DESIGN AND CONTROL IMPLEMENTATION OF FLAPPING MECHANISM FOR INSECT SIZE ROBOFLIERS

By

SINGH SPOORTHI

Thesis Submitted to the School of Graduate Studies, Universiti Putra Malaysia, in Fulfilment of the Requirements for the Degree of Doctor of Philosophy

February 2024

FK 2024 42

Abstract of thesis presented to the Senate of Universiti Putra Malaysia in fulfilment of the requirement for the degree of Doctor of Philosophy

DESIGN AND CONTROL IMPLEMENTATION OF FLAPPING MECHANISM FOR INSECT SIZE ROBOFLIERS

By

SINGH SPOORTHI

February 2024

Chairman : Professor Ir. Kamarul Arifin bin Ahmad, PhD
Faculty : Engineering

Due to the demand of Micro Aerial Vehicle (MAV) An investigation is performed into the development of an innovative, lightweight, and minimally linkage-oriented flapping actuation mechanism design for Flapping Wing MAV wing applications. Most of the research investigates the suitability of existing actuation mechanism designs for wing flapping generation. Natural flyers, such as mosquitos, can beat their wings at a high frequency of 800hz. However, as per the research survey, human-made artificial fully flyable FWMAVs, which are powered by motors, can only flap their wings at a maximum frequency. Based on a comprehensive analysis of 23 years of research data, it has been shown that there is currently a lack of mosquito characteristics mimicking models that accurately resemble natural insects with flapping wing designs driven by motors. Hence here in this research, an attempt is made, for designing few characteristics of mosquito mimicking flapping wing mechanism design. nearly Seven varieties of different mechanisms for flapping actuation are elaborated, and discussed in depth,

along with their benefits and limitations. In addition, a comprehensive parametric computational analysis has been undertaken to ameliorate flutter condition by reorganizing the design parameters of the proposed actuation mechanism. For experimental analysis, the assessment of the analytical equation is undertaken for which comprises of the proposed approach having completed computational fluid dynamics, forward and inverse kinematic testing, and simulation testing with 3D design optimization. The data collected from the created design modules are compared in order to forecast the flapping frequency based on the design criteria. Together, the wing model mounting system test rig and the data controller for data collecting have been devised and implemented. To validate the experimental method, handmade and 3D-printed prototypes were evaluated The Kinematic analysis of the novel mechanism i.e "Crank driven – triple cylindrical slidable joint and crank-slider mechanism " arrangements with direct and inverse kinematics and Jacobian representation for linear velocity and angular velocity measurements are detailed in this article. Also,3-Dimensional (3D) simulations of the mechanism design modelling have been performed to determine the flapping motion measurement and flapping link tip position tracking with two different software's.

Until now, the overall size and weight of flapping actuation designs in motor driven mechanisms has been greater owing to the complex designs of gear systems compared to linear actuated designs. Hence miniaturised unique motor actuated design concepts were in need. To further improve the design, with investigated motor modification options, an approach is made with button

vibrators as drivers to reduce the overall size and weight of the design, which subsequently evaluated their efficacy through testing. To produce natural and regulated insect-like motion, the study analyzes slider crank modified actuation materials. The inquiry has moved to design realization and analysis. Python, comp-mech GIM, and simscape multibody Computer Aided Design (CAD) models, kinematic measurements, and extensive simulations have helped in understanding the multiple design concepts. The design concepts were accomplished utilizing hand fabrication and 3D printing. Despite their fragility, handcrafted designs work. However, 3D-printed designs were bulky and faced challenges despite their potential benefits in weight reduction and thin linkages. To create compact, robust components, 3D printing techniques have been developed, showing a commitment to durable, functional designs, and constructed model, showcasing the results of their efforts. The fabrication and testing processes are meticulously documented. The study's greatest achievement is precise control of intricate wing oscillations using advanced simulation approaches. Emulating the tuned Proportional Integral Derivative (PID) controller with Simscape multibody software for the modelled design gives the research project the control needed for manoeuvring models with flapping wings.

Keywords: Crank Slider Mechanism, 3D Printed MAV, Flapping Wing Micro Aerial Vehicle, Insect Inspired MAV, Mosquito Mimicking.

SDG: GOAL 4: Quality Education

Abstrak tesis yang dikemukakan kepada Senat Universiti Putra Malaysia sebagai memenuhi keperluan untuk ijazah Doktor Falsafah

REKABENTUK DAN PELAKSANAAN KAWALAN MEKANISME FLAPPING UNTUK ROBOFLIER SAIZ SERANGGA

Oleh

SINGH SPOORTHI

Februari 2024

Pengerusi : Profesor Ir. Kamarul Arifin bin Ahmad, PhD
Fakulti : Kejuruteraan

Peningkatan dalam permintaan Kenderaan Udara Mikro (KUM), menyebabkan satu kajian telah dijalankan untuk membangunkan rekabentuk mekanisma pergerakan kepak yang inovatif, ringan, dan berorientasikan kaitan minimum untuk aplikasi Sayap Mengepak Kenderaan Udara Mikro (SMKUM). Sebilangan besar penyelidikan menyiasat kesesuaian reka bentuk penggerak sedia ada untuk penjanaan kepak sayap. Penerbang semula jadi, seperti nyamuk, mempunyai kemampuan untuk mengepakkan sayap mereka pada frekuensi tinggi iaitu 800hz. Walau bagaimanapun, berdasarkan kajian penyelidikan, FWNAV buatan manusia yang boleh terbang sepenuhnya dan dikuasakan oleh motor hanya boleh mengepakkan sayap mereka pada frekuensi maksimum. Berdasarkan analisis komprehensif terhadap data penyelidikan selama 23 tahun, didapati bahawa pada masa ini terdapat kekurangan model peniruan ciri-ciri nyamuk yang tepat menyerupai serangga semula jadi dengan reka bentuk sayap yang mengepak yang didorong oleh motor. Oleh itu, dalam penyelidikan ini, satu percubaan dibuat untuk mereka

bentuk beberapa ciri mekanisme mengepakkan sayap yang meniru nyamuk. Hampir tujuh jenis mekanisme yang berbeza untuk pengaktifan mengepak diterangkan dan dibincangkan dengan mendalam, bersama dengan kebaikan dan kelemahan mereka. Pelbagai rekabentuk mekanisme dibangunkan dan dibincangkan secara mendalam, bersama-sama dengan faedah dan hadnya. Disamping itu, analisis pengiraan parametrik yang komprehensif telah dijalankan untuk memperbaiki keadaan getaran dengan menyusun semula parameter reka bentuk mekanisme penggerak yang dicadangkan. Untuk analisis eksperimen, penilaian persamaan analisis dijalankan, yang terdiri daripada pendekatan yang dicadangkan yang telah melengkapkan pengiraan dinamik bendalir, ujian kinematik hadapan dan songsang, termasuk ujian simulasi dengan pengoptimuman rekabentuk 3D.

Sehingga kini, saiz keseluruhan dan berat reka bentuk pengaktifan kepak dalam mekanisme yang didorong oleh motor lebih besar disebabkan oleh reka bentuk kompleks sistem gear berbanding reka bentuk yang diaktifkan secara linear. Oleh itu, konsep reka bentuk unik yang diaktifkan oleh motor yang lebih kecil diperlukan. Untuk memperbaiki reka bentuk, dengan pilihan pengubahsuaian motor yang dikaji, satu pendekatan dibuat dengan menggunakan butang getar sebagai pemandu untuk mengurangkan saiz keseluruhan dan berat reka bentuk, yang kemudiannya dinilai keberkesanannya melalui ujian. Untuk menghasilkan gerakan serangga yang semula jadi dan terkawal, kajian ini menganalisis bahan pengaktifan yang diubah suai menggunakan sistem engkol gelincir. Kajian ini telah beralih kepada realisasi dan analisis reka bentuk. Model CAD multibodi Python, mekanik komputasi GIM, dan Simscape, ukuran kinematik, serta simulasi yang meluas telah membantu dalam memahami pelbagai konsep reka bentuk. Penyelidikan CFD mengesahkan ramalan prestasi aerodinamik reka bentuk asas. Kerja ini teliti dan kompeten dalam menyiasat mekanisme pengaktifan kepak Kenderaan Udara Mikro. Konsep reka bentuk dicapai menggunakan fabrikasi tangan dan pencetakan 3D. Walaupun rapuh, reka bentuk buatan tangan berfungsi. Namun, reka bentuk yang dicetak 3D adalah besar dan menghadapi cabaran walaupun mempunyai potensi manfaat dalam pengurangan berat dan pautan yang tipis. Untuk menghasilkan komponen yang padat dan kukuh, teknik pencetakan 3D telah dikembangkan, menunjukkan komitmen kepada reka bentuk yang tahan lama dan berfungsi, serta model yang dibina, menunjukkan hasil usaha mereka. Proses fabrikasi dan ujian didokumentasikan dengan teliti. Pencapaian terbesar kajian ini adalah kawalan tepat terhadap ayunan sayap yang rumit menggunakan pendekatan simulasi yang maju. Meniru pengawal PID yang disesuaikan dengan perisian multibodi Simscape untuk reka bentuk yang dimodelkan memberikan projek penyelidikan ini kawalan yang diperlukan untuk mengemudi model dengan sayap yang mengepak.

Kata Kunci: Mekanisme Peluncur Engkol, MAV Bercetak 3D, Kenderaan Udara Mikro Sayap Berkepak, MAV Inspirasi Serangga, Meniru Nyamuk.

SDG: MATLAMAT 4: Pendidikan Berkualiti

ACKNOWLEDGEMENTS

First and foremost, I would like to express my greatest gratitude to my supervisor, Professor Ir. Dr. Kamarul Arifin bin Ahmad, who guided me with constant support throughout COVID situations, which enabled me to complete this research work successfully, in addition, he gave me an abundance of technical support, mental encouragement to continue this investigation at India. Also, I wish to convey my deepest admiration to my co- supervisor, Professor Dr. Mohammad Zuber, who mentored me with technical involvement throughout COVID situations and inspired me to carry out this investigation in continuation at India with lab facilities at MIT-Manipal. Additionally, I would like to thank another co- supervisor Dr. Mohd Nizar Hamidon, who strengthened all my creative views by spending enough time to address all of my doubts and added his valuable perspectives too. Also, I would like to convey my gratitude to Dr. Adi Azriff Basri, and Dr. Norkhairunnisa Mazlan, the members of the supervisory committee, for their continuous support in providing the necessary guidance regarding the project, publications and patents filing etc, support for this research and for their insightful discussions, recommendations with quick response without any delay. I am really grateful for their time and commitment to contribute as my advisory board.

I would like to thank Universiti Putra Malaysia for providing me the best facilities and conducive environment throughout my postgraduate study period. Special thanks to Manipal Institute of Technology [MAHE], India for providing Lab facilities and equipment’s during COVID period. It helped me a lot to carry out experimental analysis very well. I wish to extend my thanks to the staff of the Department of Aerospace Engineering UPM for their friendly dealing and moral support. I gratefully acknowledge the support of the Aerospace Malaysia Research Centre (AMRC), and Institute of Advanced Technology (ITMA), for providing me space to work with required support. I also thank my friends and colleagues especially from Mechatronics Department of Manipal Institute of Technology [MAHE] India, for providing me constant support in all time.

My sincere gratitude and deepest appreciation to my parents, T Chandrashekar (father) and R S Sharada (mother), for their continuous support and encouragement for my long-life journey of learning. Thanks, must also go to my family members, my son Amrit B S and my friends, for their love, patience, understanding and encouragement as well as the wonderful environment they provided for the successful completion of this work. I am also indebted to every individual for their involvement directly and indirectly throughout this research. I really appreciate their relevant comments and encouragement during my research period. Thank you for always being there and making this pursuit a valuable journey.

This thesis was submitted to the Senate of Universiti Putra Malaysia and has been accepted as fulfilment of the requirement for the degree of Doctor of Philosophy. The members of the Supervisory Committee were as follows:

Kamarul Arifin bin Ahmad, PhD
Professor Ir.
Faculty of Engineering
Universiti Putra Malaysia
(Chairman)

Mohd Nizar bin Hamidon, PhD
Professor
Faculty of Engineering
Universiti Putra Malaysia
(Member)

Adi Azriff bin Basri, PhD
Senior Lecturer
Faculty of Engineering
Universiti Putra Malaysia
(Member)

Norkhairunnisa binti Mazlan, PhD
Associate Professor Ts.
Faculty of Engineering
Universiti Putra Malaysia
(Member)

Mohammad binti Zuber, PhD
Professor Ts.
Department of Aeronautical and Automobile Engineering
Manipal Institute of Technology
India
(Member)

ZALILAH MOHD SHARIFF, PhD
Professor and Dean
School of Graduate Studies
Universiti Putra Malaysia

Date: 11 July 2024

TABLE OF CONTENTS

	Page
ABSTRACT	i
ABSTRAK	iv
ACKNOWLEDGEMENTS	vii
APPROVAL	ix
DECLARATION	xi
LIST OF TABLES	xvii
LIST OF FIGURES	xviii
LIST OF APPENDICES	xxviii
LIST OF ABBREVIATIONS	xxix

CHAPTER

1	**INTRODUCTION**			1
	1.1	Overview		1
	1.2	Research Background		1
	1.3	Research Gap Identified		9
	1.4	Identified Problem Statement		10
	1.5	Research Objectives		10
	1.6	Scope of Work		11
	1.7	Thesis Outline		12
2	**LITERATURE REVIEW**			14
	2.1	Overview		14
	2.2	Mosquito Flapping Characteristics		14
	2.3	Classification of Flapping Actuation Mechanism Designs		16
		2.3.1	Rotary/Motor-Driven Flapping Mechanism	23
			2.3.1.1 Four-Bar Linkage Mechanism	24
			2.3.1.2 Five-Bar Linkage Mechanism	31
			2.3.1.3 Six-Bar Linkage Mechanism	32
			2.3.1.4 String-Based Mechanism	34
			2.3.1.5 Shaft-Based Mechanism	34
			2.3.1.6 Compliant Structures for Rotary Actuated Flapping Mechanism	35
		2.3.2	Hybrid Driven Flapping Mechanism	37
		2.3.3	Linear Driven Flapping Mechanism	40
			2.3.3.1 Piezo Actuation/ Driven Mechanism	43
			2.3.3.2 Piezo Driven 4 and 5-Bar Flapping Mechanism	45
			2.3.3.3 Piezo Fans for Flapping Enhancement	47
			2.3.3.4 Inertia Driven Piezo Actuated Flapping	48
			2.3.3.5 Resonant Driven Piezo Flapping Actuation	48

2.3.3.6 Shape Memory Alloy (SMA) Driven Mechanism 49
2.3.3.7 Electro Active Polymer (EAP) Driven Flapping 50
2.3.3.8 Electrostatic Driven Flapping 53
2.3.3.9 Electromagnetically Driven Flapping 54
2.4 Findings from Literature Review 59
2.4.1 Flapping Wing Design Analysis Process 59
2.4.2 FW-Flight Modes Comparison 62
2.4.3 Hovering and Forward Flight 67
2.4.4 Flapping Patterns 70
2.4.5 Flight Duration / Endurance 72
2.5 Summary of the Literature Review and Remarks 80

3 RESEARCH METHODOLOGY 83
3.1 Overview 83
3.2 Basic Design Process 84
3.3 Design Concepts with Kinematic Modelling 89
3.3.1 Model - 3C Design 89
3.3.2 Model – Crank Slider Design 97
3.4 CAD Design of FW-Mechanisms 106
3.4.1 Motor Actuated 3C Design Mechanism 107
3.4.2 X-Pattern Crank-Slider Four-Bar Mechanism Design 108
3.4.3 Concept of Proposed Design Mechanism-II 109
3.4.4 Modified SC-SDL with Single Motor (Mechanism III) 113
3.4.5 CAD Design of DC-SDL Mechanism (Mechanism IV) 115
3.4.6 SC-SDL Mechanism Designs with Coin/Button Motors 117
3.5 Fabrication Process of FW- Design Types 119
3.5.1 Fabrication of 3C Design Model 120
3.5.2 Fabrication of X-Pattern (Crank-Slider) Four-Bar Mechanism Design 122
3.5.3 Fabrication of SC-SDL Design -II 123
3.5.4 Fabrication of SC-SDL Design -III 125
3.5.5 Fabrication of DC-SDL Design -IV 129
3.6 Button Vibrator as Motor (Driving Source) for Sliding Lever Mechanism Designs 134
3.6.1 Working Principles of Button Vibrator 136
3.6.2 Fabrication of the Button Motor Driven Mechanisms 137
3.7 Controller Implementation 140
3.7.1 Simscape Modelling for DC-SDL Mechanism 142
3.7.2 DC Motor with PID Controller Tuning Approach 146
3.7.3 Modelling of New Micro DC Motor 148
3.8 Summary of the Chapter 152

4 RESULTS OF SIMULATIONS AND REAL TIME TESTING 154
4.1 Overview 154
4.2 FW Parameters Comparisons and Analysis (Literature Study) 155
4.2.1 Flapping Wing Mechanism Comparison 155
4.2.2 Flapping Frequency Comparison 160
4.2.3 Flapping Angle Comparison 163
4.3 2D/3D Modelling and Simulations of all Design 165
4.3.1 Simscape Multibody^{tm} Simulations: 3C Model 166
4.3.1.1 COMPMECH GIM Simulations:3C Model 169
4.3.1.2 Kinematics Modelling in Python Programming 172
4.3.2 Simulation Results of X-Pattern Crank Slider 4-Bar Mechanism 174
4.3.3 COMPMECH GIM Simulation Results: Design Mechanism-II 179
4.3.4 Simulation Results: Design Mechanism-III 181
4.3.5 Simulation Results: Design Mechanism-IV 184
4.3.5.1 Matlab Simulations of Design Mechanism-IV 185
4.3.5.2 Compmech GIM Simulations: Design Mechanism IV 187
4.3.6 Simulation Results: Design Mechanism-VI 189
4.4 Simulation Results: Controller Implementation 192
4.4.1 Controller Simulations: DC-SDL Mechanism 192
4.4.2 PID Controller for the Left Lever of Modelled DC-SDL Mechanism 194
4.4.3 DC Motor with PID Controller Tuning 198
4.4.4 PID Controlled DC Motor as Driving System at Right Lever of DC-SDL Model 200
4.4.5 PID Controlled DC Motor as Driving System for Both the Levers of DC-SDL Model 204
4.4.6 Implementation of Modelled New Micro DC Motor on DC-SDL Mechanism 206
4.5 Computational Fluid Dynamics 212
4.5.1 Analysis of the X-Pattern 4-bar FW through CFD 213
4.5.2 Computational Fluid Dynamic Study and Results of Design Mechanism-III 218
4.5.2.1 Geometry Simplification 220
4.5.2.2 Domain Discretization 222
4.5.2.3 Solver Setup 227
4.5.2.4 Inferences 229
4.6 Experimental (Real-Time Results) of Fabricated FW-Prototypes 236
4.6.1 Experimental Setup and Results of 3C Model 237
4.6.2 Experimental Setup and Results: Design Mechanism-III 241
4.6.3 Experimental Setup and Results: Design

Mechanism-IV 247
4.6.4 Experimental Setup and Results: Button Motor Driven SC-SDL Design 256
4.7 Summary of the Simulations and Results 261

5 CONCLUSION AND RECOMMENDATIONS FOR FUTURE RESEARCH 263
5.1 Concluding Remarks 263
5.2 Overall Conclusion 271
5.3 Future Work /Suggestions 272

REFERENCES 275
APPENDICES 308
BIODATA OF STUDENT 320
LIST OF PUBLICATIONS 321

LIST OF TABLES

Table **Page**

Table		Page
2.1	List of Advantages and Drawbacks of the 4-Bar Flapping Actuation Mechanisms	26
2.2	Material Actuation Analysis	42
2.3	List of Few Mechanisms under Rotary Driven Systems	56
2.4	List of Few Mechanisms under Hybrid Driven Systems	57
2.5	List of Few Mechanisms under Linear Driven Systems	58
3.1	Denavit Hartenberg (DH) Table	91
3.2	Difference between the Motor Types	134
3.3	List of Standard and Micro DC Motor Parameters	148
4.1	Mesh Quality Metric Evaluation	226
4.2	Design Specifications of the Proposed 3C Design Test Bench Prototype	240
4.3	Design Specifications of the Test Bench DC-SDL Prototype	248
4.4	List of All Modelled Designs and its Specifications	260
4.5	List of Simulations and Experiments Performed for All Designs	261

LIST OF FIGURES

Figure		Page
2.1	Trend of Papers Published from 2000 to 2021 a Scopus Data Survey on Flapping Wing Micro, Nano & Pico Aerial Vehicles	18
2.2	Trend of Papers Published from 2000 to 2021: a Scopus Data Survey on Driven Mechanisms Utilized in Flapping-Wing Aerial Vehicles (Motor, Hybrid & Linear Actuated) (S. Singh, Zuber, et al., 2022b)	18
2.3	a. Percentage of Micro, Nano & Pico Aerial Vehicles and b. Percentage of Fully Flyable Model and Flapping Test Bench Models from Available Data in Appendix 1	18
2.4	Classification of Types of Flapping Actuation Mechanisms Utilized in Flapping-Wing Drones	21
2.5	Percentage of Flapping Actuation Mechanisms Utilized in Overall FW Drones (S. Singh, Zuber, et al., 2022a)	22
2.6	Steps of Flapping Actuation Mechanism Design Process	60
2.7	Percentage of Flight Modes (Hover, Vertical Take-Off, Forward Flight, Guide Rail, Landing, Turns & Backward) under Fully Flyable Flapping-Wing Systems	62
2.8	Endurance and Corresponding Weight with the Yearly Representation of Rotary & Hybrid Actuated Fully Flyable Fapping-Wing System Models	62
2.9	Endurance and Corresponding Weight with the Yearly Representation of Linear Driven Fully Flyable Fapping-Wing Systems Models (Note: All Linear Driven Fully Flyable Fapping-Wing Systems Models Are under Insect Mimicking Types)	63
2.10	Yearly Progress of Rotary & Hybrid Driven Fully Flyable Fapping Wing Systems with Respect to a). Endurance, and b). Total Weight.	64
2.11	Yearly Progress of Linear Driven Fully Flyable Fapping-Wing Systems with Respect to a). Endurance, b). Total Weight	66
2.12	Percentage of Biomimetic and Biomorphic Types a). Hovering Capable Fully Flyable Fapping-Wing System Models b). Forward Flight-Capable Fully Flyable FWAV Models	69
2.13	List of Flapping Actuation Mechanisms Utilized in Flapping-Wing Systems to Generate a). Hovering Flight Condition, b).	

	Forward Flight Condition	69
2.14	Percentage of Wing Flapping Patterns Utilized under Hovering Capable Fully Flyable Flapping-Wing Drone Models	70
2.15	Flapping Patterns Performed by Several Flapping-Wing Systems under Different Flapping Actuation Mechanisms	71
2.16	Number of Launching Types Used under Each Flapping Actuation Mechanism for Fully Flyable Flapping-Wing System	71
2.17	Number of Flying Patterns after Auto / Hand Launch of Fully Flyable Flapping-Wing System	72
2.18	Flapping Actuation Mechanism Sketches from Prototypes That Lasted over 8.5 Minutes	74
2.19	Allocation of Ranking Based on the High Level of Endurance Attained over the Years	75
3.1	Flow Chart of a). Basic Design Process and b). Design Concept Types Used for Flapping Wing Actuation	85
3.2	Detailed Flow Chart of Research Methodology Implemented for Flapping Wing Prototype	88
3.3	Kinematic Structure of 3C Design Flapping Actuation Mechanism	90
3.4	Top View of the 3C Design Kinematic Structure	93
3.5	Fast Return Mechanism	99
3.6	Standard Sliding Lever Mechanism Concept	101
3.7	A Limiting Positions of the Flapping Wing Mechanism	105
3.8	Novel 3C Flapping Actuation Mechanism Design	107
3.9	CAD Model of Mechanism Design I for Flapping Actuation	109
3.10	SC-SDL Design Mechanism-II	110
3.11	X-Pattern Crank-Slider Four-Bar Mechanism Design	112
3.12	SC-SDL Design Mechanism-III	114
3.13	CAD Model of SC-SDL Design -III, a Motor Driven Single Crank - Dual Slotted Lever Mechanism for Flapping Actuation	115
3.14	Isometric View (CAD Model) of the DC-SDL Mechanism	116

3.15 Exploded View of the Proposed DC-SDL Design 116

3.16 Single Crank-Sliding Dual Lever (SC-SDL) Model with Single Button Vibration Motor as Driving Source 117

3.17 Single Crank-Sliding Quad Lever (SC-SQL) Model with Single Button Vibration Motor as Driving Source 118

3.18 Dual Crank – Slotted Dual Leavers (DC-SDL) Model with Dual Button Vibration Motor as Driving Source for Individual Wing 118

3.19 The Flapping Actuation Mechanism's Test-Bench Design 121

3.20 Flapping Frequency Measuring Setup 121

3.21 Equivalent Circuit Diagram of Flapping Frequency Measuring Setup 121

3.22 3D Printed Design of X-Pattern Four-Bar Mechanism 123

3.23 Over All Weight of Fabricated Design Mechanism II with Motor (without Wings) 124

3.24 Size of Hand Made SC-SDL Mechanism Design with 10 Cents Coin 125

3.25 Peight of Compact Handmade SC-SDL Design Mechanism with Motor (without Wings) 125

3.26 Paper Wings Attached to the Handmade SC-SDL Mechanism Design 126

3.27 SC-SDL Design III with Flapping Frequency Measuring Setup 126

3.28 Mosquito Wing Shaped Plastic Wing Attached to the Handmade SC-SDL Mechanism Design 127

3.29 Mosquito Wing Shaped Plastic Wing Design Movement 128

3.30 Overall Weight of Compact Handmade SC-SDL Design Mechanism with Motor and Wings 128

3.31 Proposed DC-SDL Mechanism Testbench Design /Prototype (Handmade) 130

3.32 Sequential Frames of the Proposed Mechanism for Less Frequency (i.e at Minimal Input Voltage), Each Frame is 167ms Apart 130

3.33 3D Printing of Wing Lever Parts 131

3.34 Printed Parts of Sliding Lever and Motor Supporting Base 132

3.35 Weights of Sliding Lever, Battery and Micro Dc Motor in Grams 132

3.36 3D Parts Assembled DC-SDL FW Prototype 133

3.37 Weights of Assembled Single and Double Motor with Sliding Lever in Grams 133

3.38 Button Vibrator Internal Structure 136

3.39 Handmade SC-SDL Design with Button Vibration Motor 138

3.40 Total Weight of Hand Made SC-SDL Design with Button Vibration Motor (without Wings) 138

3.41 Hand Made SC-SFL Design with Button Vibration Motor with its Overall Weight (without Wings) 139

3.42 Modelling of Dual Crank – Slotted Dual Leavers (DC-SDL) Mechanism in Simscape Multibody 144

3.43 Connections of Modelled Dual Crank – Slotted Dual Leavers (DC-SDL) Mechanism 145

3.44 Simscape Modelled DC Motor with PID Controller 146

3.45 Measurements of Attained PID Controlled Voltage with Output Speed of DC Motor (at P=1, I=1, D=0) 146

3.46 PID Controller Specifications and Response after Tuning 147

3.47 Modelled Micro DC Motor 149

3.48 DC Motor Current and Speed at 3.7v Input DC Voltage 149

3.49 Modeled Micro DC Motor Current and Speed at 3.7v Input DC Voltage 150

3.50 Both the Motors Obtained Current Variations are Compared in Data Inspector of MATLAB 151

3.51 Both the Motors Obtained Speed Variations are Compared in Data Inspector of MATLAB 151

4.1 Variation in Total Weight of FWAV Models in Years to Flapping Actuation Mechanism a). Rotary & Hybrid Driven Mechanisms and b). Linear Driven Mechanism 156

4.2 Flapping-Wing Systems Total Weight and Corresponding Wingspan of (a). Rotary & Hybrid Driven Mechanism, and (b). Linear Driven Mechanism 157

4.3	Correlation between Mass & Wingspan (a). Bird Like FWAV’s, (b). Hummingbird like FWAV’s	158
4.4	Percentage of a). Biomimetic and Biomorphic Type of Fully Flyable FWAV’s. and b). Number of Wings, Utilized under Fully Flyable Flapping-Wing Systems	159
4.5	Percentage of Tailed and Tailless Models Created under a Particular Flapping Actuation Mechanism in Fully Flyable Fapping-Wing Systems	160
4.6	Flapping Frequency and Corresponding Total Weight of (a). Rotary & Hybrid Driven Mechanism, (b). Linear Driven Mechanism	161
4.7	Flapping Frequency and a Corresponding Wingspan of Rotary and Hybrid Actuated Overall Fapping-Wing Systems	162
4.8	Flapping Frequency and a Corresponding Wingspan of Linear Actuated Overall Fapping-Wing Systems	163
4.9	Flapping Angle and a Corresponding Wingspan of Overall Flapping-Wing Systems	164
4.10	Similar Model Design in Simscape MultibodyTM MATLAB	167
4.11	Equivalent Model for the Mechanism in Simscape Multibody^{TM} (SimMechanics^{TM})	167
4.12	Obtained Position and Velocity of the Wing Tip	168
4.13	(a): Similar Model Design in Compmech GIM Software	169
4.14	(a)The Angle of Flapping Obtained, and (b) Flapping Velocity at the Flapping Link Tip	171
4.15	(a) Angular Velocity of the Flapping Element, and (b) Acceleration at the Flapping Link Tip	171
4.16	Angular Acceleration of the Flapping Element	172
4.17	Flapping Angle Obtained from Forward Kinematics of DH-Table 4.1	173
4.18	(a) Variation in Flapping Liver Tip with Respect to the Driving Crank Angle in x and y Direction. and (b) Variation in Liver Tip Angular Velocity with Respect to Time in x & y Direction	173
4.19	Workspace of the Modelled Design I Mechanism	175
4.20	Point Velocity Analysis of the Design I Mechanism	176

4.21	Angle between Two Vectors at Left Lever of the Design I Mechanism	177
4.22	Angle between Two Vectors at Right Lever of the Design I Mechanism	178
4.23	Element IC of Acceleration vs Time (sec)	179
4.24	Workspace of the Modeled *SC-SDL* Design Mechanism-II	180
4.25	Color Wise Representation of Variations in Velocity and Acceleration at Both Lever Paths of Motion	180
4.26	Kinematic Analysis at Lever Tip of SC-SDL Design Mechanism-I; (a)Point velocity vs. Flapping Duration; (b) Point Acceleration vs. Flapping Duration; (c) Elemental Angular velocity vs. Flapping Duration; (d) Elemental Angular Acceleration vs. Flapping Duration	181
4.27	Workspace of the Modeled SC-SDL Design Mechanism-III	182
4.28	Color Wise Representation of Variations in Velocity and Acceleration at Both Lever Paths of Motion	183
4.29	Kinematic Analysis at Lever Tip of SC-SDL Design Mechanism-I; (a)Point velocity vs. Flapping Duration; (b) Point Acceleration vs. Flapping Duration; (c) Elemental Angular velocity vs. Flapping Duration; (d) Elemental Angular Acceleration vs. Flapping Duration	183
4.30	MATLAB of DC-SDL Single Lever for Simulation	185
4.31	Velocity and Acceleration Determined by Simulation during Angular Velocity at Motor is Set to be 10rad/s	186
4.32	Changes in Velocity and Acceleration Based on the Different Angular Velocity Set at the Motor	186
4.33	Workspace of the Modeled DC-SDL Mechanism	187
4.34	Obtained Angular Speed and Acceleration for Sliding Lever Element Motion	188
4.35	Point Velocity and Acceleration Measured at the Tip of Proposed Sliding Lever Wing	188
4.36	Modelling of Four Levers (Sliding Quad Levers) Actuation through Single Motor in Compmech GIM Software with its Velocity Indications	189
4.37	Wing Tip Velocity Variations of all the Four Wings	190

4.38 Wing Tip Positional Variations of All the Four Wings 190

4.39 Wing Tip Acceleration Variations of all the Four Wings 191

4.40 Input Signal Generated from Constant & Integrator Provided at the Revolute Joint A & A1 for Actuation 193

4.41 Variations in Both the Lever Positions, Angular Velocity and Angular Accelerations of the DC-SDL Mechanism with Respect to Time 194

4.42 PID Controlled (Left Wing) Connections of Modelled Dual Crank – Slotted Dual Leavers (DC-SDL) Mechanism in Simscape 196

4.43 Left and Right Motor Input Signals with PID Controlled Signal 197

4.44 PID Controlled Variations of Left Wing Lever Position, Velocity and Acceleration with Respect to Right Wing (without PID) of DC-SDL Mechanism 198

4.45 DC Motor Output after PID Controller Tuning 199

4.46 PID Controlled DC Motor at Right Wing of Modelled Dual Crank – Slotted Dual Leavers (DC-SDL) Mechanism in Simscape 200

4.47 PID Controlled Linearly Increasing DC Motor Speed 201

4.48 Increased Right Wing Lever Flapping Velocity Compared to Left Wing 202

4.49 Variation in Right Wing Lever Flapping Acceleration Compared to Left Wing 203

4.50 Positional Tracking of Right-Wing Lever Tip 203

4.51 PID Controlled DC Motor for Both the Levers of Modelled Dual Crank – Slotted Dual Leavers (DC-SDL) Mechanism in Simscape 204

4.52 Emulation Results of PID Controlled DC Motor for Both Levers of Modelled DC-SDL Mechanism 205

4.53 Simscape Modelling of Micro-DC Motor-Controlled DC-SDL Mechanism with Chart Flow Process 206

4.54 Detailed Logic Chart for the Flapping Motion Control Process 207

4.55 Chart Controlled Inputs at Both Motors 209

4.56 Variations of the Flapping Lever Angular Speed, Acceleration and Position as Per the Chart Flow 210

4.57 Lever Position in to Normalized Frequency or Samples 211

4.58 Discretized Domain Dimensions 214

4.59 Transient Thrust Force Plot 215

4.60 Transient Coefficient of Lift Plot 215

4.61 Transient Coefficient of Drag Plot 216

4.62 Downstroke Flapping-Wing Plate with Velocity-Magnitude Contours at the 150 / 314-Time Frames 217

4.63 Local Refinement within the Dynamic and Static Fluid Zones for Uniform Residual Convergence 222

4.64 Boundary Layer Inflation Zone in Close Proximity to the Flat Plate 223

4.65 Local Capsular Discretization to Capture the Wake Distribution of the Separated Flow 224

4.66 Flapping Physics for the Computational Fluid Dynamic Ornithopter Analysis 228

4.67 Static Pressure Distribution over Flapping Flat Plate at t = 0. 001 229

4.68 Velocity Magnitude Contour over Flapping Flat Plate at t = 0. 001 230

4.69 Symmetrical (a) Downstroke and (b) Upstroke Velocity Magnitude Contours over Flapping Flat Plate at 150th and 314th Time Frame Respectively 231

4.70 Upheave Wake Induced Flow Separation over Flat Plate (a) Wake Distribution (b) Magnified View 233

4.71 Net Flow Field Metrics of Asymmetric Flapping Plate Configuration (a) Coefficient of Drag (b) Coefficient of Lift (c) Thrust Force along the Positive x Axis 234

4.72 Averaged Flow Field Metrics of Left and Right Asymmetric Flapping Plate Configuration (a) Coefficient of Drag (b) Coefficient of Lift (c) Thrust Force along the Positive x Axis 235

4.73 Measured Flapping Frequency 237

4.74 a).Variation in Flapping Frequency as a Function of Increased Input Voltage. b). Multiple Set of Tests for Flapping Frequency Analysis 238

4.75 Sequential Flapping Captured Frames of the Proposed Mechanism 239

4.76 Comparison of Obtained Flapping Angle from Forward Kinematics to Real Time Testing 240

4.77 Variation in Flapping Frequency Due to the Variable Input Voltage of the Motor 242

4.78 Digital CRO Forward and Reverse Stroke Time Difference Measurement 242

4.79 Phase Lag between Left- and Right-Wing Measuring Setup 243

4.80 Phase Lag between Left and Right Wing 244

4.81 Normal Distribution Comparison of Proposed Design Configuration's Metric against Existing Flapping Wing Design Weight Ratio Metric 244

4.82 The Captured Path of Movement by the Final Prototype 246

4.83 Ultrasonic Sensor Measurement Interfaced with Ultra2000 Software 248

4.84 Distance Variation Measured by an Ultrasonic Sensor throughout Wing Flapping 248

4.85 IR Sensor Circuit Setup for Frequency Measurement 249

4.86 Schematic Diagram of Flapping Frequency Measuring IR Sensor Circuit Setup 249

4.87 Flapping Frequency Measurement Setup with Laser Tachometer 250

4.88 Variation in Flapping Frequency a) by Laser Sensor and b) IR Sensor Based on the Varied Input Voltage of the Motor 251

4.89 Average of Laser Tachometer and IR Sensor Flapping Frequency Readings 252

4.90 Difference between the IR Sensor and Laser Tachometer Flapping Frequency Readings (i.e the Error Obtained) for 7set of Testing Performed 253

4.91 Digital CRO Forward and Reverse Stroke Time lag Measurement 254

4.92 Frequency Measurement of 3D Printed DC-SDL Mechanism with Micro DC Motor Design at an Input Voltage of 3.5v 256

4.93 Hand-Made SC-SDL Design with a Button Motor Frequency Testing Setup 256

4.94 Obtained Set of Flapping Frequencies from Button Motor Driven SC-SDL Model 257

4.95 Difference of Flapping Frequency Obtained between Left and Right Wing of Button Motor Driven SC-SDL Model 258

4.96 IR Sensor Measured Frequency Measurement of Handmade SC-SDL Mechanism with Button Vibration Motor Design at 1v Input Dc Voltage 258

LIST OF APPENDICES

Appendix		Page
A1	Flapping-Wing System Characteristics of Varieties of Rotary Driven 4–Bar Linkage Mechanism	308
A2	Flapping-Wing System Characteristics of Varieties of Rotary Driven 5-Bar Linkage Mechanism	310
A3	Flapping-Wing System Characteristics of Varieties of Rotary Driven 6-Bar Linkage Mechanism	310
A4	Flapping-Wing System Characteristics of Varieties of String-Based Rotary Driven Mechanism	311
A5	Flapping-Wing System Characteristics of Varieties of the Shaft–Based Rotary Driven Mechanism	311
A6	Flapping-Wing System Characteristics of Varieties of Compliant Structure Mechanisms for Flapping	312
A7	Flapping-Wing System Characteristics of Varieties of Hybrid Driven Mechanism	313
A8	Flapping-Wing System Characteristics of Varieties of Piezo Driven Mechanisms	314
A9	Flapping-Wing System Characteristics of Varieties of SMA Driven Mechanisms	316
A10	Flapping-Wing System Characteristics of Varieties of Electro Active Polymer (EAP)driven mechanisms	317
A11	Flapping-Wing System Characteristics of Varieties of Electrostatic (ES) Driven Mechanism	318
A12	Flapping-Wing System Characteristics of Varieties of Electromagnetic (EM) Driven Mechanisms	318

LIST OF ABBREVIATIONS

n	Link index
J	Joint coordinate
I	3 x 3 Link inertial matrix
T_n^{n-1}	4 x 4 Transformation matrix of assumed coordinate nodes/ systems from link n-1 to n
$T^{(Jn)}$	4 x 4 Transformation matrix of standard reference coordinate system
$R^{(Jn)}$	3 x 3 Rotation matrix of assumed coordinate nodes/ systems from link n to n –1
$O^{(Jn)}$	Origin of the of assumed coordinate systems from link n to n –1
$\psi^{(Jn)}$	Joint coordinate vector from link n to n –1
$q^{(Jn)}$	Generalized coordinates from link n to n –1
Ln & Pn	Link length
dn	The translation movement at the joint
$d_{z(i-1)}$	Translation along Z-axis when i=1, 2, 3… depending on the frame (i) consideration
$\theta_{z(i-1)}$	Rotational angle about Z-axis when i=1, 2, 3… depending on the joint (i) consideration
$\alpha_{x(i)}$	Rotational angle about X-axis when i=1, 2, 3… depending on the joint (i) consideration
$r_{x(i)}$	Translation along X-axis when i=1, 2, 3… depending on the frame (i) consideration

CHAPTER 1

INTRODUCTION

1.1 Overview

This chapter defines the primary concept of the present work. First, the theoretical foundations of this research are described in the research introductory paragraph, followed by a discussion of UAV's focusing on flapping wing aerial vehicles designs with nano aerial vehicles details and a lightweight design mechanism requirement in the second portion. Furthermore, in the problem statement section, the characteristics of the mosquito-mimicking model are explored. The purpose of the research is stated in the fourth part as objectives. The dissertation's scope is outlined in the epilogue.

1.2 Research Background

The new drone market, also known as unmanned aerial vehicles (UAVs), has been enriched with bio-inspired technologies and enhanced performance. Although rapid progress has been made in the design of UAV morphing, the challenges of low altitude aerial locomotives remain important and impede the spread of this technology. Aerial locomotion becomes especially difficult when it is close to the Earth's surface where winds can alter speed and direction very quickly, making UAV-type morphing unfavorable. High wind turbulence levels can be detrimental to flight and face severe flight control challenges. In finding workable solutions, scientists have discovered inspiration in biological flying systems, such as insects and birds, because they have an impressive flight technique involved in them. The idea of flight mechanism has progressed from fixed-wing or rotary-wing to flapping-wing and vibrating-wing mimicking small birds and insects, accordingly. Based on their size and weight, these miniaturized UAVs are typically categorized into four subsections: MAV (Micro Aerial Vehicles), NAV (Nano Aerial Vehicles), PAV (Pico Aerial Vehicles) and SD (Smart Dust). All these vehicles are known as "extremely small and ultra-light air vehicle systems". For MAV, the overall wingspan is 1 m, and the weight is less than 2 kilograms. For NAV, the maximum wingspan is 15 cm, and the weight is less than 50 grams. For PAV, the overall wingspan is 2.5 cm, and the weight is less than 3 grams. Smart dust (SD) consists of several small micro-electromechanical systems (MEMS) and sensors inside it, the size for SD is 0.25 cm and the weight is 0.5 grams. Explicitly, propeller-driven MAVs are basically flying wings where all avionics, energy storage, and propulsion are limited within the wing configuration. Rotary-wing implementations have yielded better performance compared to fixed wings, owing to their ability to fly slowly and even drift. Whereas during high winds or thunderstorms, the ability of MAVs to flap wings is protected due to the high lift mechanisms that have developed over the wing surface, allowing for slow controlled flight. The reason that a flapping wing is more viable than a rotor is that its energy is spread over a wider chord and oscillates from a minimum of zero thrust and boosts at either end of the flapping stroke to its maximum at mid stroke. Generally, most of the insects they see flying about are with four wings, but dipterans (meaning 'two wings') only ever use one pair. The other pair of wings has been reduced to club- like structures known as 'halteres' used for balancing upward movements. During the flight, the thorax, wing and wing hinge are all severely deformed by storing potential energy. Flapping of the wing can be achieved by employing this potential energy which can reduce the inertial cost of it (Nagai & Isogai, 2011). Without elasticity in the wing, flapping wings won't be effective than compared to rotating propellers (Hawkes & Lentink, 2016). Researchers seem to be able to build bio-inspired drive trains, using compliance components, elastic energy storage systems to reduce power consumption and prolong flying time by enhancing battery life. Many have experimented with the robotic design to enhance it by involving flexure hinges or elastic thoraces and have achieved substantial energy savings (Bluman et al., 2018; Sahai et al., 2013). Very tiny insect roboflies are very fascinating and fall under Micro Aerial Vehicles (MAV). They have been great because of their high versatility and applications all over the world. Here they will study flapping type insect roboflies and also demonstrate its stability analysis, system identification and control implementation strategies. In this proposal, the strategy follows forward with following process, focused on control and driving technology, actuation by means of motors /piezoelectric material, mechanical transmission system, suitable controller and minimal power sources.

In short, the MAV's wing flapping actuation mechanisms are guided by two fundamental principles. One is to mimic the structure with mechanisms, just like actual living birds/ insects, called the biomimetic approach of design, and the second is to use only limited characteristics observed in flying birds/ insects with advanced design features of human-made aerial vehicles, referred to as the bio-morphic approach of design (Jones & Platzer, 2006b). In 2005, Jones et.al attempted a biomorphic concept of design that involves fixed side wings to generate lift and two flapping wings at the back side (as foil) that could flap in the counter phase. Usually, whenever a bird flaps its wings, the body appears to fluctuate against the wing movements. But in this concept, the biplane framework is advantageous as it balances the aerodynamic limitations by concentrating on enhancing the thrust through mechanical parts (Jones et al., 2005; Jones & Platzer, 2003, 2006a, 2010). However, the general biomimetic approach to design has been followed by many researchers in projects like Microbat (Pornsin-Sirirak, Tai, Ho, et al., 2001), Nano hummingbird (M. Keennon et al., 2012b) etc., where flapping of side wings is mainly focused. The flapping wing system is the most sustainable mechanism when compared to rotary and fixed types. This may be because its energy is transmitted via a larger chord, oscillating from a limit of zero thrusts that boost both ends of the flapping angle to a high (higher than in mid-stroke) (Michelson, 2010). The remarkable thing about these flapping structures is that they are designed to be a flexible and efficient oscillating system with reasonable elasticity. The flapping method involves control over the wing in such a way that the movement of the wing must stop and reverse the plane for every stroke ("The Aerodynamics of Hovering Insect Flight. VI. Lift and Power Requirements," 1984). The wing kinetic power will be held on the thorax walls, which will be utilized at the end of every stroke for better lift (Madangopal et al., 2006). The versatility of wings is a major component of insect motion that efficiently generates aerodynamic power. In comparison to birds, insect wings are indeed controlled at the base, so in-flight it experiences great deflections and gradual structure adjustments accordingly. Insect wings serve as reconfigurable airfoils and have many associated supports, involving passive twist to achieve damping (Agrawal & Agrawal, 2009). The structure and tensile mobility of the framework in a stretch and a chord-like orientation determine the functional resistance of a wing to a specified density (Combes & Daniel, 2003). As a result, researchers with the concept of imitating the insect flight technique on their MAVs usually opt for a better and simpler flapping mechanism on its wing. In 2012, the mechanism of flapping techniques being categorized by Ryan et al (Ryan & Su, 2012) depending on the following conditions: workspace (generated wing trajectory), rigid body, compliant mechanism (Colmenares et al., 2015), type synthesis, mobility, and type of actuators used for wing actuation, etc. Phan and Park, in his review paper, elaborated on the motor unit, design mechanism, wing configuration, and control strategies utilized in micro-to-pico size fapping-wing drones. They described the associated electronics and power technologies that were used on the MAVs to drive actuators rather than traditional electromagnetic motors (Phan & Park, 2019). In 2019, Jiaxin et al. (Jiaxin et al., 2019) reviewed various scientific approaches of driving actuation mechanism, such as piezoelectric, motor, and electromagnetic driven fapping-wing drones. In their recent work, the advancement of the FWMAV bio-inspired mechanism concerning the driving actuation methods is well explained.

When contemplating the design of a lightweight and compact, life forms like tiny insects or flies/mosquitoes are commonly the primary source of inspiration. Until now, the majority of mosquito research has mostly concentrated on studying the aerodynamics of their wings, rather than investigating the mechanisms behind their creation or attempting to imitate their traits. Mosquitoes are currently attracting attention due to their unique flying patterns and distinctive aerodynamics features. Mosquitoes exhibit unique flapping wing characteristics that are influential for mimicking in micro aerial vehicle design. Some pertinent features include Deviation Motion, Hovering with Small Sweeping Amplitude, Increased Vertical Force via Drag and Wing-Wake Interaction. Mosquitoes have a particular wing flapping pattern that includes a significant deviation motion, characterized by relatively large deviation angles and small sweeping amplitudes. This motion greatly influences the aerodynamic performance, adjusting the angle of attack and direction during wing movement, thereby enhancing lift generation efficiently(H. Jung et al., 2024). Unlike many insects, mosquitoes are capable of hovering with a lesser sweeping amplitude but with larger deviation angles, which contributes to improved vertical force generation. This is crucial for designing MAVs that require hovering capabilities. With deviation motion, mosquitoes can convert some of the drag force generated during the early phase of a downstroke into vertical lift. This capability to generate a larger vertical force more efficiently is desirable for MAVs aiming to mimic insect flight. Mosquito wing movements lead to wing-wake interactions that are beneficial for lift generation. Understanding these interactions is valuable for the development of MAVs that need to navigate through complex aerodynamic scenarios. These aerodynamic aspects, along with the ability to generate sufficient lift while hovering and improving flight efficiency, can be considered when designing and developing MAVs that imitate the flapping-wing characteristics of mosquitoes. Although mosquitoes are responsible for transmitting the most significant infectious diseases worldwide, they are nonetheless considered exceptional flyers. Based on their size, they generally flap their wings at a rapid frequency ranging from 600 to 800 Hz. Flapping also enables them to camouflage their presence, engage in courtship behaviour, and maintain flight. Their elongated and slender wings move back and forth between the frontmost and rearmost emphasizes with a stroke amplitude of approximately 40 to 45°, which is significantly smaller than that of their natural counterparts (>120°). While most insects rely on leading-edge vortex for lift, mosquitoes possess additional aerodynamic features such as rotating drag, reinforcement of the trailing-edge vortex through wake capture, and the extra mass effect. An exhaustive examination of these three mechanisms is necessary, considering the advantages and disadvantages of high-frequency, low-stroke angles, operating much outside the typical kinematic boundary in comparison to other insects, and the influence on the enhancement of design in small drones(Ahmad et al., 2000; Bomphrey et al., 2017; Mahendra et al., 2021; B. Singh et al., 2021; van Veen et al., 2020). The progress of navigation of NAV is significantly facilitated by the lightweight, compact size, and uncomplicated flapping actuation mechanisms. In this context, they are focusing on the notable characteristics of mosquitoes, which is novel and non-existing till now.

In any flapping-wing drone design, an efficient actuation mechanism for flapping, maneuvering, and modulating the wings is required from a strategic standpoint. As a result, the mechanisms used for flapping motion in MAV, NAV, and PAV till date should be classified systematically for the benefit of the study. Such a classification would also help future development of flapping methods, especially for very lightweight bio inspired aerial vehicles. Accordingly, in our literature review, authors were able to detail the characteristics of several flapping-wing drones under each type of flapping actuation mechanism, which can be found in Appendix-1 of this paper. A brief overview of the classification based solely on flapping actuation mechanisms, which are the core of insect-inspired flapping vehicles, has been carried out, to be primarily considered when designing any flapping-wing drone. Based on the similarity of the gear and linkage connections of the various aerial vehicle prototypes, authors designed a standard combination of design mechanisms under diverse processes according to the classification in chapter 2. The equivalent block diagram representation of those design mechanisms is implemented in this review, for ease of understanding of the mechanisms. It displays the depiction of design in the form of block diagrams with variants, add-ons, and enhancements provided by various authors to their prototypes, indicated with explanations. The block diagram approach was chosen here because it offers a comprehensive concept of design mechanisms with internal connections and parts in blocks. In addition, to block diagram representation, steps for the flapping-wing drones design process which include other parameters such as flapping angle, flapping frequency, and current driving mechanisms, chosen from various literature for the generation of lifts at different sizes or scales of flapping-wing drone are also discussed. The authors classified flapping-wing drones forms such as birds, small birds, nano hummingbirds, insects, bats, and biomorphic types into rotary, hybrid, and linear actuated flapping-wing drone based on their imitable similarity.

Flight modes such as forward, backward, turn, take-off, hovering, and landing flight are described for the fully flyable model and the flapping test bench model. The best performing prototypes are addressed by assigning them a ranking based on their flight modes, flapping actuation structure designs, and long-duration flight affordability. The requirements and designs of most actuation mechanisms have been expanded by focusing on the new productivity of flapping frequency and stroke angle controllability via linkage mechanisms with awareness of flapping patterns.

1.3 Research Gap Identified

From the literature review the following important points are to be addressed as potential to bridge the gap in already conducted research work, future scope, and requirements.

- Researchers concentrated on Miniaturized flapping technique is only through linear actuation mechanism, as the size is a main constraint in NAVs.
- In motor driven mechanisms, due to the intricate designs of gear systems, the overall weight of the flapping actuation mechanisms has been higher until now.
- Natural flyers, such as mosquitos, beat their wings at a high frequency i.e 800hz, yet human-made artificial fully flyable FWNAVs driven by motors can only flap their wings Max upto 45hz frequency.
- From the literature review of 23 years research data, Mosquito characteristics mimicking FW designs- driven by motors are not there yet and it is required for insect's behavioural study.

1.4 Identified Problem Statement

- As mosquito mimicking models are currently not available for the analysis and subsequent design optimization, or evolution.
- The advancement of NAV is greatly aided by the light weight, small size, and simplest flapping actuation mechanisms, here our target is for some salient features of mosquito.
- Hence our aim is to DESIGN AND CONTROL IMPLEMENTATION OF FLAPPING ACTUATION MECHANISM FOR INSECT SIZE ROBOFLIERS that could mimic some of the mosquito characteristics like compact size, reduced weight with minimal flapping angle & better flapping frequency.

1.5 Research Objectives

The overall objectives of this research work are, Designing of flapping actuation mechanism for flapping wing micro aerial vehicle application, by exemplifying a thorough review of the available flapping actuation design concepts. The proposed design employs a lightweight design with comparable properties (like flapping frequency, angle and overall weight, size) to the existing models. To ensure that the proposed design meets the requirements of micro aerial vehicles. Supporting to the above the following objectives were formulated. In specific, this research is:

1. To design flapping wing actuation mechanisms with mathematical modelling and kinematics by focusing on reducing its overall weight, achieving compact size, and less complex design model.
2. To evaluate its performance by analyzing structural movements through 2D/3D simulations, to obtain the parameters such as flapping frequency, velocity, and accelerations.

3. To implement modelled flapping actuation designs into fabrication using handmade / 3D printing methods.

4. To validate the proposed designs through experimental analyses and simulation of control performance to assess their suitability for nano aerial vehicle applications.

1.6 Scope of Work

Designing and building a completely functional insect-scale aerial vehicle especially with respect to micro/nano scale is a difficult endeavor. yet there are no specific design methods in place, as well as no adequate manufacturing specifications such as effective actuation mechanism, compact in size, lesser weight, and unique materials. The biomechanics of flying insects are extremely complicated, and they all fit into a space smaller than a Swiss watch.

Generally, motor driven FWAV's use several gears / cranks with linking rods, rocker or couplers as connections in any design mechanism. There is currently no simple flapping actuation system with least links, like only two-bar connections, are not available yet. It is critical to reduce the complexities of actuation mechanism designs in minimizing the overall weight of the system. Hence, they are attempting to come up with a very small size motor actuated flapping wing design with better frequency, under mini motor actuated models. When considering the design of something that is lightweight and small, natural creatures such as tiny insects or flies/mosquitos are typically the main source of inspiration. So far, most of the research on mosquitoes has focused only on their wing aerodynamics, but not on its design mechanisms or mimicking its characteristics. Some researchers have also conducted experiments using piezo or linear actuated Nano FW-models. However, motorized designs in insect-sized or mosquito like versions are exceedingly uncommon.

Based on our analysis of literature, it has found that, among completely functional Flapping Wing Models, those powered by motor-driven mechanisms, until now have achieved a maximum frequency of 45 Hz only. On the other hand, models driven by linear mechanisms such as piezo, shape memory alloy, electro active polymer, electrostatic, and electromagnetic have achieved max frequency of approximately 200 Hz. According to researcher Bomphrey, the flapping frequency of mosquito's are 800hz which is highest compared to most insects, with minimal flapping angle of 45 degree. Hence, it is essential to create a design model with a micro motor driven lightweight device that mimics the characteristics of a mosquito, such as small size, high flapping frequency, and a precise flapping angle. As a limitation the wing size cannot be as small as mosquito's, due to physical driving mechanism weight impacts which obviously affects the lift of the FWNAV.

1.7 Thesis Outline

This dissertation is divided into eight chapters. The first chapter introduces micro aerial vehicles, focusing on the significance of fluttering wing vehicles in particular. In the introduction, the rationale for conducting this research, its objectives, and its scope are outlined with problem statements. The second chapter provides context for this study by examining pertinent literature in this field. In this section, the efficacy of the flapping wing used on MAVs is discussed. In addition, a review of previous work on flapping actuation mechanisms and its mosquito mimicking characteristics specified with requirements are elaborated. significant design connections and materials utilized to enhance the flight performance of MAVs are discussed. The third chapter elaborates on the slider crank mechanisms with modifications into at least three or four distinct designs. utilization of button vibrators as micro motors, their driven design. also examines the methodology for developing experimental and numerical models, including the kinematics and CAD designs involved in the development process. Chapter 4 discusses the design, modelling, simulations, fabrication, and validations of the three cylindrical joint mechanisms. Results, analyses, and discussions on flapping actuation and the design process, in conjunction with the performance of the primary flapping wing model. demonstrates the comparison of control designs and emulation results in detail. As a conclusion, Chapter 5 discusses the conclusion and future research recommendations deduced from this study.

CHAPTER 2

LITERATURE REVIEW

2.1 Overview

The fundamentals of general UAV's, focused MAV and Mosquito flight characteristics chosen for the motivation of the project work were discussed in Chapter 1. This literature review chapter presents a detail on the mosquito flapping specifications and current design practice in FWMAV's with different types of actuation mechanisms that are classified. The literature review is structured in a way that provides a comprehensive structural overview of the research done in FW-drones. Types of driving sources used for flapping actuation mechanism are also emphasized. Advantages and limitations of some specific design mechanisms are listed & compared. Comparisons of different fully flyable prototypes of two decades are plotted with respect to the yearly modifications done by the authors to their model. Before concluding the chapter, the literature findings will be presented from the review of the research followed by remarks of the direction of the research.

2.2 Mosquito Flapping Characteristics

Specific MAVs that mimic mosquito-like characteristics are at the forefront of bio-inspired robotics research and development. They may not replicate all the high-frequency and complex kinematic features of mosquitoes, but they adopt certain elements of their wing motion, like flapping patterns and deviation angles, within the constraints of current technology. Some examples may include, RoboBee(Breuer, 2019; R. Wood et al., 2013): Developed by researchers at Harvard University, this MAV utilizes a flapping-wing mechanism to mimic the flight of bees, with similarities to mosquito flight due to the small size and flapping-wing nature of both insects. DelFly(de Croon et al., 2009; De Croon et al., 2012): Created by Delft University of Technology in the Netherlands, the DelFly robots feature flapping wings and have gone through several iterations that exhibit impressive maneuverability and hovering capabilities. Nano Hummingbird:(M. Keennon et al., 2012a, 2012b, 2012c) Designed by AeroVironment, this MAV replicates the flapping-wing motion of a hummingbird, which shares certain characteristics with mosquitoes, such as hovering and lift generation through rapidly flapping wings. BionicOpter(Dragonfly, 2013; FESTO, 2013): This robotic dragonfly made by Festo can hover, fly in all directions, and even glide, using wing-flapping mechanisms similar to those found in flying insects like mosquitoes. While MAVs may not yet fully simulate the high flapping frequency or the precise deviation angles of mosquito wings, they incorporate aspects of their flight mechanics to address specific functions such as hovering, agility, and efficiency. As technology progresses, it is likely that these characteristics will be increasingly emulated in MAV designs to improve their performance.

Insects like mosquitoes use deviation motion, a motion component perpendicular to the main flapping plane, to adjust their wing kinematics for better lift and thrust. Engineers mimic this by designing MAV wings with hinges or flexure points that allow the wings to deviate from the primary flapping plane, improving lift and control. Although achieving the high flapping frequencies of mosquitoes (up to 800 Hz) is difficult with current technology, researchers work on optimizing the flapping rate within achievable limits to balance energy consumption with the aerodynamic requirements for stable hover and maneuverability. Mosquitoes have limited energy reserves, which in turn restricts their flight range. They need to feed frequently to maintain their energy levels. Due to their small size, mosquitoes are highly susceptible to environmental factors such as wind and rain, which can greatly affect their flight. Mosquitoes cannot carry additional weight beyond what their biology allows for, which limits any potential utility beyond their natural role. Understanding these limitations is important for researchers attempting to mimic mosquito flight in robotic systems, as they highlight the trade-offs between agility, energy consumption, and environmental resilience that must be managed in engineered systems(Ahmad et al., 2000; L. G. Liu et al., 2020; Miller, 2017; J. D. Zhang & Huang, 2019).

2.3 Classification of Flapping Actuation Mechanism Designs

Insect movements depend on the synchronization of their flapping wings while in flight. Therefore, enabling the insect to move sideways is not an easy maneuver. The wings of fliers are generally linked to their dual muscles, one to enhance their strength and the other to control them (Deora et al., 2015). During flight, these muscle parts deform the thorax by indirectly moving the wings via a complex hinge consisting of both compliant and rigid parts (Dickinson & Tu, 1997). In general, some insects move their flight muscles explicitly, others implicitly. In insects with explicit flight, the wing muscles are attached to the wing base, so that a little downward progress of the wing base would lift the wing upwards. Flapping of the wing can be achieved by employing this potential energy, which can reduce the inertial effect (Nagai & Isogai, 2011). Without elasticity in the wing, flapping wings will not be effective when compared to rotating propellers (Hawkes & Lentink, 2016). The impressive flight techniques associated with insects and birds, have inspired several researchers towards biological flying systems to evolve workable and efficient man-made flying mechanisms. The mechanism of flight has progressed from a fixed to a rotary, then to a flapping wing and an oscillating wing that mimics small flying creatures like birds and insects (Gursul, 2007). Based on parameters, such as size, mass, and volume, the small-sized Unmanned Aerial Vehicles (UAVs) are usually classified into four subgroups, namely, Micro Aerial Vehicles (MAV), Nano Aerial Vehicles (NAV), Pico Aerial Vehicles (PAV)(R. J. Wood et al., 2017) and Smart Dust (SD) (M. Hassanalian & Abdelkefi, 2017). All these vehicles are known as "extremely small and ultra-light air vehicle systems" (Petricca et al., 2011).

Researchers surveyed the Scopus database from 2000 to 2021, using search keywords based on size (such as flapping wing micro, nano, and pico aerial vehicles) and driving mechanism (such as motor-driven flapping wing, hybrid flapping-wing aerial vehicle, and linear actuated flapping wing). This can be seen in Figures 1 and 2 respectively.

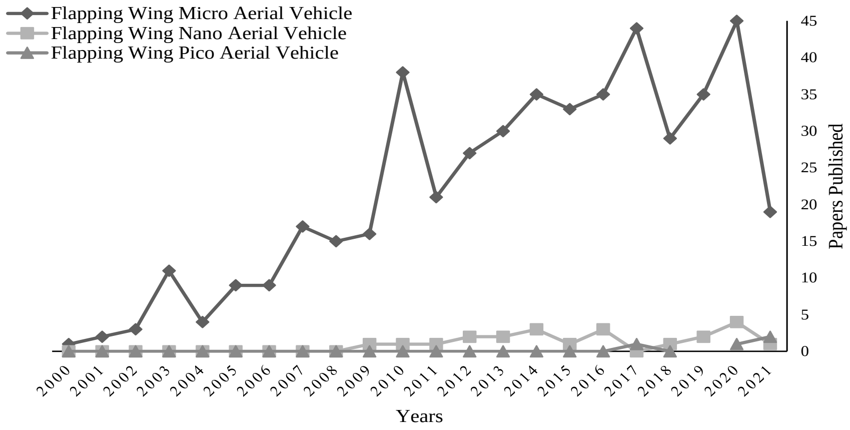

Figure 2.1 : Trend of Papers Published from 2000 to 2021 a Scopus Data Survey on Flapping Wing Micro, Nano & Pico Aerial Vehicles
(S. Singh, Zuber, et al., 2022a)

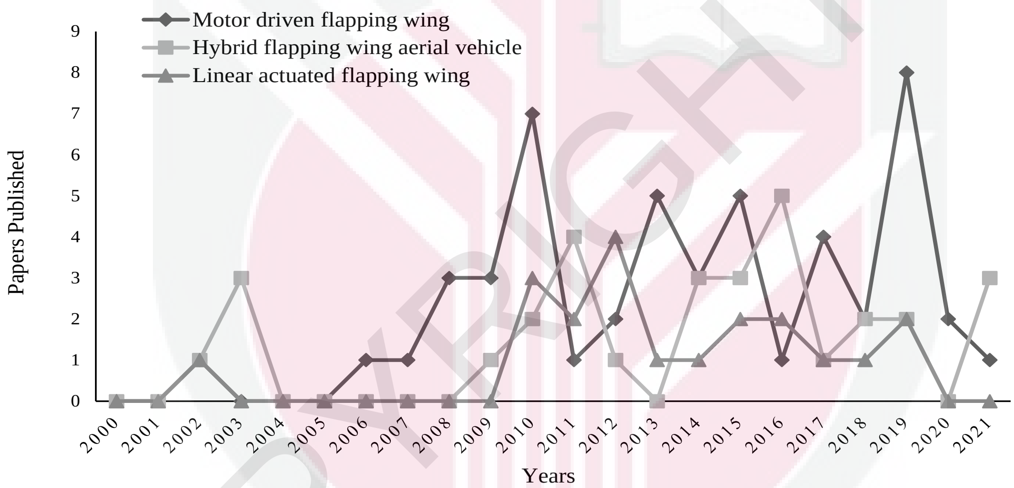

Figure 2.2 : Trend of Papers Published from 2000 to 2021: a Scopus Data Survey on Driven Mechanisms Utilized in Flapping-Wing Aerial Vehicles (Motor, Hybrid & Linear Actuated) (S. Singh, Zuber, et al., 2022b)

a. **b.**

Figure 2.3 : a. Percentage of Micro, Nano & Pico Aerial Vehicles and b. Percentage of Fully Flyable Model and Flapping Test Bench Models from Available Data in Appendix 1

It can be observed from Figure 2.1 that a large volume of research has been performed by researchers in the field of Micro Aerial Vehicles (i.e 94.83%) when compared to the Nano (4.37%) and Pico (0.79%) Aerial Vehicles. Figure 2.2 depicts how FWAVs have captivated the interest of academic researchers in designing and testing various types of actuation mechanisms over the last two decades. As per the graph collected data, the average research on overall flapping-wing drones carried out by several academicians is of the order 49.50% on motor actuation mechanism, 30.69% on hybrid actuation mechanism, and 19.80% on linear actuation mechanism during the past 21 years. This paper has evaluated all classification based on size scales (the percentage of micro, nano, and pico aerial vehicles from Appendix-1 is represented in Figure 2.3(a), and most types of flapping driven mechanism for free flight capabilities, such as fully flyable models and flapping test bench models in Appendix-1. Figure 2.3(b) shows the percentage of fully flyable models and flapping test bench models available from our published list.

For MAV, the overall wingspan is 1 m, and the weight is less than 2 kilograms. For NAV, the maximum wingspan is ≈15 cm, and the weight is below ≈50 grams. For PAV, the overall wingspan is ≈2.5 cm, the weight is nearly under ≈3 grams. Smart dust (SD) consists of several small micro-electromechanical systems (MEMS) and sensors inside it, the size for SD is ≈0.25 cm and the weight is ≈0.5 grams. Explicitly, MAVs are operated by propellers that are flying wings, in which all avionics, stored resources, and propulsion in the wing environment are reduced. Rotary-wing implementations have yielded better performance compared to fixed wings, owing to their capability of flying slowly with even drift. Flapping-wings have the benefits of greater maneuverability, less noise, and improved concealment- compared to fixed and rotating wing drones. Thus, the main module for achieving the ideal bionic quality of an aerial vehicle is surely the flapping-wing drone (“Fixed and Flapping Wing Aerodynamics for Micro Air Vehicle Applications,” 2001; Ho et al., 2003; Z. Liu & Moschetta, 2009; Sachs, 2016).

While developing any flapping-wing drone, there are numerous design options for the flapping actuation mechanism. In this paper, authors have classified flapping actuation mechanisms by referring to the papers of the past two decades, as shown in Figure 2.4. It contains detailed information on all the actuation mechanisms used by many researchers on MAVs, NAVs, and PAVs. This classification also aids in the selection of a better and more efficient flapping mechanism for the design of lightweight flapping-wing aerial vehicles. The first classification of flapping actuation is based on driving techniques, which are divided into two categories: rotary/motor-driven flapping and linear driven flapping. DC electrical motors have been the most used rotary actuators in flapping-wing drones (Anderson et al., 2011; A. Conn et al., 2006; A. T. Conn et al., 2007; de Croon et al., 2009; Q. Nguyen et al., 2014).

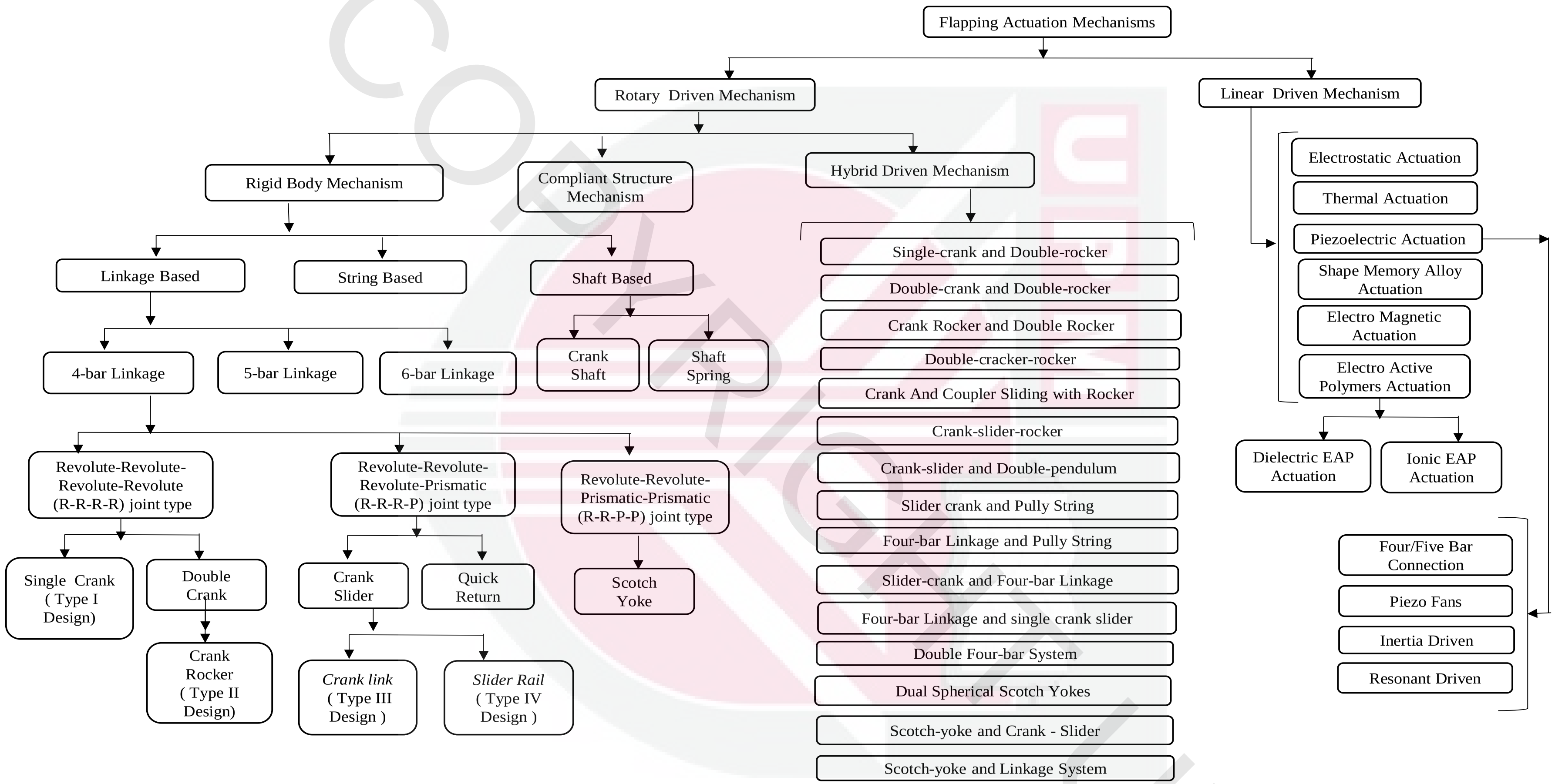

Figure 2.4 : Classification of Types of Flapping Actuation Mechanisms Utilized in Flapping-Wing Drones
(S. Singh, Zuber, et al., 2022a)

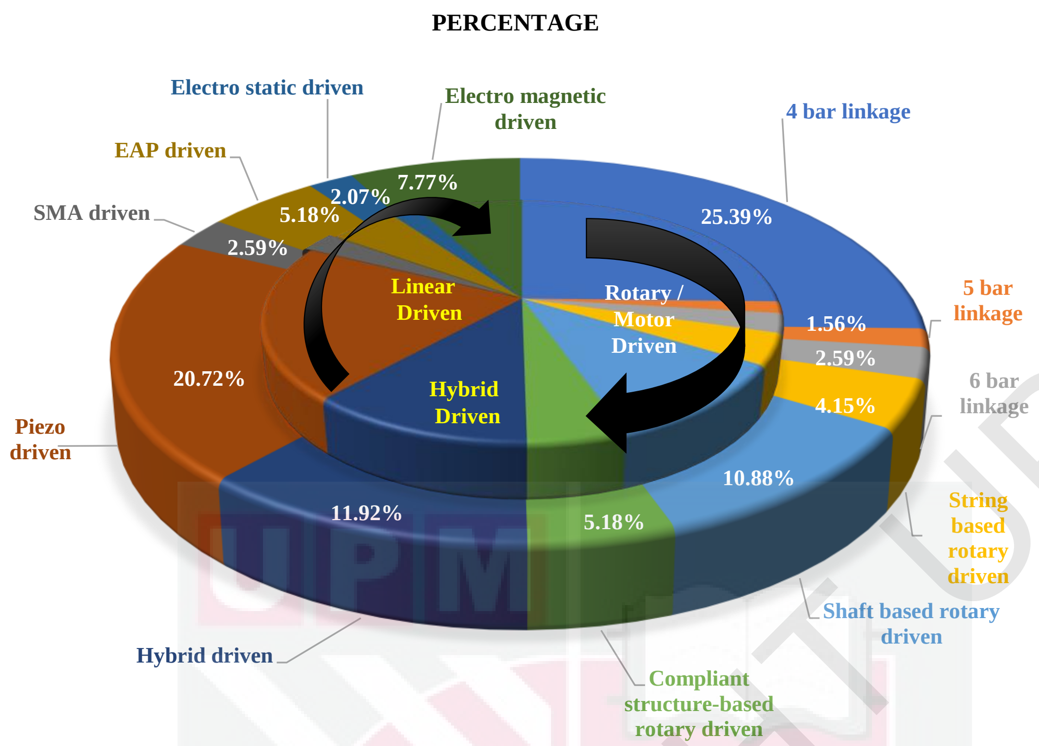

Figure 2.5 : Percentage of Flapping Actuation Mechanisms Utilized in Overall FW Drones (S. Singh, Zuber, et al., 2022a)

To develop hybrid-driven flapping techniques, double linkage mechanisms were considered to achieve high sweep amplitudes with some unique combinations of any two different or same rotary driven mechanism designs. This means that the design combination of any two rotary actuated mechanisms used in MAV, such as the four-bar linkage and pulley string mechanism, single-crank and double-rocker mechanism is considered to be a hybrid mechanism (Z. Khan et al., 2009; Q. V. Nguyen et al., 2016; Phan, Au, et al., 2016; Phan, Kang, et al., 2017; C. Wang et al., 2010). Figure 2.4 depicts classification details for these flapping actuation mechanisms. Figure 2.5 represents the overall percentage of (from Appendix-1) every mechanism used in flapping actuation of fully flyable and flapping test bench models of flapping-wing drones, with rotary, hybrid, and linear-driven mechanisms.

Flapping-wing drones forms such as biomimetic (like birds, small birds, nano hummingbirds, insects, bats) and biomorphic types have been identified under rotary, hybrid, and linear actuated flapping-wing drone based on their imitable similarity.

2.3.1 Rotary/Motor-Driven Flapping Mechanism

Obtaining the required resonance in FWs was the most essential aspect to boost the power capacity, generation of lifts, and efficiency in flight control. Rotary driven mechanism necessitates the use of a motor as a driver and translation of this rotary action to linear motion to get the flapping movement is challenging. Generally, standard rotary to linear mechanical actuators like Ball screws, chain drives, rack & pinion, and scotch yokes systems transform rotary movement to linear movement with various methods (Hussain, 2019). Under the first method (rigid body mechanism with geared motors), various transmission mechanisms are used to mimic insect flaps, some of which are based on the type of connections used, such as Linkage based mechanism, String-based mechanism, and Crank shaft mechanism, are discussed in further sections (Gaissert et al., 2014; Gong et al., 2018; M. Keennon et al., 2012a; Ristroph & Childress, 2014). Following are the linkage-based mechanisms utilized so far for flapping actuation. A mechanical contact, which is a body assembly linked to the control of force and motion, is called a linkage (McCarthy & Soh, 2011). The motion of the body or attachment is geometrically studied so that the connection is assumed to be rigid (Moubarak & Ben-Tzvi, 2013). A linkage developed as more of a network with a combination of stiff links and joints referred to as kinematic chains. In this kinematic chain, if any link or connection is fixed or set, it is a mechanism. In flapping-wing drones, the linkages are the transmission systems of movement with support. There are a lot of mechanisms with minimal linkages of 2-bar and 3-bar connections with some gear attached. However, the types of linkage mechanisms that are commonly used in flapping-wing drones are as follows: 4-bar linkage mechanisms, 5-bar linkage mechanism, and 6-bar linkage mechanisms are all examples of linkage mechanisms (Baek et al., 2009; M. Hassanalian & Abdelkefi, 2019a; Sahai et al., 2013; Yokoyama et al., 2008).

2.3.1.1 Four-Bar Linkage Mechanism

The best linkage is indeed a lever, a mechanism that rotates around a fulcrum connected to a fixed point. By considering two levers which are attached via rod such that, if force is introduced at one part, it will get transmitted to the other part called planar 4-bar link system (Lindholm & Cobb, 2014) with 4 revolute joints in it (i.e. Revolute-Revolute-Revolute- Revolute joint system). The levers are known as cranks, and the fulcrums are known as pivots. There are also 4-bar spherical and spatial connections that are used in practice (Hartenburg et al., 1965; Jang & Yang, 2018; Oppenheimer et al., 2017; Y. Peng et al., 2017). The Following are the mechanisms depending on the combination of Revolute (R) or Prismatic (P) joints which have been the most common 4-bar linkage changes available for the flapping-wing arena. The combination possibilities are R-R-R-R, R-R-R-P, and R-R-P-P as shown in Figure 2.4. Which is a combination of any 4 joint mechanisms, but there is only one degree of freedom according to Gruebler’s Equation, these types of linkages require only a single input to make any movement. Also, it involves:

single – crank, double – crank or Crank-rocker mechanism (de Wagter et al., 2018; T. Jiang et al., 2019; Karasek et al., 2018), Crank-slider mechanism (G. K. Lau, Chin, et al., 2014; Y. Peng et al., 2017; Takahashi et al., 2018), and Scotch-yoke mechanism (Galiński & Zbikowski, 2005),(Zbikowski et al., 2005) with advantages and drawbacks listed in Table1 by referring to Hassanalian (M. Hassanalian & Abdelkefi, 2019a). By referring to Yang et al (L. J. Yang et al., 2007) and Pornsin-Sirirak et al (Pornsin-Sirirak, Tai, Nassef, et al., 2001), they have considered the Golden snitch MAV mechanism here as a common reference design among 4-bar flapping actuation system research papers. Golden snitch uses the 4-bar mechanism design for flapping actuation where Gear 1 influences the flapping angle and phase lag at the wings. Recently, the author Analooee (Analooee & Ghayour, 2020) developed a flapping actuation mechanism for a small MAV, a conrod with a connector is utilized in the actuation mechanism design, where upward and downward guide rods are attached at its connector part. As Isbitirici designed the prototype for four wings MAV, four sets of connections with four motors are been utilized. PD and PID controllers are incorporated to obtain linear movement from the motor rotation and to establish closed-loop control. In 2007, Yang et al has designed two different flapping-wing drones using a 4-bar link with PVDF wing A and wing B (L. J. Yang et al., 2007). Controlling multiple stroke angles, flap symmetries, and reducing phase lag has been accomplished by modifying the dimensions of the linkages.

Table 2.1 : List of Advantages and Drawbacks of the 4-Bar Flapping Actuation Mechanisms

Actuation mechanism	Advantages	Disadvantages
Single crank	Simple and light	Wing motion not fully balanced
Double crank	Symmetrical movement	Heavy mass and volume, out of phase
Crank rocker	Planar flapping movement	Constantly changing transmission angle
Slider crank	Symmetrical flapping motion, simple design & easy implementation	Has big friction and low efficiency
Scotch yoke	Varying flapping motion	Complex in design and energy losses due to friction.

Till now, several works have added flexible components for their improvement of the 4-bar linkage system, but only a few have given constrained achievements (Baek et al., 2009). The Microbat (Pornsin-Sirirak, Tai, Ho, et al., 2001) Project, and Pornsin-Siriak et al (Pornsin-Sirirak, Tai, Nassef, et al., 2001) modelled the 4-bar (dual-pushrod) system of four separate transmission mechanisms with MEMS technology. Also used different wing combinations (beetle, bat, dragonfly, butterfly, etc.) driven by a compact 30 Hz DC motor. But two different kinds of energy sources are utilized and could obtain better efficiency with supercapacitor/cell/battery separately. Topology optimization (CHEN et al., 2020) has been applied to the small 3D printed 4-bar flapping-wing drones (Z. Chen et al., 2019) system by Chen et al, Based on various load situations. The increase in weight reduction (Z. Chen et al., 2018), ability to avoid bending, and displacement restriction based on stiffness has also been analyzed. The least-square method has been used to obtain the best optimum solution for more than four specified positions(J. S. Zhao et al., 2014). A spatial 4-bar connection with a single actuator system (Jang & Yang, 2018) is used to actuate flapping and rotating together in a dragonfly-inspired MAV. The wing root control mechanism to control the average angle of attack in the progressive rotary system and make comfortable hovering capability, could change flight mode without affecting its posture. De Croon et al came with 2 versions of Delfly in 2009 (de Croon et al., 2009), The crank mechanism of DelFly-I provided specific rods with certain moves on one axis, but the phase coordination was not equal with the wing pairs. The DelFly II is fitted with a unique drive mechanism with the axle of the motor gears which has shown strong symmetrical motion without any fuselage rocking behavior but perpendicular to flight direction (De Croon et al., 2012), (Tay et al., 2015). In 2007, Zdunich et al (Zdunich et al., 2007) tested the insect-inspired flapping-wing 4-bar mechanism based only on living hinges with electroactive polymer artificial muscles (EPAM), especially for silicones and acrylics. The mechanism could generate about 40 degrees of flapping movement at 9 Hz frequency with an actuator of 9 silicone layers. Tested with 2 prototypes SF-2.5 (IC-powered Mentor) and SF-3 (electric-powered Mentor) with 4-bar flexible linkages. For the 4-bar linkage (Perseghetti et al., 2014), and enhanced process was intended to improve the lightness of the prototype vehicle and its wing design to maintain longer flight times. Crank rocker (Y. Zhang, Wang, et al., 2020) and scotch yoke (K. C. Moses et al., 2018) related advantages and disadvantages are summarized by us with the study of concepts and are listed in Table A1 and Table A2 of Appendix 1. But the double rocker, quick return, and scotch yoke mechanisms are alone not sufficient to be used in MAV for flapping actuation. Hence, it has been used in conjunction with a variety of linkages and mechanisms, including the single-crank and double-rocker mechanism, the double-crank and double-rocker mechanism, the scotch-yoke and linkage mechanism, and so on. These mechanisms are considered as hybrid mechanisms in flapping-wing drones, elaborated briefly further under the hybrid mechanisms section. The detailed parameters of most of all 4- bar linkage flapping actuation mechanisms with specifications are listed in Table 2.1.

A. Crank-Rocker Mechanism: Usually, a basic 4-bar crank rocker is typically employed in any ornithopter-type flapping-wing vehicle to turn an electric motor's rotational movement into a balanced flapping movement (Pourtakdoust & Aliabadi, 2012). By utilizing the modal analysis method and state feedback controller, the longitudinal stability of the hovering flapping-wing drones has been analyzed in 2019, by Jiang et al (T. Jiang et al., 2019) for possible disturbances. But the wings are driven by coreless and brushless DC motors having crank rocker mechanisms in them. They have demonstrated the longitudinal dynamics of the tailed FMAV using the Newton-Euler equation. Crank rocker mechanisms similar to those used by Hong et al (Hong & Altman, 2008) were adapted from a Cybird-P1® remote control ornithopter model (Han et al., 2009), (Hu et al., 2010).. A 4-bar crank rocker compliant mechanism with rubber material has been designed by Sahai (Sahai et al., 2012) with the flexibility of interchangeable parts. The spatial crank-rock (Zhou et al., 2019) mechanism is a unique structure with symmetrical movements, during the flapping process of its wings. In any case, this mechanism is not appropriate for miniaturized MAVs since it has four or more space rockers (Zhou et al., 2019). A crank rocker-arm linkage with a nondimensional survey of a non-linear motor-as actuator (Baek et al., 2009) coupled with a mass-spring structure as a method for producing flapping through motor-drive. Here they proved a relation between the resonant frequency of the compliant system and optimal voltage for motor input, to achieve lower energy consumption. Additionally, they have tested and demonstrated the rigid-body mechanisms associated with Baek's compliant and Vamp RC rigid-body mechanisms. Compliant mechanism/ procedures were discussed well in greater detail further below.

B. Slider-crank Mechanism: is a type of 4-bar planar mechanism that essentially works as shown in Figures 2.5 and 2.3, by combining revolute and a prismatic joint, where the rigid-body attribute has a pair of wing levers. According to Yi et al (Yi et al., 2018), the slider-crank mechanism is considered in two ways, i.e the crank-link and slide-rail type. The close end of both wing levers is like a rotating guide that serves as a wing base across a pivot, separated by the next pivot and connected with a pin that is guided upright. The pin is intertwined with a motorized crank sliding structure, and each base of the wing is directed to angular fluctuation around its center. Both compliant body mechanisms with flexibility and a rigid body mechanism are being designed and tested with the slider-crank concept by Lau et al (G. K. Lau, Chin, et al., 2014). As per Yi et al (DONG et al., 2020; Yi et al., 2018) to reduce the horizontal vibrations, torque and maintain stability, it is better to opt for a slide rail mechanism. The design is based on the Dipteran insect’s flight thorax for the actuation mechanism driven by a DC motor. The flapping wing bat MAV has been developed and tested to improve the harmonic flapping motions, using an integrated Electronic Control System (ECS) with a slider-crank4-bar mechanism (Yusoff et al., 2013). The flapper is actuated via a single DC mini motor with serial number 1224A015-SR, and a speed of 901 rpm. The major issues related to its performance regulations, like continuous calibration, duration of time, and speed calculation inaccuracy, are remedied by the suggested ECS. An effort has been made to create an efficient flapping mechanism for a dragonfly, through 'Modified Slider Crank' (MSC), actuated by a motor (Fenelon & Furukawa, 2010), (bin Abas et al., 2016). In 2013, Ryan et al. worked on the mechanism with rigid body mechanics, which consists of two sliding motor-driven cranks (Ryan et al., 2013).

The concept proposed by a slider crank (Roshanbin et al., 2017) coupled to a 4-bar wing twist configuration apparatus significantly affects the average lift vector for the center of gravity by airflow rearrangement. Jang and Yang has proposed a dragonfly-inspired hierarchical 4-bar planar slider crank (Jang & Yang, 2018) MAV design. To achieve various design positions, a matrix transformation was used to establish the relationship between variables, and the kinematics of it was studied with the analysis of vectors. The wing root control system controls the average attack angle in the progressive rotational process. To minimize the negative elevation produced in wing upstroke movement, a boring-hole (Long et al., 2015) technique was adopted to the slider-crank flapping wing mechanism. Analysis, comparison, and examination of the conventional and boring-hole technique for the flapping-wing structure were carried out successfully. In 2015, Nguyen et al (Q.-V. Nguyen et al., 2015) designed a crank slider mechanism with some linkage system, that has been driving all four wings sequentially and reaping the benefits of double clap-and-fling impact in one flapping period. Finally, a better stable mechanism could be produced with the 2-stage reduction gearbox of gear ratio 1 - 20 comprising M0.3 of 9-teeth pinion, spur gear, and a brushless motor. Recently in 2020, Chen et al (S. Chen et al., 2020) used the modified version of the crank slider design for flapping wing rotor (FWR) mechanism where flapping and rotation both are included in the mechanism. The flapping frequency is very less because of the limited motor rotation speed, but it could generate lift 43% of its weight. Recently, Sochacki et al (Sochacki & Cekus, 2020) has designed an ento-mopter having the basic concept of 4-bar slider rail type with little modifications like - slotted link with a bilateral slider connection for actuating both wing-rocking lever system and wing-angle rotation system simultaneously. The detailed specifications of the 4–bar linkage flapping actuation mechanisms are listed in Table 2.1**.**

2.3.1.2 Five-Bar Linkage Mechanism

It utilizes 4-bar actuation mechanisms with an added linkage as per the design or Flapping wing model requirements. The whole mechanism of the modified 5-bar [107, 108] is equipped with aluminum in pairs with steel ball roller covers, incorporated at hinge points, that are different from one another for better advantage. This research culminated in safe flight tests through the onboard custom-designed kinematic Autopilot in combination with a closed-loop PD controller (D. Coleman et al., 2017). The process of “modified 5-bar” here enhances the standard 4-bar mechanical output of crank-rocker structure as shown in Type I design with a single gear connected to the linkages. In

2017, Coleman et al (D. Coleman et al., 2015) has focused on weight management, stability, and timeframe of flight. Simulation-based optimization model of the hinge for the development of 5-bar multi-material flapping mechanisms (Bejgerowski et al., 2010) in MAV. The MAV was worthy of reproducible flights with a payload of 31 grams that is 75 % entire MAV mass emptied (Bejgerowski et al., 2011). In conjunction with the supplementary 4-bar mechanism, the system has one degree of freedom and utilizes a 5-bar mechanism. To enhance the function parameters, a hawk moth was used with similar to Type I design of single gear mechanism (Banala & Agrawal, 2005). Manduca sexta forewings (K. C. Moses et al., 2017) is an artificial flapping-wing drones that has been built with a 5-bar, structurally diverse crank-rocker system. Experimentation for bending rigidity and lift output is assessed well to measure performance variations. In Table A2, the detailed list of most 5-bar flapping actuating mechanisms with specifications is mentioned.

2.3.1.3 Six-Bar Linkage Mechanism

Generally, it uses 4-bar actuation mechanisms with two added linkages as per the design or flapping-wing model requirements. In the Single-crank double-rocker mechanism (T. Zhang, Zhou, Zhang, et al., 2011) set of two side by side designs, one for each wing. In Stephenson 6-bar (L. J. Yang et al., 2015) the inverted design has been used with two more linkages. For the implementation of “Thunder I” flapping-wing drones (M. Hassanalian & Abdelkefi, 2016) an interior transmission system was built using 14 components that internally provide two 6-bar efficient systems. The 6-bar actuation (M. Hassanalian & Abdelkefi, 2019a) process used here resulted in large symmetrical fluttering movement with mounted connections for all elements. In 2018, Wang et al established a sequential serial chain constructed by three rotating joints denoted as R-R-R chains, which are constrained by the insertion of two (spherical joints) of SS dyads. The resulting one DOF spatial connection of the R-R-R-2-S-S could achieve a swing and flap mechanism that ensures seven precision points over the given reference paths (P. L. Wang et al., 2018). The fusion of a spatial (R-S-S-R) 4-bar link with another 4-bar linkage that reflects a 6-bar linkage has been used in the flapping-wing drone. The swing or pitch motion of wings is actuated by an actuator that drives the combined system. The obtained result was 29 prototypes that accomplished the optimum synchronization of wing swing and pitch (P. L. Wang & McCarthy, 2018). Pairs of 6-bar linkages have been established by Jeon et al (Jeon et al., 2017) for small-sized MAV wing flapping by an analysis of the unsteady blade element theory. For better performance, the tension between the links could be decreased. To resolve the phase lag of lift force issue and to improve the flapping amplitude, yang et al (L. J. Yang et al., 2015) in 2015, has combined both 4- Bar Linkage with Watt mechanism and identified it as the type of Stephenson six-link mechanism. single-crank double-rocker (T. Zhang, Zhou, Zhang, et al., 2011) and double-crank double-rocker (T. Zhang, Zhou, Wang, et al., 2011) mechanisms contribute their virtues in a simple arrangement with a six-link seven-joint mechanism and seven links with nine joints, with a gear-driven input respectively. However, the freeness of swing near the wing root was limited, so the model was tested only for "twist-flapping" motion. The list of 6-bar flapping actuators with specifications is shown in Table A3 below.

2.3.1.4 String-Based Mechanism

It goes with the pulley system very well. A mechanism with a string and pulley combination would be a better choice for amplification of the flapping actuation and smooth transferring of the displacement into the wings. In 2019, Gong et al (Gong et al., 2019) have developed a flapping-wing drones with the string and pulley combination. In 2018, a DC motor actuated string-based mechanism was used in flapping-wing drones to get better identical left-right movement and less speed of the wing tip than the linkage-based mechanism (Gong et al., 2018). It is also used to lower the movable linkages as much as possible and to increase fluttering performance with long service life to the system (M. Keennon et al., 2012c). Nano hummingbird with pulley-string mechanisms produces flapping motions that are more advanced than any other flapping-wing drones exhibiting remarkable flight performance (M. Keennon et al., 2012b). This means that it always needs FW for guided flight it imitates insect flight instead of just hummingbird (M. Keennon et al., 2012a). Table A4 below provides the list of string-based rotor-driven mechanisms with specifications.

2.3.1.5 Shaft-Based Mechanism

The 175 g dragonfly model has four wings, powered by a crankshaft (Gaissert et al., 2014) transmission brushless motor for each wing. The drives, onboard circuitry, and networking systems are powered by two 7.4 V LiPo batteries. To transform the motor-driven revolving action in the wing, the crank shaft mechanism is used in dragonflies (Gaissert et al., 2014). The curious feature of the crankshaft is how it ends the motor box in a straight line with the proximity of the crankshaft. But for the motion of the crankshaft which pulls out and releases both the strings which produce required movements at left and right pulleys connected with wings. Two more extra strings were attached at both pulleys to maintain phase matching of wings motion (M. Keennon et al., 2012a). For the crankshaft-based mechanism, a prototype model of the Chen's et al (L. Chen et al., 2018) design is considered. For a crank shaft mechanism (L. Chen et al., 2018) of complete rotary wing-flapping model to upgrade its aerodynamic performance.

The resulting vortex decreases the negative lifting magnitude substantially, thus explaining the change in the mean lifting period. In 2018, Guo with a similar crank shaft mechanism and little modifications like elastic plates and a U-frame via ball joints at bearings, the new Flapping-Wing Rotor (FWR) (Guo et al., 2018) model could efficiently demonstrate vertical takeoff without external control. Since the movement is only vertical, the Angle of Attack (AoA) of the flapping cycle differs passively hence elastic plate is required. Table A5 includes a list of flapping-wing drones features of varieties of a rotary-driven crank shaft mechanism.

2.3.1.6 Compliant Structures for Rotary Actuated Flapping Mechanism

There are three types of compliant mechanisms available, including short compliant segments, long compliant segments, and flexural joints. In 2014, to mimic the Dipteran insect flight, Lau (G. K. Lau, Chin, et al., 2014) came up with a compliant flapping mechanism, which could generate more than 25 Hz frequency. They also tried with a rigid body mechanism to obtain better frequency and flapping angle, the compliant mechanism parts (like hinges, pleural plates and process) are replaced by wing liver, and rigid slider with fulcrum. Generally, flapping wing drones with compliant mechanisms (Stanford & Beran, 2012) are driven by a motor are accompanied by a rotating spring (Baek et al., 2009) or polyimide film hinges (G. K. Lau, Chin, et al., 2014) or rubber strips (Sahai et al., 2013) to enhance the flapping more smoothly. An innovative way for bending is by using a ring-type framework (Peters et al., 2016) that consists of inbuilt modes of oscillations without any supporting framework (Bolsman et al., 2009b). These combinations of compliant thoracic systems will save energy consumption to a minimum of 30 %, as compared with the rigid-body flapper with the elasticity storage capacity. The injection-molded compliant drive structures of the 4-bar linkage flapping device were constructed with minimal mold components and sacrificial shape elements. Using an integrated shape synthesis approach, they were able to create a design that adhered to functionality and mold capability constraints (Bejgerowski et al., 2009). Chin et al (Y.-W. Chin & Lau, 2013) came up with a new word for flapping actuation in 2013 named 'Clicking process.' The plate center is driven by a DC gear motor to get physically displaced from one end to another by bending Tergum which is fully controlled by a clicking mechanism.

In 2014, Hines et al (Hines et al., 2014) applied an elastic element, helical spring directly driven by the Solarbotics GM15 motor concept to obtain a novel minimalist flapping-wing drone and could obtain 10 Hz flapping frequency. The importance of wing compliance in improving flapping-wing drone performance cannot be overstated. Increased compliance reduces wing stability and limits the force that affects the wing's capacity to sustain itself during flight. Insufficient compliance of the wing affects camber adaptability, which results in insufficient thrust. As a result, careful consideration must be given to wing compliance (Mueller et al., 2010). The list of characteristics of varieties of compliant flapping structures is given in Table A6. From the above revision of the overall rotary actuated flapping mechanism, the following are the advantages and disadvantages of the best mechanisms summarized accordingly as shown in Table 2.3.

2.3.2 Hybrid Driven Flapping Mechanism

Following possibilities of dual-lever mechanisms were considered to achieve high sweep amplitudes with some two combinations of mechanisms under rotary driven mechanisms. Like any linkage and string combination or any two combinations of rotary mechanism to obtain a hybrid technique. Few such combinations are considered here under the hybrid mechanism by referring to Figure 2.4 classification as listed. 4-bar linkage and pulley string mechanism (Phan, Au, et al., 2016; Phan, Kang, et al., 2017; Phan, Truong, et al., 2016) single-crank and double-rocker mechanism (C. Wang et al., 2010), crank-slider and double-pendulum mechanism (Zhou et al., 2019), double-crank and double-rocker mechanism (Zhou et al., 2019), slide-crank and 4-bar linkage mechanism (Yusoff et al., 2013), (Roshanbin et al., 2017), (Karásek et al., 2014) crank-slider-rocker mechanism (Q. V. Nguyen & Chan, 2019), dual spherical scotch yokes mechanism (Galiński & Zbikowski, 2005), scotch-yoke mechanism and linkage system (Q. V. Nguyen, Park, et al., 2010) and double 4-bar mechanism (P. L. Wang & McCarthy, 2018), (Steltz et al., 2007) , crank and coupler sliding with rocker (Q. Liu et al., 2019), double-cracker-rocker (Y. W. Chin et al., 2020) , scotch-yoke and crank – slider (Vu Phan et al., 2015), crank rocker and double rocker (X. Zhang et al., 2019).

In a hybrid mechanism, are combined with at least two or more of the previously discussed design mechanisms. The two planar 4-bar linkages mimicking insect's thorax (Q. V. Nguyen et al., 2016) are considered as a reference design. The double-cracker-rocker (Y. W. Chin et al., 2020) design has also followed a similar design, but with little modifications for linkage and gear size with a different way of alignment by supporting structures. A flapping system with a specific combination of a design 4-bar link and a pulley-string mechanism (Phan, Au, et al., 2016) has been designed (Phan et al., 2015),(Phan & Park, 2016) to obtain high flapping amplitudes to replicate the rhinoceros beetle's wing movement, with a clap and fling at either stroke reversal. Clap and fling played a major role in enhancing the vertical force of the flapping-wing drones. Unsteady blade element theory has been used for the flapping force measurements, the KUBeetle-S robot that can change its stroke plane with wing turn at the same time and modulate wing root spars unevenly with the stable flight conditions (Phan, Kang, et al., 2017). Estimated information demonstrated that perhaps the control mechanism could generate sufficient quantities of forces and moments for the regulation of attitudes (Phan, Truong, et al., 2016). Finally, KUBeetle-S effectively hovered and loitered for around 3 minutes with the involvement of the on-board attitude input feed for system regulation, showing the efficiency of the suggested control system (Phan et al., 2019a),(Phan, Truong, et al., 2017) The most stable and easy-to-assemble mechanical system is a single-crank and double-rocker mechanism that uses a wrench to drive two lightweight oscillatory wings. But this mechanism is weak in flight-reliable efficiency after optimizations (C. Wang et al., 2010).

Flapping structure colibri (Roshanbin et al., 2017) comprising of a slider-crank coupled to a 4-bar movement amplification system. connections with modified linkage and gear alignments. The adjustment of wing twist was obtained by triggering the root edge bars that control the wing camber and efficient pitch and roll stabilization. Both the crank-slider and double-pendulum mechanism stays symmetrical throughout the fluttering phase with the double-crank and double-rocker Mechanism, by providing a smooth forward flight. These two mechanisms have a moderately basic structure (Zhou et al., 2019). A double-cracker-rocker flapping-wing drones (Y. W. Chin et al., 2020) has three main functions (such as propulsion, lift, and drag) of the flapping mechanism, which allows powerful flight output by easy tail regulation. To explain hovering steadiness and neutral glide stability, they have utilized fin-like tail and neutral tail elevation with a thrust-based consistency. For Thorax-based (Z. A. Khan & Agrawal, 2011) flapping-wing drones' architecture, two concepts were specified, tested, and measured. Whereas concept one utilizes two 4-bar links that are moved by a corner from a standard crank to operate the rocker design. The second concept concerns an elastic (flapping spring) connector that activates the wing (Z. A. Khan & Agrawal, 2007). Zbikowski et al. have developed an insect-like flapping wing with dual spherical Scotch yokes mechanism for more insight into insect flapping wing motions (Galiński & Zbikowski, 2005). They have chosen a spherical Scotch yokes mechanism with rotational movements of transmission to avoid the limitations of the planar system mechanism. In 2014 Karasek et al came up with a hybrid mechanism with the benefits of using two phases that is independent phases of imbalances, which can be adjusted by a suitable selection of dimensions. Characteristics of hybrid-driven flapping-wing drone are listed in Table A7 in Appendix 1 and a few advantages and disadvantages of hybrid FWAV are discussed in Table 2.4.

2.3.3 Linear Driven Flapping Mechanism

To date, many investigations have been carried out on flapping-wing drones by various institutes because of their tremendous mobility, less expensiveness, less complexity of circuits, and easy programming. It is necessary to obtain a mechanical harmonic or flapping actuation mechanism at the wing for producing efficient lift. This can be accomplished by applying any of the following four modes under a linear driven mechanism. i.e. material stretching, contraction, torsion, or bending. The first two modes of deformation are omitted by implicated heavy mechanical loads. The downside of using torsion is the normal requirement of support systems. Bending is the storage mode of greatest attraction.

The focus is placed on linear actuation which enhances flapping movement with a simplified mechanical transmission system through suitable material excitation techniques. At cm to mm scales, because the actuator size is decreased, they require high power densities at its favorable scaling effect. A variety of material excitation techniques have been researched till now by many institutions to achieve linear actuation that produces intrinsic wing flap mechanisms. The key theme of this work is relatively mature technologies used in the field of micro flapping-wing drones. The material excitation techniques generally involve compliant structures that could be selected for the analysis and is divided into following categories: electrostatic (Kim et al., 1997), thermal (Prasanna & Spearing, 2007), piezoelectric (Q.-M. Wang & Cross, 1998), shape memory alloy (Tomozawa et al., 2009), dielectric elastomer/ electro active polymers (Cao et al., 2019; C. T. Nguyen & Choi, 2015; Pei et al., 2004) and electromagnetic actuators (McIvor & Chahl, 2020; Roll et al., 2013). To evaluate the performance of the material actuation analysis to deflection, stress, strain, and speed, simplified measurements been considered from Conn et al (A. T. Conn et al., 2007), Pelrine et al (Pelrine et al., 2017), Yousaf et al (Yousaf et al., 2020), Chao et al (Chao, 2016) and Karpelson et al (C. Chen et al., 2013), have attempted to represent actuation geometries as described below in Table 2.2 in this paper. The advantages and disadvantages of all rotary, linear and hybrid mechanisms are listed in table 2.3,2.4 and 2.5 respectively.

Table 2.2 : Material Actuation Analysis

Actuator	Deflection frequency	stress	strain	Elastic energy density (J/g)	Operating principle with speed	Important notes
Electrostatic	Low	Very low	High	0.0015	Electrostatic force, fast	Requires MEMS manufacturing process with high voltage
Thermal	Medium	-	-	0.15	Thermal expansion, slow	Versatile geometries, large material selection
Piezoelectric cantilever	High	High	Very low	0.013	Converse piezoelectric effect, fast	Simple planar structure, high operating voltage
Shape memory alloy	High	Very high	Medium	>15	Thermally induced change of phase, slow	Maximum energy density
Dielectric elastomer	Highest	High	Medium	3.4	Maxwell stress forming viscoelastic deformation, medium	Capable of 300% strain, increased voltage requirements
Electromagnetic	High	High	High	0.003	Electromagnetic force, very fast	Low voltage consumption and high-power density benefits

High operating frequency and power density of an electrostatic actuation in flapping generation imply a potential for robots on a micro gram size with lower power consumption used for stepping and ratcheting purposes (Hollar et al., 2003). Thermal and Shape Memory Alloys (SMA) are current-mode actuators that operate at high currents and low voltages. However, piezoelectric, electrostatic, and dielectric elastomers require higher voltages with a low current to operate, which are referred to as voltage-mode actuators (C. Chen et al., 2013). Attributable to pre-requisite size, speed, piezoelectric, Dielectric Elastomer Actuators (DEAs), electrostatics, and electromagnetic actuators are effective co-modeling choices in comparison to smaller-scale bionic flapping-wing drones (C. Chen & Zhang, 2019). According to Conn et al, (A. T. Conn et al., 2007) the insect muscle has a linear stroke, with a very high tensile capacity. However, this is an obvious concern because any MAV flapping system must be extremely compact. The mode coefficients and mass of the wing are important to be considered when the piezo electric actuation is used for the operation of an external flapping-wing (Ballas et al., 2006). The advantages and disadvantages of a few linear actuated flapping-wing drones are listed in Table 2.5.

2.3.3.1 Piezo Actuation/ Driven Mechanism

The piezoelectric material transforms the electrical input to a carefully controlled mechanical displacement. Piezoelectric actuators can be operated by a bipolar or a unipolar signal. (Karpelson et al., 2011). Piezoelectric actuation model has elaborated by Wang et al (Q.-M. Wang & Cross, 1998) in 1998, which comprises analytical abilities based on design variables and material properties, blocked strength, and an optimum operating frequency. The PZT-4 and PZT-5H formats are various PZT formulations that can be regarded as “hard” (Sitti et al., 2001)or “soft” (Sitti et al., 2001) piezo-electric materials. PZT-5H is used frequently in NAV applications(R. J. Wood et al., 2005). Also, it includes the system plan, design, and development of the unimorphic actuators (Cox et al., 1999). To enhance the displacement for any application, flex tensional and cantilever beam actuators are in use (Kommepalli et al., 2009). Flex tensional piezoelectric actuators like Moonie, cymbal, and recent uni flex usually opt for elastic elements to increase the displacement (Robbins et al., 1991). Piezoelectric materials have high conversion efficiency and sufficient deformation strength compared to mini electric motors for actuating the wing flapping mechanism (Lv et al., 2015; Sahai et al., 2006; R. J. Wood, 2007) . A unimorph piezoelectric actuator single-crystal PIN-PMN-PT legitimately drives the wing with no transmission system. With this mechanism, they accomplished a 1.45 mN lift force that is 1.9 occasions bigger than the total weight of the actuator (Ozaki & Hamaguchi, 2018b).

The Harvard Robobee (Chirarattananon et al., 2015; K. Y. Ma et al., 2013, 2015; Teoh et al., 2012), is a modified version of Mobee where square aerodynamic dampers are attached at its top and bottom side for its stable vertical takeoff. The system takes translational redirection at its contribution from the piezo actuator to give rakish avoidance at its yield, which causes fluttering. They utilized the spring-level model and topology improvement to get the structure of the component (Chattaraj et al., 2021). With the combination of Residual Current Devices (RCD) passive snubber flyback DC/DC step-up converter (Markose et al., 2014), bidirectional active half-bridge and the driver circuit have been structured by concurrent drive technique. Mobee's is an FWNAV, assembly scaffold is based on a Sarrus linkage (Sreetharan et al., 2012) with overall weight of 90mg. A Diode-Pumped Solid-State (DPSS) laser method is applied for micromachining and lamination operations of each part with a minimal size of nearly 10 μm. The damper-stabilized robobee has been designed with the inherent instability of the RoboBee, where they could be able to test free-flight without attaching vertical guide wires as shown in paper (Teoh et al., 2012). In 2019, (Jafferis et al.,

2019) To boost aerodynamic efficiency, the 90-milligram (Jafferis et al., 2019) vehicle having four wings propelled by two piezoelectric actuators reinforced with alumina has been built by Jafferis to attain a sustained untethered flight. Electro adhesives are created, characterized, and used for the demonstration of a robotic flying insect actuated by piezo materials, which can stick strongly over various materials such as glass, wood, and natural leaves (Graule et al., 2016). To give better and smooth enhancement for piezo oscillations, different connecting techniques like 4-bar and 5-bar connectivity through MEMS are experimented by several researchers are discussed in the next section.

2.3.3.2 Piezo Driven 4 and 5-Bar Flapping Mechanism

Linkage systems or bars are not only used in rotary actuation mechanisms, but they have also been used for piezo actuation systems. For giving better support and flapping enhancement for MAVs to PAV linkage mechanism, 4-bar or 5-bar connecting systems are been used for the transition motion in combination with piezo materials (Lindholm & Cobb, 2014). In the micromechanical flapping segment, the detailed analysis is carried out for the wing function based on a 4- bar compliant framework (Sitti, 2003). Cox et al. (Cox et al., 1999), have considered two different design mechanisms separately for both 4 and 5-bar linkage systems, that has involved in an electro-mechanical emulation of mesoscale flapping flight. However, the half-scaled small prototype could give better lift force and flapping frequency compared to the full-scale prototype. A Micromechanical Flying Insect (MFI) (R. J. Wood et al., 2008) structure with smart composite microstructures (SCM) process has been developed with 4-bar and slide crank concepts that could generate the highest wing beat frequency of 200 Hz. SCM is a resolution to MEMS vulnerabilities and macro-mechanical machining techniques constraints. In 2010, Fearing et al (Fearing & Wood, 2010) for the same MFI design, with the unique combination of SCM and piezo actuators, could obtain 275 Hz of frequency and ±35° of flapping angle. Fearing et al. have modeled a piezo actuated 4-bar design of micro-mechanical thorax of flapping insect. The flyback converter is constrained by pulse width modulation in irregular conduction mode to guarantee the strength of the output high voltage (Fearing et al., 2000; Gan & Xu, 2020; Kong & Su, 2019; Q. T. Truong et al., 2011). For achieving a linear actuation construction, a movable frame is used as an actuator, which makes contraction and expansion motion to produce reciprocating linear movement like a slider, for crank-slider mechanism without any gear system (Y. Peng et al., 2017). By considering the geometry of the links as a key factor in determining the optimal flapping frequency, a dummy mass is added at the center of 4-bar mechanism. In contrast to the original model, the revised approach resulted in a 70% rise in the frequency of flapping and an 8% reduction in the flap angle. To obtain linear motions along the guide path, the linear actuator consisting of a PZT with a permanent magnet acts according to the principle of the Impact-Drive Mechanism (IDM) (Higuchi et al., 1990; Y. X. Peng et al., 2011; Q.-T. Truong et al., 2009). The bending motion of the unimorphic LIPCA (lightweight piezo-composite actuator)(Syaifuddin et al., 2006) having a connection with a 4-bar linkage mechanism could generate a flapping motion with a frequency of approximately 9 Hz. Mobee having three main degrees of freedom (DoF) along with the withdrawal of three internal struts enables to work like a fully functioning micro-machine with the parallel production of 16 PC-MEMS spherical 5-bar linkages (Sreetharan et al., 2012). A spatial 5-bar (Topology: RSRRR) (Avadhanula et al., 2002) with two degrees of freedom that is a blend of a differential mechanism with a flat 4-bar mechanism, converting small piezo movement input into the MFI wing output as flapping.

2.3.3.3 Piezo Fans for Flapping Enhancement

Piezo fans (Toda & Osaka, 1979) were initially studied at the end of the 70s (Toda, 1981) to attain maximum amplification to get better movement (Wait et al., 2007). Piezo fans were prominent as portable electronic cooling fans (Kimber et al., 2009). Piezo electric fan works by pairing a piezoelectric unimorph with a connecting elastic blade, which can produce large deflections at its resonance. Two parallel coupling piezo fans are used to obtain two DOF actuation that is powered by sinusoidal voltages of varying period delays over them to understand the fluttering and twisting wing configuration gestures (H. C. Chung et al., 2008). With an angle of 16◦, the twisting motion was found to be peaked at 47.4 Hz frequency. Additionall changes are observed, during the phase delay with the increased twisting movements, and decreased angle of bending (H.-C. Chung et al., 2008). In 2008, the analysis of the efficiency of the dynamic piezo fan structure was carried out by Chung using a linear analytical model insisting that the Strouhal and a minimum number of parameters help to pick the best piezo fans for flapping-wing drones optimization (H. C. Chung et al., 2009). In 2012, Shijun introduces a revolutionary piezoelectric actuated flapping-wing rotor MAV supportive of Vertical Take-Off and Landing (VTOL) ability through hypothetical and practical solutions with better power supply. If a model is enhanced by incorporating the amplification system onto the FW rotary mechanism, the MAV will anticipate a substantial increase in a lift (Guo et al., 2012). The characteristic parameters of piezo actuated flapping-wing drones are listed in Table A8.

2.3.3.4 Inertia Driven Piezo Actuated Flapping

The piezo actuator has a very minor stroke of microscopic movement. As an amplification method, the concept of inertia drive was introduced by Zhang et al. The method is performed on the piezo actuator with a sequence of asymmetric waveform voltage as an input with a duty ratio greater than 50 percent. Bearing motions are regulated by inertia by imposing drastic voltage variations on piezo material (Y. Zhang, Peng, et al., 2020). The oscillation at the flapper is generally measured through a laser beam and oscilloscope.

2.3.3.5 Resonant Driven Piezo Flapping Actuation

Resonance is described as the process of driving a device with a level equivalent to its natural frequency. It is said that a device is powered with a periodic signal with a natural frequency. The development of rapid and high-frequency flapping movements with restricted size, weight, and power has become one of the main factors for flapping-wing drones. A unimorph piezo electric actuator drives the wing directly using an external power source but without any transmission mechanism (Ozaki & Hamaguchi, 2018a). The direct-driven mechanism is being used, which can produce a lifting power more prominent than their weight. Recently a resonant method has been used by Ozaki et al, on the piezo material to enhance the flapping motion at the wings (Ozaki & Hamaguchi, 2020) part. Also tested different combinations of wings driven by resonant actuation process on unimorph piezoelectric material by eliminating the coupling of a wing to body and wing to wing oscillations.

2.3.3.6 Shape Memory Alloy (SMA) Driven Mechanism

SMA can be used as an actuator, it is simpler compared to the motor (servo) and piezoelectric actuation methods. SMA is a memory metal that gets contract when warmed and comes back to its underlying shape after distortion (Jayender et al., 2008; Krulevitch et al., 1996; C. C. Ma et al., 2000) . Through some exploration, it was discovered that the poly dimethyl siloxane (PDMS) covering to SMA actuator will prompt expanded productivity with improved time reaction and decreased overshoot (Jumat et al., 2019). Shape memory alloy wires have been utilized as actuators (Basaeri et al., 2014).Shape memory alloys (SMA), shape memory polymers (SMP), electro-chemo-mechanical conducting polymers (EMCP), thermal polymers and mechano-chemical polymers (MCP), and ferromagnetic shape memory alloys (FSMA) are more capable of withstanding enormous free strain and high resistance, though they may exhibit mild reactions and reduced efficiency, making them inadmissible for use in flapping-wing drones (Furst et al., 2013; Ganor et al., 2009; Madill & Wang, 1998; Marimuthu et al., 2014) . An inductor is considered to be the main element for integrating carbon fiber, MAV is designed using a multi-physics and lumped variable method. Computation enables the inductor to get adjusted to different shapes and sizes. Grouped values are created based on the target values for the MAV inductor (Fearday et al., 2017). Shape memory alloy (SMA) actuator wires and super-elastic SMA ribbons were used by Stephen. For the design of elbow and shoulder joints to imitate a bat's flapping sequence. Bending and stress are calculated and adjusted using the necessary force model and optimization algorithms (Furst et al., 2012). For multiple flexure integration with tunable stiffness, in 2012 Hines et al (Hines et al., 2012) have used SMP (shape memory polymers) to increase elevation without altering Waveform controlling of the piezoelectric element successfully. In 2017, Kamaruzaman et al (Kamaruzaman & Abdullah, 2017) made two separate approaches, i.e., the spring form and the wire form of Nickel-Titanium SMA (NiTi) for the flapping-wing MAVs. Heat is produced on the wire/spring using an electrical current supply for contraction also the system is cooled by convection with the natural atmosphere for expansion. The spring style SMA showed a better response for both by high compression and expansion. Because of the SMA wire tension restoration and elasticity restrictions for a longer duration, it is not much used for flapping mechanism actuation, but as a supporting material, it has been used as a muscular portion of the MAV's. The characteristic parameters of SMA actuated flapping-wing drones are listed in Table A9.

2.3.3.7 Electro Active Polymer (EAP) Driven Flapping

When an Electro active polymer is been activated by an electric field, it displays a modification in its size or shape (Bashir & Rajendran, 2018). The Dielectric Elastomer EAPs, and Ionic EAPs are two types of polymers generally used for flapping-wing drone's applications. If two compliant electrodes with applied voltage differences are interspersed with a polymer, which induces thickness contraction and expansion in the region of the polymer film, this effect is pointed to be dielectric elastomers (Pei et al., 2004). Dielectric Elastomer as Electro Active Polymers/actuator (Uh et al., 2016) has been well described by Pelrine (Pelrine & Kornbluh, 2016). In an electrostatic-based actuator, dielectric elastomers can be used to increase actuating stress (Pelrine et al., 2017). It is incredibly difficult to build the drive system for a MAV wing flap as it needs bending or twisting movements. Due to its high volume-specific density of power and high strain efficiency, silicone-based dielectric elastomers have been used in the actuator content of flapping-wing drones (Burgess et al., 2009). In 2014, Lau et al (G. K. Lau, Lim, et al., 2014) have used Rolled Dielectric Elastomer Actuator (DEA) as an indirect longitudinal muscle for the flapping-wing drone model, which is been considered. To avoid membrane wrinkling, a pre-stretch is required. Cap's end maintains the hoop stretch, and the axial stretch is protected by a diamond shaped CFRP shield. The initially compressed shell relaxes during activation through supply by elongating the rolled actuator to create variations. These variations will affect the CFRP shell indirectly causing flapping at wings through Tergum (G.-K. Lau et al., 2017). In 2015, Zhao et al (J. Zhao et al., 2015), made an flapping-wing prototype of dielectric elastomers, As DE-film is actuated, it flattens by transforming to a saddle surface, and restores to its original state by contraction as soon as the voltage is removed. Wings are connected at their end and could obtain the flapping frequency of 5 Hz. If the natural frequency is lower than the expected frame frequency, regaining the frame's reaction will restrict the frequency of the lift, as the retrieval force is from the stored frame energy. In 2018, Cao et al (Cao et al., 2019) have devised the flapping mechanism incorporates a slider-crank system that converts the DEA linear movement to a reciprocal flap movement, while the double rocker system amplifies the flutter amplitudes (Cao et al., 2018). Macroscopic objects must be neglected by using two physical stops on the slider part.

Ionic EAPs or Ionic polymer-metal composites (IPMC) consisting of polymer of ionic gel planting with the electrode of a metal, generally it's been used to obtain relatively large responses with applied low voltages (Mukherjee & Ganguli, 2010). In 2006, Gie Lee et al (Lee et al., 2006) to improve the performance of IPMC based flapping, a rack-and-pinion mechanism is built within it. Gold was plated on the surface of cast IPMC to get improved surface conductivity and to reduce the evaporation of solvents by electrically heated electrodes. The prototype tested could be able to fly at low frequency with large wings. In 2018, Yang Zhao et al (Y. Zhao et al., 2018) have applied a unique material called IPMC [236],(Rosly et al., 2018)on flapping-wing drone for its wing flapping. Where the IPMC drive has been forced on one side by a clamp and the wings have been linked to the other way to move available actuating force of IPMC drive on the wing for flapping generation. The reduced amplitude with increased frequency of flatting on the wing has been realized when the IPMC actuation frequency is over the resonant frequency. The characteristic parameters of EAP actuated flapping-wing drones are listed in Table A10 in Appendix 1.

2.3.3.8 Electrostatic Driven Flapping

The electrostatic force is obtained when an alternating voltage is applied across two electrodes placed parallel (Tyson & Frazier, 2012). Here the electrostatic force is used for the movement of the metal beam to get oscillations as an application to flapping-wing drones**.** In 2015, Yan et al (Yan et al., 2015) presented a self-lifting artificial insect with a wing actuated by an electrostatic mechanism, where electrodes were activated through supply voltage to get deflection at metal beams, with less power consumption and adaptable wing movements for best flight. In 2016, Liu et al (Z. Liu et al., 2016) tried to introduce the pivot spar bracket concept for electrostatic actuated FW mechanism to get increased lift force. the fulcrum bar is replaced by a pivot spar bracket concept, and multiple parallel bars are reduced to a pair of metal rods, to get the limited and smooth movement of wing flapping. But the overall weight of the prototype got increased. To get a lightweight prototype in 2018, Liu et al (Z. Liu et al., 2018) induced more powerful wing rotation in analogy with little modifications to his previous model. By providing DC bias voltage in between the electrode plates placed in parallel to form an electrostatic field which intern generates sustainable vibration at wings. With a frequency of 35 Hz, it has obtained better lift force efficiency and a lightweight simple design compared to other works. In 2016, Yang et al (Y. Yang, 2016) used the same concept, but with reduced size and minimal components. Where fulcrum bars are been avoided, a U-type arrangement of electrodes with very small size four parallel beams to wing connection is used, to obtain mosquitoes size FW actuated prototype. The characteristic parameters of electrostatic actuated flapping-wing drones are listed in Table A11.

2.3.3.9 Electromagnetically Driven Flapping

Electromagnetic actuators use lower processing voltages and have high power density, making them the best tool for flapping-wing mechanisms. In 2016, Zou et al (Zou et al., 2016) introduced a combination of two 4-bar mechanisms to the electromagnetic-actuated flapping-wing drone. By minimizing its weight, could obtain an increase in flapping frequency and is able to sustain the flight of 7 minutes in the air. An electromagnetic actuator that transforms an electrical signal into a magnetic field and generates a linear motion, is a linear solenoid actuator. In 2013, Bontemps et al (Bontemps et al., 2013) used the spring-mass concept for FWNAV, but without 4-bar linkages and few modifications in the design like compliant linkage with hinges connected across thorax like a pendulum. This mechanism could generate a 4 µN lift force with a 51° angle of flapping and a frequency of 100hz.

In 2019, Liu tried to incorporate the efficient design mechanism that could produce an efficient lift with better flapping frequency. The flexible hinge bending stiffness has been customized with a unique design to achieve better lifting in electromagnetically actuated (Z. Liu et al., 2019) flapping-wing drone. Optimization strategies include the substitution of the iron core with even more appropriate materials like Ni-Zn ferrite for greater electromagnetic force and enhanced flapping frequency improvement by the steadiness of the cantilever vibratory system. The 5.5V low voltage-driven electromagnetic actuator (Z. Liu et al., 2017) is used to induce vibration through a cantilever-plate-like framework to actuate the flapping of insect scale flapping wings. The prototype was tested with two different size magnets which could produce a transmitting mechanism with a flap angle of 20 degrees at 101.4 Hz frequency and 30-46 degrees at 75 Hz, respectively, for large and small magnets. Dargent et al (Dargent et al., 2009) described a novel approach to SU-8 in which the elastic energy is stored directly in the wings will vibrate at their natural frequency using a linear electromagnetic actuation technique. The frequency of the oscillation can be adjusted to the frequency of the wing resonance. Recent work by et al (McIvor & Chahl, 2020) on electromagnetic energy efficiency analysis on flapping-wing drone has shown that a reasonable amount of 13% reduction in input power requirements as compared with the original energy consumption. In 2013, Roll et al (Roll et al., 2013) carried out a series of electromagnetic flapping-wing drone experiments and studies with 16 separate wing profiles. Successful in design and production with improved efficiency and decreased overall costs. In 2015, Bolsmana et al (Bolsman et al., 2008) implemented this solenoid-actuated ring structure combination of nearly four different varieties of structures for flapping generation and enhancement. However, the oscillatory behavior of the rings was affecting the other controlling equipment's which were a part of the flapping-wing systems (Bolsman et al., 2009a). The characteristic parameters of electromagnetically actuated flapping-wing drones are listed in Table A12.

Table 2.3 : List of Few Mechanisms under Rotary Driven Systems

Best Mechanism	Advantage	Disadvantage
Golden Snitch, 4-bar linkage gear transmission (L. J. Yang et al., 2012)	Moldflow software for better design, modeling, and simulations verification	In this study, the stroke angle of flapping-wing drone is restricted by the phase distinction between two wings.
Third type of Stephenson 6-bar linkage (L. J. Yang et al., 2015)	Decreased phase lag to a minimal level	High vibrations were triggered during fluttering due to weight and more links.
Flapping-wing 4-bar slider-crank mechanism (G. K. Lau, Chin, et al., 2014)	The thoracic mechanism with compliant materials could retrieve the wing inertial energy to flexible elastic energy.	The structure for the rigid body has no elastic energy storage capabilities.
Novel flapping wing rotor of crank shaft mechanism (Guo et al., 2018)	In the lever system, the Elastic plate plays a significant role. The FWR model offers a beneficial platform and provides a much wider variety of aerodynamic lift and performance combinations. The flyable prototype result demonstrated that it's self-stabilized.	Switch only in the vertical direction & hover inside a limited space illuminated.
Beetle (Scotch yoke mechanism) (Q. V. Nguyen et al., 2009)	The flap actuation test and strength analysis show that wing rotation helps to generate force.	Due to the deterioration of the linkage device, the decrease in the flapping angle and flapping frequency of the MAV. Owing to reduced rigidity and vibration of the guiding rail, the forward speed of flapping-wing drone against the long-distance can never be completely observed.
Clicking mechanism with compliant structure (Y.-W. Chin & Lau, 2013)	It is more effective aerodynamically than harmonic sinusoidal movement	Because of the position locking, an abrupt stop at the end of the wing flap stroke

Table 2.4 : List of Few Mechanisms under Hybrid Driven Systems

Best Mechanism	Advantage	Disadvantage
Hybrid System mechanism of Saturn and Nano Hummingbird (M. Keennon et al., 2012a)	Wing rotation and twist modulations are being used, enhanced control characteristics in cross-coupling, and pitch or yaw to roll coupling	-
Scotch-yoke mechanism and linkage system (Q. V. Nguyen, Park, et al., 2010)	-	Owing to the restricted linkage method, the flapping angle of the beetle cannot be reproduced. Because of the minimal motor torque, the flapping frequency of the wing is not as high as the actual bug.
Two planar 4-bar linkages mimicking insect's thorax(crank - coupler rocker-mechanism) (Q. V. Nguyen et al., 2016)	Two flapping and two fixed wings are used, which is advantageous to obtain high thrust	If too fast beginning to turn control at a low angle of the body is used, it can enter a spiral dive by an almost horizontal axis of the body.

Table 2.5 : List of Few Mechanisms under Linear Driven Systems

Best Mechanism	Advantage	Disadvantage
Robobee (piezo actuation) (Teoh et al., 2012)	Stabilized vertical flight	Lateral drift due to inherent torque bias because of inevitable assembly asymmetry.
SMA actuators in flapping-wing MAV (Kamaruzaman & Abdullah, 2017)	Wire type SMA has given the fastest contraction as compared to the spring type SMA. For the cooling process, wire type SMA has given the fastest time to cool as compared to the spring type SMA	-
Novel Piezo actuation based on inertia drive (Y. Zhang, Peng, et al., 2020)	It is easier to perform using friction contact, without using any transmitting mechanisms like crank-rocker or crank-slider. This could mainly provide unlimited stroke with an arbitrary type of flapping motion.	-
Electromagnetic actuator (Z. Liu et al., 2017)	Conventional electromagnetic actuators could provide a rotating motion with low voltage consumption and high-power density benefits.	Influence of external materials especially metals
SU-8 (Dargent et al., 2009)	The excitation frequency can be adapted according to the wing resonance frequency	-
Micromechanical Flying Insect (MFI) (R. J. Wood et al., 2008)	Smart Composite Microstructures (SCM) attachment to the system could generate the highest wing beat frequency of 200hz	-
Ring-type structure with solenoid actuator (Bolsman et al., 2008)	The independence of wing coupling choices, the avoidance of the need for a support frame, and space for the actuator to be mounted in the center of the ring.	The vibratory behavior of rings may adversely impact sensors
Resonant Driven Piezoelectric actuation (Ozaki & Hamaguchi, 2020)	Improved lift and flapping frequency with resonant driven mechanism concept	Cross talk between stroke amplitude of the actuators, the prototype demands an increased overall weight and cost of manufacturing.

2.4 Findings from Literature Review

From the literature review the following important points are to be addressed as potential to bridge the gap in already conducted research work, future scope, and requirements. Researchers concentrated on Miniaturized flapping technique is only through linear actuation mechanism, as the size is a main constraint in NAVs.In motor driven mechanisms, due to the intricate designs of gear systems, the overall weight of the flapping actuation mechanisms has been higher until now. Natural flyers, such as mosquitos, beat their wings at a high frequency i.e 800hz, yet human-made artificial fully flyable FWNAVs driven by motors can only flap their wings Max upto 45hz frequency. From the literature review of 23 years research data, Mosquito characteristics mimicking FW designs- driven by motors are not there yet and it is required for insect's behavioural study. As mosquito mimicking models are currently not available for analysis and subsequent design optimization, or evolution. The advancement of NAV is greatly aided by the light weight, small size, and simplest flapping actuation mechanisms, hence targeting for some salient features of mosquito would be the better option.

The comparison results of the literature review with required process flow to design and analyze any flapping actuation system is discussed in further sections.

2.4.1 Flapping Wing Design Analysis Process

To build any flapping-wing drone, it is necessary to opt for whether it should be of the bio-mimic type of bio-morphic type design. Because the biomimetic design perfectly mimics the physiology of living creatures such as birds, insects, and so on (Jones et al., 2004) .

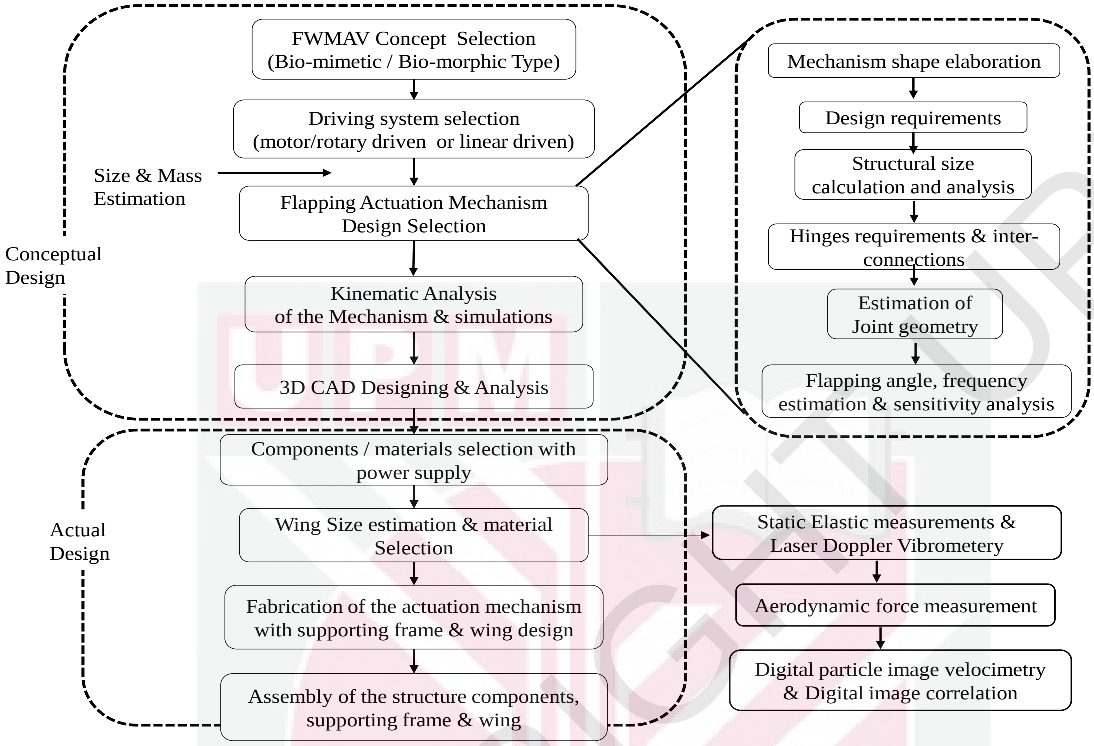

Figure 2.6 : Steps of Flapping Actuation Mechanism Design Process

The biomorphic designs are influenced by the concepts of living creatures, but they are not exact replicas of living organisms (H. K. Jung et al., 2015). De Wagter's DelFly (de Croon et al., 2009) and Platzer's biplane Flapping MAV (Jones et al., 2003) are two classic biomorphic models. In this paper, unconventional flapping-wing systems with various combinations of wing connections and more than two wing combination models are biomorphic. Biomorphic and biomimetic types are indicated in appendix-1 for the respective FWAV models/designs. It is not easy to select an appropriate actuation structure for flapping-wing design concepts from the available mechanisms (see Figure 2.4), depending on the size, mode of flight, and flapping frequency requirements. Choosing the type of driving actuator (like rotary / linear actuation) and corresponding components required for the conceptual design based on the estimated target mass/size of overall FWAV to be achieved is important. Hence the summary of the flow or steps for the FWMAV design process, as shown in Figure 2.6 by referring (Bejgerowski et al., 2010), (Jeon et al., 2017) papers. Focusing on the internal connections of the design mechanism concerning - how many links, joints are connected to gears, bearings, strings, and hinges are required to be within it. It is important to keep minimal connections or links as more the number of links and joints, could make the structure heavy and complex, also may hamper the smooth flapping movement at wings. These connections play a key role in the transmission movements; hence it is important to design its virtual measurements of mechanical structure with required calculations in CAD software. Giving importance to the structure or framework and design complications of the overall actuation mechanism must be focused. The structure is implicit in most designs within complexity, where the actuators are nevertheless influential in few cases. The structure itself or the actuator design might be a source of uncertainty sometimes hence it has to be taken care of while designing any flapping-wing drone. It is important to maintain the delicacy, lightness, and stiffness of inner and outer supporting frames in a system. But also reducing the structural complexity is a challenging task, which indirectly helps to build a lightweight and more accurate flapping actuation mechanism.

2.4.2 FW-Flight Modes Comparison

During the flight, birds/insect's wings concentration is not only in forward movements, it also attempts to flap up/down (pitch), clap & fling, plunge/sweep, depending on their flapping ease to create a balanced lift and thrust by responding to changing environmental conditions (Shyy et al., 2016). With wide speed range activities, it also offers excellent flying stabilization and dynamics with its flight modes like forward, backward, turn, take off, hovering and landing flight, etc. Here in this paper, they have attempted to analyze the flapping patterns and flight modes as shown in Figure 2.7 of various flapping-wing systems as listed in Appendix-1.

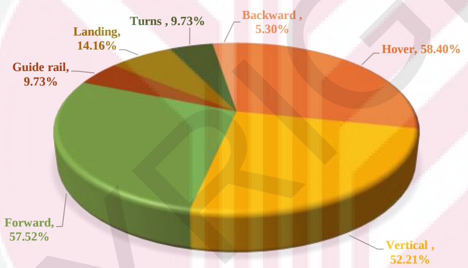

Figure 2.7 : Percentage of Flight Modes (Hover, Vertical Take-Off, Forward Flight, Guide Rail, Landing, Turns & Backward) under Fully Flyable Flapping-Wing Systems

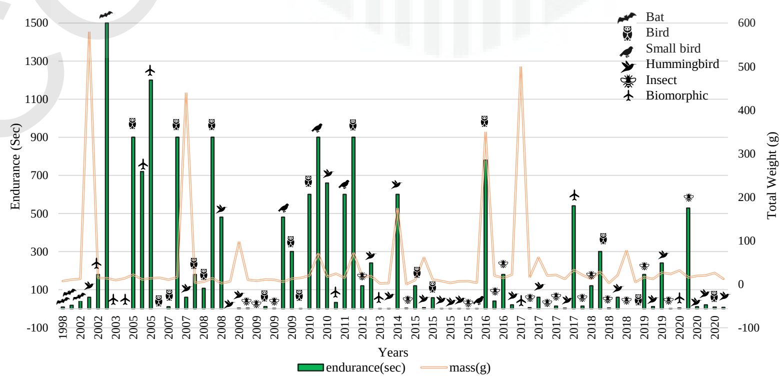

Figure 2.8 : Endurance and Corresponding Weight with the Yearly Representation of Rotary & Hybrid Actuated Fully Flyable Fapping-Wing System Models

In Appendix-1 free stream flight flapping-wing systems (fully flyable models) and flapping test bench setup (half model) are listed by indicating the characteristics like type of mechanism, structure/shape similarity like insect /bird type, flight modes (forward, backward, turn, take off, hovering and landing flight, etc.), endurance, total mass/weight, flapping frequency, flapping angle and wingspan, etc. Figure 2.8 And Figure 2.9, indicates the duration of the flight (endurance) with respect to the total weight of fully flyable flapping-wing systems of rotary & hybrid driven, and linear driven systems with expanded projection. (Note: rotary & hybrid actuated are 76 + linear actuated are 37 = total 113 fully flyable FWAVs considered from Appendix 1). From Figure 2.8 And Figure 2.9 the lightweight flapping-wing systems could achieve a better duration of the flight with less power consumption compared to heavy weight systems.

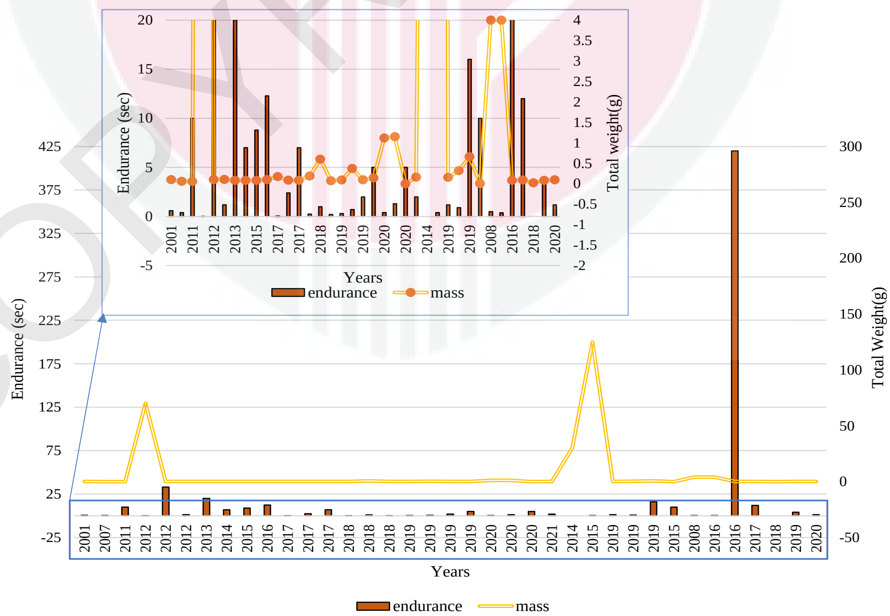

Figure 2.9 : Endurance and Corresponding Weight with the Yearly Representation of Linear Driven Fully Flyable Fapping-Wing Systems Models (Note: All Linear Driven Fully Flyable Fapping-Wing Systems Models Are under Insect Mimicking Types)

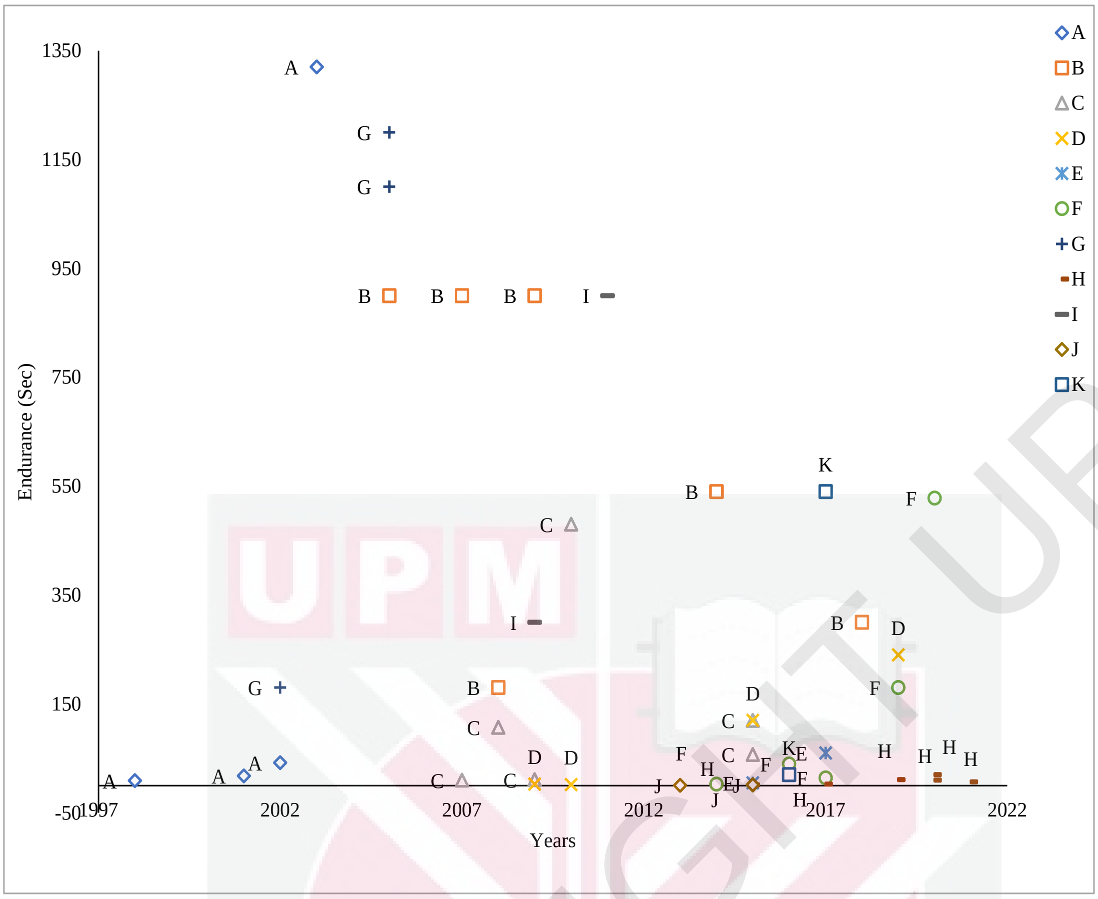

a).

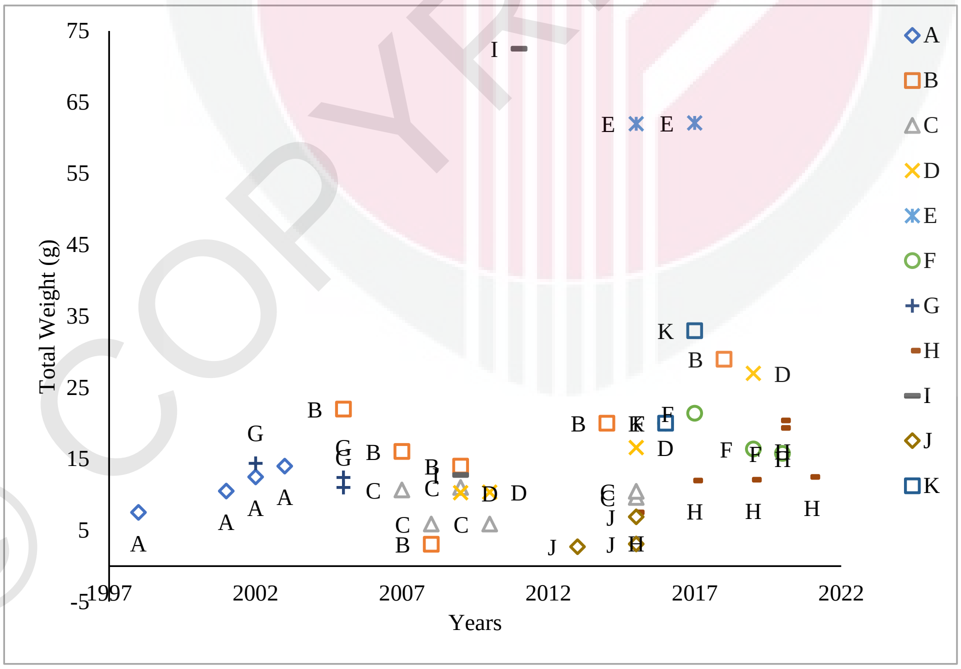

b).

Figure 2.10 : Yearly Progress of Rotary & Hybrid Driven Fully Flyable Fapping Wing Systems with Respect to a). Endurance, and b). Total Weight.

(A). Microbat (Pornsin-Sirirak, Tai, Ho, et al., 2001), (M. T. Keennon & Grasmeyer, 2003a), (Pornsin-Sirirak, Tai, Ho, et al., 2001) ,(M. T. Keennon & Grasmeyer, 2003b). (B). Delfly (de Croon et al., 2009) ,(de Wagter et al., 2014a) ,(Lentink et al., 2010) ,(Tay et al., 2015) ,(de Croon et al., 2009), (Karasek et al., 2018) . (C). Lung jieh's Fwmav (L. J. Yang et al., 2007), (L. J. Yang et al., 2012), (Hsiao et al., 2012), (L. J. Yang, Hsu, Han, et al., 2009), (L. J. Yang, Hsu, Hsiao, et al., 2009), (L. J. Yang, 2012), (L. J. Yang et al., 2015) . (D). Nguyen's FWMAV (Q. V. Nguyen et al., 2009), (Q. V. Nguyen, Truong, et al., 2010), (Q.-V. Nguyen et al., 2015), (Q. V. Nguyen & Chan, 2019) . (E). David coleman's hummingbird (D. Coleman et al., 2015), (D. Coleman et al., 2017). (F). Kubeetle (Phan, Kang, et al., 2017) , (Phan et al., 2019b), (Phan et al., 2020), (Phan, Kang, et al., 2017), [143]. (G). M Platzer's Flapping MAV (Lai & Platzer, 2001) (Jones et al., 2005), (Jones & Platzer, 2006a), (H). J zhang's hummingbird [305-309], [330]. (I). Bejgerowski's small bird (Bejgerowski et al., 2009), (Bejgerowski et al., 2011). (J). Hines FWMAV (Hines et al., 2014), (Hines et al., 2015). (K). M Karásek's colibri

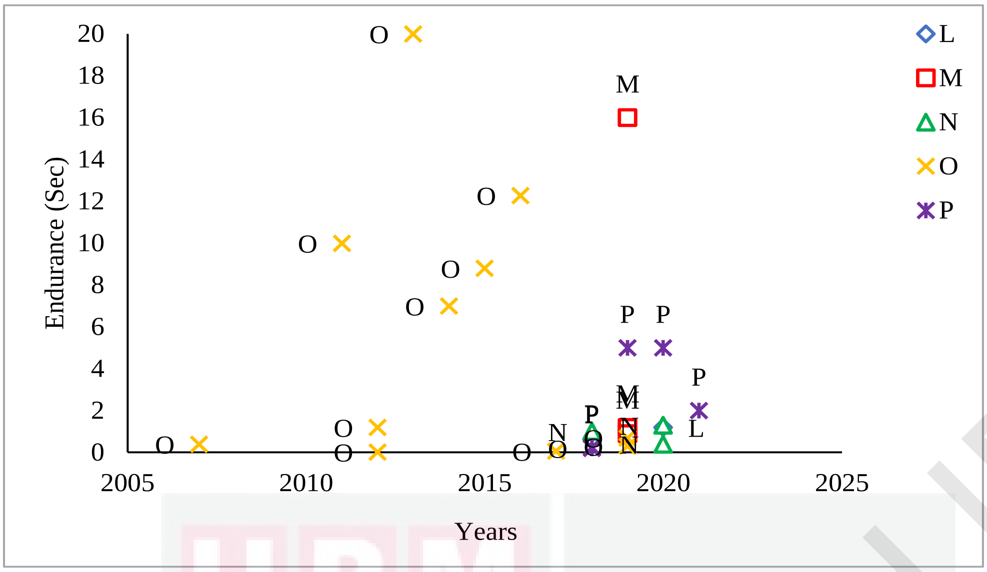

a).

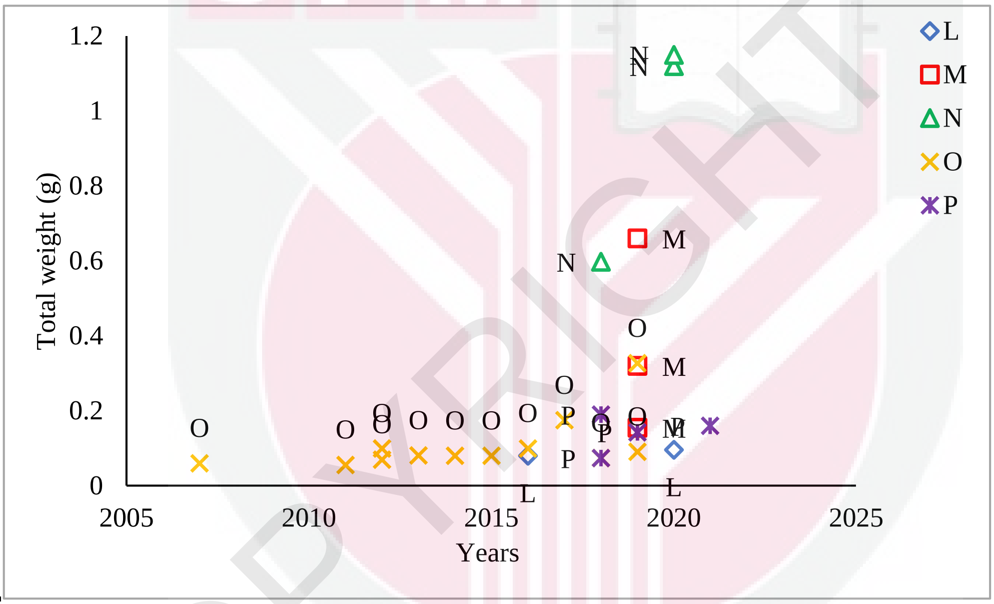

b).

Figure 2.11 : Yearly Progress of Linear Driven Fully Flyable Fapping-Wing Systems with Respect to a). Endurance, b). Total Weight
(L). Y Zou's SJFLY model I & II (Zou et al., 2016), (C. Wang et al., 2020) . (M). Y Chen's Flapping micro robot model I, II, & III (Y. Chen et al., 2019). (N). T Ozaki's FWMAV models (Ozaki & Hamaguchi, 2020), (Jimbo et al., 2020), (Ozaki & Hamaguchi, 2018a). (O). R J Wood's FWNAV models (R. J. Wood, 2008) , (R. J. Wood, 2007), (Jafferis et al., 2019) , (K. Y. Ma et al., 2013), (Graule et al., 2016) , (Pérez-Arancibia et al., 2011) , (Y. Chen et al., 2015) , (Chirarattananon et al., 2014) , (Y. Chen et al., 2017) , (K. Y. Ma et al., 2012) , (Y. M. Chukewad et al., 2018) , (Teoh et al., 2012) . (P). Fuller's Robofly models (Y. Chukewad & Fuller, 2021) , (Dhingra et al., 2020) , (Fuller, 2019) , (Y. M. Chukewad et al., 2018) .

From the collected data of Appendix 1, the distingsion between fapping-wing system types depending on their imitating similarities, such as bird, small bird, nano hummingbird, insect, bat, and biomorphic type, under rotary and hybrid actuated types. Linear actuated insect FWAVs are also identified and their percentage among all free-stream flapping-wing drones can be seen in Appendix 1 is included in the pie graph of Figure 2.2. Some of the rotary flapping wing MAVs are considered under bio-morphic type, as it involves rotation of the wings with flapping performance (because bio-morphic type flapping-wing drones are a combination of partially bio-mimetic and semi advancement of human-created design). Flight modes/patterns (like forward, backward, turn, takeoff, hovering, and landing flight as shown in Figure 2.7 of fully flyable model and flapping test bench model of flapping actuation mechanisms are listed in Appendix 1. From Figure 2.10(a) and 2.10(b), it can be seen that the yearly progress made by the authors/ researchers in their rotary & hybrid actuated fully flyable FWAV's with respect to endurance & total weight. Similarly in Figure 2.11(a) and 2.11(b), the yearly made by the authors/ researchers in their linear actuated fully flyable fapping-wing systems with respect to endurance & total weight.

2.4.3 Hovering and Forward Flight

Generally, only hummingbird mimicking flapping-wing drones can only be seen performing hovering flight mode, but by identifying some bird & insect imitating free stream (fully flyable) flapping-wing drone that could also perform the hovering flight. Up to today, out of 113 free streams flapping-wing systems (from appendix 1), nearly 66 flapping-wing drone models were able to hover as well. The percentage-wise segregation of hovering capable and forward flight-capable flapping-wing drones as per appendix-1 is shown in Figure 2.12. Where nearly 39% of insects imitating full stream FWAVs are capable of hovering. As per Zdunich (Zdunich et al., 2007) in 2007, the aero-elastic properties offer sufficient twisting with camber for both hover and diagonal translation flying in flapping-wing systems. With the aid of reduced cost rate gyro systems with suitable system algorithms, the functional prototype could be able to achieve extraordinary hovering flight stability. Sometimes excessive heat of brushed dc motors appears to mean that the flapping-wing prototype may not produce enough thrust for hovering, and therefore brushless motor use would be the likely solution. The flapping mechanism of DelFly II can produce great symmetrical mobility with maximum thrust, which delivers force across the fuselage axis, by continuing to increase the flapping amplitude to accomplish hovering. the direction of wing movement and corresponding forces of hovering of Delfly can be seen clearly in their schematic representation (de Croon et al., 2009).

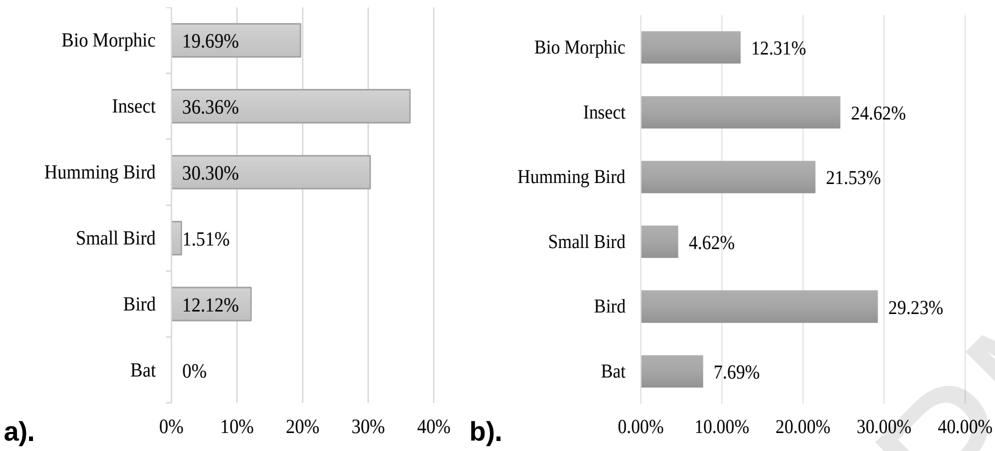

Figure 2.12 : Percentage of Biomimetic and Biomorphic Types a). Hovering Capable Fully Flyable Fapping-Wing System Models b). Forward Flight-Capable Fully Flyable FWAV Models

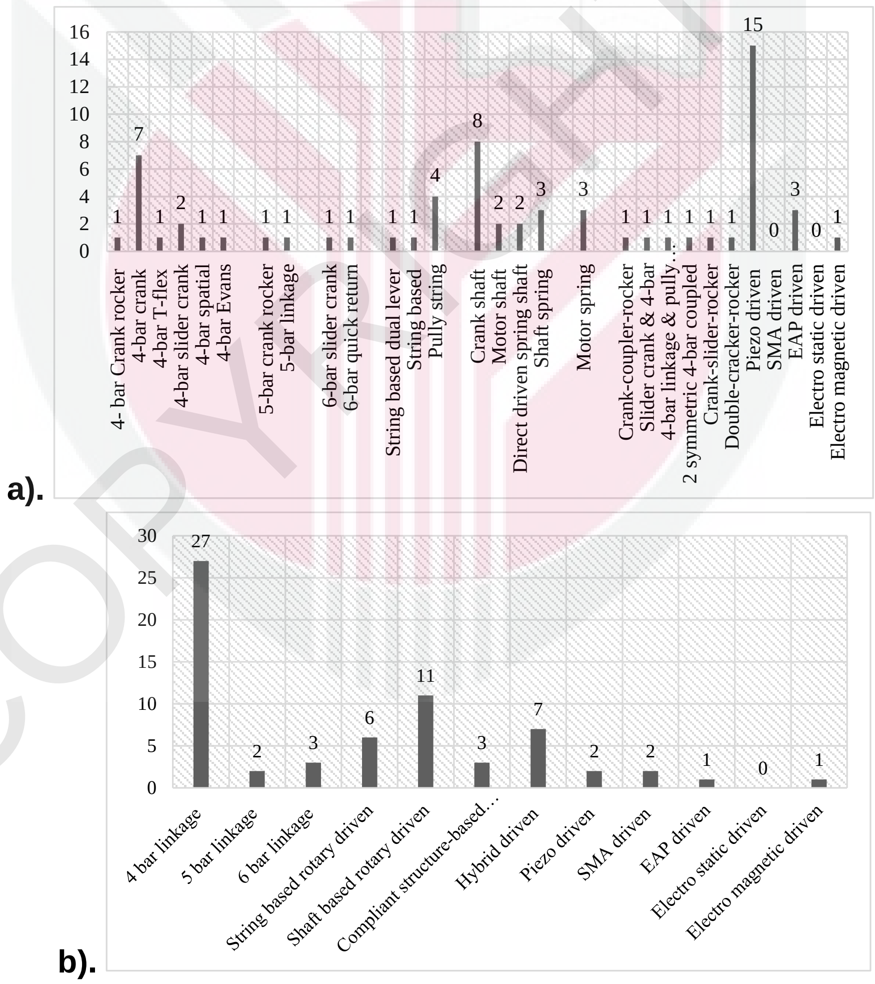

Figure 2.13 : List of Flapping Actuation Mechanisms Utilized in Flapping-Wing Systems to Generate a). Hovering Flight Condition, b). Forward Flight Condition

The list of several rotary, hybrid, and linear actuated mechanisms, specifically used by the researchers for their FWAVs that can perform hovering flight mode, is listed in Appendix-1. The number of flapping-wing systems that utilize a particular mechanism to generate hovering flight mode are depicted specifically in Figure 2.13. Where rotary actuated 4-bar linkage mechanisms (such as crank-rockers, crank-sliders) and hybrid mechanisms were often used in flapping-wing systems to perform hovering flight operations.

2.4.4 Flapping Patterns

In any FWAV, choosing the flapping pattern is essential, as its frequency aids in the generation of lift and thrust, as well as hovering. under Hovering capable fully flyable flapping-wing drone models the percentage of patterns of flapping is indicated in Figure 2.14.

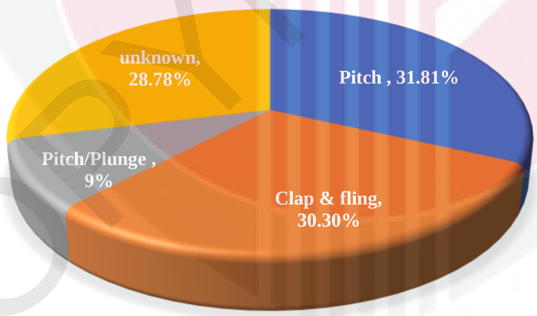

Figure 2.14 : Percentage of Wing Flapping Patterns Utilized under Hovering Capable Fully Flyable Flapping-Wing Drone Models

The clap/fling approach is recognized by Fogh(WEIS-FOGH, 1973), as an aerodynamic factor that occurs during the maneuvering of the wing kinematics. It is one of the appropriate methods of increasing lift, particularly among small fliers. from a 100mm MAV (Kawamura et al., 2008) having a total mass of 2.3 g found that clap-and-fling movement of wing resulted in increased thrust, which is likely to be influenced by comparative wind speed. Clap fling and pitch patterns are commonly used by most biomimetic type FWAV's, but pitch/plunge pattern of flapping is used only in biomorphic type FWAV's.

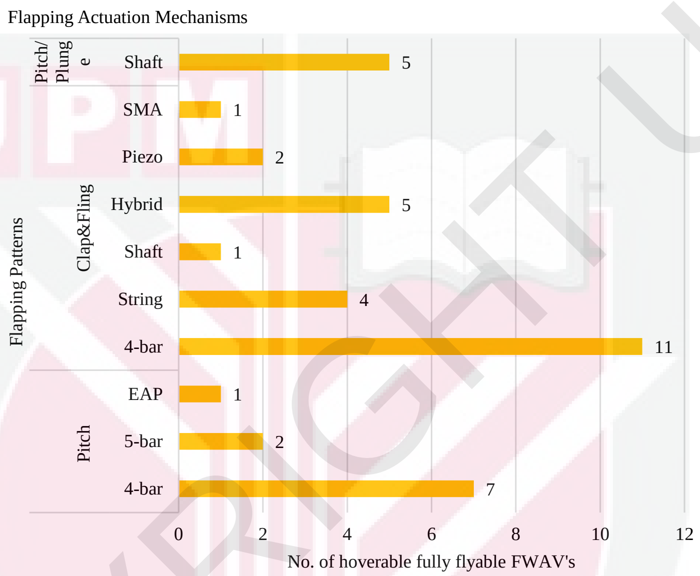

Figure 2.15 : Flapping Patterns Performed by Several Flapping-Wing Systems under Different Flapping Actuation Mechanisms

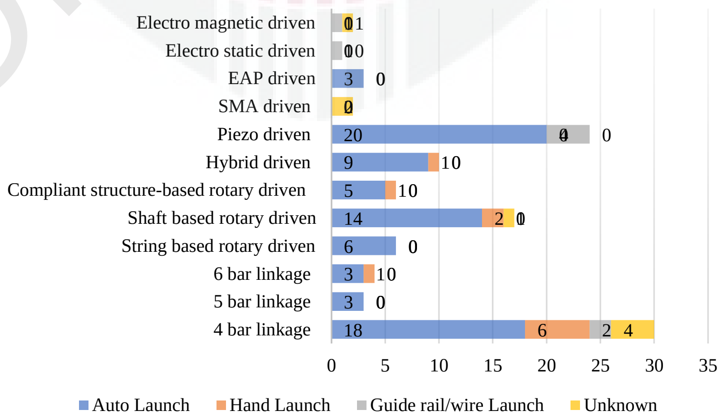

Figure 2.16 : Number of Launching Types Used under Each Flapping Actuation Mechanism for Fully Flyable Flapping-Wing System

As per Platzer et al (Jones et al., 2005; Lai & Platzer, 2001) it is more efficient to use wing flapping with proper phasing between pitch and plunge to obtain a better lift. Figure 2.15 shows flapping patterns performed by several Hovering capable fully flyable FWAV's under different flapping actuation mechanisms. Figure 2.16 shows the percentage of launching types such as auto-launch, hand launch & guide rail launch of fully flyable flapping-wing drones under each flapping actuation mechanism. Figure 2.17 indicates the flying patterns (like only hovering flight, only forward flight, both hover and forward flight) of flapping-wing system after the Auto / Hand launch of the prototype.

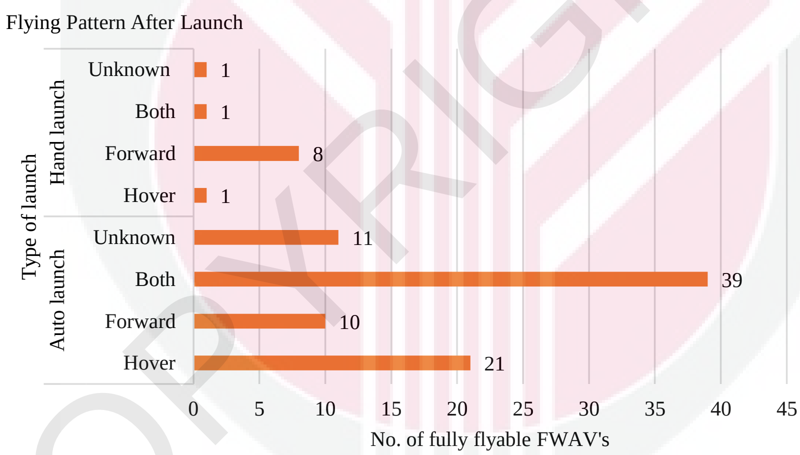

Figure 2.17 : Number of Flying Patterns after Auto / Hand Launch of Fully Flyable Flapping-Wing System

2.4.5 Flight Duration / Endurance

Increased flight duration is a significant advantage in almost any venture. The vehicle's overall endurance is determined by it's power consumption and also reduced drag at its wing, resulting in increased flight endurance (M. M. A. Hassanalian, 2014). One of the main drawbacks of small-scale flapping-wing air vehicles is their low endurance when compared to larger drones. As a solution, wing design performance/optimization analyses must be carried out to minimize drag, to obtain increased flapping-wing efficiency with endurance (M. Hassanalian et al., 2017). The flapping actuation mechanism can sometimes play a significant role in producing quality lift, and also sustainability of flight can be achieved by providing external material/ connections to the system as a stabilization factor. Prototypes that are maintained and adjusted for a longer period during flight by controlling wing movements through their design mechanism are more functionally like their biological counterparts. Astonishingly, there has been so little progress in extending endurance and expanding the amount of fully flyable vehicles built since Microbat in 2003, particularly over the last two decades. Hence the number of prototypes that achieved endurance of more than 8.5 minutes from appendix-1 are considered here, and their flapping actuation mechanism designs/sketches are shown in Figure 2.18. They have investigated on the mechanisms of these vehicles to see, what role the flapping mechanism played in lift generation and flight duration sustainability discussed below. Based on the high endurance achieved over the years and attempted to assign ranks to indicate the superior prototype mechanism as a result of our research, indicated in Figure 2.19.

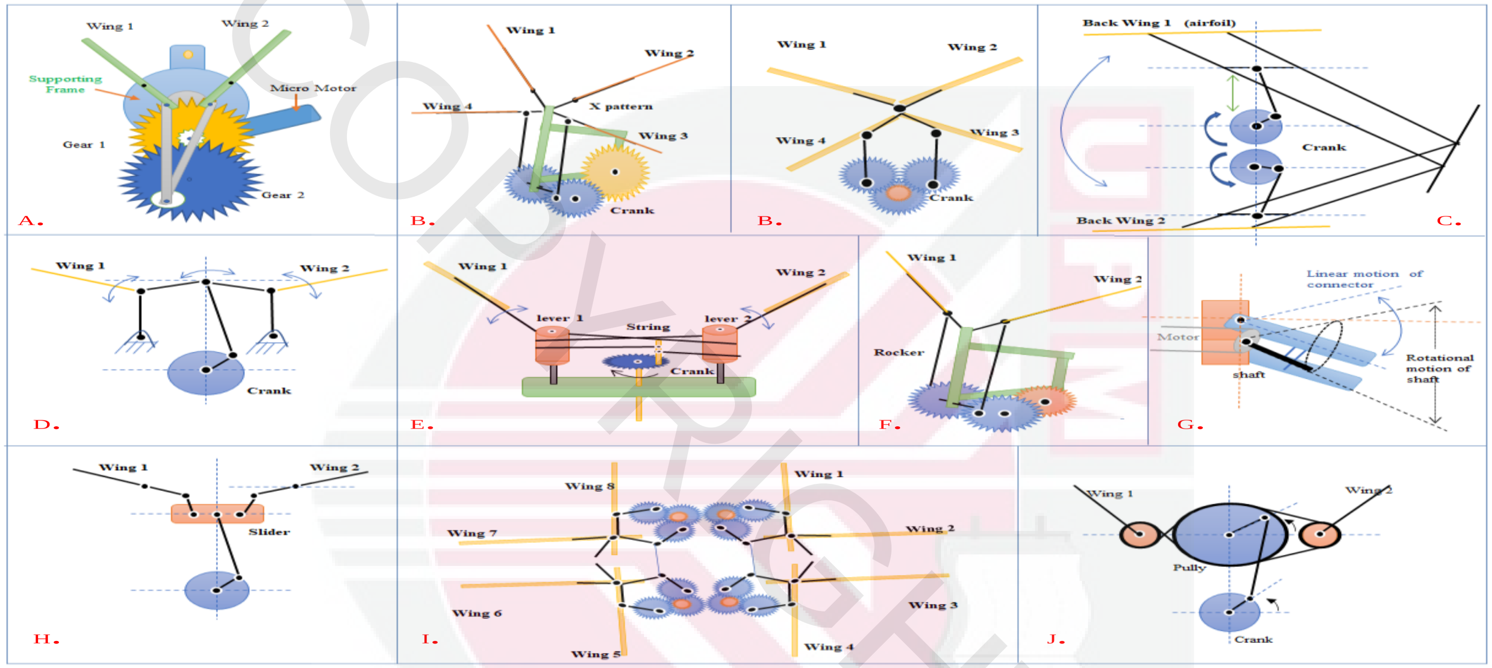

Figure 2.18 : Flapping Actuation Mechanism Sketches from Prototypes That Lasted over 8.5 Minutes
(A). AeroVironment Microbat MAV (4-bar single crank mechanism) (M. T. Keennon & Grasmeyer, 2003a) (Pornsin-Sirirak, Tai, Ho, et al., 2001) , (B). delfly (de Wagter et al., 2014b) (Lentink et al., 2010) (Tay et al., 2015) (de Croon et al., 2009) , (C). Radio-controlled flapping-wing MAV (Model 3) & Improved NPS FWmodel (Jones et al., 2005) (Jones & Platzer, 2006a) , (D). small bird (Crank rocker mechanism with short compliant segments) (Bejgerowski et al., 2010) (Bejgerowski et al., 2011) (Mueller et al., 2010) , (E). Saturn Prototype (string based dual lever mechanism) (M. Keennon et al., 2012a), (F). FWMAV Model (Spatial Single-Crank Double-Rocker mechanism) (T. Zhang, Zhou, Zhang, et al., 2011), (G). BionicOpter by festo (Gaissert et al., 2014) , (H). Hassanalian's Thunder-I (slider crank mechanism) (M. Hassanalian & Abdelkefi, 2016) (M. Hassanalian & Abdelkefi, 2019b) , (I). Quad-thopter FW robot (crank-shaft mechanism) (de Wagter et al., 2017) , (J). KUBeetle-S (Pully stringmechanism) (Phan et al., 2020)

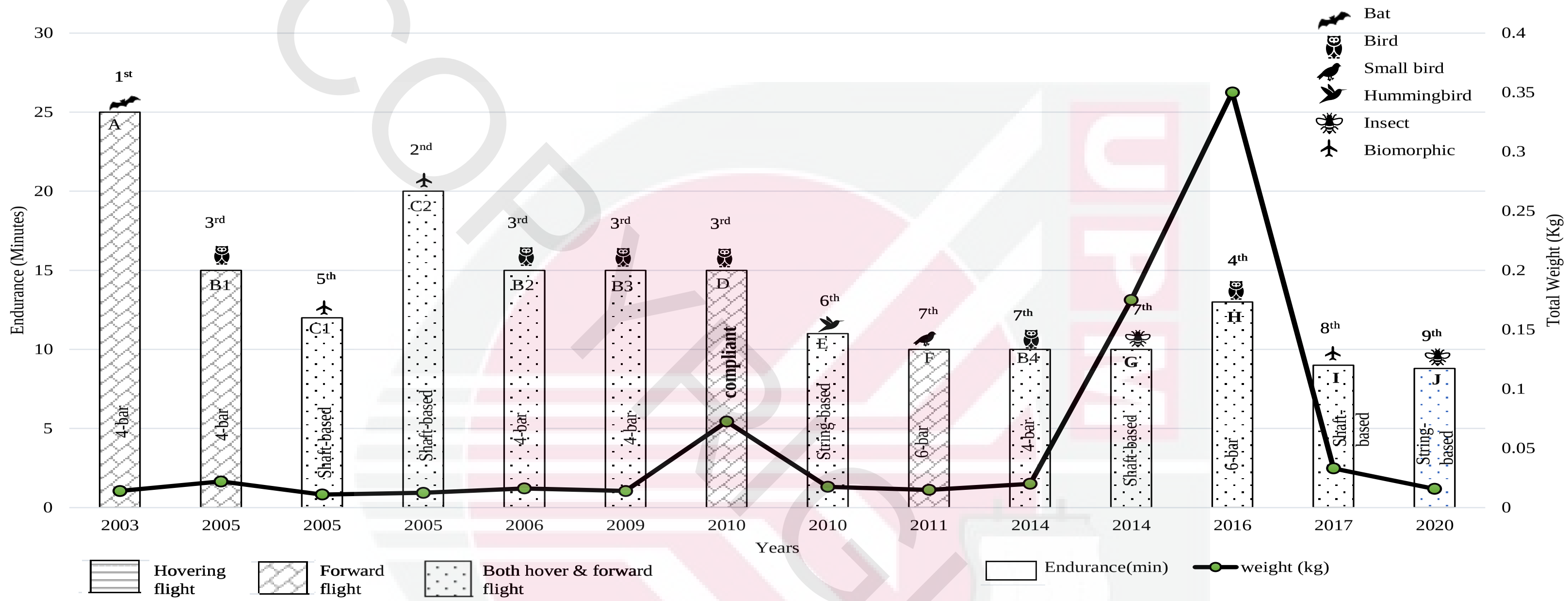

Figure 2.19 : Allocation of Ranking Based on the High Level of Endurance Attained over the Years
(A). AeroVironment Microbat MAV (4-bar single crank mechanism) (M. T. Keennon & Grasmeyer, 2003a) (Pornsin-Sirirak, Tai, Ho, et al., 2001) , (B1, B2, B3, B4). Delfly (de Croon et al., 2009), (Tay et al., 2015), (de Wagter et al., 2014b) (Lentink et al., 2010) , (C1, C2). Radio-controlled flapping-wing MAV (Model 3) & Improved NPS FWmodel (Jones et al., 2005), (Jones & Platzer, 2006a) , (D). a small bird (Crank rocker mechanism with short compliant segments) (Bejgerowski et al., 2010) (Bejgerowski et al., 2011) (Mueller et al., 2010), (E). Saturn Prototype (string-based dual lever mechanism) (M. Keennon et al., 2012a), (F). FWMAV Model (Spatial Single-Crank Double-Rocker mechanism) (T. Zhang, Zhou, Zhang, et al., 2011), (G). BionicOpter by festo (Gaissert et al., 2014) , (H). Hassanalian's Thunder I (slider-crank mechanism) (M. Hassanalian & Abdelkefi, 2016) (M. Hassanalian & Abdelkefi, 2019b) , (I). Quad-thopter FW robot (crank-shaft mechanism) (de Wagter et al., 2017) , (J). KUBeetle-S (Pully string mechanism) (Phan et al., 2020).

A compact and efficient mechanism was developed to convert the rotational movement of the motor shaft into the flapping movement of the wings for microbat (M. T. Keennon & Grasmeyer, 2003a; Pornsin-Sirirak, Tai, Ho, et al., 2001) as shown in Figure 2.18(A) only the actuation C method was developed and built out of the four flapping actuation design considerations, as those designs limited flapping movements to a plane perpendicular to the drive shaft. It has been discovered that span-wise rigidity is a significant factor influencing lift performance in flapping flight. For similar size prototypes, wings with stiff leading edges generate higher lift coefficients than those with flexible leading edges. Even as the battery begins to discharge, the frequency of flapping and the generation of lift decreases. The biomorphic type delfly (de Croon et al., 2009), (Tay et al., 2015), (de Wagter et al., 2014a), (Lentink et al., 2010) having variants like delfly I, II, delfly micro & delfly explorer, having crank mechanism as shown in Figure 2.18(B) as the basic structure with few modifications for its variants. The leading-edge of the wings transit in a horizontal figure -8-shape while each cycle is due to the aerodynamic, elastic, and inertial influence on its wing. due to its biplane wing configuration, the clap-and-peel pattern is present in each stroke which is beneficial to increase thrust (lift) force. Clap-and-peel is a variance of the clap-and-fling pattern. here the wings peel away rather than flinging apart more rigidly, which is because of the fluid-structure interplay between the air and the flexible membrane wings. This allows the circulation to build up more gradually, which can help avoid an unbalanced LEV from shedding into the wake. A MAV by Jones et al (Jones & Platzer, 2006a) with front fixed wings for lift and back flapping wings for thrust generation (having single, tandem, or biplane combinations) with crank-shaft mechanism as shown in Figure 2.18(C), provided with flexible joints for connecting the wings that allowed for passive aeroelastic pitching, was a unique design. Where the thrust varies linearly with the change in amplitude and frequency during a single air foil flapping in a perfect plunge sequence. By providing 90-degree phasing between both the plunge and pitch flaps, the performance and thrust can be increased. Locating a stationary airfoil below the plunging airfoil transforms the vertical energy shed, leading to a rise in thrust. The tandem configuration appears to outperform the biplane configuration. The two wings perform similarly in the biplane case, but the forewing generates most of the thrust in the tandem scenario. The tandem combination has the highest efficiency. A small bird mimicking the Crank rocker mechanism (Bejgerowski et al., 2010),(Bejgerowski et al., 2011),(Mueller et al., 2010)as shown in Figure 2.18(D) is designed with short compliant segments. The wing's main and secondary spars will deform through their flaps, modifying the camber and mid-chord velocities, influences its lift and thrust forces. The compliance of the primary spar adjusts the apparent wing area along/perpendicular to the flapping axis and ensures stability at high harmonics. The increase in overall thrust caused by improved wing compliance was measured experimentally. The Saturn prototype (M. Keennon et al., 2012a) employs a rotating crankshaft with a string-based dual lever mechanism as shown in Figure 2.18(E) powered by an electric motor, with two strings linked to it, each of which is controlling the oscillations of the corresponding pulley system at the wing hinge. The flapping angle pattern is periodic, but the intensity of the tip velocities is significantly lower when compared with the linkage-based system. Because of the design mechanism and wing pitch maneuverability such as rotation and twist distribution, control in the pitch, roll, and yaw axes was possible. The helicopter swashplate design helped to provide controlled input signals at actuators with much smaller bandwidth than the flapping frequency. Due to the extreme wing design configurations, the influence of flap stroke proved to have the best results during wing membrane camber reversal.

The flapping-wing drone (T. Zhang, Zhou, Zhang, et al., 2011) model having Spatial Single-Crank Double-Rocker mechanism as shown in Figure 2.18(F) offers a simpler, small size, and kinematically stabilized design. The positioning of the flapping wing and tail influences the productivity of flapping-wing flights. Plunging airfoils with plain or curly leading edges invariably produce a converse Von Karman vortex street in the wake, resulting in positive thrust values. While the angle of attack is held constant, the tubercles have very little impact on gliding flight. Whereas protuberances on the leading edge of wings can enhance gliding flight performance at non - zero attack angles. The dragonfly mimicking BionicOpter by Festo (Gaissert et al., 2014) having four wings that are governed by the main motor's crankshaft design mechanism as shown in Figure 2.18(G), which transforms the rotary movement of the motor into oscillating mobility of the wing. The crankshaft's proximal part leaves the housing having to carry the motor in a straight line, which is an intriguing feature of the crankshaft. Through eight servo motors, the BionicOpter can fluctuate the amplitude and twisting angle of each wing flaps independently, making it nearly as agile and quick as its natural counterpart. Vibrations are reduced the most when the forewing leads the motion, and a phase shift of 40 degrees provides a fairly stable flight. Hassanalian's Thunder I (M. Hassanalian & Abdelkefi, 2016) ,(M. Hassanalian & Abdelkefi, 2019b)prototype combines the variant arrangement with the slider-crank system design as shown in Figure 2.18(H), except instead of sliders, it utilizes guiding bars. A six-bar system with 14 components connections via hinges was used to achieve uniform flapping motion at both wings, yielding better lift. To fly and accomplish quick maneuverability, the MAV by Wagter et al (de Wagter et al., 2017) uses 4 separately operated sets of flapping – wings with a crank-shaft mechanism as shown in Figure 2.18(I) Comparable to a quadrotor, the wing pairs are organized so that variable thrust produces the needed roll/ pitch moments. Yaw movement is developed by alternate direction of tilting of two set wings. There is a risk of out of phase flapping, which can cause large yaw moments at the fuselage and result in fuselage spinning/loss of flapping amplitude/lift. To solve this problem, a phase lockable set of wings was used instead of a single flapping wing. the design does not correspond to any known biological counterpart, hence considered to be bio-morphic type. The insect mimicking KUBeetle-S (Phan et al., 2020) as shown in Figure 2.18(J) implements a four-bar linkage with a pulley–string mechanism to produce near-clap-and-fling effects at both dorsal and ventral stroke reversals, resulting in increased lift. In this case, the larger stroke amplitude of flapping wings and the additional payload were favourable in achieving better lift and stable flight duration.

2.5 Summary of the Literature Review and Remarks

This chapter summarizes and addresses various types of flapping-wing systems, with a focus on all flapping actuation mechanisms, structure-based designs for flapping enhancement, and hybrid flapping actuation techniques. A detailed classification of flapping-wing drones is defined by categorizing the various types of rotary/motor, hybrid, and linear driven flapping actuation mechanisms. The authors attempted to deconstruct a few basic and important actuation mechanisms into their equivalent block diagram representations. The authors also propose some alternative approaches and important parameters to consider for micro to nano-size flapping-wing systems with a significant advantage over flying light weight PAVs. Most actuation mechanisms' specifications and configurations are elaborated and focused on the high requirements of flapping frequency and stroke angle controllability via linkage mechanisms with insight into flapping patterns. The long-term stability obtained by flapping patterns/flight modes of the FWAV is investigated with the appropriate flapping mechanism contributions after manual/automatic launch. The intricacy of gear systems in motor-driven mechanisms has led to an increased total weight for the flapping actuation devices. Mosquitoes, being natural fliers, are capable of flapping their wings at an exceptionally high frequency of around 800 Hz. On the other hand, artificial flapping wing navigation systems (FWNAVs) created by humans and powered by motors can only reach a maximum wing flapping frequency of 45 Hz. An analysis of 23 years of research data reveals that there is still a deficiency in motor-driven designs that accurately replicate the properties of mosquito wings. This deficiency hinders investigations into insect behavior and the consequent improvement or development of designs.Since there is currently a lack of mosquito-mimicking models for in-depth study, it is evident that future research should prioritize the development of these models. NAV progress can greatly benefit from aspects like lightweight structure, compact size, and simplified flapping actuation systems. Therefore, focusing on the prominent characteristics of mosquitoes would be a highly promising strategy for the development of future FW-aerial vehicles.

Furthermore, yearly progress such as variations of weight, endurance, size of fully flyable FWAV prototypes by their respective authors in 2 decades has been highlighted. The best performing prototypes are ranked based on their flight modes, lift generation through flapping actuation mechanism designs, and long-duration flight sustainability. At present, the simplest method for design and manufacture is the motor-driven flapping control mechanism for bio-inspired artificial flight. As a solution to weight and size constraints, the piezo actuated and electrostatic actuated models are likely similar to real insects of very small size. But there are certain issues, including short flight difficulties, lower flapping frequencies, variations in flapping angles, etc. The wireless electricity demand of bio-inspired flapping-wing drones need to be further explored. Except for the above, for creating mosquito-scale aerial vehicles, the invention of new types of driving mechanisms with molecular level flapping actuation system are in the exploratory phase.

Based on the survey of the relevant literatures, they have determined that there is a demand for a method that is both simple yet lightweight FWMAV's.

Therefore, for the purpose of implementing the micro flapping wing model, there is a need to devise a new or original mechanism design that can transform rotary action into flapping movement or make use of an existing simplex mechanism designs. In the next chapters, the various sorts of designs that are being modeled are tested and discussed in greater depth.

CHAPTER 3

RESEARCH METHODOLOGY

3.1 Overview

This chapter presented a discussion on research methodology to achieve the aforementioned research objectives as in Chapter 1. This chapter is constructed with different design concepts through the following 4 sections. Here authors are aiming for opting and designing a unique actuation mechanism for generating flapping at wings as an application for micro aerial vehicles. The main purpose or intention of the design is to obtain better flapping frequency like mosquito flapping range. In this chapter, the work process is described in detail. The flow chart of the basic design process is as in Figure 3.1 below. The workflow is broken down into four stages, the first of which is the preference of design concepts (as shown at Figure 3.2 below) based on a literature review. Once the conceptual design is thorough, the driving force must be identified. The conceptual mechanism is then modelled in CAD with design structures and assembly to visualize its functioning. Then, analytical equations must be determined by calculating specific linkage dimensions to accomplish the necessary flapping actuation through it. Sources for mathematical equations encompass geometric shapes, characteristic features, physical properties (material), boundary conditions (constraints and loads), presumptions of initial conditions, and complexities (restriction from complex models or theoretical formulation). With these parametric data, the analytical equations for the design concept are accomplished and validated via MATLAB programming. The proposed mechanism is novel and has not been utilized in any previous prototypes; its kinematic analysis is carried out in stage two according to the flow chart depicted in Figure 3.4 Actual design model fabrication occurs in stage three and includes hand-made and 3D-printed models, as well as dummy wing testing for frequency analysis demonstrated in further sections of this chapter. As a controlling implementation with simscape emulations, they have controlled the frequency of flapping and direction with individual wing flapping controlling.

3.2 Basic Design Process

Factors such as efficiency, weight, simplicity, controllability, power consumption, and manufacturability must be considered when selecting the appropriate flapping actuation mechanism for a Micro Aerial Vehicle (MAV). Contemplating the positive aspects and drawbacks of the subsequent prevalent flapping actuating mechanisms is a must. Hence by referring to the literature survey of 20-decade research work and publications have been listed out the available types of flapping actuation mechanisms in chapter2 with details.

As a basic design process the following steps are followed which are represented in flow chart as shown in Figure 3.1(a). also, the design concept selection part is elaborated in flow chart of Figure 3.1(b) below. Initially the selection of design is considered with its design modelling and kinematic analysis as in Figure 3.2. and then the 3D design of it is created with Catia software.

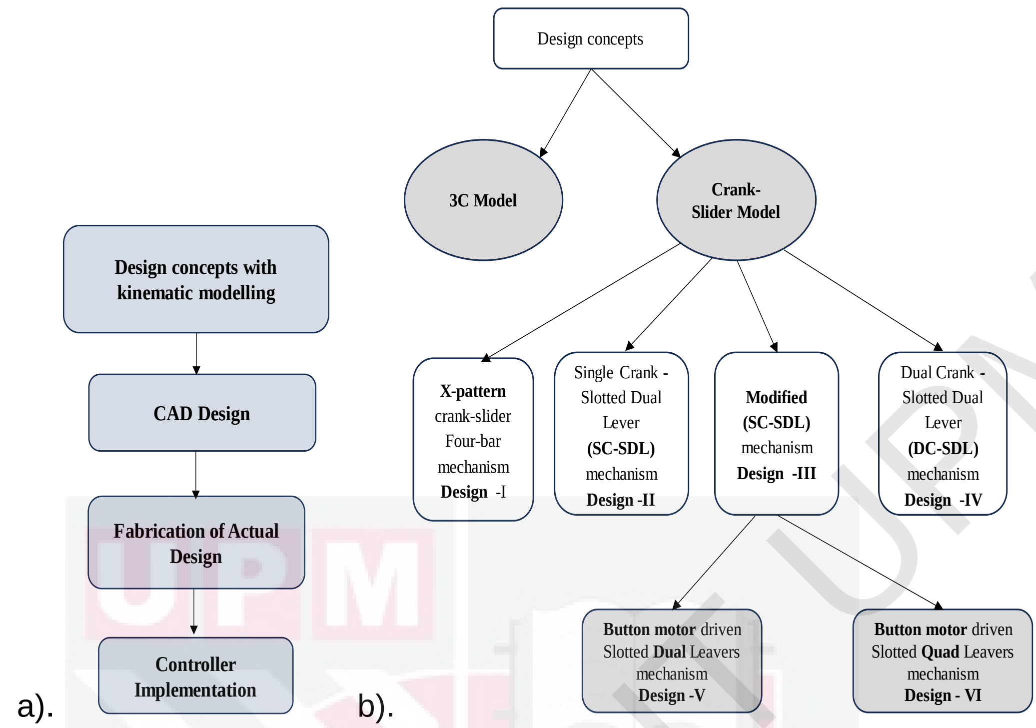

Figure 3.1 : Flow Chart of a). Basic Design Process and b). Design Concept Types Used for Flapping Wing Actuation

Choosing the proper flapping actuation mechanism for an insect-like robot is very important. By referring the types of flapping actuation designs from chapter 2, the slider crank mechanism of quick return technique has been considered and modified to obtain x-pattern four bar mechanism, Single Crank - Slotted Dual Lever (SC-SDL) & Dual Crank - Slotted Dual Lever (DC-SDL) designs as a design selection part as per Figure 3.1(b). The flapping actuation mechanism emulates the natural motion of insects while assuring efficiency, controllability, and lightweight design. Dielectric elastomers, pneumatic artificial muscles, or shape memory alloys can be used to replicate the way insect muscles inspired actuators that contract and expand. These materials can provide convincing motion, but the complexity of control and design may be heavier. Piezoelectric materials can provide precise and rapid motion, making them suitable for simulating the motion of insect wings. They can be incorporated into the structure of the wing to accomplish natural flapping. However, their force output may be constrained, making cautious design and optimization critical. Choosing micro-DC motors as the most suitable drivers for FWMAVs that mimic insects has enabled to reduce their overall weight and increase their efficacy. Coreless micro-DC motors Coreless motors lack the traditional iron core found in brushed DC motors, thereby reducing their inertia, and enabling greater acceleration and responsiveness. The lack of a massive iron core reduces inertia, allowing for quicker acceleration and deceleration. Due to their lightweight construction, they can attain high rotational speeds, making them suitable for applications requiring rapid motion. These motors typically have high levels of efficacy, converting a large proportion of electrical energy into mechanical motion. Consider voltage requirements, speed-torque characteristics, size, weight, and compatibility with applications like power source and control systems when selecting a coreless micro-DC motor. To ensure optimal performance and efficiency, it is essential to match the motor's specifications with the project's requirements. The complete operation of a micro-DC motor is detailed with various designs as shown in figure 3.1(b). the basic design process is detailed further.

All the individual design concepts have been formed and modelled in CAD, and each has been illustrated in further sections. The kinematic measurements and analyses have been done using the programming language Python. Additionally, the three-dimensional modelling of it is done in the comp mech GIM software, and the simulations in Simscape multibody are very detailed. Fabrication of tangible designs is performed in two ways: by hand and by 3D printing. Handcrafted designs were attainable but delicate, whereas 3D-printed designs were cumbersome, as it was difficult to acquire contemplate though lighter weight and very thin design links. Numerous efforts have been made into 3D printing in order to produce small, durable components. All the real-time fabricated models are illustrated in detail in this Chapter.

Controller design: Since it must navigate models with flapping wings, individual wing flapping control is a significant factor. As such, the distinctive wings of the final design IV manipulated in emulation by the simscape multibody software via PID controller tuning and chart flow process. which directs the forward, reverse, left, and right rotation of the flapping wing prototype efficiently, detailed in result chapter.

This research methodology elaborates on the process of addressing the objectives outlined in Chapter 1. It also includes a flow chart with clear labels to illustrate each step of the process.

The process of covering objectives defined is detailed in this research methodology with labeling at flow chart of Figure 3.2 below.

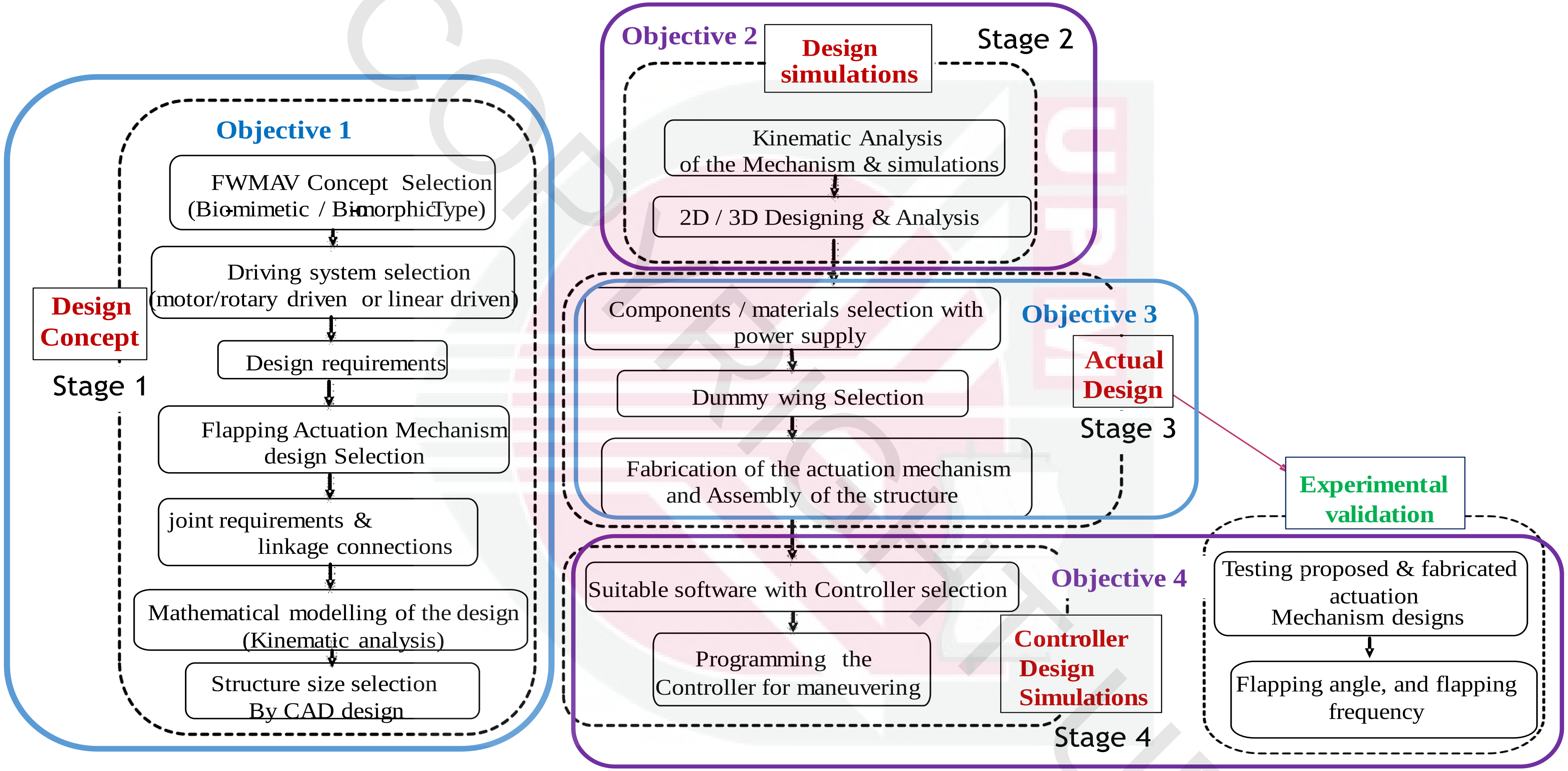

Figure 3.2 : Detailed Flow Chart of Research Methodology Implemented for Flapping Wing Prototype

3.3 Design Concepts with Kinematic Modelling

Kinematics is the discipline of physics that focuses purely on the analysis of motion, specifically without grabbing notice of the forces that are responsible for creating the motion. Researchers can get insight into the relative motion of different components inside a mechanical system by deducing kinematic equations. Having this comprehension is essential for devising mechanisms that can carry out specific tasks with effectiveness and efficiency. As illustrated by the types of design configurations considered at figure 3.1(b), the kinematic modelling of 3C design and crank-slider design are performed to verify its linkage movements. The details are as shown below.

3.3.1 Model - 3C Design

The linkage movement analysis is performed through forward kinematics and inverse kinematics (graphical method), also its angular velocities of final flapping link is analyzed through Jacobian velocity propagation method, as detailed below.

A Forward Kinematics

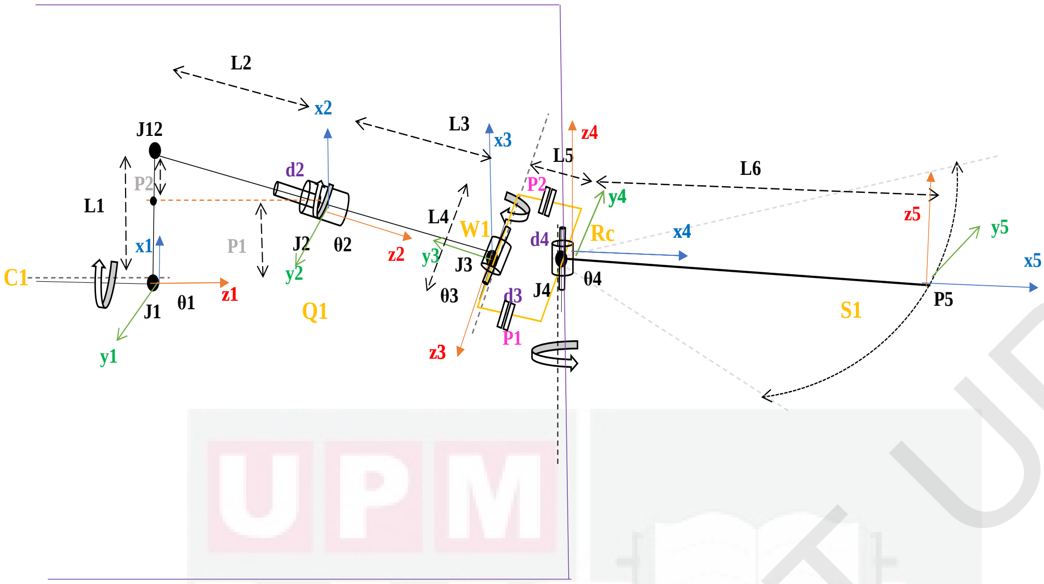

Figure 3.3 : Kinematic Structure of 3C Design Flapping Actuation Mechanism

The crank-driven mechanism's motion is characterized by the joint coordinate ψ (Jn), which is an aspect of the believed common coordinate vector (Andrzej Harlecki & Andrzej Urbaś, 2016; Harlecki & Urbaś, 2015) used in Figure 3.3 Where J represents joint coordinates of the system and n represents its position.

Assumed coordinates at joints C1,Q1,W1,Rc & S1 are as shown below and also in Figure 3.3:

$$q^{(J1)} = \{q_{C1}{}^{(J1)}\}_{C1=1} = \psi^{(J1)}$$

$$q^{(J2)} = \{q_{Q1}{}^{(J2)}\}_{Q1=1} = \psi^{(J2)}$$

But P1 ıı P2, considered to be single link L5, as the rectangle component at its one end it performs as a supporting inner link for cylindrical joint J3 to rotate along z3 axes. The another end the rectangle component is connected perpendicular to outer structure of cylindrical joint J4. Hence the whole rectangular component is here considered to be R_c. The tip of the wing is considered to be P5.

$$q^{(J3)} = \{q_{W1}{}^{(J3)}\}_{W1=1} = \psi^{(J3)}$$

$$q^{(J4)} = \{q_{R_c}{}^{(J4)}\}_{R_c=1} = \psi^{(J4)}$$

$$q^{(P5)} = \{q_{S1}{}^{(P5)}\}_{S1=1} = \psi^{(P5)}$$

The DH-Table obtained for the above shown mechanism i.e Figure 3.3 is as follows.

Table 3.1 : Denavit Hartenberg (DH) Table

n	$d_{z(i-1)}$	$\theta_{z(i-1)}$	$\alpha_{x(i)}$	$r_{x(i)}$
1	P2*tan(φ1)	θ1	0	P1
2	L3+d2	θ2	-90˚	- P1
3	± d3	-90˚+θ3	-90˚	L5
4	± d4	θ4	0	L6

They attempted to obtain the homogeneous transformation matrices from the DH-Table and assumed coordinate nodes linked to the standard reference are computed as follows:

$$T_1^0 = \begin{bmatrix} c\theta 1 & -s\theta 1.c(0) & s\theta 1.\text{s}(0) & (P1).c\theta 1 \\ s\theta 1 & c\theta 1.c(0) & -c\theta 1.\text{s}(0) & (P1).s\theta 1 \\ 0 & \text{s}(0) & \text{c}(0) & P2*tan(\varphi 1) \\ 0 & 0 & 0 & 1 \end{bmatrix}$$

$$T_2^1 = \begin{bmatrix} c\theta 2 & -s\theta 2.c(\text{-}90^\circ) & s\theta 2.\text{s}(\text{-}90^\circ) & (-P1).c\theta 2 \\ s\theta 2 & c\theta 2.c(\text{-}90^\circ) & -c\theta 2.\text{s}(\text{-}90^\circ) & (-P1).s\theta 2 \\ 0 & \text{s}(\text{-}90^\circ) & \text{c}(\text{-}90^\circ) & L3 + d3 \\ 0 & 0 & 0 & 1 \end{bmatrix}$$

$T_3^2 =$

$$\begin{bmatrix} c(\text{-}90^\circ + \theta 3) & -s(\text{-}90^\circ + \theta 3).c(\text{-}90^\circ) & s(\text{-}90^\circ + \theta 3).\text{s}(\text{-}90^\circ) & (L5).c(\text{-}90^\circ + \theta 3) \\ s(\text{-}90^\circ + \theta 3) & c(\text{-}90^\circ + \theta 3).c(\text{-}90^\circ) & -c(\text{-}90^\circ + \theta 3).\text{s}(\text{-}90^\circ) & (L5).\text{s}(\text{-}90^\circ + \theta 3) \\ 0 & \text{s}(\text{-}90^\circ) & \text{c}(\text{-}90^\circ) & \pm d3 \\ 0 & 0 & 0 & 1 \end{bmatrix}$$

$$T_4^3 = \begin{bmatrix} c\theta 4 & -s\theta 4.c(0) & s\theta 4.\text{s}(0) & L6.c\theta 4 \\ s\theta 4 & c\theta 4.c(0) & -c\theta 4.\text{s}(0) & L6.s\theta 4 \\ 0 & \text{s}(0) & \text{c}(0) & \pm d4 \\ 0 & 0 & 0 & 1 \end{bmatrix}$$

Where $c\theta n = Cos\psi^{(Jn)}$ and $s\theta n = Sin\psi^{(Jn)}$

Hence, the position of the flapping link is related to its initial reference position (Pn) by

T = $T_1^0 * T_2^1 * T_3^2 * T_4^3$

The flapping lever position and posture of during its actuation are characterized by the generated matrix in the following way, in accordance with the homogeneous transformation obtained from DH table 3.1.

$$T = \begin{bmatrix} R11 & R12 & R13 & PX \\ R21 & R22 & R23 & PY \\ R31 & R32 & R33 & PZ \\ 0 & 0 & 0 & 1 \end{bmatrix}$$

where T is a 4 × 4 transformation matrix whose elements are given by

R11 = $[C(\theta1 + \theta2)*S\theta3 * C\theta4] + [S(\theta1 + \theta2) * S\theta4]$

R12 = $[-C(\theta1 + \theta2)*S\theta3 * S\theta4] + [S(\theta1 + \theta2) * C\theta4]$

R13 = $[C(\theta1 + \theta2)*C\theta3]$

PX = $[C(\theta1 + \theta2)*S\theta3 * L6 * C\theta4] + [S(\theta1 + \theta2) * L6 * S\theta4] + [d4 * C(\theta1 + \theta2) * C\theta3] + \{[L5 * C(\theta1 + \theta2) * S\theta3] - [d3 * S(\theta1 + \theta2)] + P1[C\theta1 - C(\theta1 + \theta2)]\}$

R21 = $[S(\theta1 + \theta2)*S\theta3 * C\theta4] + [C(\theta1 + \theta2) * S\theta4]$

R22 = $[-S(\theta1 + \theta2)*S\theta3 * S\theta4] + [C(\theta1 + \theta2) * C\theta4]$

R23 = $[S(\theta1 + \theta2)*S\theta3]$

PY = $[S(\theta1 + \theta2)*S\theta3 * L6 * C\theta4] + [C(\theta1 + \theta2) * L6 * S\theta4] + [d4 * S(\theta1 + \theta2) * S\theta3] + \{[L5 * S(\theta1 + \theta2) * S\theta3] + [d3 * C(\theta1 + \theta2)] + P1[S\theta1 - S(\theta1 - \theta2)]\}$

R31 = $[C\theta4 * C\theta3]$

R32 = $[-C\theta3 * S\theta4]$

R33 = $-S\theta3$

PZ = $(C\theta3 * L6 * C\theta4) - (d4 * S\theta3) + [(L5 * C\theta3) + L3 + d3 + (P2 * \tan(\varphi1))]$

B Inverse Kinematics (Graphical Method)

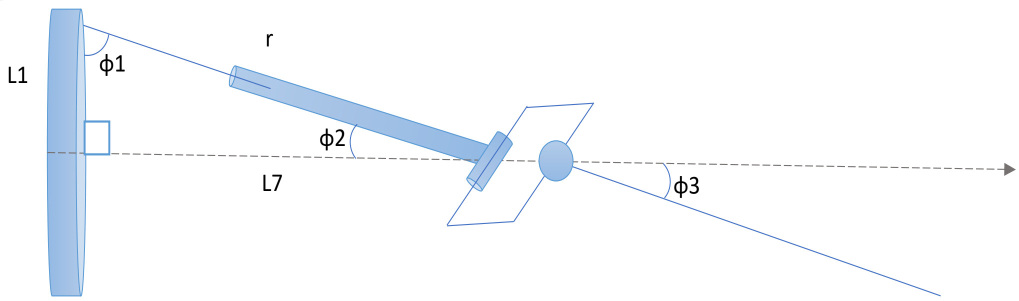

Figure 3.4 : Top View of the 3C Design Kinematic Structure

$\Theta 1 = \Theta 2$ as both are related to each other

Assume $r = L2 + d2 + L3$

From the top view of Figure 3.4, by using right angle triangle it can be written as

$$(r)^2 = (L1)^2 + (L7)^2$$

$$L7 = \sqrt{(r)^2 - (L1)^2}$$

$$= \sqrt{(L2 + d2 + L3)^2 - (L1)^2}$$

$\tan \varphi 2 = L1/L7$ i.e $\varphi 2 = \tan^{-1}\left[\frac{L1}{L7}\right]$

$\tan \varphi 1 = L7/L1$ i.e $\varphi 1 = \tan^{-1}\left[\frac{L7}{L1}\right]$

because L6 is in the same plane of r, it can say $\varphi 2 = \varphi 3$

hence $\Theta 3 = 2 * \varphi 2$ & $\Theta 4 = 2 * \varphi 3$

C Jacobian Velocity Propagation Analysis

The Jacobian matrix plays a vital role in the design of flapping actuation mechanisms. It helps to quantify the relationship between the actuator inputs and the resulting motion of the mechanism. As a result, the Jacobian matrix is crucial for understanding and optimizing the performance of flapping mechanisms, as it provides valuable insight into how different actuator inputs will affect the motion and overall behaviour of the mechanism. Flapping wing systems involve complex motion patterns, including translations, rotations, and deformations of the wings. The Jacobian matrix helps in analysing the kinematics of these motions by relating changes in joint angles or wing configurations to resulting changes in position and orientation of the wings.

This is crucial for understanding how different wing motions which indirectly affects airflow and aerodynamic performance too. Furthermore, the Jacobian matrix allows for the analysis of velocity and force relationships within the mechanism, helping to ensure efficient and precise motion control(Chimakurthi et al., 2009, 2011).

The Jacobian Analysis describes the relationship between the linear velocity and the angular velocity of the flapping link. The Jacobian-matrix transforms the linear velocity of the flapping link space in with respect to its joint actuator space. Also, it is very much necessary for motion analysis and trajectories path follow-ups.

$$J = \begin{bmatrix} J_V \\ J_w \end{bmatrix}$$

The Obtained Jacobian for the above derived mechanism / model is as shown below.

i.e the structural model referred from Figure 3.4.

$$J = \begin{bmatrix} -Y4 & -(Y4-Y1) & C_{12}(Z4-Z2) & S_{12}S_3(Z4-Z3)+S_3(Y4-Y3) \\ -X4 & -(X4-X1) & -S_{12}(Z4-Z2) & C_{12}C_3(Z4-Z3)+S_3(X4-X3) \\ 0 & 0 & -S_{12}(Y4-Y2)-C_{12}(X4-X2) & C_{12}C_3(Y4-Y3)-S_{12}S_3(X4-X3) \\ 0 & 0 & -S_{12} & C_{12}C_3 \\ 0 & 0 & C_{12} & S_{12}S_3 \\ 1 & 1 & 0 & S_3 \end{bmatrix} \begin{bmatrix} \dot{\theta}_1 \\ \dot{\theta}_2 \\ \dot{\theta}_3 \\ \dot{\theta}_4 \end{bmatrix}$$

$\boldsymbol{Note}$: $C1 = Cos\,\theta1$ and $S1 = Sin\,\theta1$

$C_{12} = Cos\,(\theta1 + \theta2)$ and $S_{12} = Sin\,(\theta1 + \theta2)$

$S_{12*} = Sin\,(\theta1 - \theta2)$

$$J=\begin{bmatrix}\dot{X}\\ \dot{Y}\\ \dot{Z}\\ \dot{\omega}_X\\ \dot{\omega}_Y\\ \dot{\omega}_Z\end{bmatrix}=$$

$$\begin{bmatrix}(-Y4*\dot{\theta}_1)-[(Y4-Y1)\dot{\theta}_2]+[C_{12}(Z4-Z2)\dot{\theta}_3]+[(S_{12}S_3(Z4-Z3)+S_3(Y4-Y3))\dot{\theta}_4]\\ (-X4*\dot{\theta}_1)-[(X4-X1)\dot{\theta}_2]-[S_{12}(Z4-Z2)\dot{\theta}_3]+[(C_{12}C_3(Z4-Z3)+S_3(X4-X3))\dot{\theta}_4]\\ \{[-S_{12}(Y4-Y2)-C_{12}(X4-X2)]\dot{\theta}_3\}+\{[C_{12}C_3(Y4-Y3)-S_{12}S_3(X4-X3)]\dot{\theta}_4\}\\ (-S_{12}*\dot{\theta}_3)+(C_{12}C_3*\dot{\theta}_4)\\ (C_{12}*\dot{\theta}_3)+(S_{12}S_3*\dot{\theta}_4)\\ \dot{\theta}_1+\dot{\theta}_2-S_3\dot{\theta}_4\end{bmatrix}$$

Where,

X1 = (P1* C_1)

Y1 = (P1* S_1)

Z1 = *P2*tan(φ1)*

X2 = P1$[C_1 - C_{12}]$

Y2 = P1$[S_1 - S_{12*}]$

Z2 = L3+d3+ *P2*tan(φ1)*

X3 = (L5$*$ $C_{12} * S_3$) – (d3*S_{12})+P1($C_1 - C_{12}$)

Y3 = (L5$*$ $S_{12} * S_3$) – (d3*C_{12})+P1($S_1 - S_{12*}$)

Z3 = (L5*C_3)+ L3+d3+ *P2*tan(φ1)*

X4 = PX = $[C_{12}{*}S_3 * \mathrm{L6} * C_4] + [S_{12} * \mathrm{L6} * S_4] + [\mathrm{d4} * C_{12} * C_3] + \{[\mathrm{L5} * C_{12} * S_3] - [\mathrm{d3} * S_{12}] + \mathrm{P1}[C_1 - C_{12}]\}$

Y4 = PY = $[S_{12}{*}S_3 * \mathrm{L6} * C_4] + [C_{12} * \mathrm{L6} * S_4] + [\mathrm{d4} * S_{12} * S_3] + \{[\mathrm{L5} * S_{12} * S_3] + [\mathrm{d3} * C_{12}] + \mathrm{P1}[S_1 - S_{12*}]\}$

Z4 = PZ = $(C_3 * \mathrm{L6} * C_4) - (\mathrm{d4} * S_3) + [(\mathrm{L5} * C_3) + \mathrm{L3} + \mathrm{d3} + (\mathrm{P2} * \tan(\varphi 1))]$

Generally, the Jacobian matrix is determined utilizing rotation matrix derivative, which is a vital resource for relating the joint space velocity to the flapping link velocity and interpreting nonlinearities within the working area. Likewise, the Jacobian matrix serves as the foundation for assessing Yoshikawa's measure and calculating the Manipulability Ellipsoid, indicating the flapping link's capacity to transform location and direction when given a joint configuration.

From the above equation the $\dot{X}, \dot{Y}$ *and* $\dot{Z}$ equations provides us the linear velocities in all x, y and z directions, similarly the $\dot{\omega}_X$, $\dot{\omega}_Y$ and $\dot{\omega}_Z$ provides the angular velocities in all x, y and z directions with respect to the wing tip.

3.3.2 Model – Crank Slider Design

A crank-slider mechanism has a crank, which is an arm that rotates, and a slider, which is an element that moves linearly. The crank-slider mechanism, in its conventional configuration, is commonly employed for achieving speedy return motion. In this setup, the crank undergoes uniform rotational motion, resulting in the slider moving swiftly in one direction and returning gradually in the opposite direction. This motion is advantageous in many applications such as reciprocating engines, presses, and shapers. Here the crank slider mechanism is initially considered as quick return form / fast return design for its movement analysis with analytical analysis of the basic design is performed. Then the same design is modified to four bar pattern analysis to generate flapping.

A. Analytical Modelling of Crank-Slider Design

While birds / aircraft travel, their own wings are conducted at a low angle, lightly trying to deflect air downwards. As a result, air pressure rises beneath the wings and lowers above them. The pressure difference produces lift, a force positioning approximately directly on wing upper layer that prevents the bird or aircraft from falling. Both lift and thrust are generated by forward and return flappable strokes. In contrast to normal hovering, asymmetric flapping generates the largest amount of vertical force during its downward stroke movement. 76% of the vertical force produced by asymmetric flapping is attributable to aerodynamic drag, demonstrating the quality of the performance (*Aerodynamics of Flapping Flight*, n.d.; Clawson et al., 2020; Fenelon & Furukawa, 2010; Park et al., 2012; Thierry et al., 2009).

By using slider crank technique as a basis, the authors developed a unique process consisting of two levers paired in a cross-x pattern, which is operated by a crank motor drive, as shown in Figure 3.5. In this instance, the fundamental architecture for transforming rotational movement to regulated angular flapping movement is indeed the X-shaped arrangement of two rapid return processes. As seen in Figure 3.6, this distinctive configuration of the rapid return technique is referred to as the main design concern. The critical elements of the concept of the flapping configurations are best illustrated using Figure 3.5, which was created using CAD program through Fusion 360 illustrated in further sections.

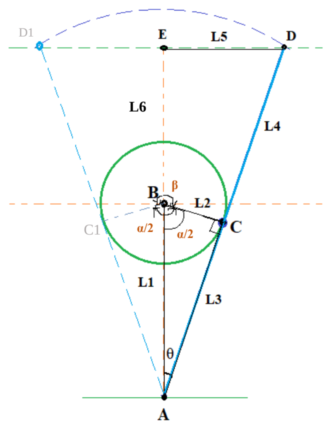

L1 = distance from A to B (fixed)
L2 = distance from B to C (crank radius)
L3 = variable length between A and C (piston sliding the slotted lever)
L4 = variable length between C and D
L5 = variable length between E and D (reciprocating lever and centre line)
L6 = distance from B to E (fixed)
α = angle of return motion from C to C1
β = angle of forward motion from C1 to C
2θ = angle of lever motion from D to D1

Figure 3.5 : Fast Return Mechanism

As illustrated in Figure 3.5, the rapid return system comprises of novel design coupled toward a disc which spins so at steady velocity. According to the motion of crankshaft, its arm glides across the slots grip, making the slotted lever to move linearly. The inclination of front motion over the crank is denoted by β, whereas the inclination of reverse motion is denoted by α. As according given in equation, the inclination about forward travel at the crank is proportional to the angle of return motion at the crank (eqn. 3.1). Moreover, the processing module period necessary for lever forth some motion exceeds the time necessary for lever returning motion. As the returning movement of the sliding-lever is rapid compared to its front movement, this type of connection can be said to be rapid return technique.

$$\frac{time\ for\ forward\ motion}{time\ for\ return\ motion} = \frac{t_f}{t_r} = \frac{\beta}{\alpha} = \frac{2\pi - \alpha}{\alpha} \qquad (3.1)$$

If the flaps produced at wings are symmetrical without bending or twisting, the average lift across one cycle-period must be nil. however, asymmetric flapping at wings results in a positive average lift. In symmetric flapping, the time spent for downstroke and upstroke is the same. Moreover, in asymmetric flapping, the time required for downstroke (t_{down}) is much greater than the time required for upstroke (t_{up}) (Yu & Tong, 2005). In 2011, Shreyas *et.al.,* (Shreyas et al., 2011) demonstrated the flow field development of symmetric and asymmetric flapping, indicating t_{down} is less than $t_{up.}$ In contrast, inclination including forward progress at the crank exceeds the inclination of return motion at the crank. As a result, the time needed for lever forward motion is longer than return movement of lever. Hence the Angular velocity for forward motion is different compared to the angular velocity of return motion.

Symmetry and asymmetry in relation to flapping wing drones can manifest themselves in the following ways.

1. Variation in speed/ timing of forward and return stroke movements.
2. Distinct ranges of motion for both side wings.
3. Left or right wings having same range but move at a different time/speed.

   (The above said conditions could occur as a result of a flapping actuation mechanism design or a variation in linkage alignments).
4. Controlled asymmetric flapping (to make controlled flight turns).
5. Transmission from Symmetry to asymmetry and vice versa is possible to achieve desired flight maneuvers.
6. In-phase Symmetric and asymmetric flapping.

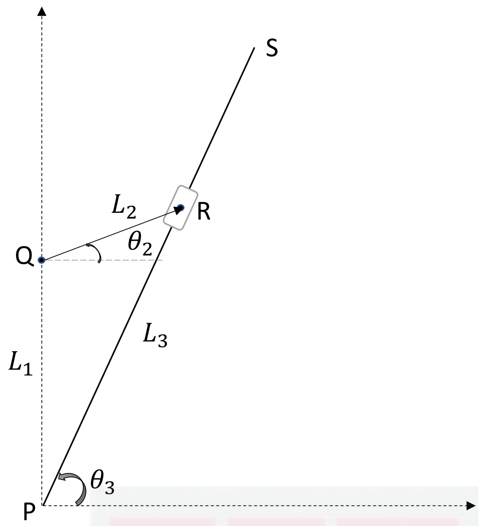

Note:
PS: flapping lever
QR: crank radius
R: slider point at crank
Q: centre point of crank
P: flapping lever end connected to a hinge
S: free end of the flapping lever
L1: length of QP (fixed)
L2: length of crank radius (fixed)
L3: length of PR (varying)
θ2: crank rotation angle
θ3: lever flapping angle

Figure 3.6 : Standard Sliding Lever Mechanism Concept

Depending on the crank rotation, the arm slides along the lever another edge, producing forward and return motion of the lever. The angle of forward motion at the crank, is greater than the angle of return motion at the crank. As a result, the time required for lever forward motion is greater than the time required for lever return motion. Because the lever's backward movement is quick than its in-flow movement, it is also known as the slotted lever mechanism. the proposed sliding lever system is considered here to be asymmetric due to its flapping speed variations in its forward and return stroke. Figure 3.6 is same representation of Figure 3.5 with length indications.

- ***Analytical Solution:***

By obtaining analytical solutions for velocity and acceleration, its easy to gain valuable insights into the behaviour of mechanical designs, and predict their performance under different conditions, for the optimization of their design parameters to obtain desired outcomes. These solutions are essential for the design, analysis, and control of a wide range of mechanical systems and mechanisms. Kinematic equations can be utilized to develop analytical solutions for the velocity and acceleration of mechanical designs. These equations delineate the correlation between position, velocity, and acceleration for various forms of motion. An analytical solution has been obtained from PQR in Figure 3.6.

From ΔPQR,

$$\cos\left(\frac{\pi}{2}+\theta_2\right) = \frac{(L_1)^2+(L_2)^2-(L_3)^2}{2(L_1L_2)}$$

$$(L_3)^2 = (L_1)^2 + (L_2)^2 - Cos\left(\frac{\pi}{2}+\theta_2\right)2(L_1L_2)$$

$$L_3 = \sqrt{(L_1)^2 + (L_2)^2 - Cos\left(\frac{\pi}{2}+\theta_2\right)2(L_1L_2)} \quad \text{or}$$

$$L_3 = \sqrt{(L_1)^2 + (L_2)^2 + 2(L_1L_2)Sin(\theta_2)}$$

Also $L_3(Cos\,\theta_3) = L_2(Cos\,\theta_2)$

$$\theta_3 = Cos^{-1}\,\frac{L_2(Cos\,\theta_2)}{L_3}$$

- ***Velocity:***

$$V = \frac{d}{dt}\theta_3 = \frac{d}{dt}\left[Cos^{-1}\,\frac{L_2(Cos\,\theta_2)}{L_3}\right]$$

Let $x = \left[\frac{L_2(Cos\,\theta_2)}{L_3}\right]$

$$V = \frac{d}{dt}[Cos^{-1}(x)]$$

$$V = \frac{-1}{\sqrt{1-x^2}} \cdot \frac{dx}{dt} \quad = \frac{-1}{\sqrt{1-\left[\frac{L_2(Cos\,\theta_2)}{L_3}\right]^2}} \cdot \frac{d}{dt}\left[\frac{L_2(Cos\,\theta_2)}{L_3}\right]$$

$$V = \frac{-1}{\sqrt{1-\left[\frac{L_2(Cos\,\theta_2)}{L_3}\right]^2}} \cdot \left[\frac{-L_2(Sin\,\theta_2).w}{L_3}\right] \qquad \text{Where} \qquad w = \frac{d}{dt}\theta_2$$

- ***Acceleration:***

$$Accel = \frac{d}{dt}\,V = \frac{d}{dt}\left[\frac{-1}{\sqrt{1-\left[\frac{L_2(Cos\,\theta_2)}{L_3}\right]^2}} \cdot \left[\frac{-L_2(Sin\,\theta_2).w}{L_3}\right]\right]$$

Let $y = \frac{L_2}{L_3}.w$, hence $Accel = \frac{d}{dt}\left[\frac{y}{\sqrt{1-[x]^2}}.[\,Sin\,\theta_2\,]\right]$

$$Accel = y(Sin\,\theta_2).\left[\frac{x}{[1-(x)^2]^{\frac{3}{2}}}\right].\frac{dx}{dt} + \frac{y}{\sqrt{1-[x]^2}}.[\,Cos\,\theta_2\,].w$$

$$Accel = y\left[(Sin\,\theta_2).\left[\frac{x}{[1-(x)^2]^{\frac{3}{2}}}\right].\frac{dx}{dt} + \frac{1}{\sqrt{1-[x]^2}}.[\,Cos\,\theta_2\,].w\right]$$

$$= \frac{L_2}{L_3}.w\left[(Sin\,\theta_2).\left[\frac{\left[\frac{L_2(Cos\,\theta_2)}{L_3}\right]}{\left[1-\left[\frac{L_2(Cos\,\theta_2)}{L_3}\right]^2\right]^{\frac{3}{2}}}\right].\left[\frac{-L_2(Sin\,\theta_2).w}{L_3}\right] + \right.$$

$$\left.\frac{1}{\sqrt{1-\left[\frac{L_2(Cos\,\theta_2)}{L_3}\right]^2}}.[\,Cos\,\theta_2\,].w\right]$$

B. Four Bar Pattern Analysis

As demonstrated in Figure 3.5, the modified design process is employed to produce a regulated inclination of flapping out of a spinning crank-slider design. It serves the exact required purpose as regular slider-crank device or a rapid backward movement method and is beneficial whenever the necessary sweep of the reciprocating motion is modest relative to the proportions of the operating crank**.** Figure 3.5 consists of a crank and slider mechanism driven by a motor. The sliding levers relate to two rod linkage forming triangular approach of connection as shown in Figure 3.7. Hence it is a 4-bar linkage (*Four-Bar Linkage - Wikipedia*, n.d.), connection for converting rotary movement to specific angular flapping movement. Like the torque increases, the crankshaft attached to it starts turning towards the identical orientation, forcing the cranked lever to operate adjacent slotting lever throughout the reverse manner. The fixed hinge O is considered to be origin of the coordinate connected at link1 (l_1), and the link1 is driven by a crank slotter mechanism. θ1 is the instantaneous angle created by slider link1 at origin, θ2 and θ3 are the instantaneous angle created by link2 and 3 in coordination. θ4 is the angle created by the link3 at point C. As illustrated in Figure 3.7, the range of link 1 is limited due to the fact that it is driven by a crank slider mechanism. The movement of links 2 and 3 is dependent on the crank-driven movement of link 1. Because the linkages self-assemble in the shape of a triangle, it can obtain the required relationships between the crank slider mechanism's links by applying the triangle inequality (Natesan, n.d.).

That is ,

$$(l_1 - l_4) < (l_2 + l_3) \tag{3.2}$$

however, from Figure 3.7,

$$(l_1 + l_2) > (l_3 + l_4) \tag{3.3}$$

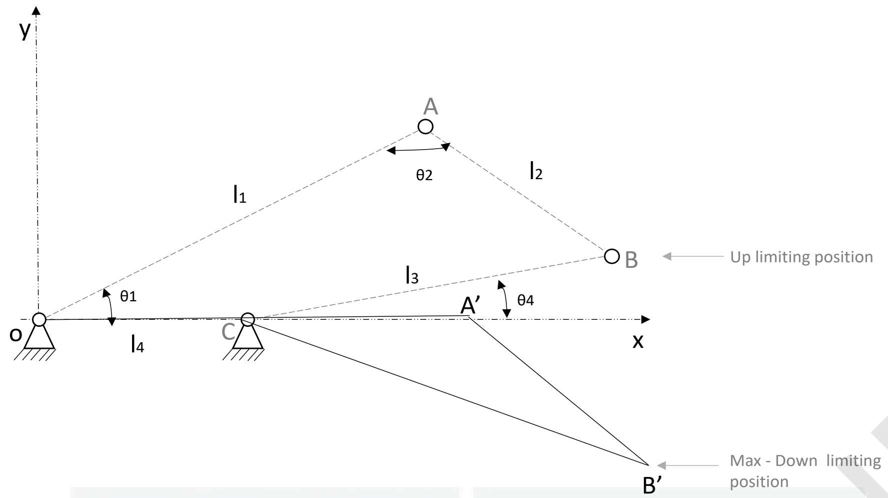

Figure 3.7 : A Limiting Positions of the Flapping Wing Mechanism

Also from eqn (3.5),

$$\textit{time ratio (Q)} = \frac{time\ of\ nornmal\ stroke}{time\ of\ quick\ retun\ stroke} \geq 1 \qquad (3.4)$$

Equations for the angular displacement obtained from geometry is,

$$[l_1 \cos(\theta 1)+l_2 \cos(\theta 2)] > [l_3 \cos(\theta 3)+l_4 \cos(\theta 4)]$$

$$[l_1 \sin(\theta 1)+l_2 \sin(\theta 2)] > [l_3 \sin(\theta 3)+l_4 \sin(\theta 4)] \qquad (3.5)$$

When the slider position at the crank exceeds 90 degrees, link1 reaches its maximum position, dragging link3 via link2 along with it. When the slider position at the crank exceeds 270 degrees, link1 reaches its minimum position, dragging link3 via link2 along with it. The up and down limiting positions are as shown in the Figure 3.7. Minimum transmission angle (H. Jiang et al., 2017), can be obtained from triangular relationship during maximum down limiting position.

i.e $\rho = \arccos[((l_2)^2 + (l_3)^2 - (l_1 - l_4)^2)/2.l_2.l_3]$ (3.6)

The perforated mechanism travels in the both directions linearly with a rotational pitch motion, producing a 25°-35° range of movement. In Flapping Wing Micro Aerial Vehicle (FWMAV) applications, the lever's fluttering action could also be leveraged to create movement by mounting winged design to the slot connection. One complete round of the crankshaft enables the notched fulcrum to generate two flaps. By modifying the dimensions of links AB, BC, and AD as shown in Figure 3.5, also it can easily modify the stroke angles and flapping asymmetry (the lag effect between both the two wings during its flapping motion). Figure 5.4 depicts the simulations of the lever motion analysis. The structural analysis of the fast return mechanism for the flapping wing was done using commercially available modelling software. The analysis involves four main steps to solve any modelled problem. In the preliminary step, the creating of the geometry, mentioned the type of analysis and elemental parameters. The pre-processing steps were carried out by adding the material properties and boundary conditions. The solution steps have mesh plot and form of restraints and loads. The final stage is postprocessing, which involve deformation, mode shapes and stress distribution are to be computed. In the present study, the flapping wing structure of the model is developed and evaluated its stresses and deformation under static loading conditions.

3.4 CAD Design of FW-Mechanisms

The utilization of Computer Aided Design modelling for flapping actuation mechanisms allows engineers to effectively create, analyse, and optimize the design, resulting in the production of durable and high-performing mechanisms for a wide range of applications. For the flow chart of design types shown in Figure 3.1(b), the 3D CAD designs are built and briefed as follows.

3.4.1 Motor Actuated 3C Design Mechanism

There is currently no simple flapping actuation mechanism with triple cylindrical joints axes arranged in a perpendicular direction to each other that can be used for flapping generation. It is critical to reduce the complexity of the flapping actuation mechanism designs, which in turn reduces the overall weight of the system consequently.

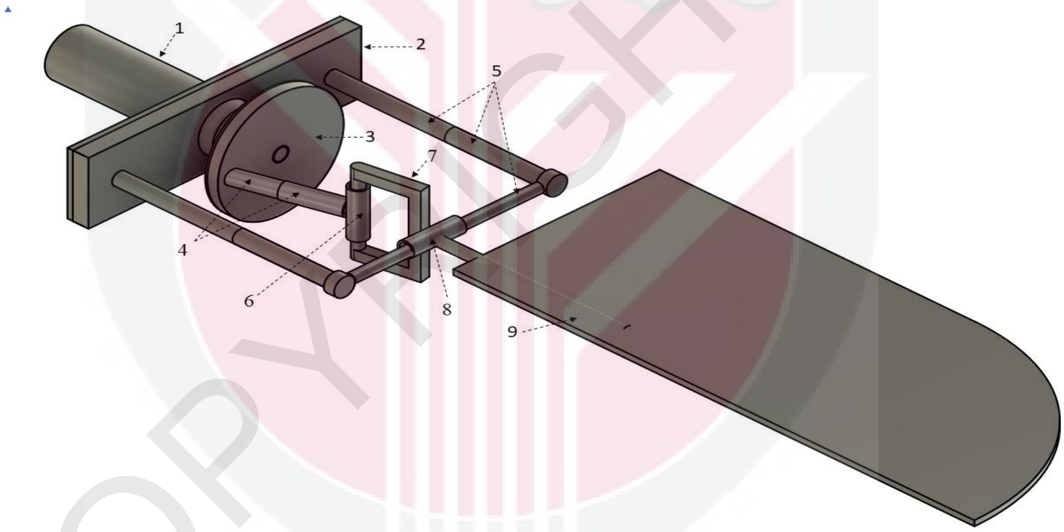

Figure 3.8 : Novel 3C Flapping Actuation Mechanism Design

They developed a novel and less complex mechanism for flapping actuation called the "Crank driven – triple cylindrical slidable and rotatable joint " mechanism arrangement. The fundamental connection for converting rotary motion to specific angular movement of flaps in this case is a horizontal path formed by three cylindrical joints, where the axes of all three joints are perpendicular to each other. Using joint coordinates and homogeneous transformation matrices, the geometry of the system was described. A crank driven triple cylindrical connection arrangement is unique and easily designable with minimal components. In this mechanism, generated motion and flapping is considered for the all-cylindrical joints C_n of the proposed mechanism design. the mechanism is arranged in freely rotatable and slightly slidable joint. where in the first cylindrical joint one end of the outer cylinder is connected to a crank and another end is open. Similarly, one end of the indirectly connected link inside the cylindrical is open/ freely movable and another end of it is connected to second cylindrical joint as shown in Figure 3.8. The rotational force reaction acting on the connected links are elaborated in Figure 3.4 above. The built CAD model is from the derived basic concept of Figure 3.3.

3.4.2 X-Pattern Crank-Slider Four-Bar Mechanism Design

Typically, a sliding attachment with crank is a 4-bar (F. .Sukarman, 2017) coupling system that includes 3R (joints with revolute motion) and one 1P (sliding/prismatic-joint), and has been utilized frequently in applications involving flapping wing aerial vehicles. In any FWMAV, the rotation of the crank drives the linear movement/ sliding, which generates downward and upward strokes at the levers. There are two primary kinds of slider-cranks: in-line and offset. In an in-line configuration, the slider is positioned so that the line of passage of the slider's hinge joint follows the supply joint of the crank.

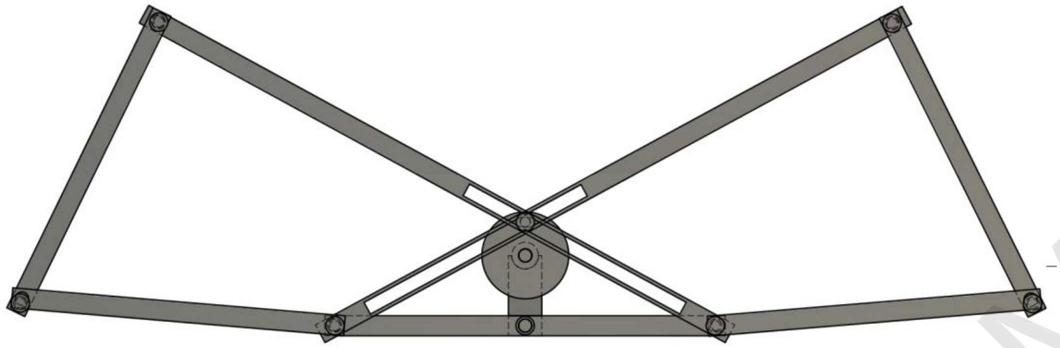

Figure 3.9 : CAD Model of Mechanism Design I for Flapping Actuation

Because the crank rotates, a symmetrical linear motion of the slider is produced in both opposite directions. In a slider with an offset configuration, the axis of passage of such slider's rigid frame doesn't really travel through crank's primary pivot, resulting in a lopsided action. However, its speed in reverse is greater than its speed in forward travel. This is called a rapid return technique. Numerous additional design processes have revealed variances or latencies in the wing inclination trajectory of both side wings (Park et al., 2012). The CAD model of figure 3.9 was constructed based on the derived fundamental notion of figure 3.7.

3.4.3 Concept of Proposed Design Mechanism-II

Generally, a slider actuated crank connection is a 4-bar linkage system, made up of three revolute joints and one prismatic (or sliding) joint, used commonly in flapping wing aerial vehicle application. Where the rotation of the crank drives the specific angular movement, or slider creating flaps of up and down strokes at the lever in any FWMAV.

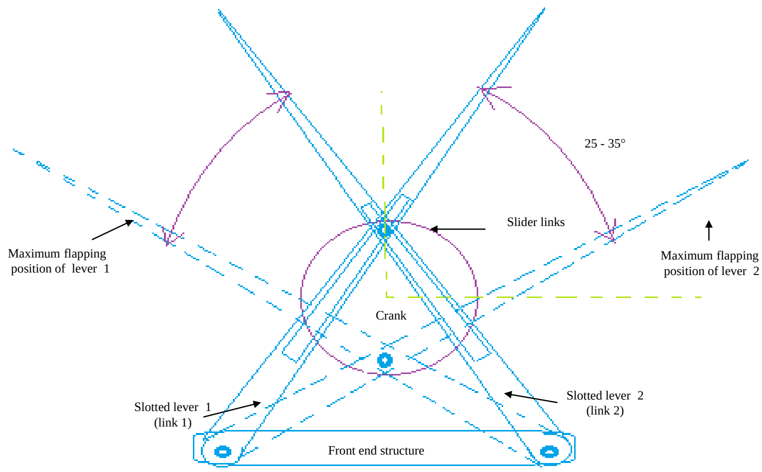

Figure 3.10 : SC-SDL Design Mechanism-II

Slider cranks are classified into two main types: in-line and offset. The slider on an in-line arrangement is placed such that the line of transit of the slider's hinge joint moves according to the source joint of the crank. i.e., As the crank spins, this causes a corresponding symmetric slider motion in up and down pattern. while in the slider on an offset arrangement, the line of transit of a of the slider's hinge joint does not pass via the source pivot of the crank, creating the slider motion is asymmetric way. but it moves more quickly in the returning path than the forward path of its motion. This is referred to as a quick-return mechanism. Using the slider crank mechanism as a reference model, a novel design known as the Single Crank - Slotted Dual Lever (SC-SDL) mechanism is being created as in Figure 3.10. The basic design for converting rotary motion to specific angular motion in this case is the arrangement of two quick return mechanisms in an X fashion. this unique arrangement of the quick return mechanism is referred here as the single crank and slotted dual lever mechanism, as shown in Figure 3.10, which is modified version of Figure 3.6.

The quick return mechanism is composed of an arm connected to a disc that revolves at a consistent speed. Based on the movement of the crank, the arm slides along the slotted lever, causing the lever to swing forward or return stroke angle pattern. But at the other side, the angle of forward motion of the lever is greater than the angle of reverse motion. Consequently, the time required for the lever forward stroke exceeds the time required for lever return stroke. Because the return motion of the lever is quicker than its forward motion, this mechanism is known as the quick return mechanism. A single crank - dual slotted lever mechanism is being utilized to generate a repeated angle of flapping motion driven by a crank rotation. It performs the similar function as a slider-crank mechanism or a quick return concept and It is particularly helpful when the necessary stroke of the actuated flapping angle is less in comparison to the dimensions of the driving crank system. As the motor rotates, the crank connected to it begins to rotate in the same direction, causing the crank to drive both slotted levers in the opposite direction. The lever will move in a specific angular motion, i.e pitch action in the opposite direction, creating a 25°-35° angle of motion. By connecting wings at the tip of the slotted lever, the flapping motion of the lever could be used to generate lift in FWMAV applications. One full rotation of the piston causes the slotted lever to create 2 flaps, i.e., up and down strokes. Figure 3.10 depicts the simulations of the lever motion analysis.

The basic components of the flapping actuation mechanism design-I are best described using the Figure 3.11, with its CAD modeling in Fusion 360 software. It consists of the following components:

- Base – serves as a support for the front and back-end structure frames.
- Front end structure – a frame that supports two lever slots that are connected across it.
- Backend structure - consists of a triangular-shaped supporting frame that holds the motor.
- Motor – a micro-DC motor for rotation that is linked to a crank.
- Crank – a rotary gear-like structure with no teeth and a rod-like projection on one side.
- Slotted lever- two levers with rectangular slots in the middle that connect to the crank in an X pattern.

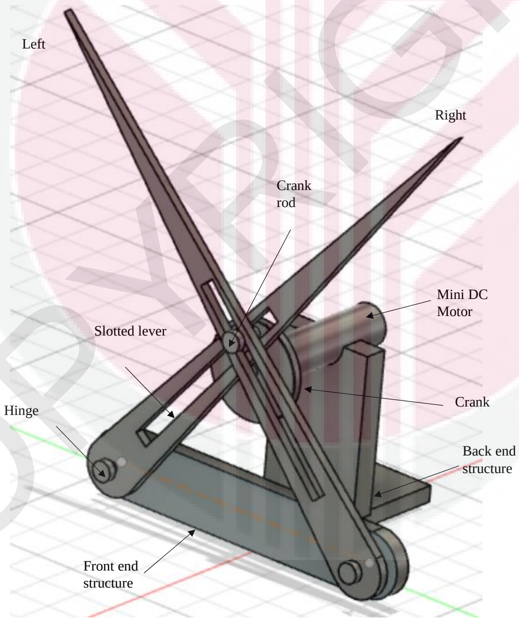

Figure 3.11 : X-Pattern Crank-Slider Four-Bar Mechanism Design

The 3D design and modelling of Double-Slider piston mechanism, (which converts rotary motion of the motor linked with the piston gear into flapping movements of the needles where sliders of the needles are connected through piston in X pattern) has been carried out successfully in Catia V5 software. The Finite Element Analysis is versatile approximation tool for designing and optimization of the flapping actuation model which is applied here to check its structural deformation ability. Two different size meshes are applied and compared for the results of von stresses and displacement of it. The optimization is carried out only for the critical parts of the model, like flapper needle and gear with piston, by changing the material from aluminum to steel. For piston and flapper needle by altering its thickness from 0.8 mm to 1mm hence it can get better and improved design model. These changes will strengthen the components of the model, allowing us to increase the load capacity of the base. Also, it is possible to minimize the vibration at body during flapping generation through the needles, because of the usage of the strong material steel.

3.4.4 Modified SC-SDL with Single Motor (Mechanism III)

In this revised design mechanism-III (Crank and Lever Transmission of Revised Design), both the hinges and the motor shaft with crank are aligned to the origin of the horizontal plane. In comparison to the design mechanism -III, the lever in this case is also extended beyond the hinge connection and is regarded as a flapping lever tip. As illustrated in Figure 3.12, both levers are placed opposite each other. The front-end and back-end structures are avoided in this revised mechanism to reduce overall design weight. The base structure is used here on the motor's top edge to provide support for both hinges. As in the first design, a single motor drives the crank, and the crank's rotation is converted to specific angular motion/flaps by a sliding arrangement at one end of the lever via its slots. The angle of motion produced at its hinge connection will be almost 20-30 degree, which is bit lesser when compared to design-II flapping angle. Figure 3.13 depicts the CAD modelling of the revised design mechanism -III**.**

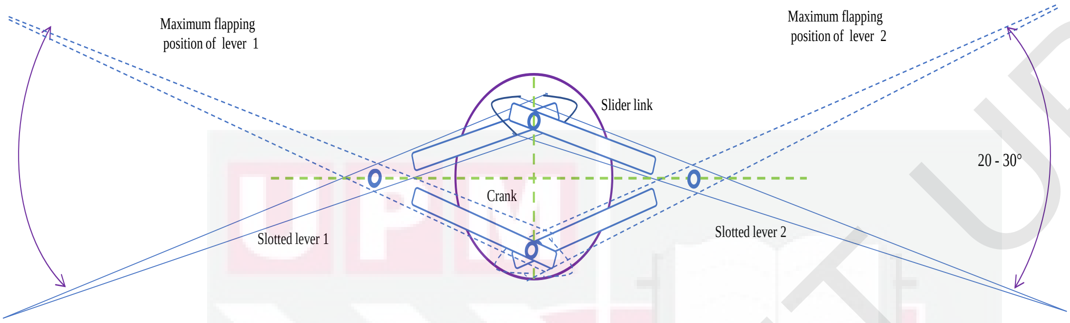

Figure 3.12 : SC-SDL Design Mechanism-III

Figure 3.13 best illustrates the basic components of the flapping actuation mechanism design-II, which was CAD modelled using Fusion 360 software.

- Base structure – serves as a support for the hinges and levers, fitted on the motor top edge.
- hinges–are a bolt-and-nut idea structure that stands on the base structure to provide support for two levers along its holes that are coupled.
- Slotted lever-two levers with rectangular curved slots on one edge (that surrounds the crank rod by stacking on each other) and a sharp tip on the opposite edge of the lever (where the wings will be attached)
- Motor - a miniature DC motor for driving the crank, which indirectly drives the slotted levers.
- Crank - a circular framework with no teeth and a rod-like extension on its one side.

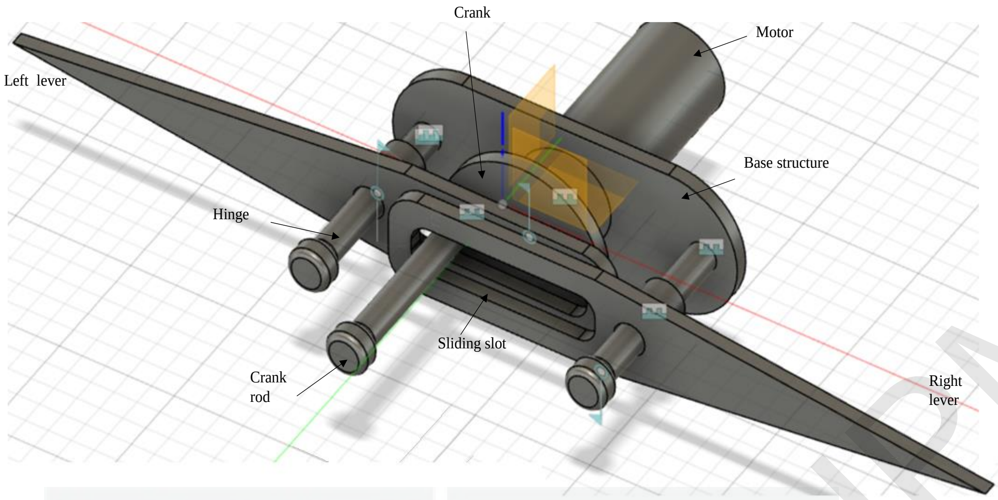

Figure 3.13 : CAD Model of SC-SDL Design -III, a Motor Driven Single Crank - Dual Slotted Lever Mechanism for Flapping Actuation

3.4.5 CAD Design of DC-SDL Mechanism (Mechanism IV)

In the proposed design mechanism, both the hinges and the motor shaft with a crank are aligned to the origin of the horizontal plane. In comparison to the basic design of sliding lever concept (S. Singh, Muralidharan, et al., 2022), the lever in this case is extended beyond the hinge connection and is regarded as a flapping tip. As illustrated in Figure 3.14, both levers are placed opposite each other. The base structure is used here on the motor's edge to provide support for both hinges. the individual motor drives the respective crank, and the crank's rotation is converted to angular flaps by a sliding arrangement at one end of the lever via connected slots.

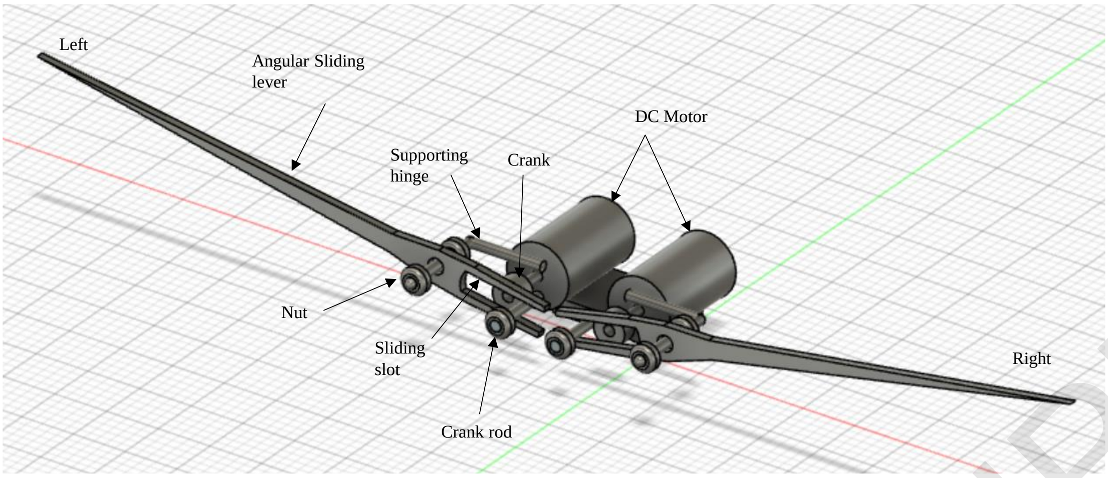

Figure 3.14 : Isometric View (CAD Model) of the DC-SDL Mechanism

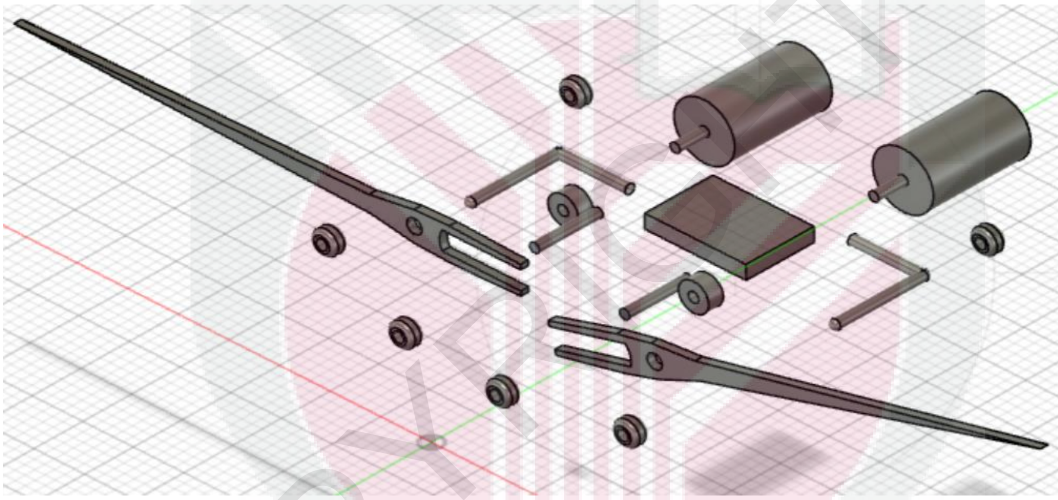

Figure 3.15 : Exploded View of the Proposed DC-SDL Design

The angle of motion produced at its hinge connection will be between 30-50 degrees depending on the arrangement. Figure 3.14 depicts the isometric view (CAD model) of the design mechanism. Figure 3.15 depicts the explode view of the proposed system design.

3.4.6 SC-SDL Mechanism Designs with Coin/Button Motors

In this section, the design proposed is same as revised design mechanism-III (Crank and Lever Transmission of Revised Design, i.e SC-SDL) where both the hinges and the motor shaft with crank are aligned to the origin of the horizontal plane as in Figure 3.16. Only the driving motor is replaced by the button motor. In electronic devices, button vibrators have been used as linear actuators by providing vibration and haptic feedback. However, they endeavored to use it as a rotating motor for flapping action in an effort to create the smallest insect-like structure possible. The Single Crank-Sliding Dual Lever mechanism design with single button motor is as shown in Figure 3.16 below.

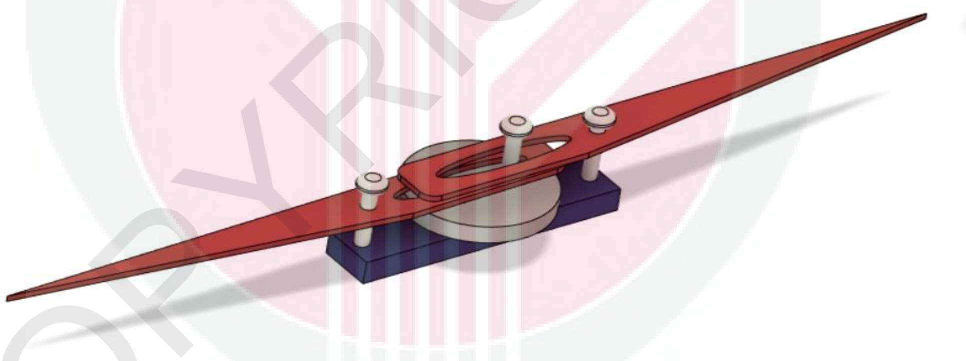

Figure 3.16 : Single Crank-Sliding Dual Lever (SC-SDL) Model with Single Button Vibration Motor as Driving Source

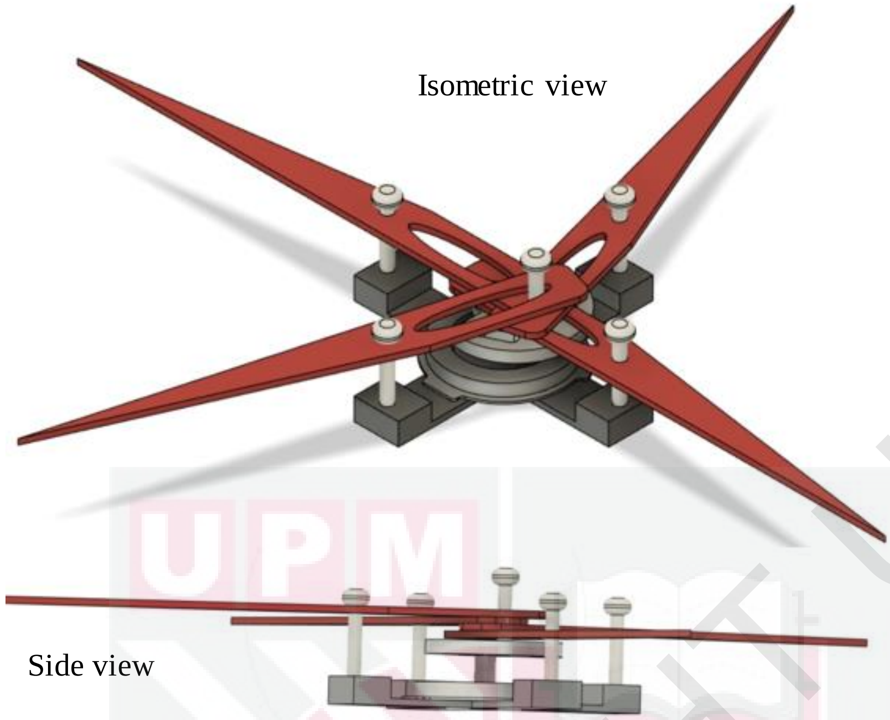

Figure 3.17 : Single Crank-Sliding Quad Lever (SC-SQL) Model with Single Button Vibration Motor as Driving Source

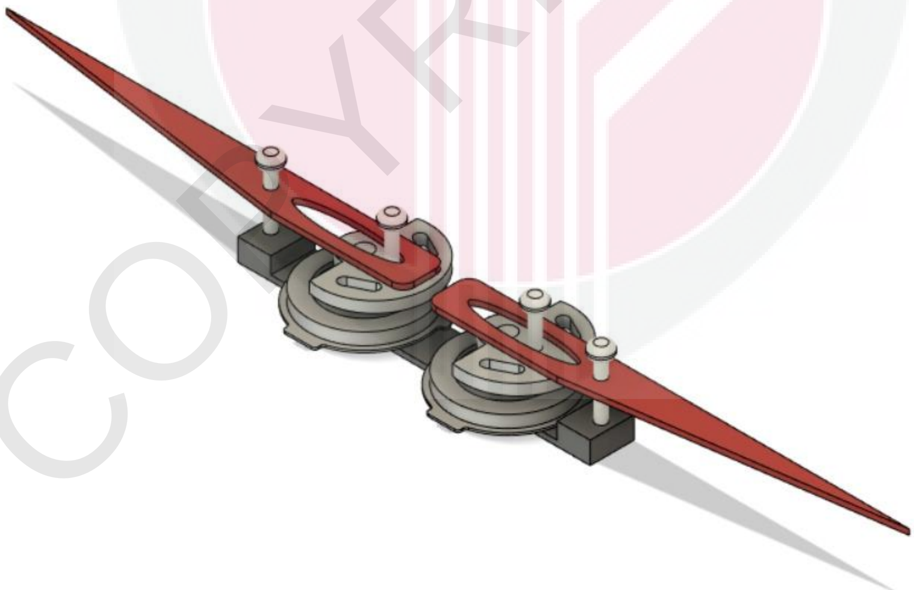

Figure 3.18 : Dual Crank – Slotted Dual Leavers (DC-SDL) Model with Dual Button Vibration Motor as Driving Source for Individual Wing

The proposed design is being implemented in CAD as shown in Figure 3.16. where button vibration motor is been used as driving crank for both the levers that are placed opposite each other. a single button vibration motor drives the crank, and the crank's rotation is converted to specific angular motion/flaps by a sliding arrangement at one end of the lever via its slots. The angle of motion produced at its hinge connection will be almost 15-22 degree, which is bit lesser when compared to flapping angle of above discussed chapters designs. The same design is modified by adding two additional levers, resulting in slotted quad levers as shown in Figure 3.17. Also depicts side view illustrating how the levers are stacked one on top of the other to facilitate ease movement of all four levers. Figure 3.18 depicts the CAD design of the revised design mechanism -III, driven by button motor, i.e. Dual Crank – Slotted Dual Leavers (DC-SDL) model with dual button vibration motor as driving source for individual wings.

3.5 Fabrication Process of FW- Design Types

Micro DC motors play an essential role in flapping wing designs, particularly in miniature or micro aerial vehicles (MAVs) that mimic the flight of birds or insects. Here are several significant reasons why micro-DC motors are essential for flapping wing designs, as Flapping wing designs necessitate a small, lightweight driving source to generate the required motion. Micro DC motors acquires the necessary less power to propel the wing flapping motion. They can deliver high torque and rotational speed, enabling efficient wing motion. Micro DC motors are designed to be compact and light, making them suitable for use in miniature robotic systems. These motors are typically small, enabling the miniaturization of flapping wing mechanisms, which is essential for MAVs that must be agile and manoeuvrable.

Therefore, the Micro DC motor is regarded as the primary power source for the construction and assembly of flapping wing models. The fabrication process encompasses two distinct methods: one is the manual design approach, while the other involves the use of 3D printed designs. Handmade designs are sometimes used due to the need for micro-sized designs. However, when it comes to achieving exact design sizes, 3D printers are preferred for their ability to ensure uniformity in lever design standards. The fabrication procedure for several flapping wing design models is outlined below.

3.5.1 Fabrication of 3C Design Model

By referring to the CAD design from Figure 3.8, The 3C model design is fabricated using a manual approach to decrease its overall size, as it comprises of three joints as in Figure 3.19 below. The wing is directly attached to the output link of a rotary to flapping conversion mechanism. The design possesses the minimal friction and fast mechanical transmission characteristics necessary to achieve better flapping motion. However, it could obtain max 18-20 degrees of flapping angle through this actuation mechanism, which is similar to the simulation results. The actuator's flapping consistency is measured through a photoelectric sensor with a counter utilized to measure its frequency as shown in Figure 3.20.

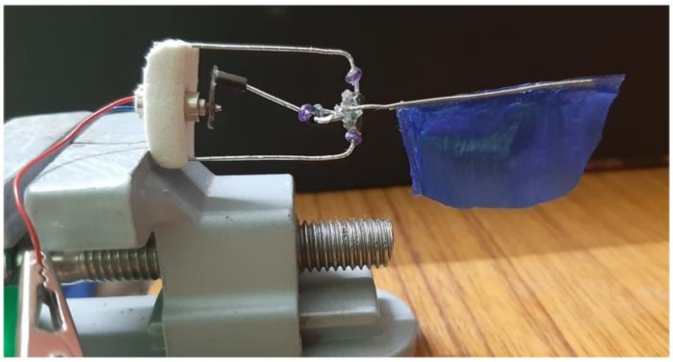

Figure 3.19 : The Flapping Actuation Mechanism's Test-Bench Design

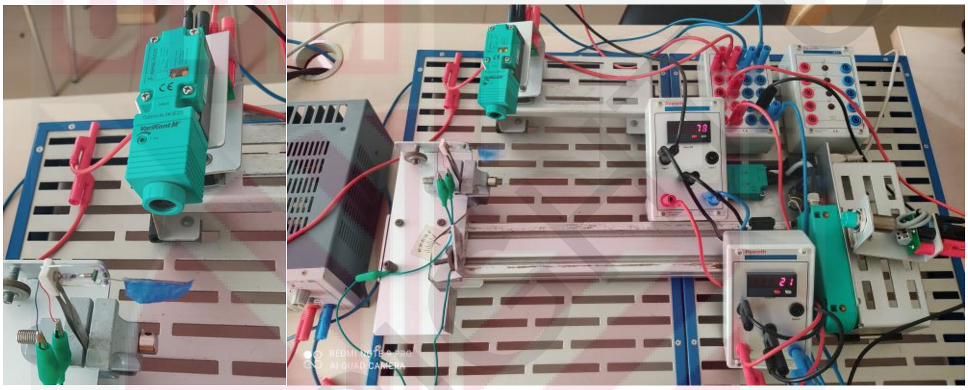

Figure 3.20 : Flapping Frequency Measuring Setup

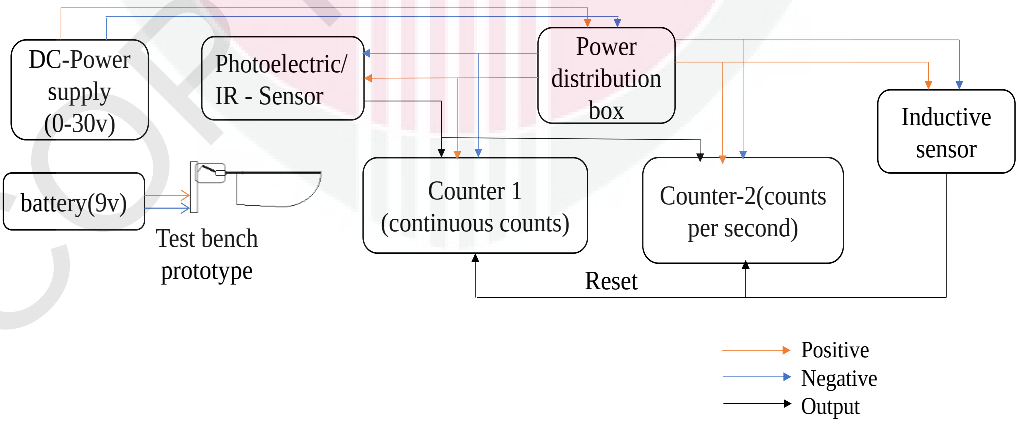

Figure 3.21 : Equivalent Circuit Diagram of Flapping Frequency Measuring Setup

By considering dc input power of 30v at the distribution box, and the same supply is distributed to proximity sensors and counters, as shown in Figure 3.20 and Figure 3.21. A constant 9v battery source has been applied separately to power the test bench model. also took care of Calibration of sensors during initial tests. When the infrared sensor detects wing motion, it begins transmitting its output to counters. Counter-1 counts the detected flaps continuously by displaying them, and counter-2 is programmed to count the number of flaps/counts per second, i.e., frequency. Additionally, the inductive sensor's output resets the values of the counters.

3.5.2 Fabrication of X-Pattern (Crank-Slider) Four-Bar Mechanism Design

A motor-driven crank-controlled fast return mechanism designed for flapping actuation of Micro Aerial Vehicle wings is fabricated in 3D printer with X-pattern Four-bar mechanism as in Figure 3.22. Because of its rapid return qualities of its lever, the ratio between both strokes differs. Consequently, investigations and computational methods of flapping properties have substantiated the proposed approach. Process factors analyzed throughout simulated results include flapping intensities, flap angles, angular speed, angular acceleration, torque, and force applied on the system architecture. Additionally improper boundary conditions resulted in lag in one of its levers during flapping. The proposed motor-driven flapping actuation mechanism is structurally analyzed and validated to ascertain its suitability for micro aerial vehicle applications.

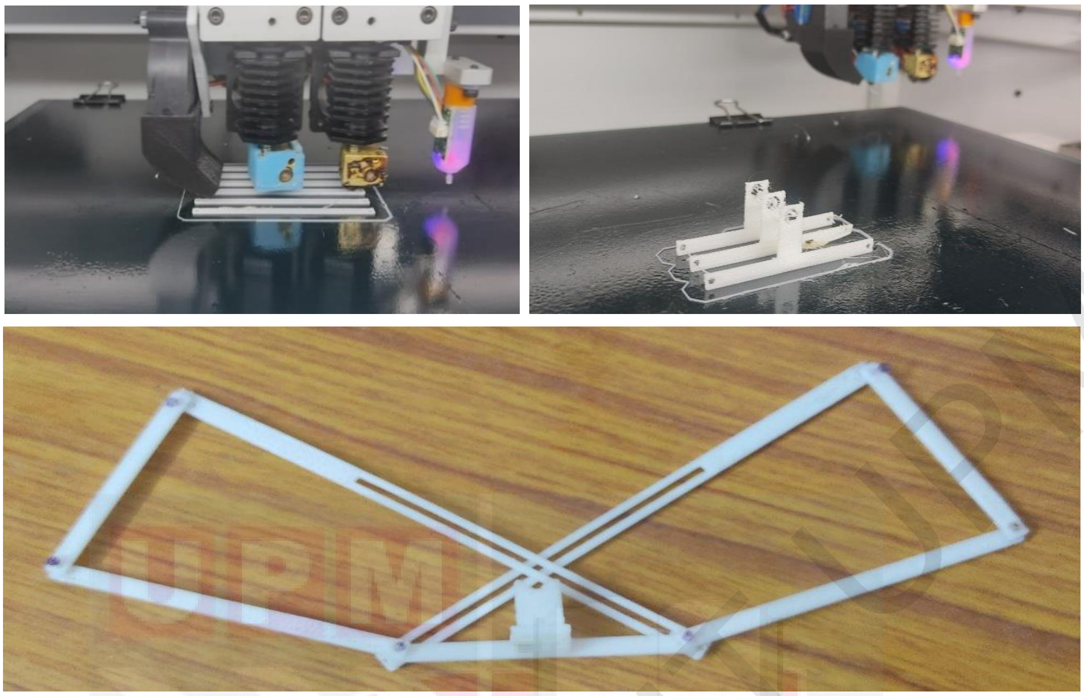

Figure 3.22 : 3D Printed Design of X-Pattern Four-Bar Mechanism

After assembling the individual 3d printed designs, it’s been realized that the overall weight was creating imbalance in its wing lever movement. Also, levers were clashing while movement, which was affecting the flapping lever movement. Hence the modification in its design is performed, to obtain mechanism -II discussed in further section below.

3.5.3 Fabrication of SC-SDL Design -II

Due to the requirement of sophisticated transmission mechanism with light weight and minimal intervening connections. This innovative mechanism was created to answer the need for a producible structure that is small in size, mass and has reduced design linkages. The proposed Single Crank - Slotted Dual Lever (SC-SDL) mechanism transforms rotational motion into specific angular motion at different velocities for each of its two strokes, i.e., the forward stroke and the return stroke. The discovery of a lag between the left and right lever motions in our design mechanism-I leads us to the conclusion that the flapping is asymmetric. To eliminate the position lag, the design has been altered and a new design mechanism-II has been developed. The overall weight of the handcrafted wooden structure shown in figure 3.23 includes the motor but excludes the wing. The above proposed design mechanism-II can generate flaps at its lever, but its velocity and acceleration vary greatly. This is due to structural design constraints, i.e., the time of flapping of both levers is not the same but varying.

Figure 3.23 : Over All Weight of Fabricated Design Mechanism II with Motor (without Wings)

Therefore, the above mechanism design -II is not creating symmetric flapping, hence it is incompatible with Flapping Wing MAV applications. However, by making minor changes to the design mechanism-II, it has yielded a revised design model known as mechanism design-III. Where the revised design mechanism-III can minimize the phase lag between the flapping coordination of both wing motion paths with respect to time discussed further.

3.5.4 Fabrication of SC-SDL Design -III

To fabricate the proposed prototype, the skeletal of the mechanism is built by hand, and then it is validated in terms of its size by being compared to a coin valued 10 cents, as seen in the Figure 3.24. The size and components of the design were simplified to achieve the goal of overall weight reduction. As a result, a 0.85g flapping mechanism design was achieved including the micro dc motor weight within it as shown in Figure 3.25.

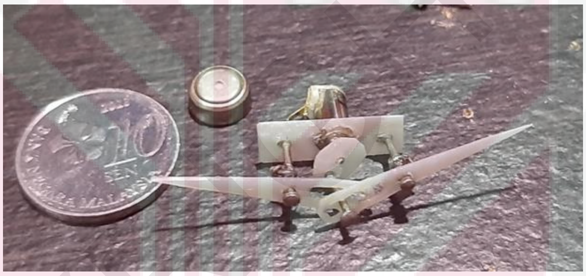

Figure 3.24 : Size of Hand Made SC-SDL Mechanism Design with 10 Cents Coin

Figure 3.25 : Peight of Compact Handmade SC-SDL Design Mechanism with Motor (without Wings)

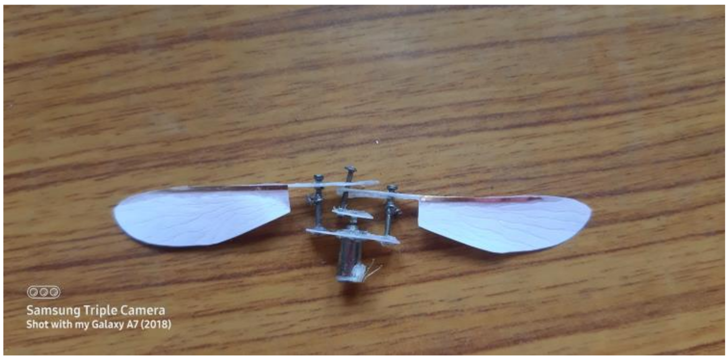

Figure 3.26 : Paper Wings Attached to the Handmade SC-SDL Mechanism Design

Figure 3.27 : SC-SDL Design III with Flapping Frequency Measuring Setup

The paper wing attached handcrafted SC-SDL design prototype as shown in Figure 3.26 was tested with the appropriate power supply; however, due to the stiffness of the paper wing, the flapping noise was excessive, and the flapping frequency measured was low. Because of this, the paper wings were eventually replaced with tissue paper wings, which are more flexible and weigh less than their predecessors. As a result, the noise level was reduced, and the frequency at which the wings flapped increased.

Figure 3.28 : Mosquito Wing Shaped Plastic Wing Attached to the Handmade SC-SDL Mechanism Design

With the limited materials availability, the working prototype with necessary circuit connections is created and to actuate the wings, miniature brushless DC motors are installed. One of the crank-slider mechanisms has been accomplished in this flapping actuation design as outlined above. The crank's rotational motion is converted into a specified angular flapping motion at both the levers. Flapping action is enhanced by incorporating low friction and quick mechanical transmission into the design. The wing is firmly connected at the output link of the proposed model, which transmits the rotational motion of the crank to specific angular flapping motion. The design features- low friction and rapid mechanical transmission, which are essential for improving flapping motion. It is observed that a flapping angle range between 25-35 degrees using this actuation system has been achieved. The consistency of the actuator's flapping is measured using a photoelectric sensor, and its flapping frequency is determined using a counter, as seen in Figure 3.27.

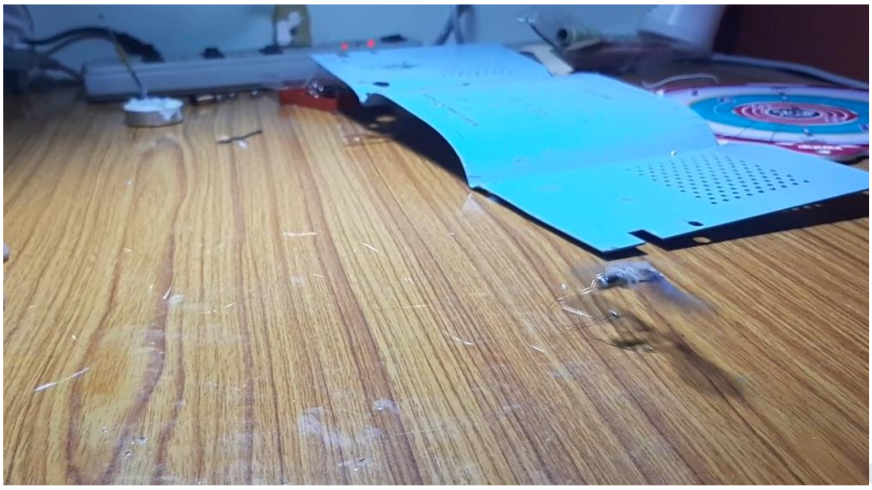

Figure 3.29 : Mosquito Wing Shaped Plastic Wing Design Movement

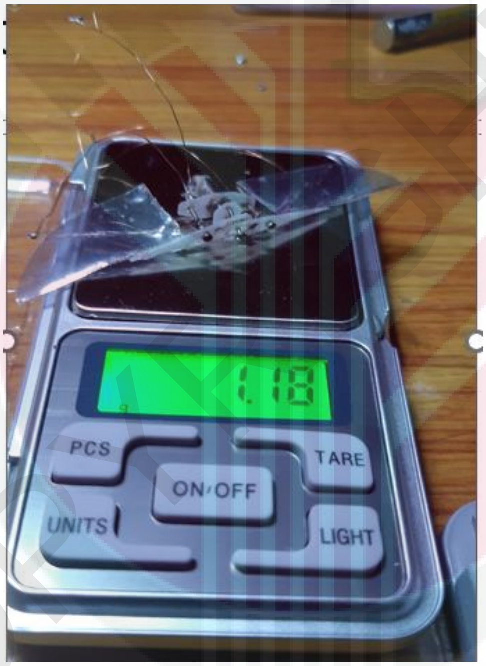

Figure 3.30 : Overall Weight of Compact Handmade SC-SDL Design Mechanism with Motor and Wings

As depicted in Figure 3.28, also attempted to substitute the tissue paper wing with a plastic wing in the shape of a mosquito wing. When the power supply is offered, however, it began traveling in the reverse direction as in Figure 3.29. To make it move forward, once more attempted to alter the wing shape. The prototype of the final wing design is depicted in figure 3.30. With the provision of the supply, the prototype initiated forward motion, demonstrating its ability to generate thrust without generating lift. To address the issue of insufficient lift generation, a separate drive source is installed at each wing lever to enhance lift and movement. This improvement in design is referred to as mechanism design IV.

3.5.5 Fabrication of DC-SDL Design -IV

Due to time constraints, fabrication of the prototype with the minimal available materials was crucial; the final test bench prototype is as depicted in Figure 3.31 and 3.32. Wherein two miniature brushless DC motors are used to flap both wings. Above described one of the crank-slider mechanisms i.e slotted lever type flapping actuation design has been implemented. The wings are firmly connected to both the levers of the proposed model, which converts the rotational motion of the crank to a specific angular flapping motion. Low friction and rapid mechanical transmission are essential for enhancing flapping motion and are incorporated into the design.

As shown in Figure 3.31, the left wing could flap at an angle of 51 degrees, while the right wing could flap at an angle of 43 degrees. If the origin is considered along both hinges, the angle above the origin is 20 degrees for the left wing and 13 degrees for the right wing. Also, the flap angle compiled below the origin is 31 degrees for the left wing and 30 degrees for the right wing. Also portrayed in Figure 3.32 are the sequential frames of the proposed mechanism for minimal flapping frequency. Where input of less than 1 volt is provided to capture flapping motion, frames are captured at 167ms intervals. They were able to observe the varying angular movements of both wings at distinct periods.

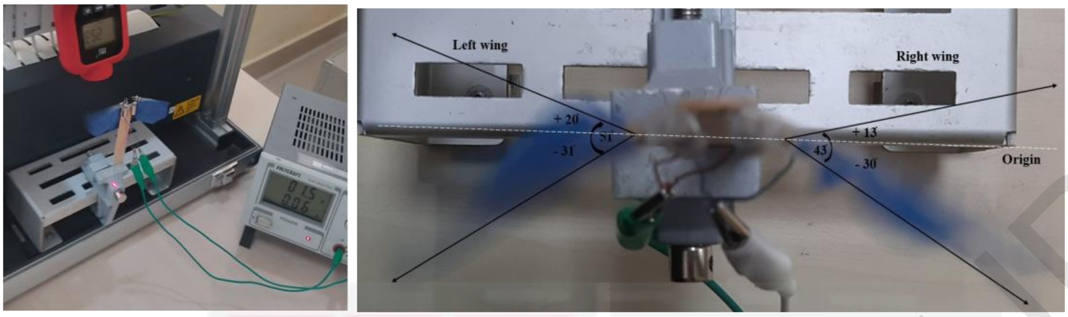

Figure 3.31 : Proposed DC-SDL Mechanism Testbench Design /Prototype (Handmade)

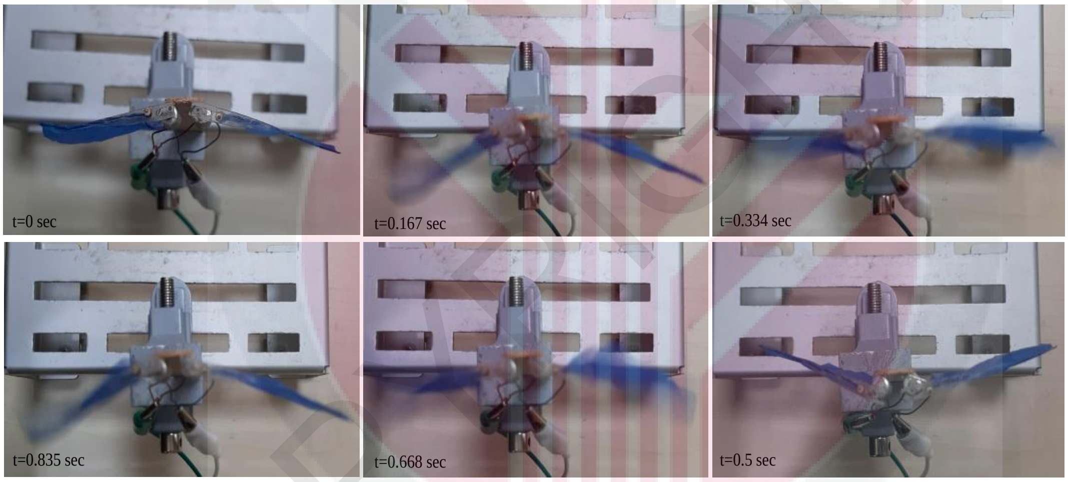

Figure 3.32 : Sequential Frames of the Proposed Mechanism for Less Frequency (i.e at Minimal Input Voltage), Each Frame is 167ms Apart

Yao wei et al (Y.-W. Chin & Lau, 2013) have utilized little different slotted lever concept in their prototype in a unique way, as per them- the rapid flap change in direction has an additive bonus that improves lift production. Due to the wing's flexibility in the spanwise horizontal way, the sudden variation in that plane results in a significant passive -wing movement about the leading-edge. The wing pitching during the downstroke across the click technique is larger, also lasts durable across sinusoidal period of movement, even though the static system flaps at a highest frequency (12.5 vs. 9.4 Hz) than the click mechanism. where in our proposed mechanism, the forward stroke lats longer than the return stroke period. Also, when compared with the clicking mechanism, our prototype has achieved higher flapping frequency i.e 72Hz.

3D Printed design: At the innovation center makerspace facility of Manipal Academy of Higher Education, the Pratham printer has been used to 3D print the CAD designs of individual parts using PLA material. Figure 3.33 depicts the base layer printing performed by the Pratham printer as a foundation for printing the actual sliding lever design.

Figure 3.33 : 3D Printing of Wing Lever Parts

Because the sliding lever sections in our hand-made designs were highly sturdy despite their thinness and also quite lightweight, they attempted to produce a size equivalent to that utilizing a 3D printer. Figure 3.34 depicts the 3d printed four sliding levers and 12 motor supporting structures. The actual weights of single sliding lever, lipo battery and micro dc motor in grams are as shown in Figure 3.35 below.

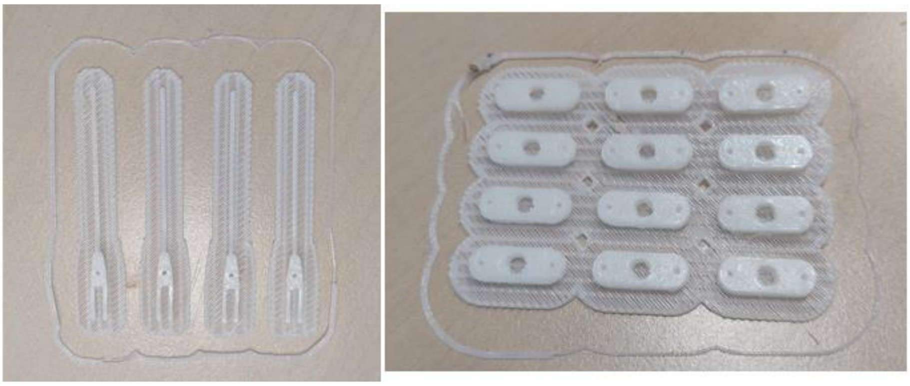

Figure 3.34 : Printed Parts of Sliding Lever and Motor Supporting Base

Figure 3.36 depicts the assembly of 3D-printed components with two motors and dummy plastic wings. where each motor will be responsible for driving its own separate wing. As a result, there is neither a phase lag nor a mismatch between the left wing and the right wing.

Figure 3.35 : Weights of Sliding Lever, Battery and Micro Dc Motor in Grams

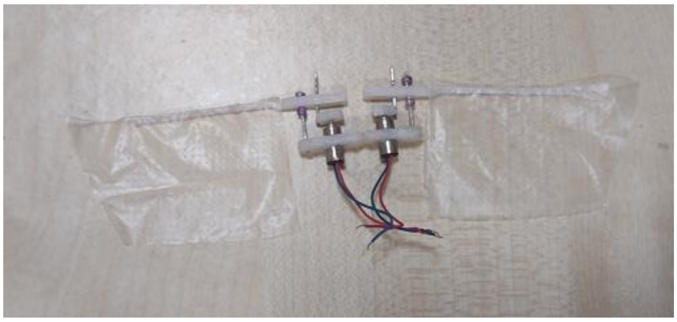

Figure 3.36 : 3D Parts Assembled DC-SDL FW Prototype

Figure 3.37 : Weights of Assembled Single and Double Motor with Sliding Lever in Grams

The weight of single and double motor with its individual wing connection are as shown in Figure 3.37. There is a difference of 0.05 grams in weight between the hand-made DC-SDL prototype (1.82g) and the 3D printed DC-SDL prototype (1.87g), which can be seen by comparing both the designs.

3.6 Button Vibrator as Motor (Driving Source) for Sliding Lever Mechanism Designs

Vibration is typically the method of choice when it comes to providing feedback in contemporary applications such as touchscreens and gaming controllers. Coin vibrators are generally coreless DC motor, and these motors are relatively small in size. coin vibrators are also known as shaftless or pancake vibrators, used as Pico size Vibration producing device. Pancake motors are compact and user-friendly. till now these motors are being used in mobiles for indicating the user that they have received a call causing vibrations. The design structures of general vibrators can be divided into three different types, namely the coin type, the Eccentric Rotating Mass (ERM / cylindrical) type, and the Linear Resonant Actuator (LRA) type, its differences are listed in Table 3.2 below. Coin vibrators likewise make use of a spinning offset mass, but their form factors are flatter and more compact, and they are completely enclosed as opposed to being open to the air. Rather than having a lengthy cylindrical shaft with axle and an offset mass, the shaft is extremely short, and the interior includes a flat mass that is offset from the centre of rotation (so that it can fit in the shape of a coin)(Dementyev et al., 2020; Garcia-Valle et al., 2021; Hao et al., 2022; Oldiges & Bajaj, 2022; Pomplun et al., 2022; Sadia et al., 2020).

Table 3.2 : Difference between the Motor Types

Motor types	ERM type	Coin type	LRA type
Form factor	Cylindrical	coin	coin
Working method	Eccentric Rotating Mass	Eccentric Rotating Mass	Linear Resonant Actuator
Built in connection	Simple/direct	Simple/direct	Uses LRA driver

The coin-based vibrator is based on ERM (Eccentric Rotating Mass) motors. Therefore, they can be driven in the same manner as their pager motor counterparts. They have the same motor drive principles, including H-bridge circuitry for active braking. The 3-pole commutation circuit for brushed coin vibrators is built out around an internal shaft in the center of a flat PCB. A flat plastic disc with a bearing in the center that rests on a shaft, two "voice coils," and a tiny mass make up the vibrator rotor. The voice coils, which produce a magnetic field, are powered by two brushes on the underside of the plastic disc that come into touch with the PCB commutation pads. The flux produced by a disc magnet that is fastened to the engine chassis interacts with this field. The N-S pole pairs built into the neodymium magnet are affected by the commutation circuit, which changes the field's orientation through the voice coils. The disc spins resulting in vibrations because of the built-in eccentric mass that is off-center. In short, As the ERM rotates, the centripetal force of the offset mass is asymmetric, resulting in a net centrifugal force, and this causes a displacement of the motor i.e vibrations. In order to provide haptic feedback when the user interacts with a device, button vibrators are frequently paired with touchscreens or buttons. This feedback improves the user experience by providing tactile confirmation of button presses or touch gestures, thereby making the interaction more intuitive(Dementyev et al., 2020; Sadia et al., 2020; Shen et al., 2023; Y. Zhang et al., 2022). These motors are utilized to produce appropriate vibration patterns for capsule motility while it is traveling through the digestive system of the patient. in which capsule endoscopy is a specialist sector, and where the development of a comprehensive system requires competence in electronics, firmware development, and medical regulations (Ciuti et al., 2012).

3.6.1 Working Principles of Button Vibrator

A compact electric motor, an eccentric rotating mass (ERM), and a power source are the primary components of a button vibrator. The motor is typically a small direct current (DC) motor, and the eccentric rotating mass is a small, unbalanced weight affixed to the motor's shaft as depicted in Figure 3.38. A rotating magnetic field is generated when an electrical current is applied to the motor. This magnetic field interacts with the permanent magnets present in the motor to rotate the shaft. As the motor shaft rotates, so does the eccentric weight that is affixed to it (Muthuselvi et al., 2022; Oldiges & Bajaj, 2022).

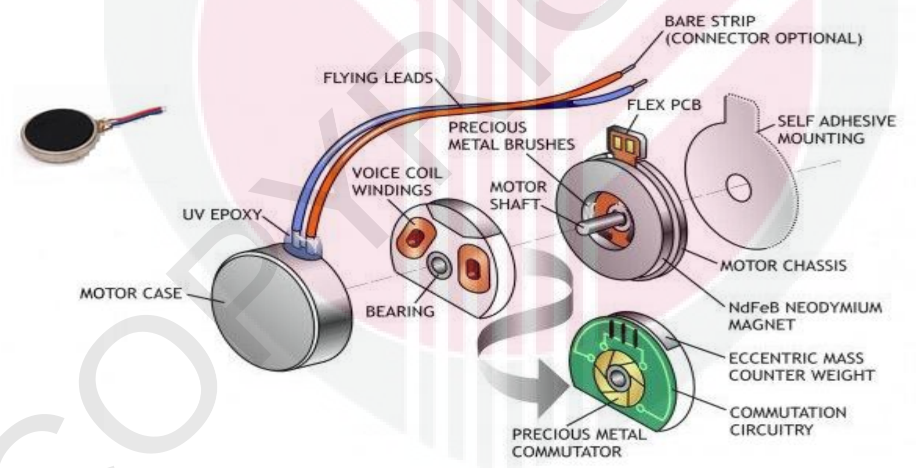

Figure 3.38 : Button Vibrator Internal Structure

The rotation of the eccentric weight creates an imbalance in the system of the motor, causing vibrations. These impulses are then transmitted to the device or surface that the motor is mounted to. By adjusting the motor's speed and direction, the vibrations' intensity and pattern can be modified to provide the user with a variety of tactile feedback. They attempted to open the outer casing/shielding of the coin/button vibrator, to operate it as a motor by supplying it with dc power. The additional metal piece (added as extra mass for vibration generation) has been removed to eliminate vibrations. Therefore, it operates with a 1v to 9v dc supply, and as the input voltage is increased, the rotation increases linearly. The coin/button vibrators that have been converted into micro motors are referred to as coin/button motors here.

3.6.2 Fabrication of the Button Motor Driven Mechanisms

At first, the authors experimented with a hand-made version of the SC-SDL concept by attaching a single button vibration motor to both the links, as illustrated in Figure 3.39. As shown in Figure 3.40, the total weight of the mechanism design with button vibration motor but without wings has reached 0.88g. As per our literature survey, 0.88 grams is the least amount of mass of any of the currently available motor-actuated flapping wing mechanisms with motor and without wings design. However, if they compare its weight to that of our SC-SDL model, which can be found in Figure 3.24 of this chapter, but the weight of the micro dc motor actuated design is 0.85. There is a variation of 0.03 grams in its overall weight between the two designs, when driving source has been replaced.

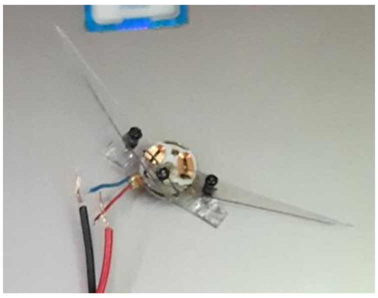

Figure 3.39 : Handmade SC-SDL Design with Button Vibration Motor

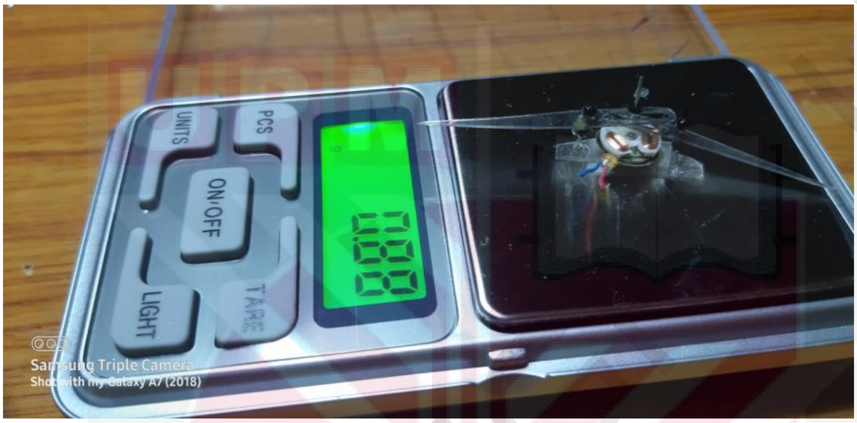

Figure 3.40 : Total Weight of Hand Made SC-SDL Design with Button Vibration Motor (without Wings)

An attempt was made to add two more wing levers to the same model, and as a result, they were able to achieve the four-lever mechanism that is operated by a single motor. Additionally, the same thing is being constructed as a design made by hand, as illustrated in Figure 3.41, where 1.07 grams is the quantity that it weighs. coin motors are typically designed for simple vibration applications and might not have sufficient power or torque to drive a complex mechanical arrangement like a slider-crank mechanism with four levers. As a result, the motor might struggle to overcome the resistance caused by the linkages, leading to uneven movements and reduced lift.

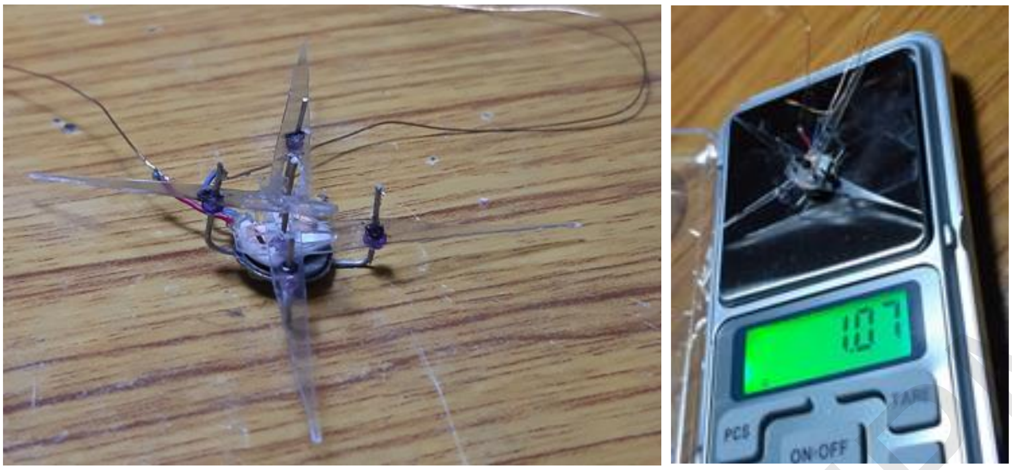

Figure 3.41 : Hand Made SC-SFL Design with Button Vibration Motor with its Overall Weight (without Wings)

In a four-lever arrangement, each lever's load and resistance might vary depending on the specific geometry of the mechanism. If the linkages and levers are not designed with balanced load distribution in mind, it can result in certain levers receiving more force than others. This imbalance can lead to erratic movements and poor coordination. Achieving proper timing and synchronization of the four levers' movements is critical for generating consistent and sufficient lift. If the levers are not precisely coordinated, they might interfere with each other's motion, leading to disruptions in the desired movement pattern. The mechanical design of the linkages, levers, and crank plays a crucial role in the smooth operation of the mechanism. If there are inaccuracies or tolerances in the design, it can result in binding, friction, or misalignment, which in turn can hinder coordination and lift generation. Coin motors often lack the precise control and feedback mechanisms needed for intricate mechanical systems. Without accurate position or speed control, it becomes challenging to ensure that the lever movements are synchronized and coordinated effectively.

3.7 Controller Implementation

To achieve sustained flight and manoeuvrability, flapping wing designs frequently necessitate precise control of wing motion. Micro DC motors provide superior speed control and responsiveness, enabling precise adjustments to the frequency, amplitude, and phase of wing flapping. This control enables unmanned aerial vehicles to adapt to changing flight conditions and execute complex aerial manoeuvres. Micro DC motors are renowned for their high efficiency, which enables them to convert electrical energy into mechanical power with minimal losses. This efficacy is crucial for maximizing the flight duration and range of flapping wing designs, especially in battery-powered UAVs. Micro DC motors contribute to extended flight durations and increased operational capabilities by minimizing energy consumption. Micro DC motors can be utilized in a variety of flapping wing designs, accommodating a variety of wing configurations, sizes, and materials. Their versatility makes them appropriate for a variety of applications, such as surveillance, environmental monitoring, search, and rescue, and even entertainment. Overall, micro-DC motors are essential components of flapping wing designs, allowing for the efficient and controlled movement of wings on UAVs. Miniature robotic systems rely on their small size, light weight, precise control, and energy efficiency to achieve sustained flight, manoeuvrability, and prolonged operation.

A significant challenge in this field is the efficient regulation of the DC motors responsible for the flapping movement of the wings. An effective method to tackle this difficulty is the implementation of a Proportional-Integral-Derivative

(PID) controller, which is a commonly utilized control technique in diverse engineering fields. A PID controller is a feedback device that modulates the input to a system in response to the discrepancy between the desired and actual output. Within the framework of a flapping-wing mechanism, the PID controller can be employed to govern the velocity of the DC motor, hence managing the frequency and magnitude of the wing flapping. Several variables contribute to the necessity of a PID controller in flapping-wing actuation for controlling the speed of a DC motor. The dynamics of a flapping-wing system are intrinsically intricate, encompassing the interconnected behavior of the motor, gearbox, linkages, and flexible wing structures.

The interaction between motor speed, wing loads, and structural flexibility can lead to deviations in the aerodynamic forces experienced by the wing spars compared to what is expected from simulations that assume rigid spars and constant motor velocity. To precisely simulate and regulate the movement of flapping wings, a more advanced method is necessary, such as the Jacobian formulation described in this study. Furthermore, the flapping-wing mechanism is susceptible to a multitude of disruptions and uncertainties, including alterations in load, fluctuations in motor performance, and variations in ambient circumstances. The PID controller can effectively reduce the impact of these disturbances and sustain the required motor speed, so guaranteeing consistent and dependable wing flapping.

Furthermore, the PID controller can be adjusted in order to attain the required response characteristics, including rapid settling time, low overshoot, and complete elimination of steady-state error (Ahmed et al., 2021; E.El-Telbany, 2013; Onal et al., 2013; K. Peng et al., 2017; Rashid & Hussain, 2021).

3.7.1 Simscape Modelling for DC-SDL Mechanism

Simscape is a MATLAB physical modeling utility that enables simulation and analysis of physical systems. Among the stages of simscape modeling are:

- Activating MATLAB and generating a fresh Simscape multibody model file. Usage of the "simscape" commands in the MATLAB command window to accomplish this. Specify the physical characteristics of the flapping wing system. This includes wing length, wing mass, wing rigidity, and any additional applicable properties.

- Constructing the proposed flapping wing's mechanical structure using Simscape multibody components. Its important to employ "Rigid Transform" to position the wing in space, "Beam or lever" to represent the wing's structure, and "Joint connection" to designate the rotational motion.

- Describe the flapping wing's activation technique depending on the design mechanism movements. This could be a motor or some other mechanism responsible for the flapping motion. i.e representing the actuator using the appropriate Simscape components by setting its speed of rotation and connecting it to the lever or wing structure.

- Configuring the simulation's parameters, for the execution of the simulation. Defining the system's initial conditions, time interval, and any input signals to be employed. Run the simulation to observe the flapping motion and evaluate the behavior of the wing i.e its speed of movement.

- For Analyzing the results of the simulation, Simscape provides various post-processing and data-analysis tools to obtain simulation data. From the simulation results, plotting and visualizing the wing's motion, calculating forces and moments, by deriving other pertinent information's is very much crucial. Considering that the specific implementation details of the proposed flapping wing design may vary based on the system's complexity and requirements. Based on proposed design, it may need adjustments and refinement for the model that must be implemented.

- It should also be noted that developing an accurate and realistic flapping wing model can be a difficult undertaking, as it involves both mechanical and electrical factors. To ensure accuracy, it may require iterative refinement and validation against experimental data, by repetitive executions with modified control parameters or values.

Figure 3.42 presents an illustration of the simscape multibody modeling of the DC-SDL mechanism. This modeling demonstrates how different sections have been developed as blocks and then integrated according to the requirements. Without establishing the solver configuration for the design, it will not be feasible to actuate the design. Figure 3.43 provides a visual representation of the detailed joint connections to the blocks that are required for its actuation with solver setups.

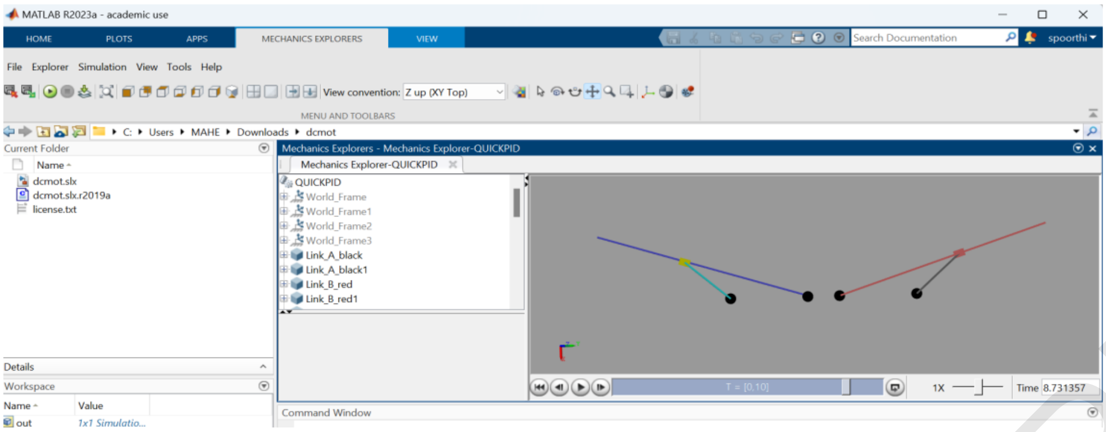

Figure 3.42 : Modelling of Dual Crank – Slotted Dual Leavers (DC-SDL) Mechanism in Simscape Multibody

Initially, the single lever actuation mechanism is constructed, and its movement is validated by actuating it. The left and right lever mechanisms are subsequently developed and activated using two distinct solvers. The input signal is considered as a straightforward signal input for motor joint actuation. Figure 3.42 demonstrates that the blue lever represents the left side wing connection, while the red lever represents the right-side wing connection. The dummy wing has not been affixed here, as only lever movements are being analyzed, as they are focusing solely on the mechanism that controls the flaps. Both side levers' motor-actuated cranks are rotated in opposing directions.

From Figure 3.43, The translation of two independent frames that correspond to the base and follower frames of the joint is limited to pure rotation around a central axis by the Revolute joint A &A1, which acts as a constraint on that motion. The axis of rotation is parallel to the z-axis of the joint base frame, which ensures proper alignment. The base and follower frame share an origin and a z-axis, and the follower frame revolves about the z-axis while the base frame remains stationary.

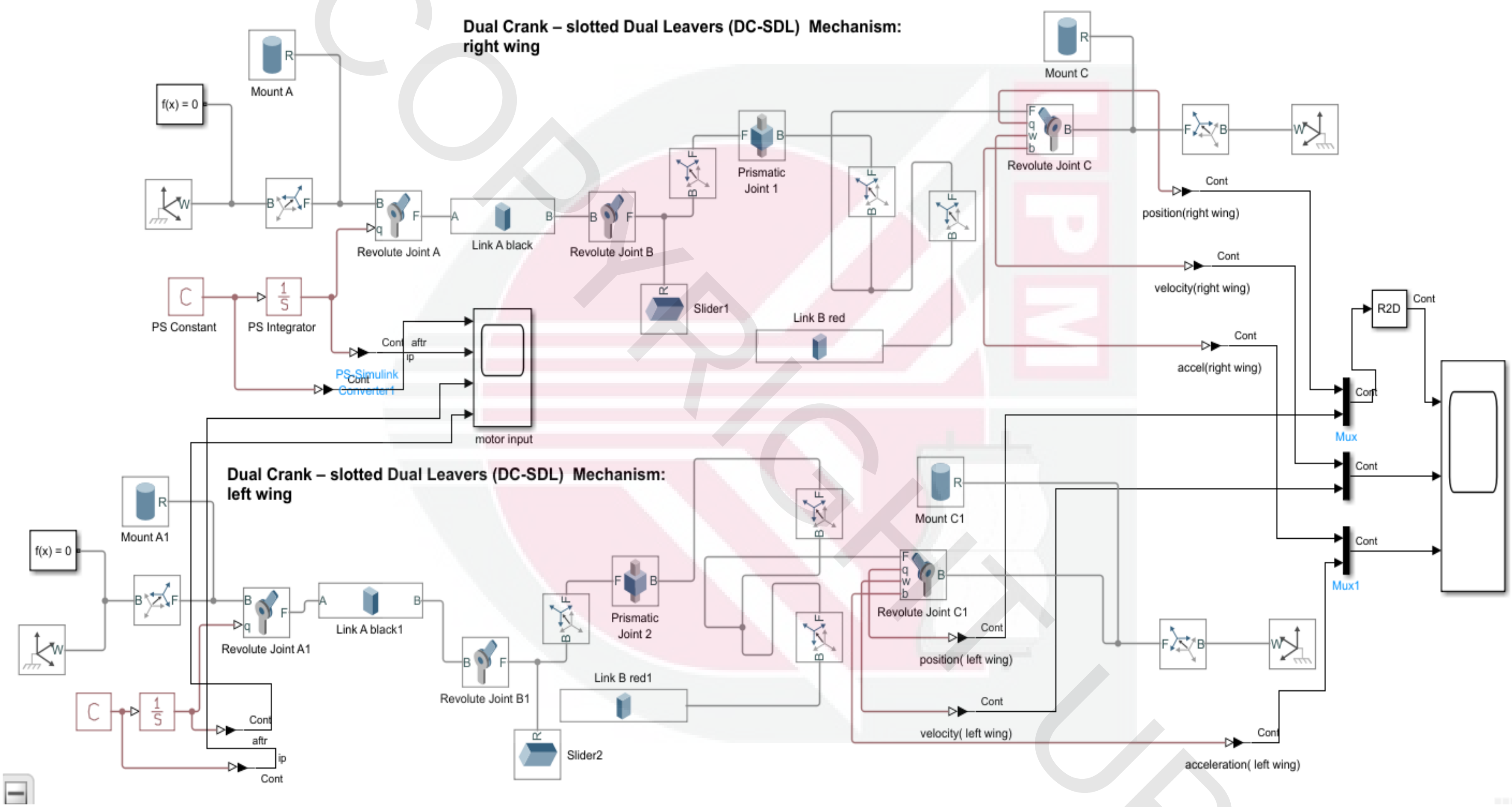

Figure 3.43 : Connections of Modelled Dual Crank – Slotted Dual Leavers (DC-SDL) Mechanism

3.7.2 DC Motor with PID Controller Tuning Approach

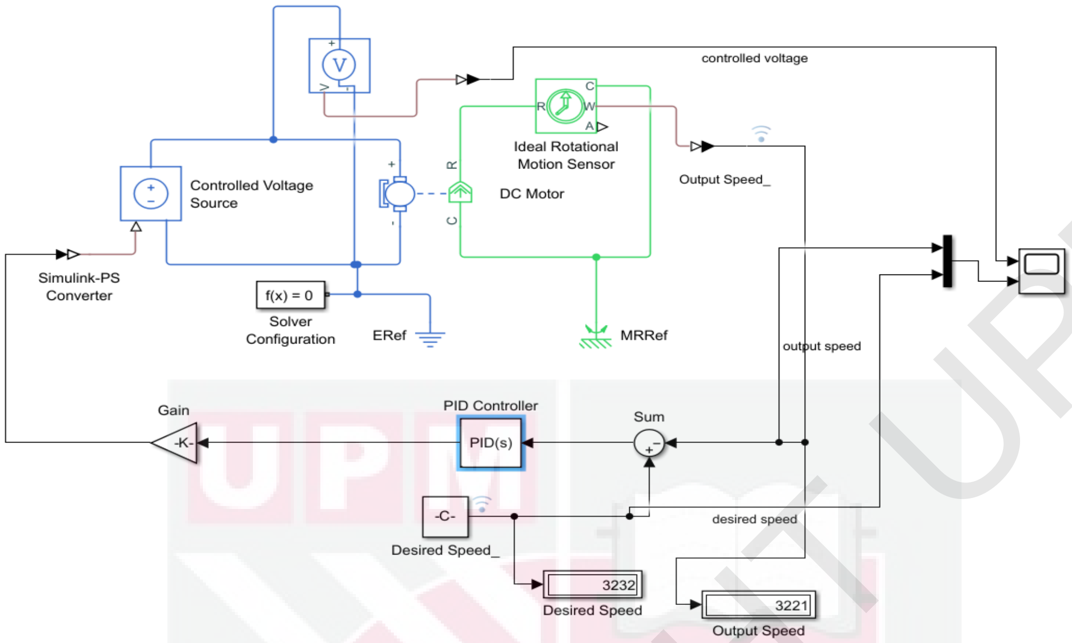

Figure 3.44 : Simscape Modelled DC Motor with PID Controller

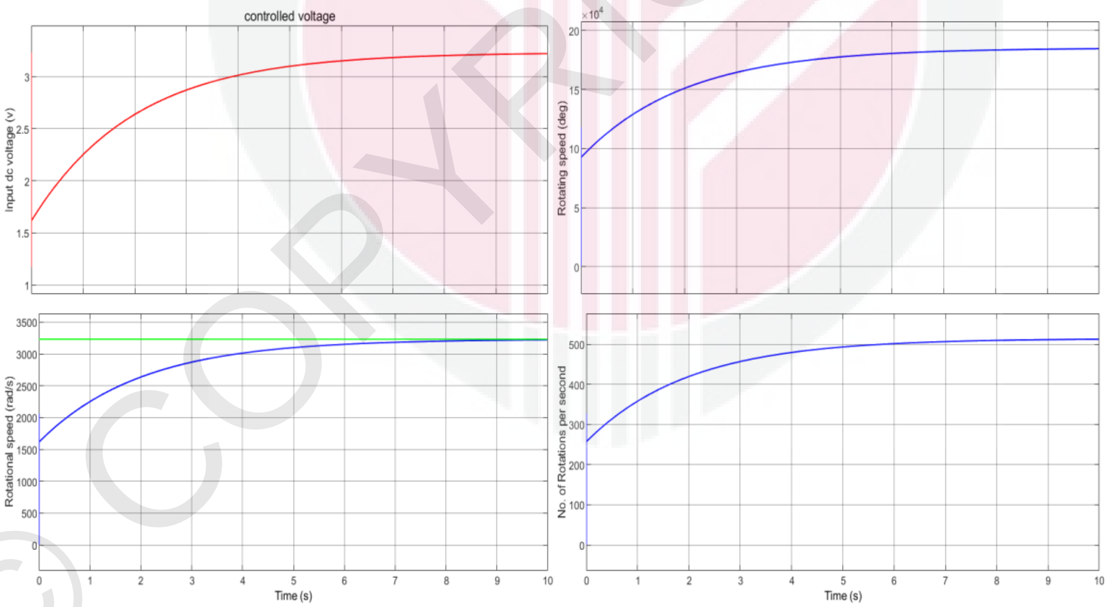

Figure 3.45 : Measurements of Attained PID Controlled Voltage with Output Speed of DC Motor (at P=1, I=1, D=0)

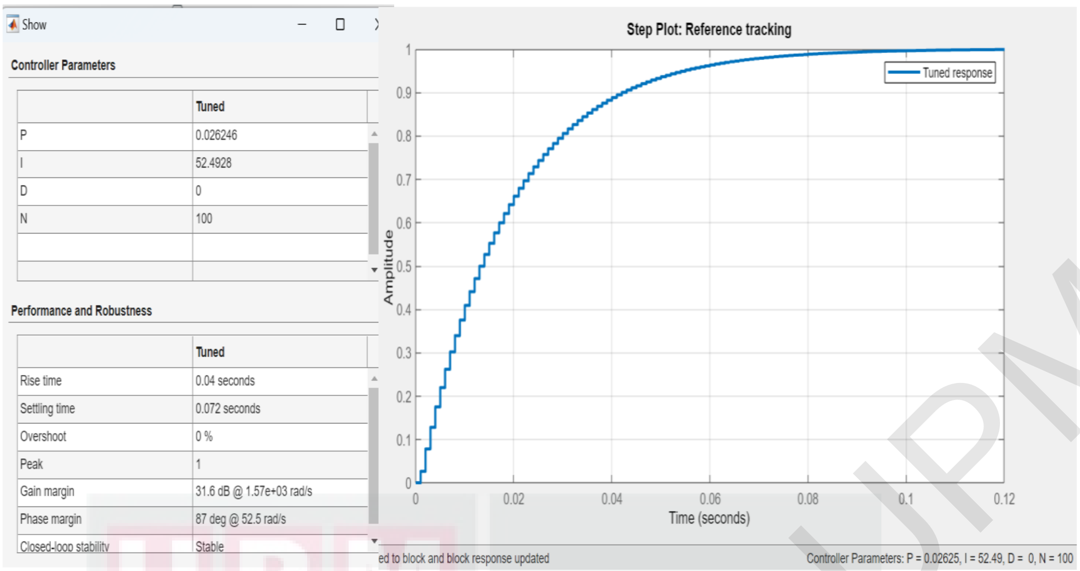

Figure 3.46 : PID Controller Specifications and Response after Tuning

Here the PID controller calculates the error by subtracting the setpoint from the actual speed measured by the sensor. The output generated by the proportional term of the PID controller is proportional to the present error. A greater error leads to a greater control output. In the context of a DC motor, the proportional term modifies the applied voltage according to the speed error. To reduce the error, this operates the motor. The PID controller's integral term addresses the accumulation of prior errors over time. It aids in the elimination of steady-state errors caused by friction or imbalances. The integral term modifies the output of the controller in accordance with the integral of the speed defect.

The simulations of the attained output speed of DC motor with PID controller at P=1, I=1, D=0, is as shown in Figure 3.45. where desired speed set is 3232 rad/s, the obtained motor output speed is 3221rad/s as in Figure 3.44. After tuning the PID controller, the finalized parameters of P,I & D with its obtained performance are as shown in Figure 3.46. where the P value is set to 0.026246 and the I value is 52.4928, but D is zero, this indicates that only the PI controller is being applied in the discrete time domain with a parallel sampling time of 0.001 consideration. Following the tuning process, the settling time that was obtained was within 0.1 seconds, which is a faster time. At a controlled input voltage of 3.3 volts obtained via PID controller, the modeled dc motor was able to achieve 514 rotations per second.

3.7.3 Modelling of New Micro DC Motor

The new micro-DC motor has been designed (Figure 3.47) in Simscape electricals of MATLAB, using the [Resistance (R) and inductor (L)] RL circuit, taking into account inertia, damping constant, and other factors. This was accomplished through investigating on the permanent magnet dc coreless micro motor (Karnavas & Chasiotis, 2016), where the specifications are as listed in the Table 3.3 seen below.

Table 3.3 : List of Standard and Micro DC Motor Parameters

Parameters	Standard Dc motor Values with units	Micro Dc motor Values with units
Input dc voltage	1.5-9v	1.5-5v
Resistance	0.5 ohms	3.9 ohms
Inductance	750 uH	12 uH
Rotor inertia	0.3 kg*m^2	$1x10^{-9}$ kg*m^2
Damping constant	0.01 N*m*s/rad	$1.22x10^{-7}$ N*m*s/rad
Back EMF constant	0.5 V*s/rad	0.00068 V*s/rad
Current	0.1 A	0.5 A
Angular velocity or speed	7 rad/s	2681 rad/s

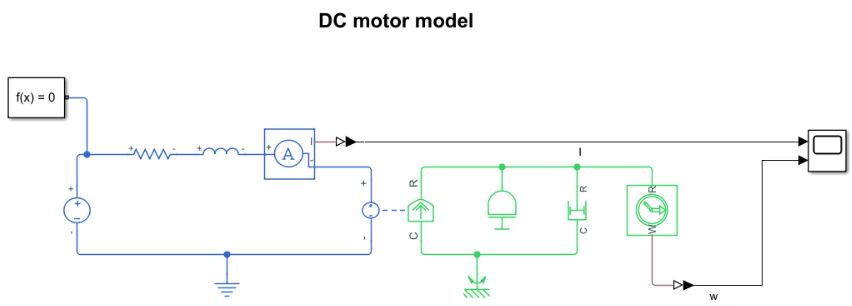

Figure 3.47 : Modelled Micro DC Motor

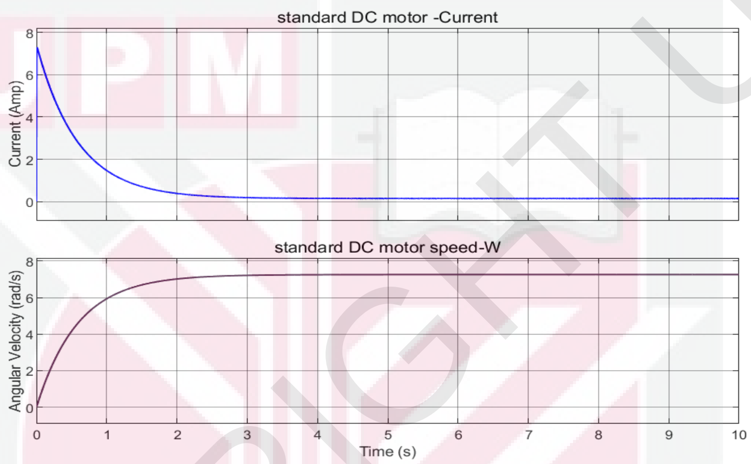

Figure 3.48 : DC Motor Current and Speed at 3.7v Input DC Voltage

In most cases, the load on the motor will cause it to draw a greater amount of current in order to keep its speed constant. However, the architecture of the motor and the input voltage may cause this connection to have some boundaries. Figure 3.48 shows the current and speed of an early-discussed DC motor operating at 3.7v input dc voltage. Figure 3.49 shows the current and speed of a newly modeled micro DC motor operating at the same voltage. By contrasting the two sets of findings shown in Figure 3.48 and Figure 3.49, it has been determined that the newly modeled micro dc motor, with its improved specifications, is capable of producing increased speed while consuming a less amount of voltage.

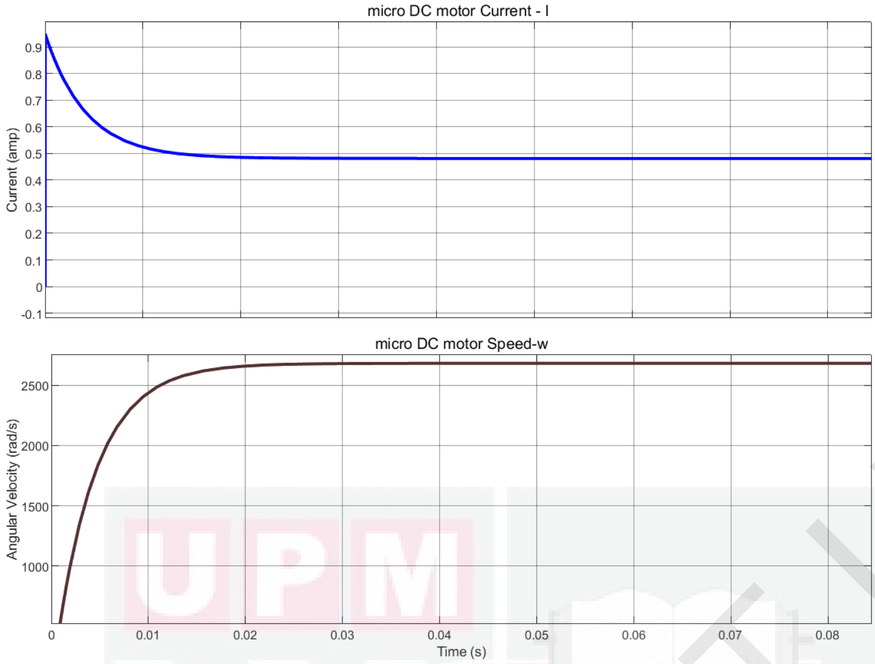

Figure 3.49 : Modeled Micro DC Motor Current and Speed at 3.7v Input DC Voltage

Certainly, the use of MATLAB's Data Inspector simulation for analyzing the current and speed characteristics of two distinct varieties of DC motors (DC motor and micro-DC motor) is a potent method for conducting a comprehensive investigation, as shown in Figure 3.50 and Figure 3.51. This method enables engineers and researchers to obtain insight into the performance of these motors under varying conditions, thereby informing design decisions and optimizations. The Data Inspector tool enables users to directly calculate multiple performance metrics from plotted data. Due to data inspector simulation, the variation in its difference and tolerance can be observed in the figures provided above.

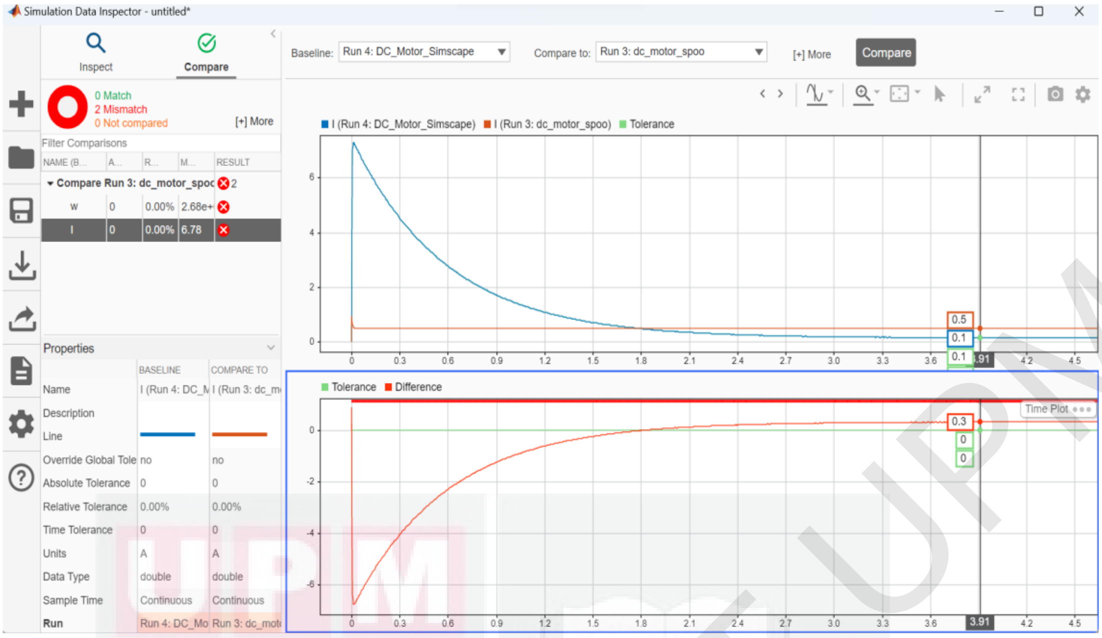

Figure 3.50 : Both the Motors Obtained Current Variations are Compared in Data Inspector of MATLAB

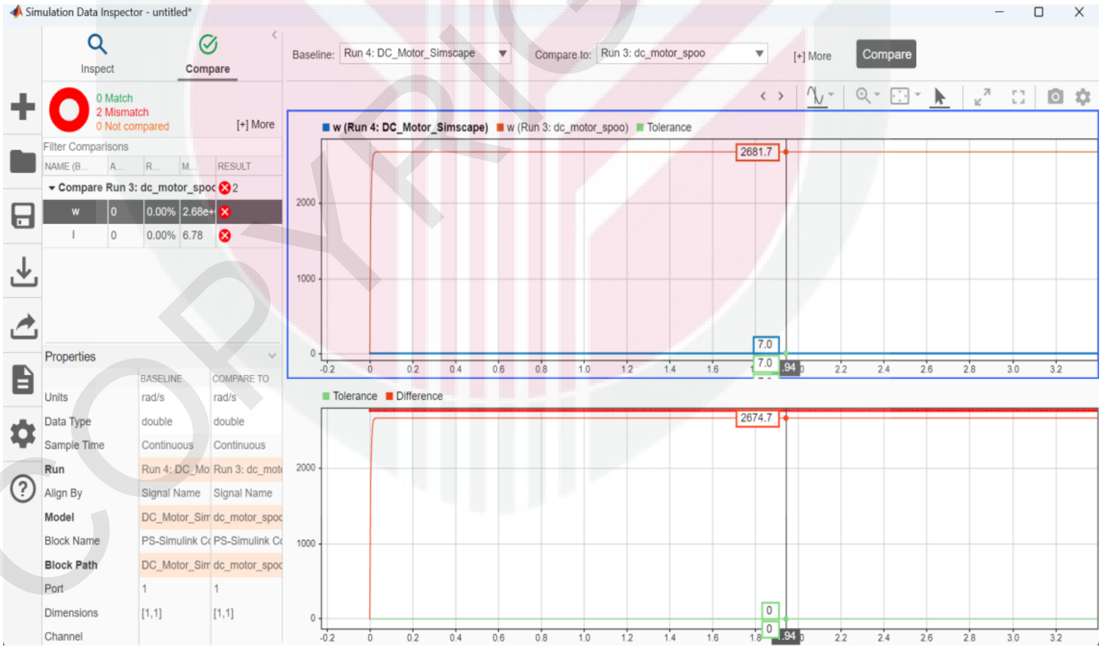

Figure 3.51 : Both the Motors Obtained Speed Variations are Compared in Data Inspector of MATLAB

As the modelled micro-DC motor worked well, it has been used for the DC-SDL mechanism for both the levers. Where the input voltage is being replaced by a controlled voltage source block, to regulate the voltage depending on the requirements. The speed is being set low for the following emulations so that they can recognize the fluctuations in the flapping position, angular speed, and acceleration.

3.8 Summary of the Chapter

The current chapter discusses efforts to construct a six different types of revolutionary test bench models of flapping wing actuation mechanism with the goal of applying it to bionic MAVs. The authors have presented the Kinematic analysis of the Crank driven – triple cylindrical slidable and rotatable joint " mechanism and crank slider type too, arrangement with direct, inverse kinematics and Jacobian representation for linear velocity and angular velocity measurements in this chapter. 3C-joint mechanism can be qualified to a specific family of the spatial one-DOF linkage mechanisms which contain triple cylindrical joints perpendicular to one another in a horizontal plane. Where as crank slider mechanism is with minimal links reduced size light weight approach perfectly suitable for micro aerial applications. The Authors have performed 3D simulations of all the mechanism designs with modelling to determine the flapping motion performance measurements and track the position/path of flapping link tip with two different software's. A novel flapping wing actuation mechanism on Crank driven – triple cylindrical slidable and rotatable joint technique and all crank slider mechanism designs are fabricated and simulation of motion analysis was performed. The simulated results followed the mechanism's expected kinematics. The developed kinematic model can determine the mechanism's design parameters and delivers the benefit of scalability in MAV design. Effective modelling and simulation have established a strong foundation for future research into dynamic analysis and mechanism manufacture.

In summary, using a PID (Proportional-Integral-Derivative) controlled micro-DC motor speed variation system is a practical and effective approach for controlling flapping wing actuation systems in micro air vehicles. Inspired by the natural flight patterns of birds and insects, these devices require precise and controlled motion to achieve steady flight and maneuverability. The advantages of incorporating PID control include precision flapping, flight stability, responsive adjustments, energy efficiency, and tenable parameters. Accurate speed regulation by the PID controller ensures precise and lifelike wing movements, maintaining constant flapping frequencies crucial for flight stability and control. The PID controller's real-time adjustments to fluctuating loads and aerodynamic conditions enhance stability and efficiency, extending flight time and range. Additionally, the controller's adjustable parameters allow for adaptation to different environmental conditions. However, challenges such as mechanical constraints, dynamic changes, integration with navigation systems, and temperature sensitivity must be addressed. Advanced modelling and adaptive control systems could further optimize performance. Overall, PID-controlled micro-DC motor speed systems offer a robust solution for precise and stable wing flapping motion, with future advancements in control theory promising even greater capabilities.

CHAPTER 4

RESULTS OF SIMULATIONS AND REAL TIME TESTING

4.1 Overview

This section involves summarizing the main findings of the simulations and experiments conducted and highlighting key data points and trends observed. The accuracy of the simulation model in replicating the real-world phenomena can greatly influence results. Simplifications or assumptions made in the model could lead to variations from real-world behavior. The efficiency of control algorithms and their ability to handle real-time computations can affect the performance in both simulated environments and actual tests. Initially, the findings of the literature study and analysis are presented in graphical form. From Chapter 3, the various designs that are meticulously considered and compared are modelled through Compmech GIM / MATLAB software and testing of fabricated prototypes. These software modelling results are grounded in extensive discussions of the simulations performed using 2D and 3D structural analysis. The simulations provide a comprehensive view of the structural behaviors and performance characteristics of each design, offering valuable insights that are visually summarized in the graphs. This chapter not only highlights the key differences and similarities among the designs but also underscores the effectiveness of using advanced Realtime testing components for flapping wing mechanism analysis in engineering research.

4.2 FW Parameters Comparisons and Analysis (Literature Study)

The comparison of flapping wing actuation models across various studies involves examining how different actuation mechanisms influence kinematics, aerodynamics, and overall efficiency of flapping flight. Researchers in the fields of bio-inspired robotics, aeronautics, and biomechanics have explored various designs and principles to mimic the complex motion of flapping wings, as seen in insects, birds, and bats. Here's a structured way researchers compared these models based on actuation mechanisms.

4.2.1 Flapping Wing Mechanism Comparison

Tiny artificial insect fliers have interesting applications, but their transmission mechanism requires light weight and reduced linking frameworks. In this section, how weight loss has progressed in FWAV's over nearly two decades is clearly elaborated. Figure 4.1(a) and 4.1(b) represents the actuation mechanism wise segregation of FWAVs, with yearly weight variations evidenced. Wingspan and mass (total weight) are important parameters to consider when designing an flapping-wing drone because they explicitly define the overall size of the flapping-wing system. From Appendix-1 fully flyable flapping-wing systems total weight and a corresponding wingspan of (a). Rotary & hybrid driven, (b). Linear-driven mechanisms plotted are shown in Figure 4.2(a) and 4.2(b). While exploring most of the existing flapping-wing drones, there are similar trends in the relationship of common mimicking type flapping-wing systems to the total weight (mass) and wingspan. The correlation between body mass and the wingspan is expressed using the power function. For the data of parameters like wingspan and mass of corresponding bird and hummingbird mimicking fully flyable flapping-wing drones are referred from Appendix-1.

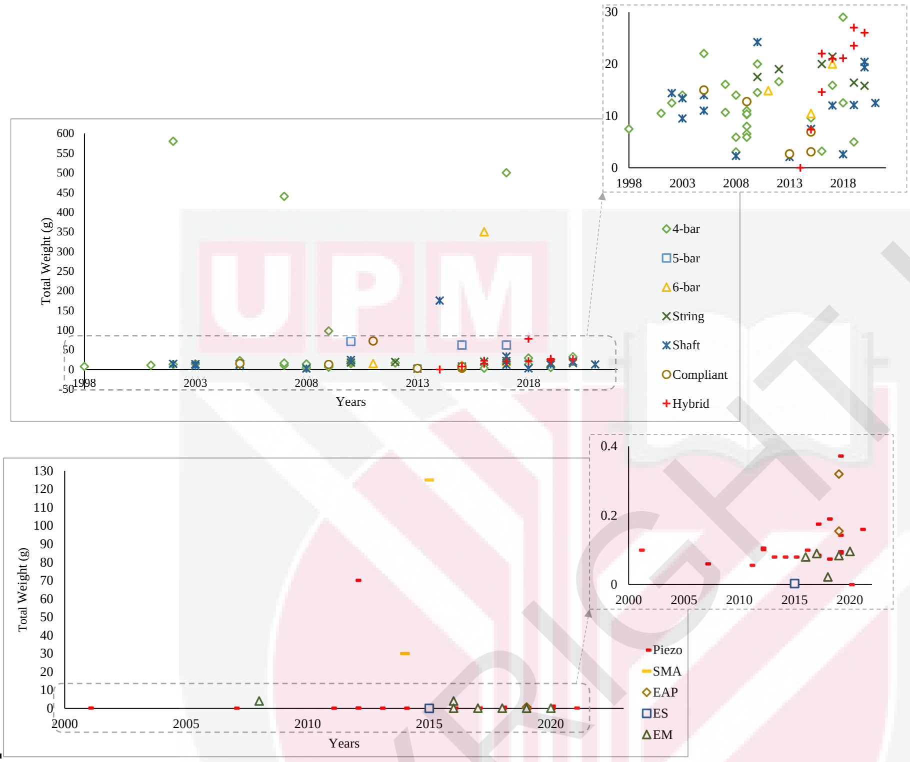

Figure 4.1 : Variation in Total Weight of FWAV Models in Years to Flapping Actuation Mechanism a). Rotary & Hybrid Driven Mechanisms and b). Linear Driven Mechanism

a.

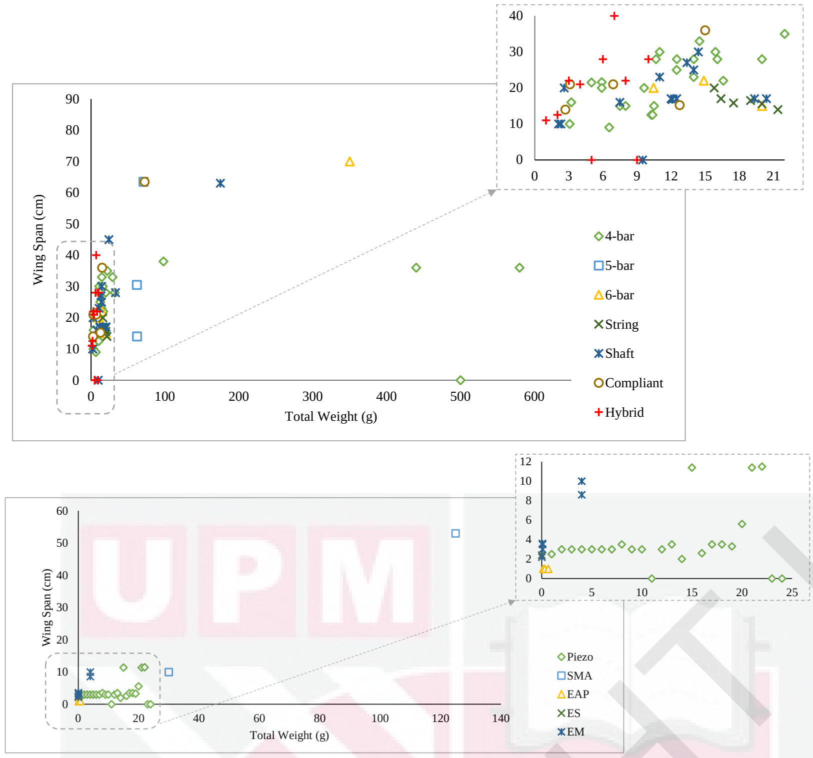

b.

Figure 4.2 : Flapping-Wing Systems Total Weight and Corresponding Wingspan of (a). Rotary & Hybrid Driven Mechanism, and (b). Linear Driven Mechanism

From Figure 4.3(a), the scaling relationship of a bird-like flapping-wing systems wingspan *b*, by body mass *m* may be represented as follows:

$$Y = 10.206\, X^{0.335} \approx b = 10.206\, m^{0.335} \quad \text{..(1)}$$

From Figure 4.3(b), the scaling relationship of a Hummingbird like flapping-wing systems wingspan *b*, by mass *m* may be represented as follows

$$Y = 9.8916\, X^{0.2321} \approx b = 9.8916\, m^{0.2321} \quad \text{.......................................(2)}$$

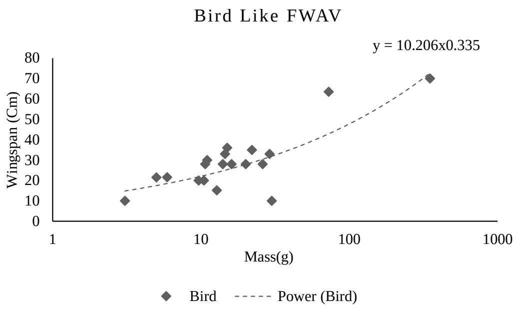

a.

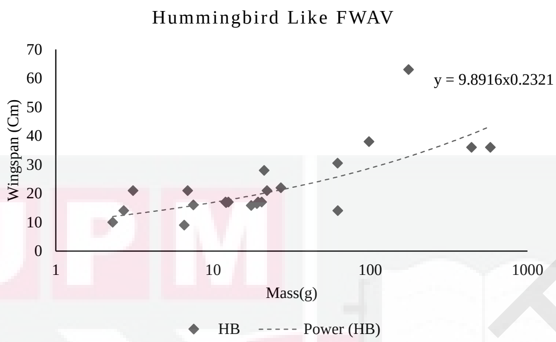

b.

Figure 4.3 : Correlation between Mass & Wingspan (a). Bird Like FWAV's, (b). Hummingbird like FWAV's

The wing base is inextricably linked to the actuation mechanism design that produces the flapping movement in the majority of flapping-wing drones. Adjusting the wing kinematics is required to gain better control over flapping-wing drones, but doing so with servo motors is difficult, so trailing edge wing roots may be a better solution. Figure 4.4(a) depicts the percentage of biomimetic and biomorphic types from Appendix-1.

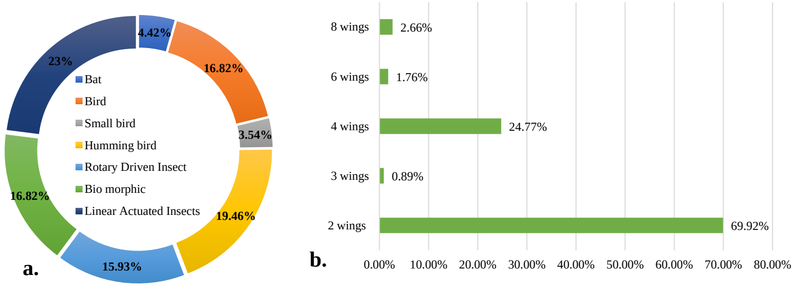

Figure 4.4 : Percentage of a). Biomimetic and Biomorphic Type of Fully Flyable FWAV's. and b). Number of Wings, Utilized under Fully Flyable Flapping-Wing Systems

The above-obtained scaling relationship of wingspan with body mass for bird and hummingbird are very much different when compared with the reference index of Shyy et al (*Introduction (Chapter 1) - An Introduction to Flapping Wing Aerodynamics*, n.d.; Shyy et al., 2013). The following is a list of important parameters to consider when designing an efficient and better-suited flapping actuation mechanism under the FWAV design requirements.

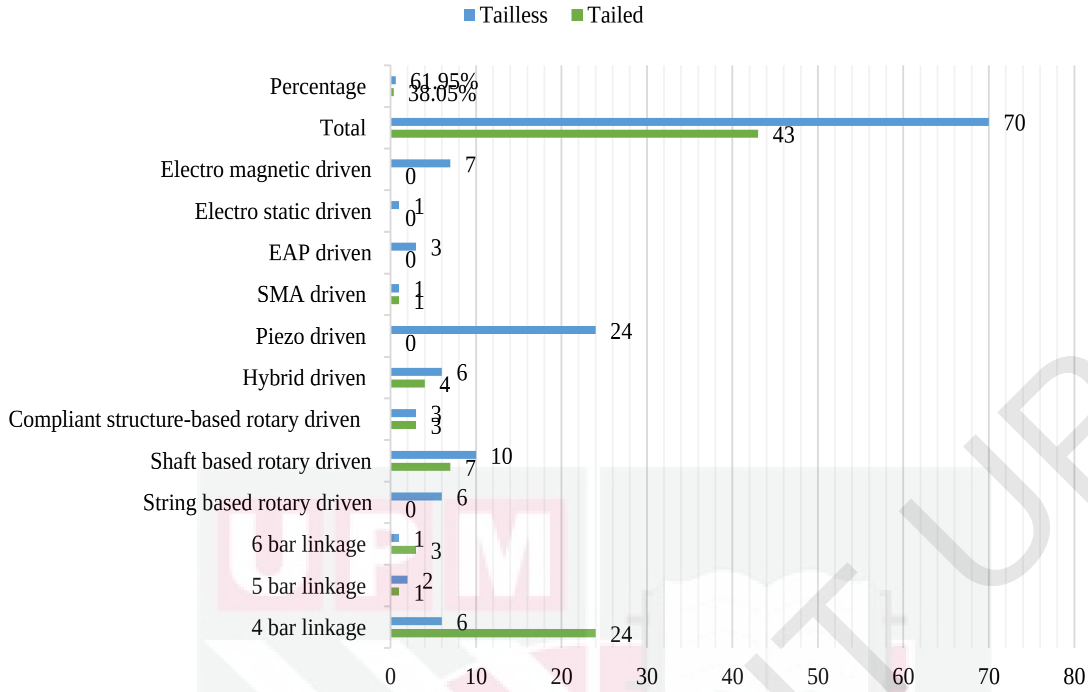

Figure 4.5 : Percentage of Tailed and Tailless Models Created under a Particular Flapping Actuation Mechanism in Fully Flyable Fapping-Wing Systems

Figure 4.4(b) depicts the percentage of a particular number of wings used in flapping wing fully flyable models. In Figure 4.5, the number of tailed and tailless models created under each flapping actuation mechanism in percentagewise. from Figure 4.4 to Figure 4.5 all the percentages are obtained from the Appendix-1 data list.

4.2.2 Flapping Frequency Comparison

While designing an actuation mechanism for flapping, it is necessary to set an expected frequency as a goal to achieve proper lift. To obtain the expected frequency the design and mass of the mechanism must be calculated accordingly. the calculation of the ratio of wing beat frequency to the natural frequency has been observed by Truong et al in 2013, is to be between 0.13

and 0.67 ratios for insects flapping at a lower wing beat frequency (less than 100 Hz) and above 1.22 ratio for insects flapping at a higher wing beat frequency (more than 100 Hz) (Ha et al., 2013). For various flapping frequencies, a spectrum of masses must be calculated and if the frequency is provided, the corresponding optimal sustaining mass for it will be estimated. if the wing operates in the predetermined interval of varying hover flight, the oscillating amplitude declines to the rise in flapping frequency (Du & Sun, 2015).

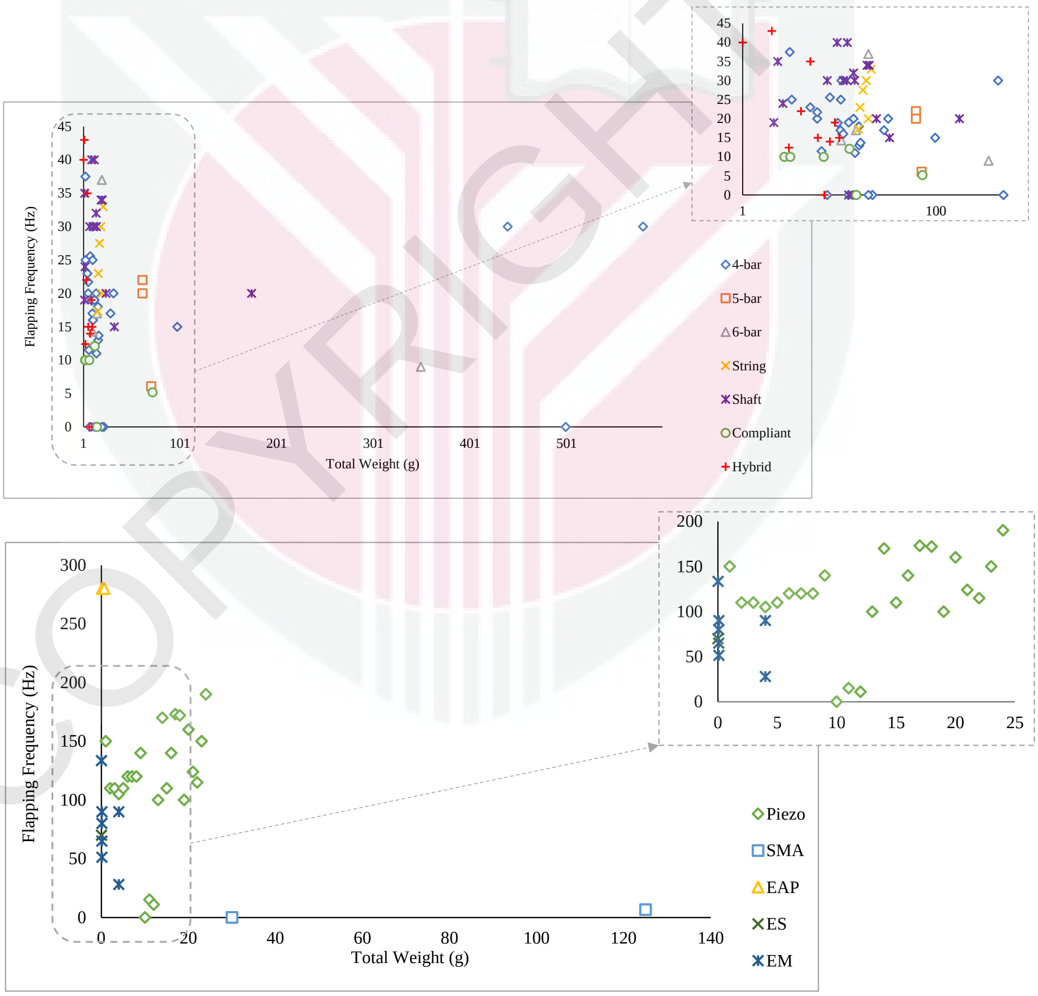

a. b.

Figure 4.6 : Flapping Frequency and Corresponding Total Weight of (a). Rotary & Hybrid Driven Mechanism, (b). Linear Driven Mechanism

Depending on the data are collected in this paper as shown in Appendix 1 through the survey on flapping frequencies and corresponding total body mass of fully flyable Flapping wing aerial vehicles in specifically rotary & hybrid driven mechanisms and in Figure 4.6(a)&(b) and Figure 4.7. linear driven mechanism has been obtained.

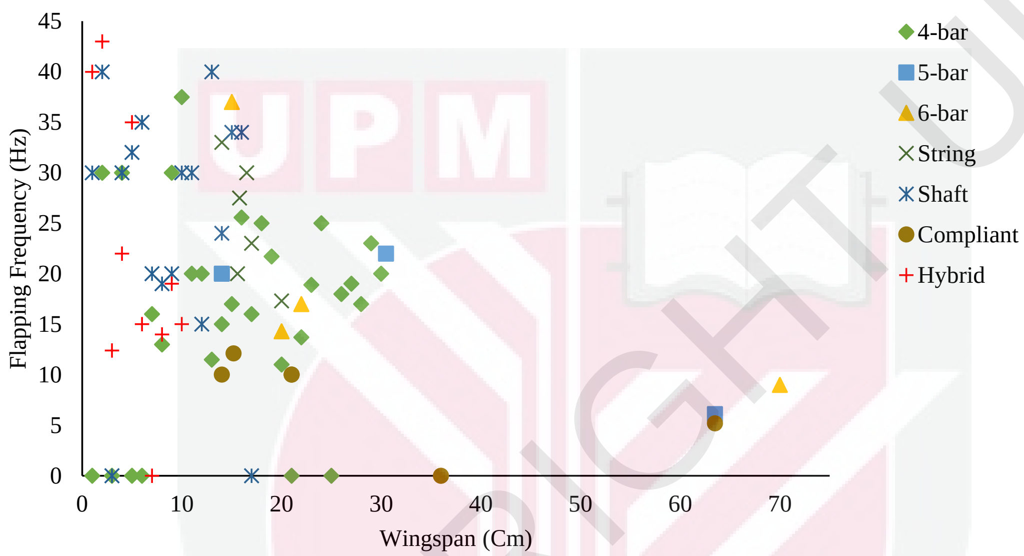

Figure 4.7 : Flapping Frequency and a Corresponding Wingspan of Rotary and Hybrid Actuated Overall Fapping-Wing Systems

Based on the flapping-wing drone designs, the total mass and flapping frequency of aerial vehicles are slightly inversely proportional which is also shown in Figure 4.6(a) and 4.6(b). It then implies that, by pursuing lightweight flapping-wing systems, they can achieve a higher frequency of flaps, which indirectly contributes to the aerial vehicle's lift-off efficiency.

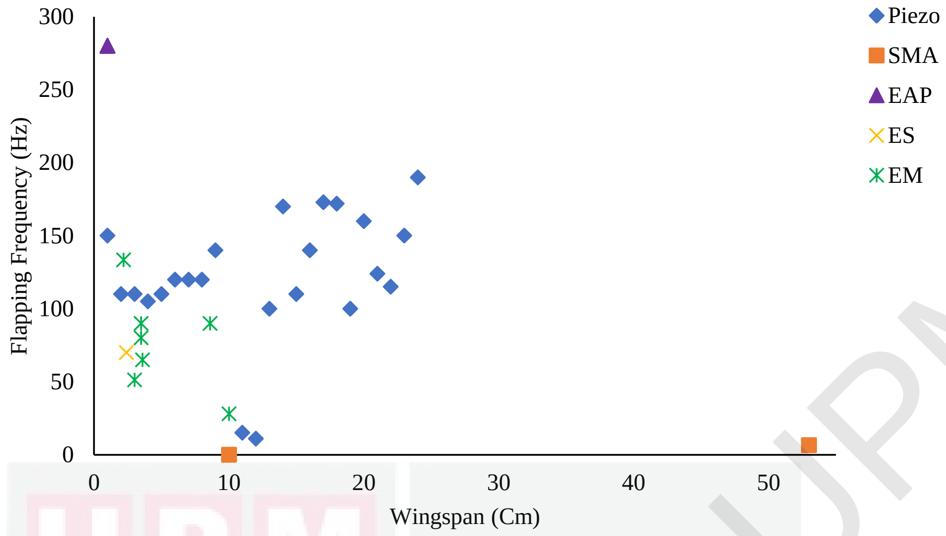

Figure 4.8 : Flapping Frequency and a Corresponding Wingspan of Linear Actuated Overall Fapping-Wing Systems

The Micro, Nano, and Pico size are being assumed depending on the mass consideration of 600 to 30g, 30 to 3g, 3 to 0.1g, respectively. Rotary & hybrid (4-bar,5-bar,6-bar, string, shaft, compliant, hybrid), and linear actuated (Piezo, SMA, EAP, ES, EM) flapping mechanisms are being differentiated with color indications for each on the graph itself. The wingspan versus flapping frequency of rotary, hybrid, and linear actuated flapping-wing drones are plotted through the data available in Appendix 1 as shown in Figure 4.7 and Figure 4.8. By analyzing this data, they found that the reduced size of wingspan models could produce better flapping frequency.

4.2.3 Flapping Angle Comparison

The wings undergo pitch and oscillatory or rotation motions, by creating some angle of the flap, which is essential to generate lift. It is necessary to create the required flapping angle, fluttering frequencies, and rotary-wing twist at specific times during the flutter cycle to generate adequate aerodynamic forces for flight to occur. The actuators of the system produce either linear or angular movements in the actuation mechanism, which may be transformed into large angles of flaps at wings. Flapping angle generation mainly relies on the actuation mechanism, design scale of the structure, size, and components/material of the wing. The flapping angle can be altered by increasing the load (wing mass) or by changing the wing alignment. As the angle of flapping is very important to generate lift, it is important to decide about the wing size/wingspan.

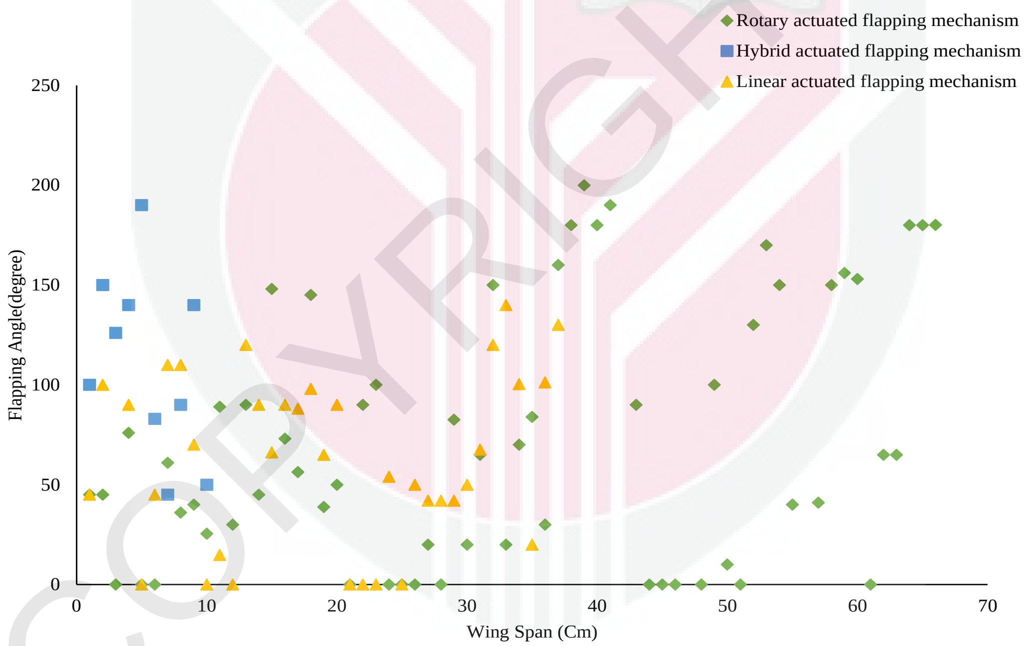

Figure 4.9 : Flapping Angle and a Corresponding Wingspan of Overall Flapping-Wing Systems

While defining a flap angle of motion in any flapping wing mechanism, it is important to ensure that the lead-edge spar rigidity is set in such a way that Figure 4.9 shows the distribution of flapping angle and wingspan for various mechanisms as per the data collected in this paper. From the analyzed designs, wingspan and flapping angle alone do not have any direct or linear relation but depend on various design parameters. the adjacent spar edges at the extremities of the stroke are closed, but not disturbed. Generally, it consumes enormous energy with created extra noise without a gain in thrust, during the contact of leading-edge spars. Rib rigidity could be altered to generate more bending at the wing edges to obtain maximum speed (Zdunich et al., 2007). In piezo actuated mechanisms, it is seen that as the phase delay and difference change, the angle of bending will get altered correspondingly affecting the flaps at wings (H.-C. Chung et al., 2008). It is important while making linkage alignments and connections appropriately joining to wings as it affects the flapping angle indirectly.

4.3 2D/3D Modelling and Simulations of all Design

2D and 3D simulations both play critical roles in the study and design of flapping wing mechanisms. 2D simulations allow a simplified representation of the wing's motion, reducing computational complexity. This enables quicker iterations for optimization and understanding of fundamental fluid-structure interactions. Preliminary design concepts can be rapidly evaluated in 2D to test their viability before moving to more complex 3D models. Key parameters such as wing shape, angle of attack, and flapping frequency can be systematically varied in 2D to study their effects on lift, drag, and thrust generation. Hence 2D simulations help in understanding the basic flow structures around the wing, such as vortex formation and wake patterns, which are integral to lift generation.

Wings are inherently three-dimensional structures, so 3D simulations provide a more accurate representation of the actual wing geometry and its interactions with the surrounding air.3D simulations can capture complex dynamics resulting from the interaction of wingtip vortices, spanwise flow, and three-dimensional unsteady effects that are not present in 2D simulations. 3D simulations are used to compute detailed aerodynamic forces and moments, providing insights into performance that can be used for the design and control of flapping wing aircraft. By combining 2D and 3D simulations, researchers and engineers can efficiently refine simulation approaches aid in understanding the complex physics behind flapping wing flight and contribute to the development of practical flapping wing vehicles.

4.3.1 Simscape Multibody^{tm} Simulations: 3C Model

For further dynamics analysis and validation of the mechanism design, the above model (Figure 4.4) was partially designed by leaving the rectangular frame structure in Simscape MultibodyTM as shown in Figure 4.10. The equivalent actuation circuit for the designed mechanism is shown in Figure 4.11. To demonstrate the significance of rectangular frame structure in the proposed design, simscape multibody 3D design modelling is carried out.

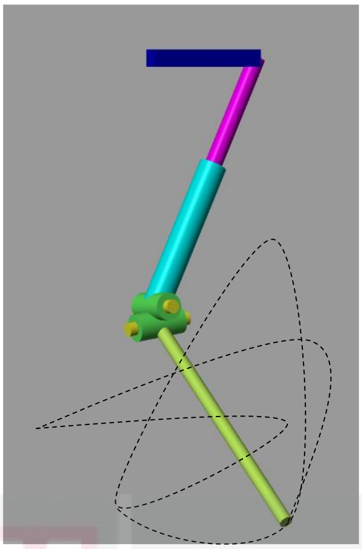

Figure 4.10 : Similar Model Design in Simscape MultibodyTM MATLAB

Additionally, by specifying the joint coordinates, the model enables us to calculate position, and velocity, as well as generate automatic 3D animations to visualize the system's behavior. The individual solids blocks are selected with the aluminum material having density of 2.7g/cm^3. Ramp input signal is driving the first revolute joint as in Equivalent Model shown in Figure 4.11.

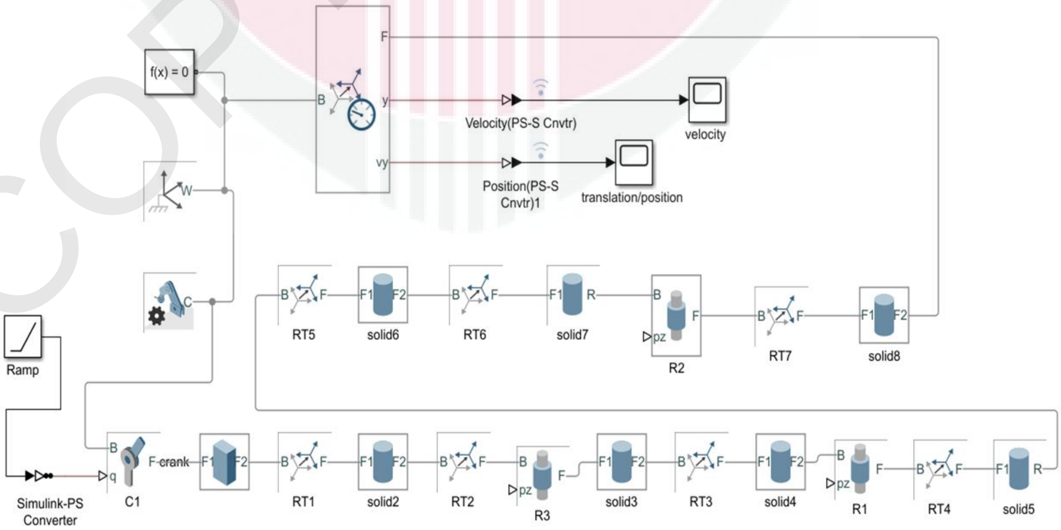

Figure 4.11 : Equivalent Model for the Mechanism in Simscape Multibody^{TM} (SimMechanics^{TM})

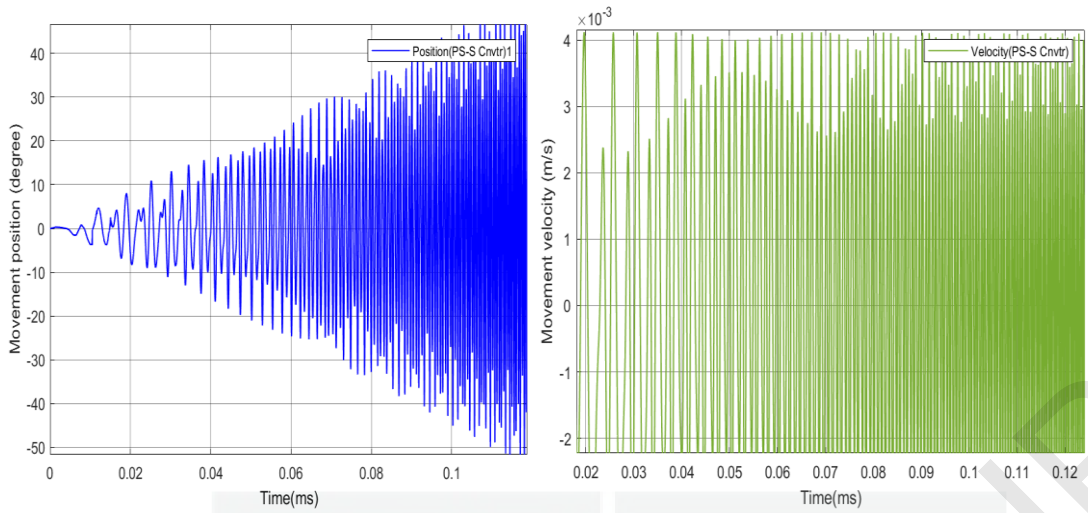

Figure 4.12 : Obtained Position and Velocity of the Wing Tip

To test the model, the joint’s evolution (Figure 4.12) the position and velocity of the flapping link is evaluated according to the direct kinematics derived in above section. To analyze the motional fluctuations of the flapping link two cylindrical joints relate to each other as shown in Figure 4.10. However, the obtained path or position of motional flapping is not symmetrical, but rather random. As a result, a rectangular framework is intended to provide a better flapping motion via the modelling of 3D mechanism's design in Compmech GIM software. Below section B shown simulations demonstrates the significance of adopting a rectangular frame structure for the desired motion direction in this design.

4.3.1.1 COMPMECH GIM Simulations:3C Model

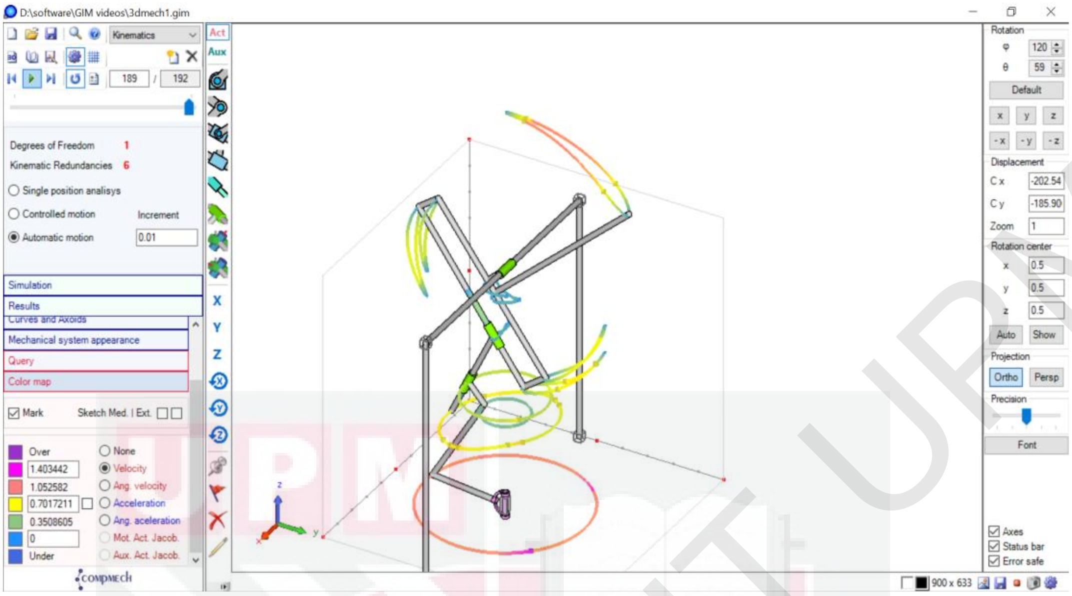

Figure 4.13 (a): Similar Model Design in Compmech GIM Software

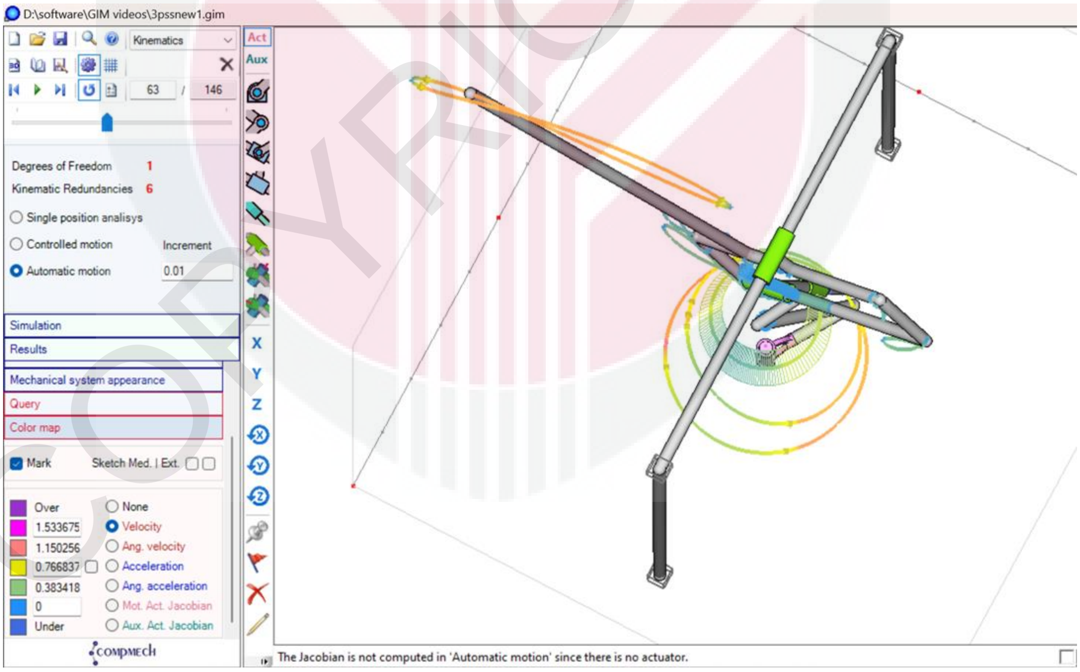

Figure 4.13(b) : Flapping Lever Tip Position Tracing

The mechanism was also simulated using Compmech Gim Software, where kinematic redundancies considered are for six. The workspace with the velocity across the motion path is clearly illustrated in Figure 4.13(a) through color representation from under to over as color variation with respect to change in velocity of motion. As they descend, the flapping represents one complete wingbeat cycle. Figure 4.13(b) is created by adjusting the size of the rectangular frame and links 1, 2, and 3. It is clearly apparent that the variance in link lengths has caused the final position fluctuation of the flapping lever tip. As in Figure 4.13(a), the obtained tracing of the liver tip has a leaf-like shape, whereas the liver tip tracing in Figure 4.13(b) has a figure-of-eight shape. As shown in Figure 4.14(a), the flapping angle obtained is the path taken by the flapping element.

The maximum angle of flapping obtained through angle between two vectors (i.e. between the alignment of final flapping element and the fixed supporting structure of Figure 4.10(a) is obtained as flapping angle range 25-40 degrees, as shown in Figure 4.15 (a), i.e 40-25 = 15 degrees. it is the angle of flapping obtained per wing beat cycle. The variation in wing beat angle velocity and acceleration, obtained in simulations per wing beat cycle is as shown in Figure 4.15(b) and Figure 4.16. The point velocity and acceleration analyzed at the flapping link tip per wing beat cycle is as shown Figure 4.14(b) and Figure 4.15(b) respectively.

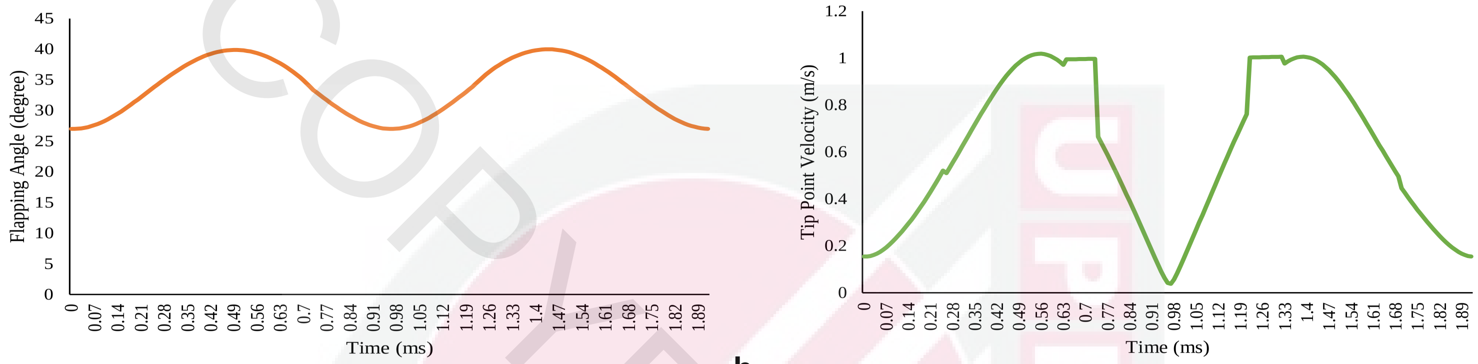

a. **b.**

Figure 4.14 : (a)The Angle of Flapping Obtained, and (b) Flapping Velocity at the Flapping Link Tip

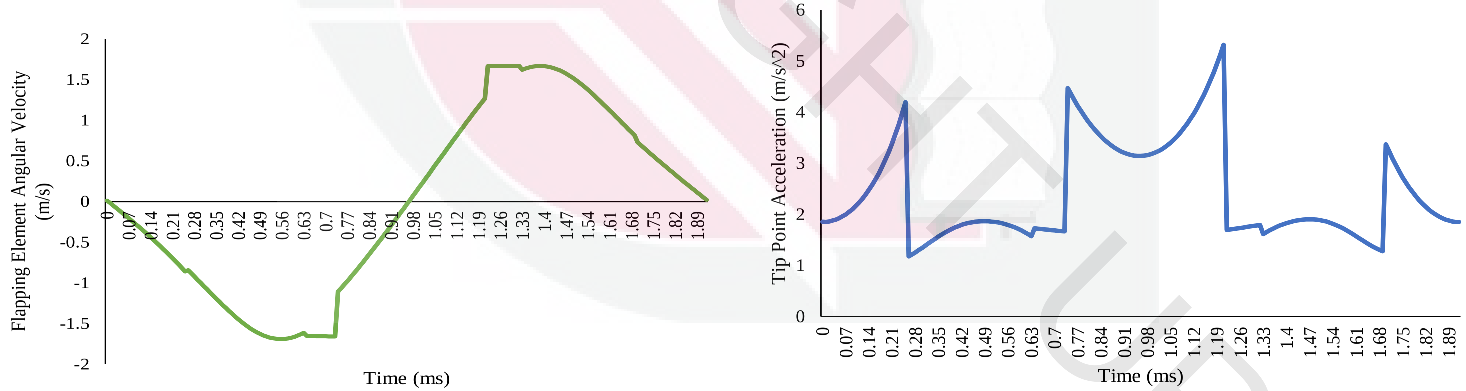

a.

Figure 4.15 : (a) Angular Velocity of the Flapping Element, and (b) Acceleration at the Flapping Link Tip

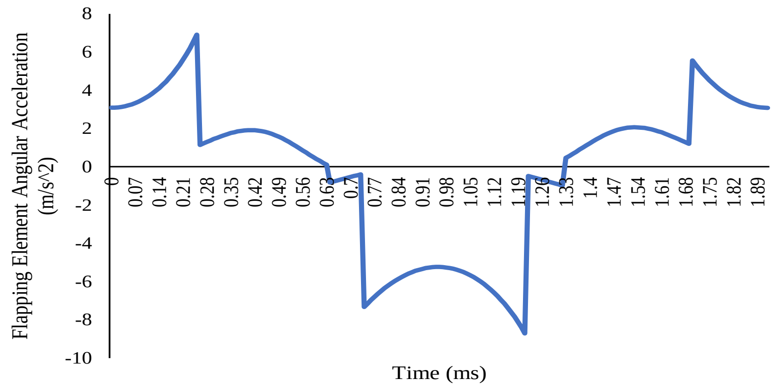

Figure 4.16 : Angular Acceleration of the Flapping Element

Because the levers' design lengths are variable, the obtained lever tip velocities of both python-programmed and comp mech-3d modelled design simulations are very similar to one another. The disparity in velocity can be reduced to an acceptable level by further refining the proposed design of connecting link sizes.

4.3.1.2 Kinematics Modelling in Python Programming

Kinematics modeling for flapping wing designs is a crucial aspect in the development of bio-inspired flying robots, such as ornithopters. This modeling helps in understanding and predicting the motion of the wings, optimizing the flapping mechanisms, and achieving efficient and stable flight. Implementing kinematics modeling in Python involves using mathematical descriptions of the wing motion, such as angular velocities, positions, and accelerations. Here's a step-by-step approach to developing kinematics modeling as discussed in chapter 3 are programmed in Python the obtained results are as shown below Figure 4.17 & Figure 4.18.

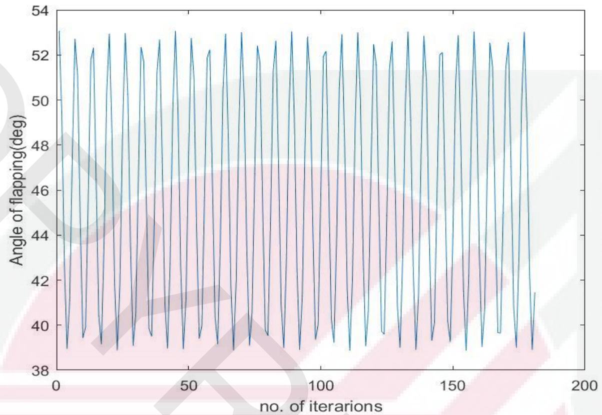

Figure 4.17 : Flapping Angle Obtained from Forward Kinematics of DH-Table 4.1

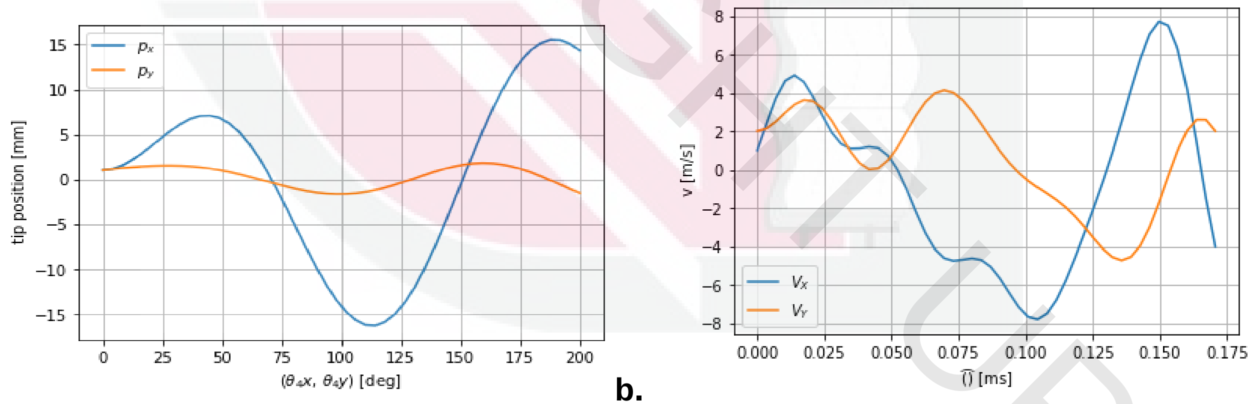

Figure 4.18 : (a) Variation in Flapping Liver Tip with Respect to the Driving Crank Angle in x and y Direction. and (b) Variation in Liver Tip Angular Velocity with Respect to Time in x & y Direction

The forward kinematic equations derived in the above section i.e chapter 3 for 3C design, are implemented into PYTHON programming with a controlled inputs at x, y and z coordinates, looping to obtain the theta 4 value as shown in Figure 4.17 .it can see the angle of flapping obtained at theta 4 is between 39-53 degree along with the number of iterations/samples. i.e 53 – 39 = 14 degrees. The PYTHON-implemented DH table has been used for homogeneous transformation matrix conversions and simulations. The variation in flapping liver (22mm length) edge/tip motion in millimetres relative to the driving crank motion in degrees is depicted in Figure 4.18(a) above. The Jacobian calculated matrix was implemented in Python as a continuation of the dh-parameters, and the velocity variation of the liver tip movement with respect to time in the x and y directions was obtained. This information is depicted in Figure 4.18(b). In comparison to the angular velocity obtained at Figure 4.15 (a), the kinematics results of angular velocity at figure 4.18(b), During the process of doing the two-dimensional kinematic analysis, the variations that are acquired are with respect to the x and y directions. The initial portion of flapping encounters greater fluctuations compared to the latter half. as the lever tip positional analysis is performed at 4.13(b), the similar validation of position through kinematics can be seen in Figure 4.18(a) in x & y directions ensuring 2D performance.

4.3.2 Simulation Results of X-Pattern Crank Slider 4-Bar Mechanism

In this paragraph, the author describes the functioning of the flap process and equipment with needed couplings and its biomechanical modelling using the GIM® software [26], that is a recognized program of the Mechanical

Engineering Department at UPV/EHU.

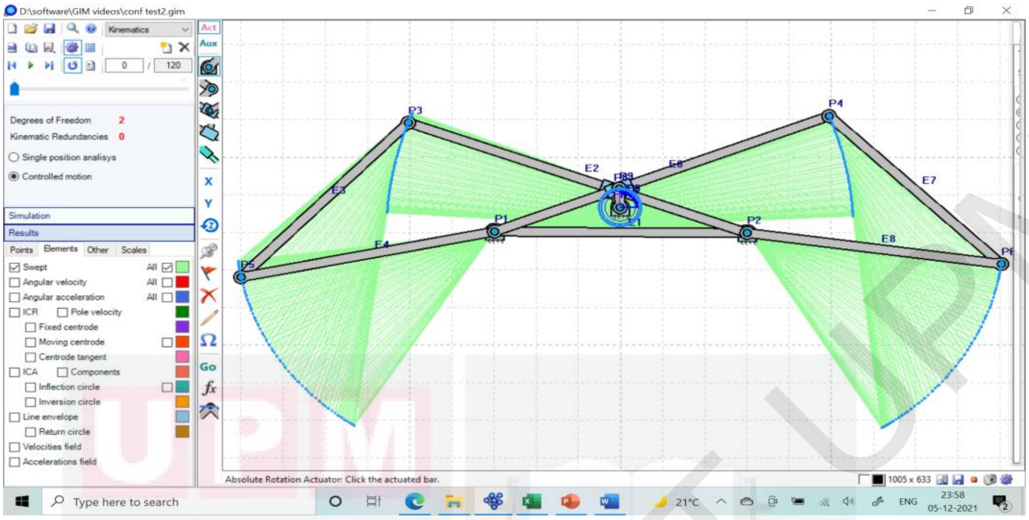

Figure 4.19 : Workspace of the Modelled Design I Mechanism

A kinematic illustration is a geometric representation of a framework wherein suitable joints with elements were being modelled as flawlessly rigid bodies. Figure 4.19 depicts the layout process with a cranked and two slotting mechanisms coupled in an X-fashion as modelled in GIM® software, along with the resulting work area. The differences in underneath or above concentrations of both flap-acceleration and flap-velocity during both lever motions are displayed by varying colour within every occurrence. The disproportionate movement of the slider is visible from the colored display of generated point velocity in Figure 4.19. To demonstrate, a model of a slider-crank mechanism has been created as shown in Figure 5.3, and the trajectories of points of interest can be visualized. Also, the mechanism's geometry has already been defined and its motion simulated in GIM software. Both actions are accomplished through the use of the Geometry and Kinematics modules. While both the wings have almost the similar angle of flaps (i.e 20-25 degrees) at elements E6/E2 and (30-35 degrees) at elements E8/E5 as shown in Figure 4.19. there is an unavoidable movement coordination lag of 1.5-8 degrees in both designs that may be because of the crank and slotted lever transmission's operation principles. The delay seen at both levers while flapping action along with the Cross synchronization between the levers is caused by the offset nature of proposed design arrangement.

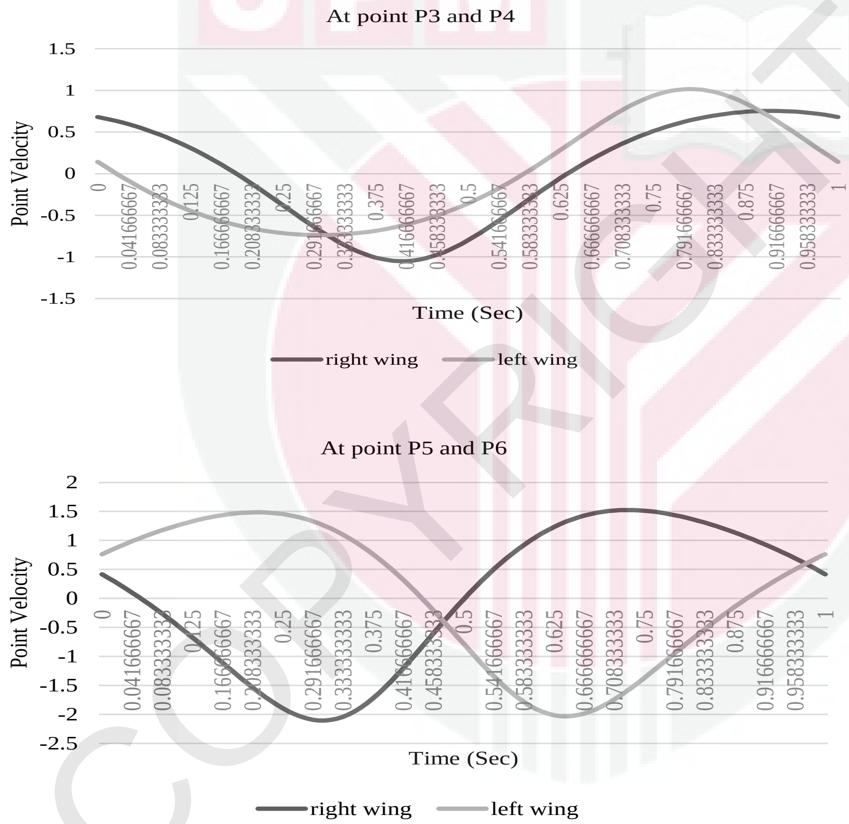

Figure 4.20 : Point Velocity Analysis of the **Design I Mechanism**

Relative speeds of both the side levers edge/tip locations are with delayed motion compared to one another, that’s why there is a lag or velocity distinction between the two-lever motion. To acquire the simulation results, a multi-body technique derived from the basic coordinates is used. The motion of the design mechanism is simulated with all nodal trajectories, velocities, and accelerations at required points or position velocity as shown in Figure 4.20.

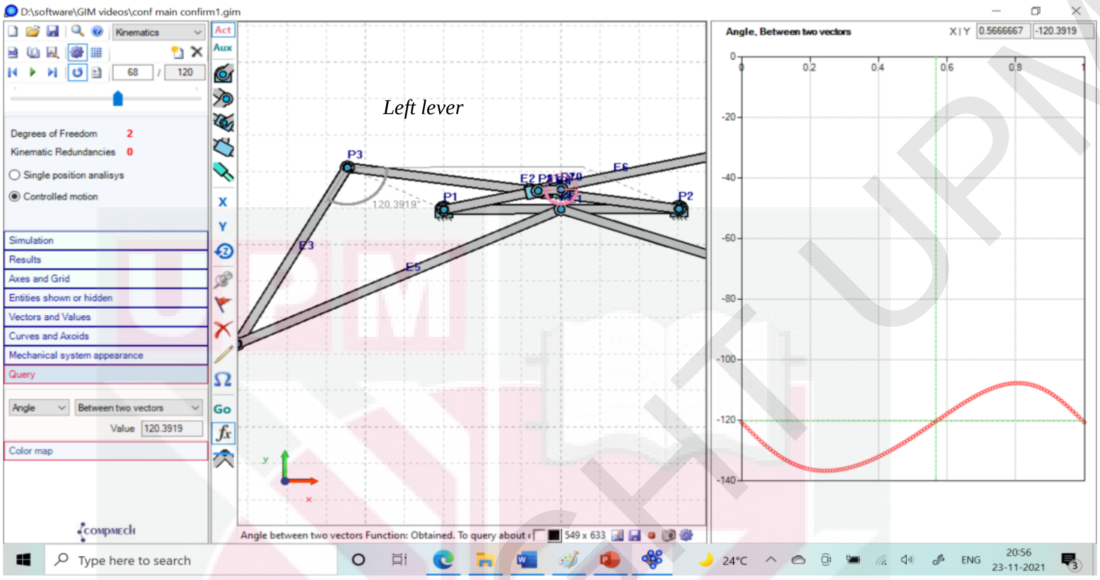

Figure 4.21 : Angle between Two Vectors at Left Lever of the **Design I Mechanism**

However, through GIM software (Macho et al., 2021), the obtain simulated results about the kinematic analysis of the design model for the elements E2/E6 and E3/E7 as shown. Figure 4.22 and Figure 4.23 show the angle between two vectors at the design mechanism's left and right linkage connections. At the left lever, element E3 forms a maximum angle of 136.66 degrees and a minimum angle of 107.7 degrees at point P3 about the angle formed by two vectors at the design mechanisms with the chosen points P2, P3, P4, and P1 as in Figure 4.21. At the right lever, element E7 forms a maximum angle of 136.46 degrees and a minimum angle of 107.11 degrees at point P5 relative to the angle formed by two vectors at the design mechanisms' chosen points P1, P5, P6, and P2 as in Figure 4.22. The Figure

4.23 depicts the Instantaneous Centre of Acceleration (ICA) of element E7 in relation to the entire design model (Viaña et al., 2017). Variations in Instantaneous Canter of Acceleration along the paths of element E7 movements are illustrated, with color-coding's indicating under and over-speed of motion representations.

Although the above-mentioned design mechanism can generate flaps near sliding joint connections, its measured point and element velocity and acceleration are highly variable. This seems to be because of constructability restrictions, in that the time required for both levers to swing is not equal but varied with some lag. Consequently, the mechanism design is asymmetric, as it is unable to perform both wings flapping simultaneously with same angle.

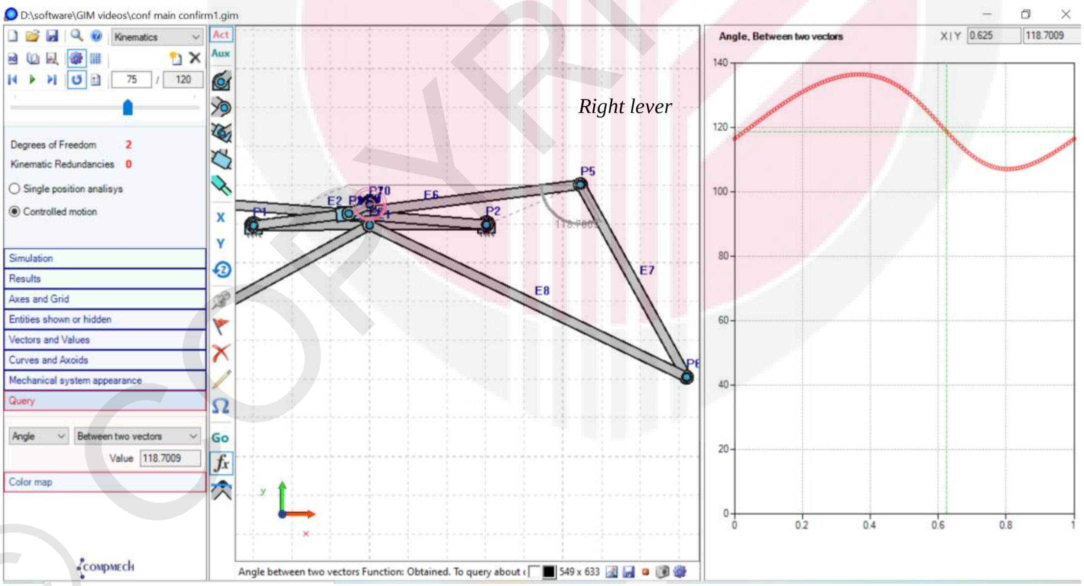

Figure 4.22 : Angle between Two Vectors at Right Lever of the Design I Mechanism

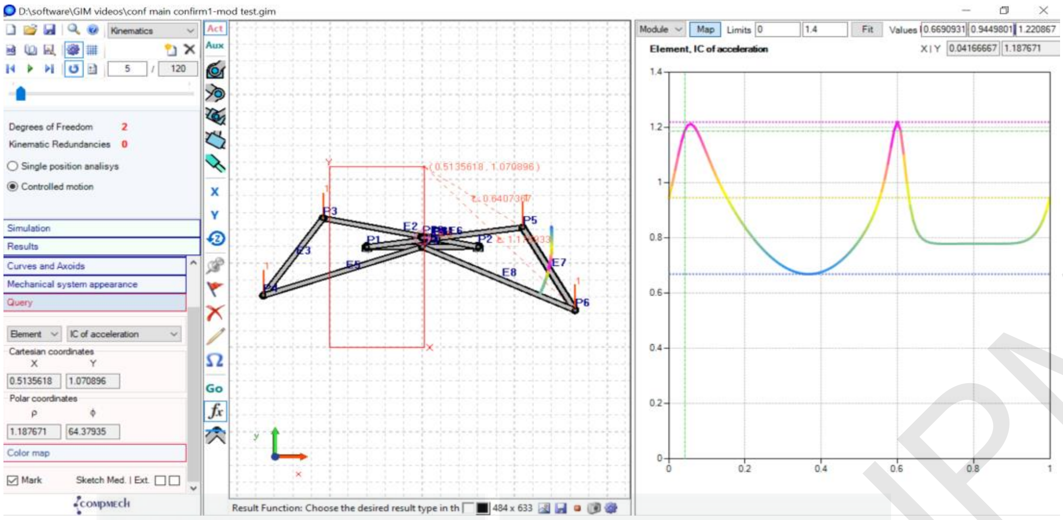

Figure 4.23 : Element IC of Acceleration vs Time (sec)

4.3.3 COMPMECH GIM Simulation Results: Design Mechanism-II

In this section, the operation of the flapping actuation mechanism with required linkages and its kinematic analysis using the GIM® software is reported, which is a registered software of the Department of Mechanical Engineering, UPV/EHU. the design mechanism-II with a single crank and dual slotted levers is modelled in GIM® software, and its generated workspace is presented in Figure 4.24 below. The angle formed at both the levers are same i.e 40 degree. But the phase lag between the left and right wing is 10 degrees as shown in Figure 4.24 i.e when right lever tip is at 40 degree, the left-wing tip is at 30 degree.

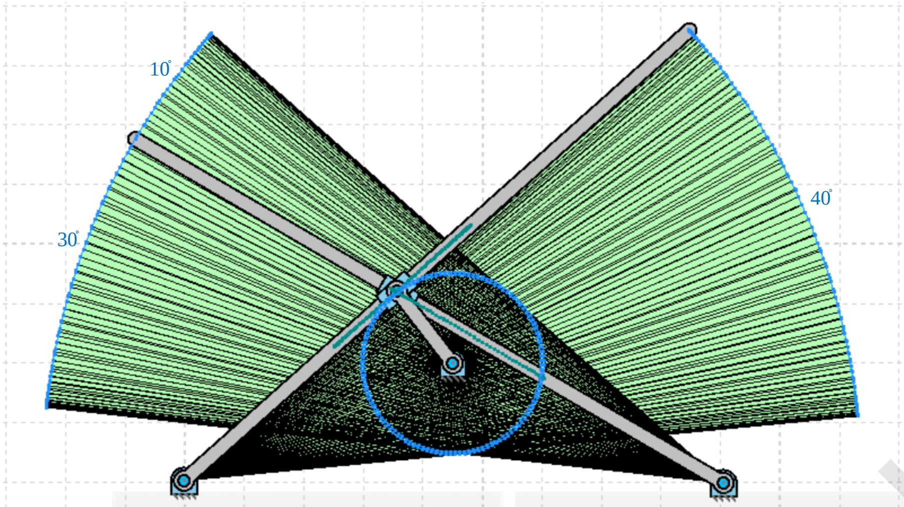

Figure 4.24 : Workspace of the Modeled *SC-SDL* Design Mechanism-II

Figure 4.25 represents the variations of under and over intensities of velocity and acceleration during both lever motions, at each instance is clearly indicated by color. The asymmetric slider motion is evident from the colored simulated output of velocity and acceleration in Figure 4.25. The lag between both the lever flapping motion is due to the offset type of a crank slider mechanism's natural characteristic and the X pattern of alignment between the levers. Figure 4.26 (a&b) indicates the results of a point velocity and acceleration analysis performed with the GIM® software.

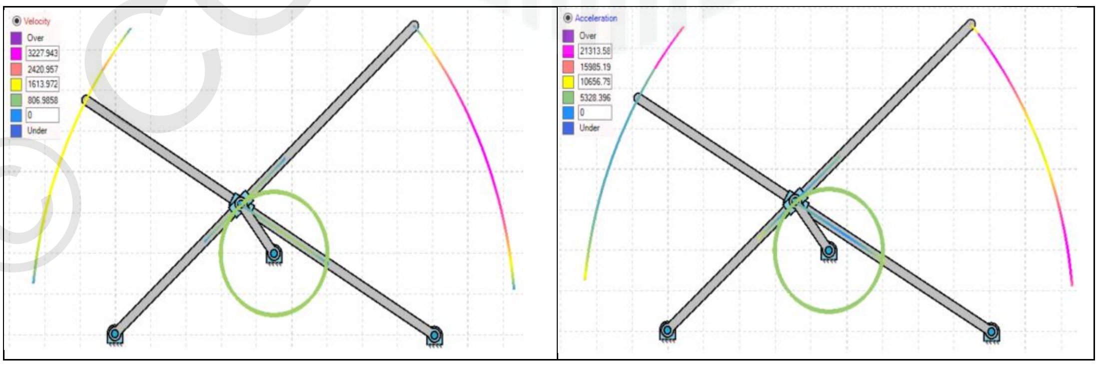

Figure 4.25 : Color Wise Representation of Variations in Velocity and Acceleration at Both Lever Paths of Motion

The velocity at the left and right lever tip points are completely opposite to each other, that's why there is a phase difference and speed difference between both the lever motion. Also, it is seen that the variation in angular velocity and acceleration with respect to left and right slotted lever elements at Figure 4.26 (c&d).

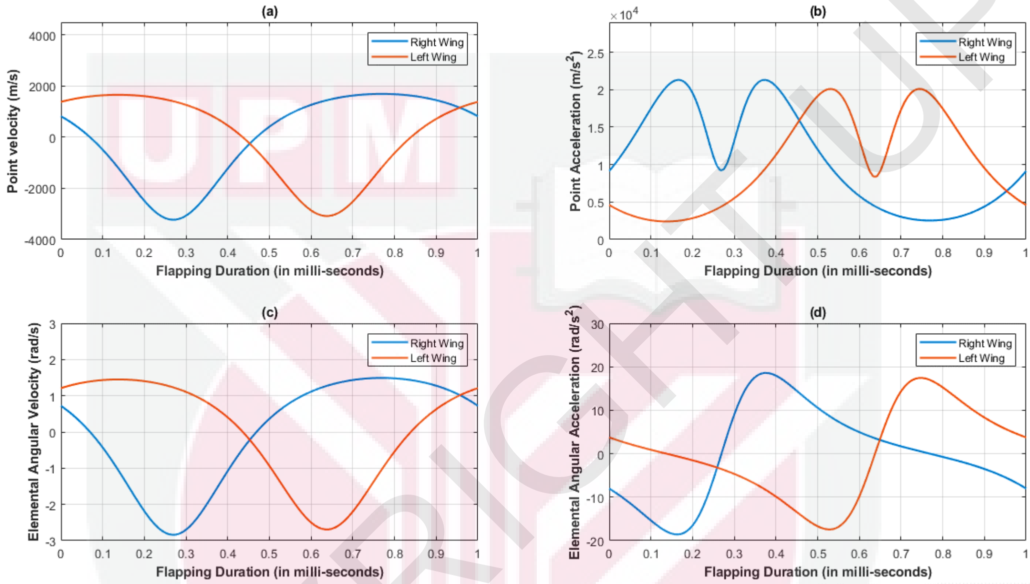

Figure 4.26 : Kinematic Analysis at Lever Tip of SC-SDL Design Mechanism-I; (a)Point velocity vs. Flapping Duration; (b) Point Acceleration vs. Flapping Duration; (c) Elemental Angular velocity vs. Flapping Duration; (d) Elemental Angular Acceleration vs. Flapping Duration

4.3.4 Simulation Results: Design Mechanism-III

The flapping motion of the slotted lever design mechanism-III could be used to generate lift FWMAV applications by connecting wings at its lever tip. With one full rotation of the piston, the slotted lever produces two flaps, i.e. up and down strokes. The simulation modeling of the lever motion analysis with workspace is shown in Figure 4.27*.* The angle generated by both levers is 37 degrees, which is identical. Figure 3 illustrates that the phase lag between the left and right wing is 2 degrees, thus while the right lever tip is at 37 degrees, the left lever tip is at 35 degrees.

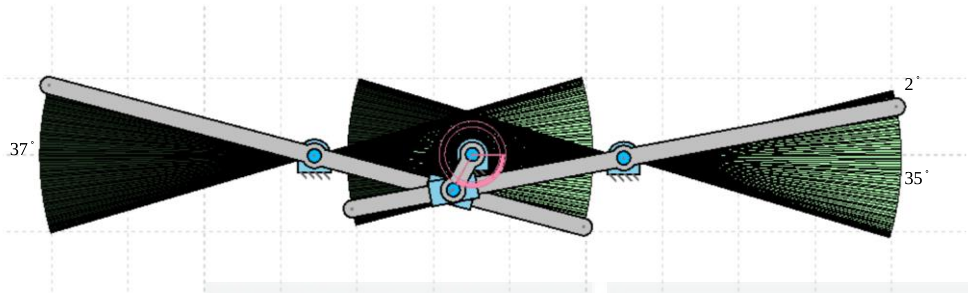

Figure 4.27 : Workspace of the Modeled SC-SDL Design Mechanism-III

But Figure 4.28, shows the variations in the speed and acceleration levels below and above, with a clear color indication in each case. From the colored simulated velocity output and acceleration in Figure 4.28, the asymmetric flapping is noticeable. Since both levers are operated by a single crank, the velocity distribution along their paths is distinct. But because of the reconfigured orientation of the lever and crank connections, the shortfall between the lever flapping is reduced in comparison to the first design.

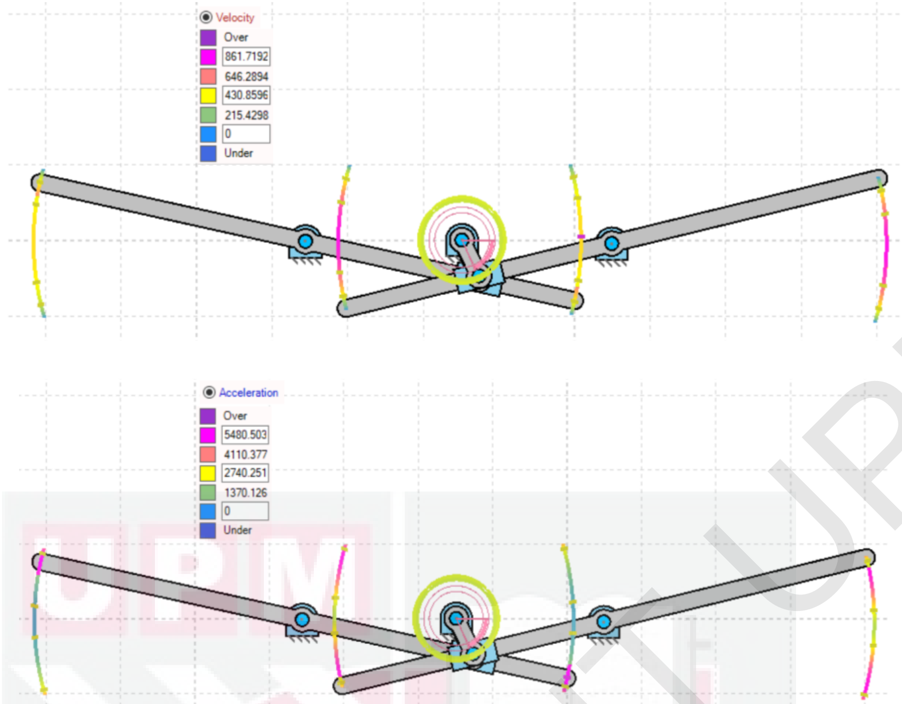

Figure 4.28 : Color Wise Representation of Variations in Velocity and Acceleration at Both Lever Paths of Motion

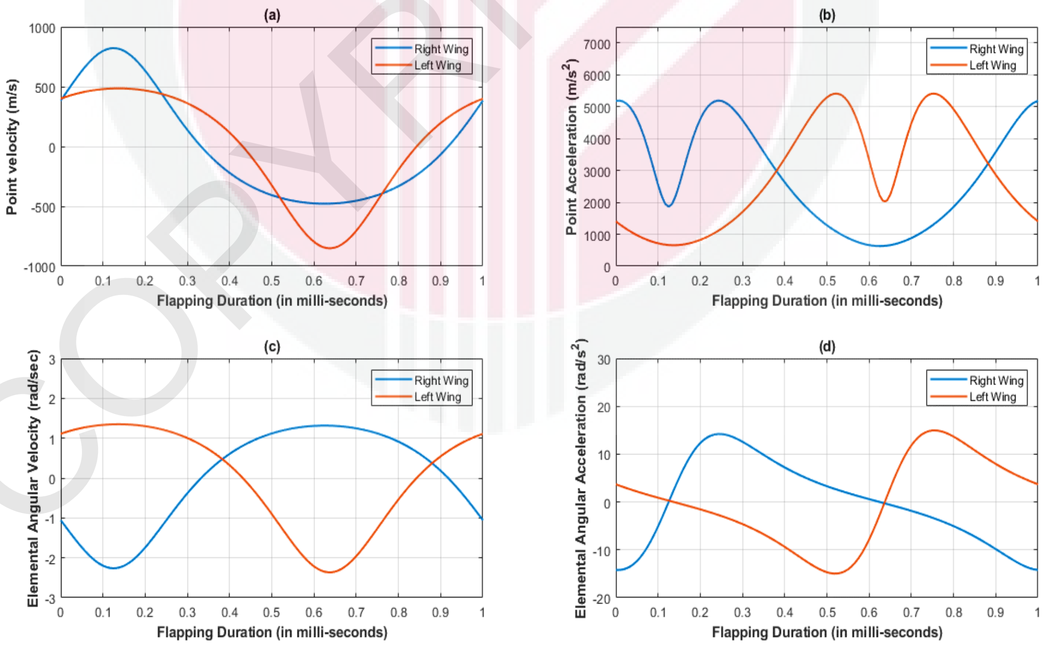

Figure 4.29 : Kinematic Analysis at Lever Tip of SC-SDL Design Mechanism-I; (a)Point velocity vs. Flapping Duration; (b) Point Acceleration vs. Flapping Duration; (c) Elemental Angular velocity vs. Flapping Duration; (d) Elemental Angular Acceleration vs. Flapping Duration

Figure 4.29 (a&b) illustrates the summary of the GIM® software point-velocity analysis, demonstrating that at left lever element there is a small decrease in speed when compared it with the right lever element. Figure 4.29 (a&b) also illustrates the decreased point velocity ratio between the left and right lever tips. However, the acceleration patterns observed in design mechanism -II and III are identical. In addition, the angular velocity and acceleration of the lever element are comparable in designs mechanism II and III as in Figure 4.29 (c&d). In design mechanism-II the phase lag was 10 degrees whereas in design mechanism-III the phase lag is 2 degrees. However, the phase delay between the wing's movement is minimized in revised design mechanism - III, so this design could be suited for FWMAV applications. Hence, the authors of this paper attempted a parametric study for its motional analysis, which is elaborated in the further sections here.

4.3.5 Simulation Results: Design Mechanism-IV

The flappable movements of the sliding lever design mechanism is being used here to actuate flapping for MAV applications by connecting wings at its lever tip. With one full rotation of the crank, the sliding lever produces two flaps, i.e. forward and return strokes. They attempted to validate the design analytically using MATLAB programming and kinematically using Compmech GIM software. Both simulated results have been compared in this section to complete a structural validation of the proposed mechanism.

4.3.5.1 Matlab Simulations of Design Mechanism-IV

The analytical solution derived in the above section are programmed in MATLAB and its animation design is as illustrated in Figure 4.30 below. Where link L1 (black) represents the fixed distance from the origin of crank to the sliding lever hinge. The length of L1 is set here for 15mm. the crank (blue) link L2 is set to be 9mm, i.e the radius of the crank. The sliding edge of the flapping (green) link L3 is set to 40mm in length to demonstrate the flapping motion conversion from crank rotation.

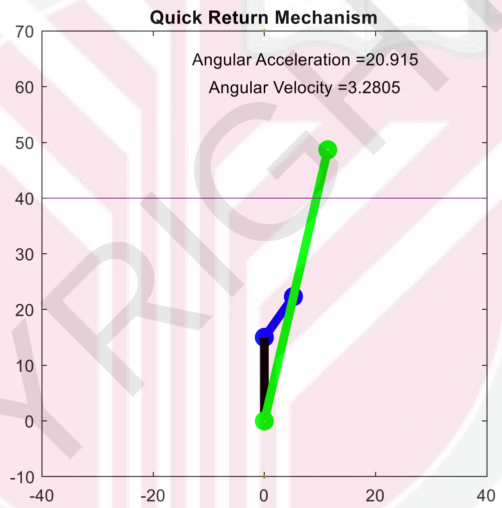

Figure 4.30 : MATLAB of DC-SDL Single Lever for Simulation

The output results obtained from the MATLAB simulated program with respect to lever angular velocity and angular acceleration for a given crank/motor angular velocity of 10 rad/sec as an input is as shown in Figure 4.31. When an input angular velocity of the crank/motor is varied between 5 to 25 rad/sec, the corresponding variations in angular velocity and angular acceleration can be seen in Figure 4.32.

The obtained angular velocity is not equivalent to a symmetric sinusoidal wave because its forward and return strokes are of varying kind. It is evident from Figure 4.27 that the return stroke is faster than the forward stroke. Similarly, variation in corresponding acceleration is also depicted in it. The above Figure 4.31 graph depicts the changes in sliding lever velocity and acceleration, when the input angular velocity of the crank/motor is varied from 5 to 25 rad/sec.

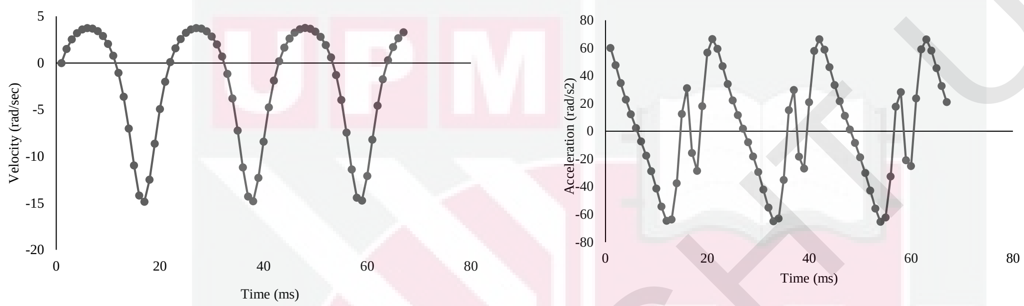

Figure 4.31 : Velocity and Acceleration Determined by Simulation during Angular Velocity at Motor is Set to be 10rad/s

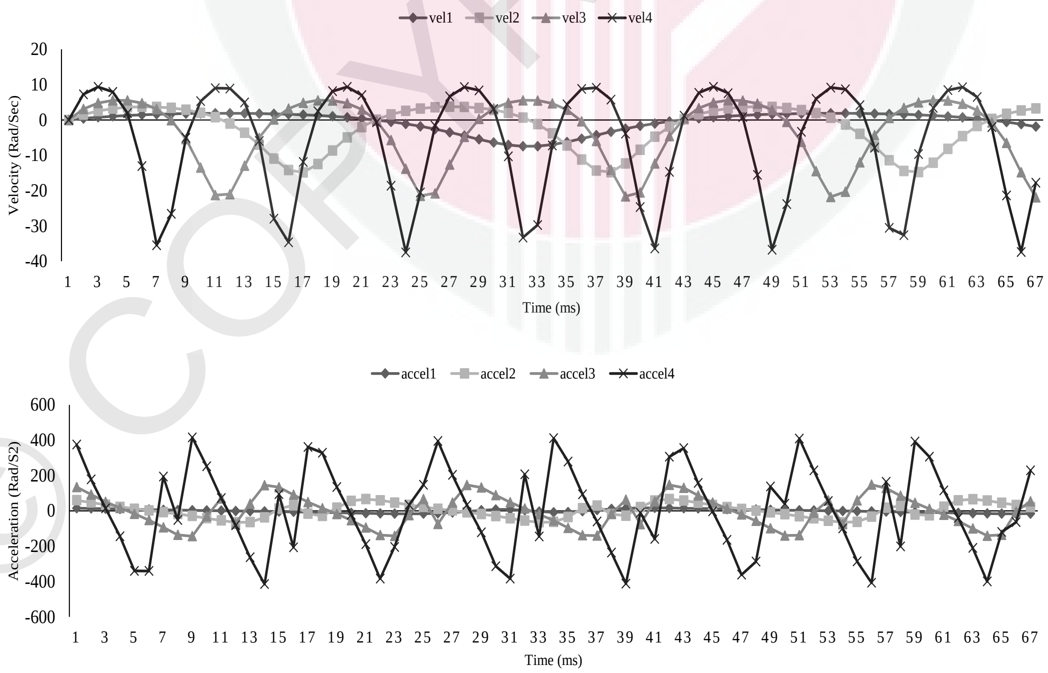

Figure 4.32 : Changes in Velocity and Acceleration Based on the Different Angular Velocity Set at the Motor

Figure 4.32 depicts the variation in lever velocity (i.e. vel1, vel2, vel3, vel4) and acceleration (i.e. accel1, accel2, accel3, accel4) corresponding to the variation in crank/motor input angular velocity (i.e. 5, 10, 15, 25 rad/sec). As the crank/ motor's velocity increases, the amplitude of flapping lever's velocity and acceleration increase proportionally which can be seen in above Figure 4.32.

4.3.5.2 Compmech GIM Simulations: Design Mechanism IV

At the levers of DC- SDL With one full rotation of the crank/motor, the sliding lever produces two flaps, i.e. forward and return strokes. The simulation modeling of the lever motion analysis with workspace are shown in Figure 4.33**,** Where individual wing motion is driven by a separate motor, the mechanism for controlling the individual lever motion will be superior. Figure 4.34 illustrates the summary of the GIM® software simulation for our proposed mechanism, i.e flapping velocity analysis, demonstrating that at forward stroke there is a small decrease in speed whereas in return stroke it is with high speed.

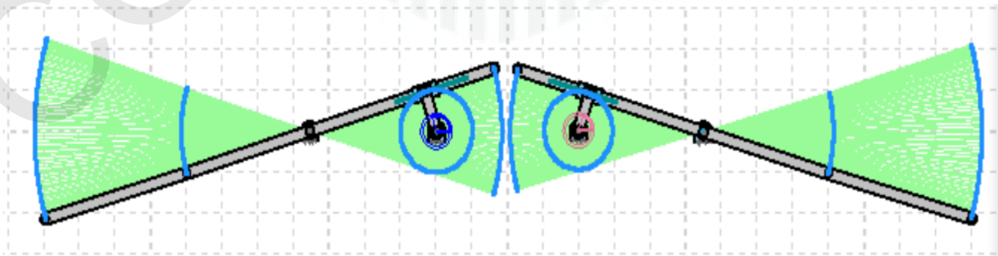

Figure 4.33 : Workspace of the Modeled DC-SDL Mechanism

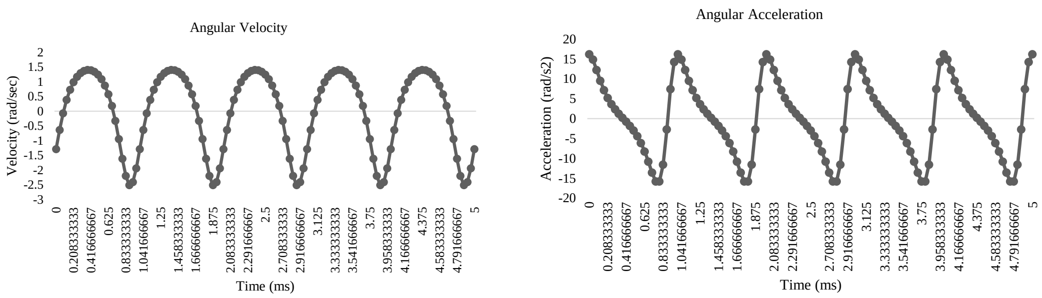

Figure 4.34 : Obtained Angular Speed and Acceleration for Sliding Lever Element Motion

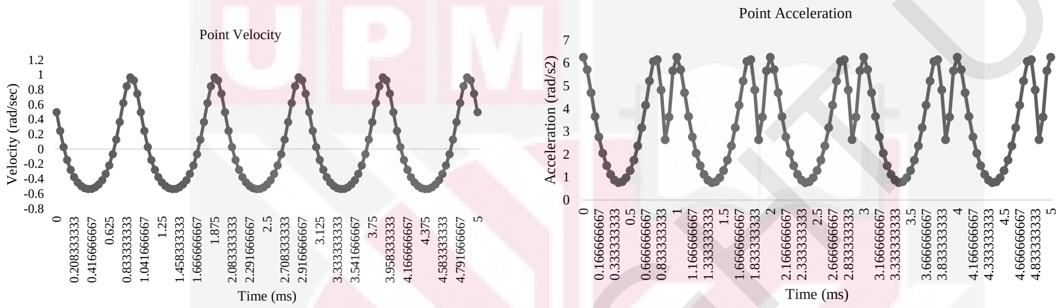

Figure 4.35 : Point Velocity and Acceleration Measured at the Tip of Proposed Sliding Lever Wing

By obtaining the velocity variation at the liver tip i.e where the wing will be attached, to know the flapping speed at that point, as shown in Figure 4.35. Figures 4.34 and Figure 4.35 demonstrate that the velocity of the lever element and the velocity of the lever tip are opposites to each other. The pattern of angular velocity and acceleration obtained through analytical derivation in Figure 4.31 is identical to the simulation results obtained from the Compmech GIM software i.e Figure 4.34 and Figure 4.35. The simulation design matches the mathematical derivation of the design model precisely, confirming the mathematical derivation of the design model. Consequently, proceeded with proposed research to fabricate the design and built a test bench model.

4.3.6 Simulation Results: Design Mechanism-VI

Modelling of four wings actuation through single motor in Compmech GIM software is as shown in Figure 4.36. The obtained wing lever tip angular velocity with respect to left, right, up, and down levers are as shown in figure 4.37 below. The polynomial curve obtained is highlighted with its equation and R squared value within the graph. The wing tip positional variations in degrees and angular acceleration for all four levers are depicted in Figure 4.38 and Figure 4.39 below. The lack of coordination (see in Figure 4.38) in the lever movements and the resulting insufficient lift can be attributed to various factors like Motor Power, Torque, Uneven Load Distribution, Timely Synchronization, Mechanical Design and Tolerances etc. coin motors are typically designed for simple vibration applications and might not have sufficient power or torque to drive a complex mechanical arrangement like a slider-crank mechanism with four levers.

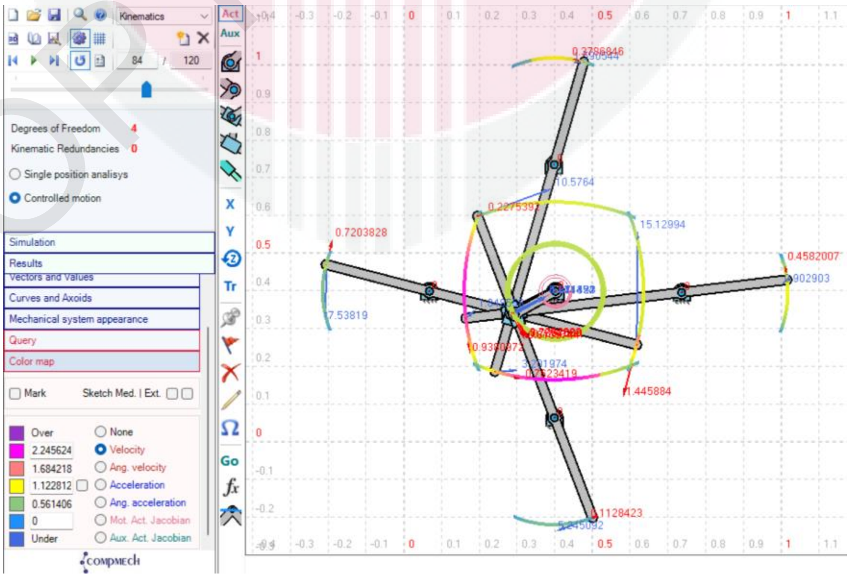

Figure 4.36 : Modelling of Four Levers (Sliding Quad Levers) Actuation through Single Motor in Compmech GIM Software with its Velocity Indications

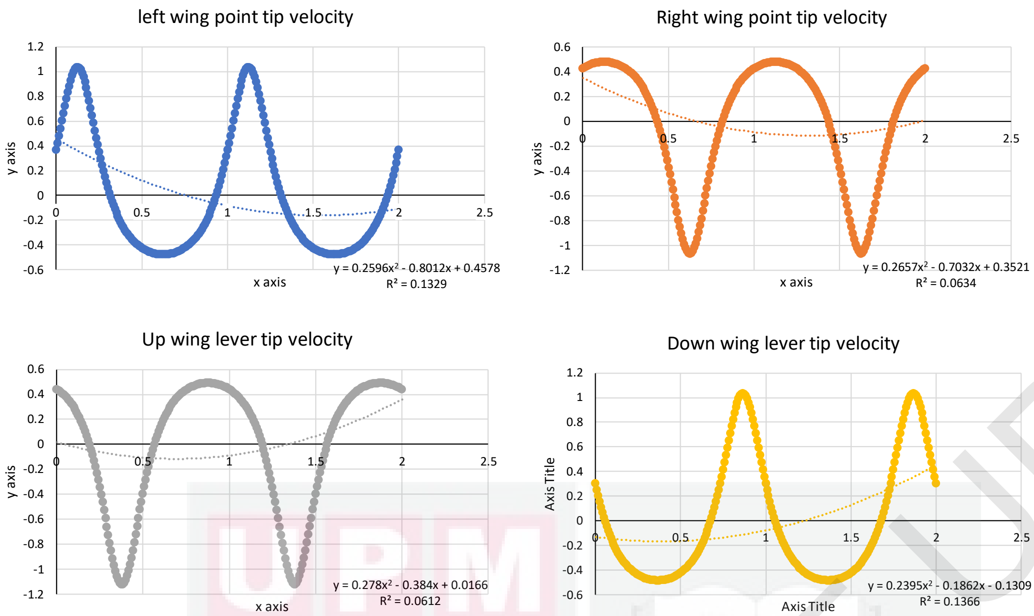

Figure 4.37 : Wing Tip Velocity Variations of all the Four Wings

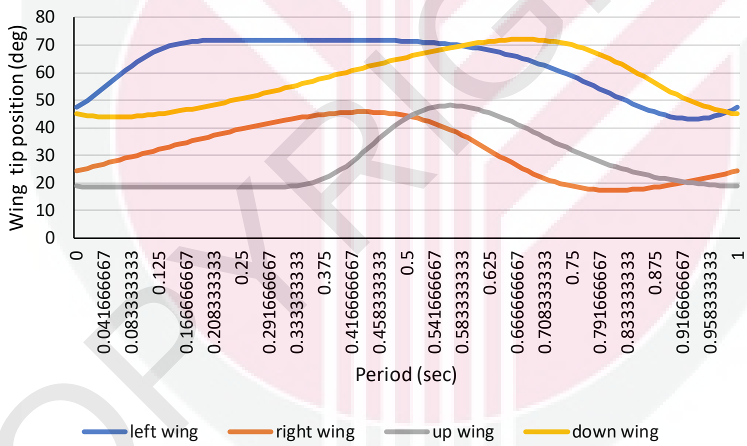

Figure 4.38 : Wing Tip Positional Variations of All the Four Wings

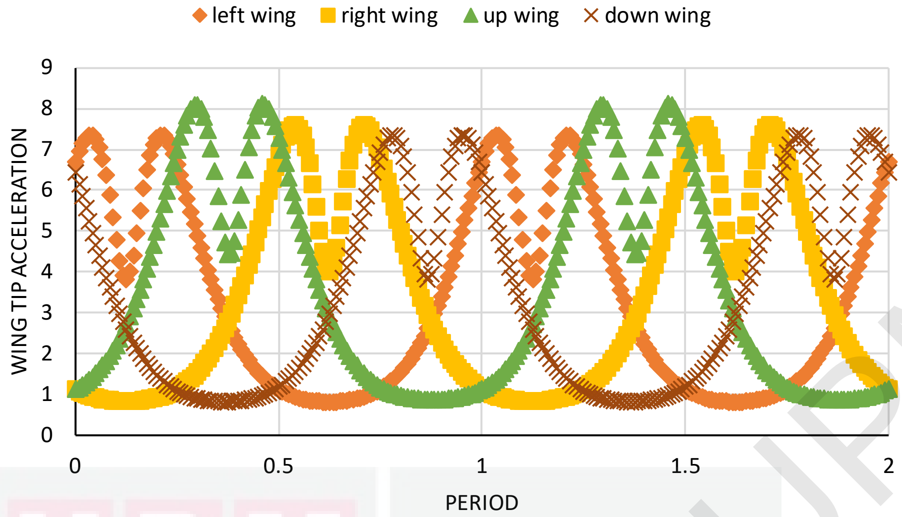

Figure 4.39 : Wing Tip Acceleration Variations of all the Four Wings

As a result, the motor might struggle to overcome the resistance caused by the linkages, leading to uneven movements and reduced lift. In a four-lever arrangement, each lever's load and resistance might vary depending on the specific geometry of the mechanism. If the linkages and levers are not designed with balanced load distribution in mind, it can result in certain levers receiving more force than others. This imbalance can lead to erratic movements and poor coordination. Achieving proper timing and synchronization of the four levers' movements is critical for generating consistent and sufficient lift. If the levers are not precisely coordinated, they might interfere with each other's motion, leading to disruptions in the desired movement pattern. The mechanical design of the linkages, levers, and crank plays a crucial role in the smooth operation of the mechanism. If there are inaccuracies or tolerances in the design, it can result in binding, friction, or misalignment, which in turn can hinder coordination and lift generation. Coin motors often lack the precise control and feedback mechanisms needed for intricate mechanical systems. Without accurate position or speed control, it becomes challenging to ensure that the lever movements are synchronized and coordinated effectively.

4.4 Simulation Results: Controller Implementation

The implementation of a controller in any flapping wing actuation design is pivotal for several reasons. Controllers are essential to maintain precise wing movements, which are critical for the stability of the flight. Slight deviations in flapping motion can greatly affect the lift, thrust, and maneuverability. Active control allows the flapping mechanism to adapt to varying flight conditions, such as changes in wind speed or direction, ensuring the system can respond to external disturbances. A well-designed controller can optimize the flapping motion to minimize energy expenditure, enhancing the efficiency and endurance of the flying device. A controller can execute complex sequences of movements to perform these maneuvers, like hovering, turning, and rapid ascent or descent. Hence, the controller implementation in flapping wing actuation designs plays a central role in achieving precise, efficient, and effective flight. It integrates sensor data, actuator performance, and environmental input to manage the complex dynamics of flapping flight.

4.4.1 Controller Simulations: DC-SDL Mechanism

Utilizing Simscape for modeling flapping wing designs offers several advantages like, it allows for the creation of physically accurate models based on actual system components and properties, leading to more realistic simulations. It supports the integration of multiple physical domains, such as electrical, mechanical, hydraulic, and thermal, within a single environment, which is essential for the complex interactions in flapping wing mechanisms. Simscape uses a block diagram approach similar to Simulink, which is intuitive for users familiar with MATLAB and makes it easier to assemble and visualize the system. Working within the MATLAB environment enables seamless data exchange between the simulation and other MATLAB tools used for data analysis, processing, and visualization. Simscape works effectively with Simulink for designing and implementing control strategies, enabling the investigation of controller performance in the overall system. The simulations are carried out at simscape by modelling DC-SDL mechanism as shown in chapter 3 of Figure 3.42 with its circuit connections, in Figure 3.43, the input signals provided at left and right motors are as in Figure 4.40 below.

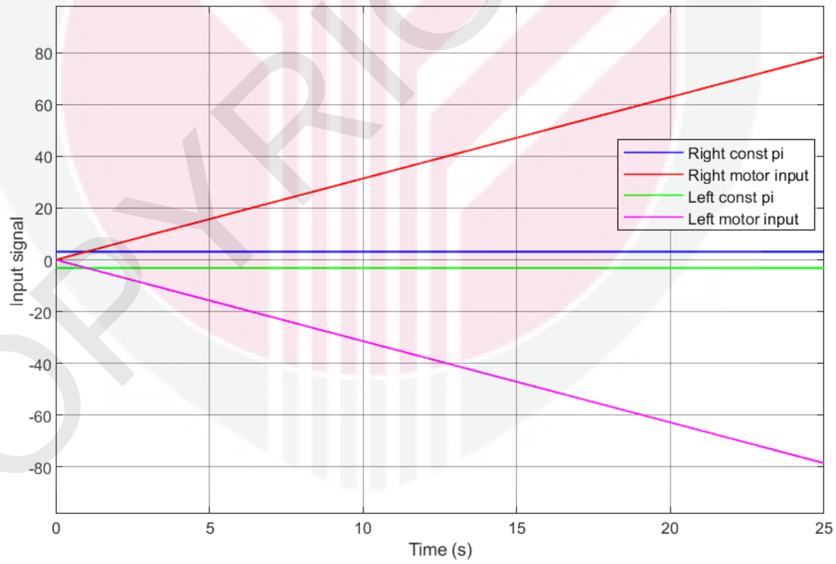

Figure 4.40 : Input Signal Generated from Constant & Integrator Provided at the Revolute Joint A & A1 for Actuation

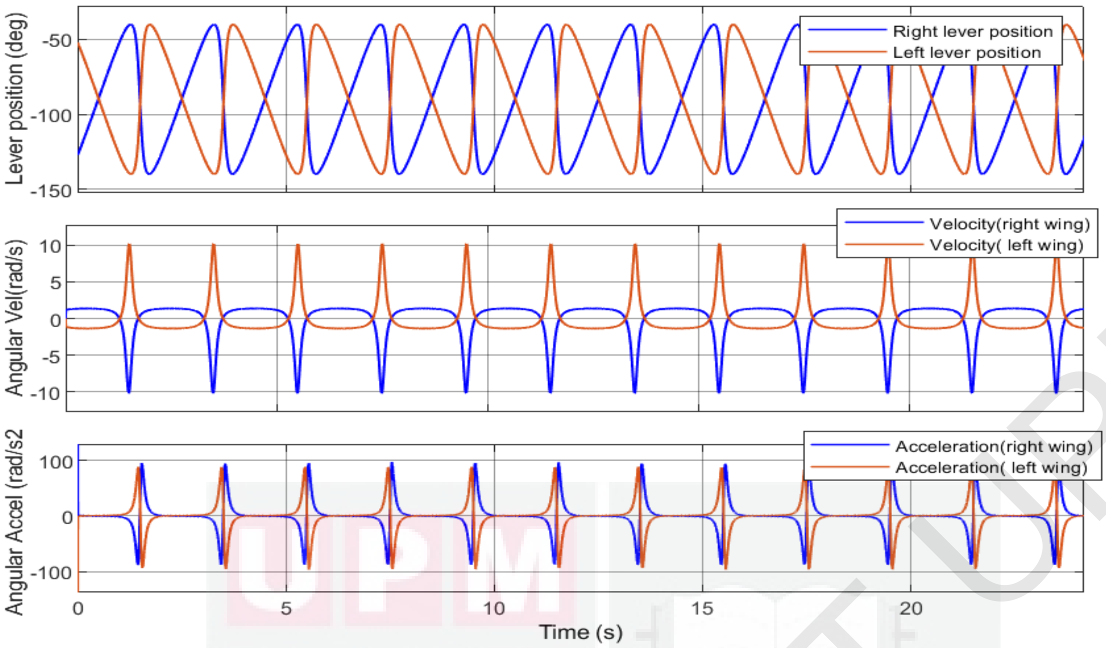

Figure 4.41 : Variations in Both the Lever Positions, Angular Velocity and Angular Accelerations of the DC-SDL Mechanism with Respect to Time

The input signal for the revolute joint is generated using a physical signal (PS) constant block with unit values for Pi (3.142) and a physical signal (PS) integrator block with unit values for Pi/180. Figure 4.40 illustrates the generated sample signal provided at right and left lever revolute joints as an input for its actuation. The corresponding lever flapping obtained as an output by DC-SDL model with left and right lever positions, angular velocity and angular acceleration are depicted in Figure 4.41

4.4.2 PID Controller for the Left Lever of Modelled DC-SDL Mechanism

The tuning of a PID (Proportional-Integral-Derivative) controller is critically important for any flapping wing system due to several reasons that directly impact the performance, stability, and efficiency of the system. Proper tuning ensures that the flapping wing system remains stable during flight. Without appropriate tuning, the system might become unstable, leading to erratic wing movements and potentially causing the system to crash.

The PID controller has been applied to the left lever of the DC-SDL modeled mechanism for continuous time domain configuration. Where proportional gain is set to 1, integral gain is set to 1, derivative gain is set to zero, and filter coefficients of 100 are being used. The PID block incorporated into the modeled circuit is depicted in Figure 4.42. The input signals for the left and right motors, along with the PID controlled signal, are illustrated in Figure 4.43. Using a PID-controlled mechanism for flapping actuation has the potential to improve the system's oscillating frequency and overall performance. Here illustrates the way a PID controller may influence the flapping frequency of an actuation mechanism. The impact of the PID controller on the actuation speed of the left lever in relation to the right lever can be noticed in Figure 4.44. A proportional-integral-derivative controller, often known as a PID controller, is a sort of feedback control system that is an essential component in the process of controlling the behavior and performance of a DC motor. PID controllers are effective in accomplishing desired control objectives, which has led to their widespread adoption in a variety of applications, including those involving DC motors. By modelling a DC motor with a PID controller (as in Figure 7.8), they attempted to learn about the properties of the DC motors by tuning it. The circuit consists of a controlled voltage source modulated by the PID controller depending on the desired angular speed provided. Controlling the speed of a DC motor by modifying the voltage source.

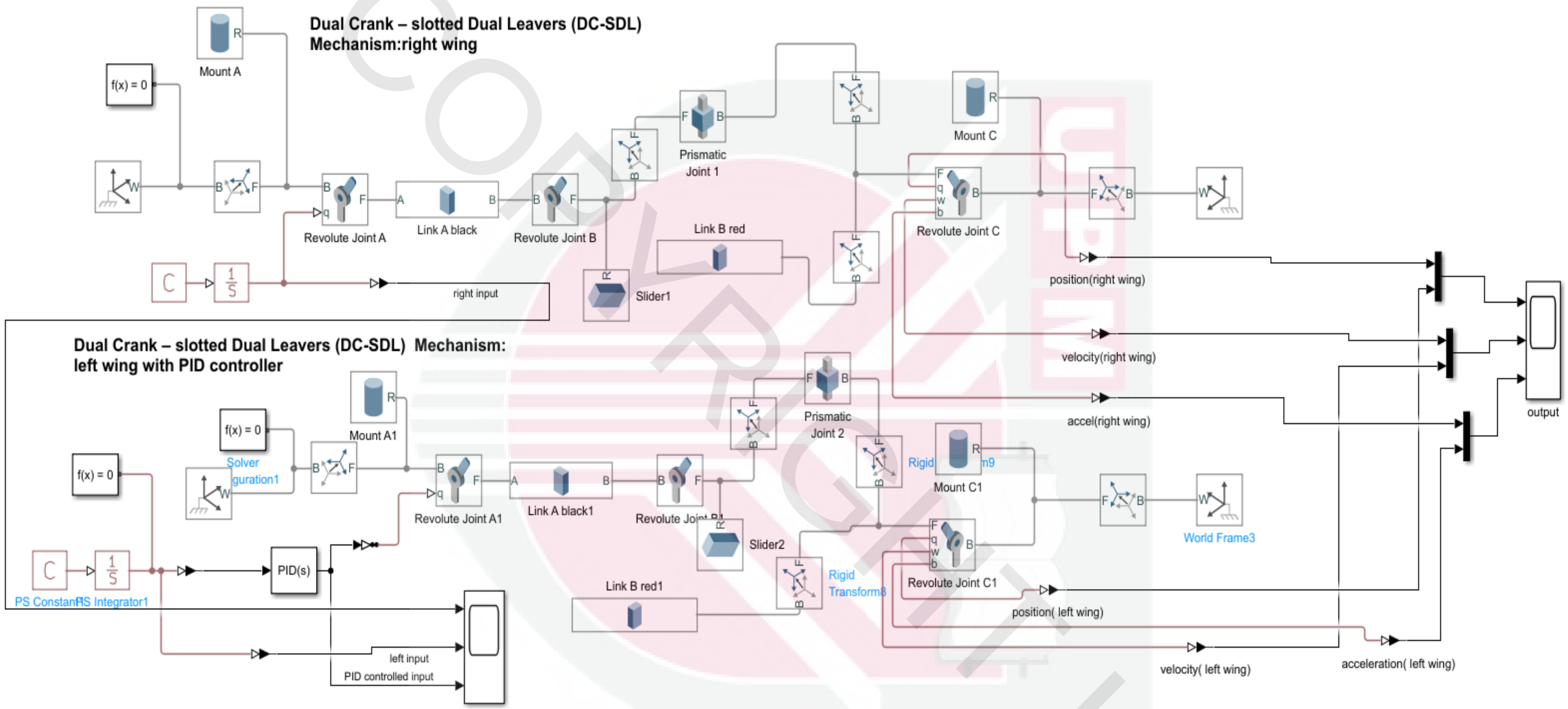

Figure 4.42 : PID Controlled (Left Wing) Connections of Modelled Dual Crank – Slotted Dual Leavers (DC-SDL) Mechanism in Simscape

Using a PID controller is a classic and effective application of control theory. Some form of sensor feedback is required to measure the actual motor speed to modulate its speed. This could be an encoder or tachometer affixed to the motor shaft, which provides information about the actual rotational speed of the motor.

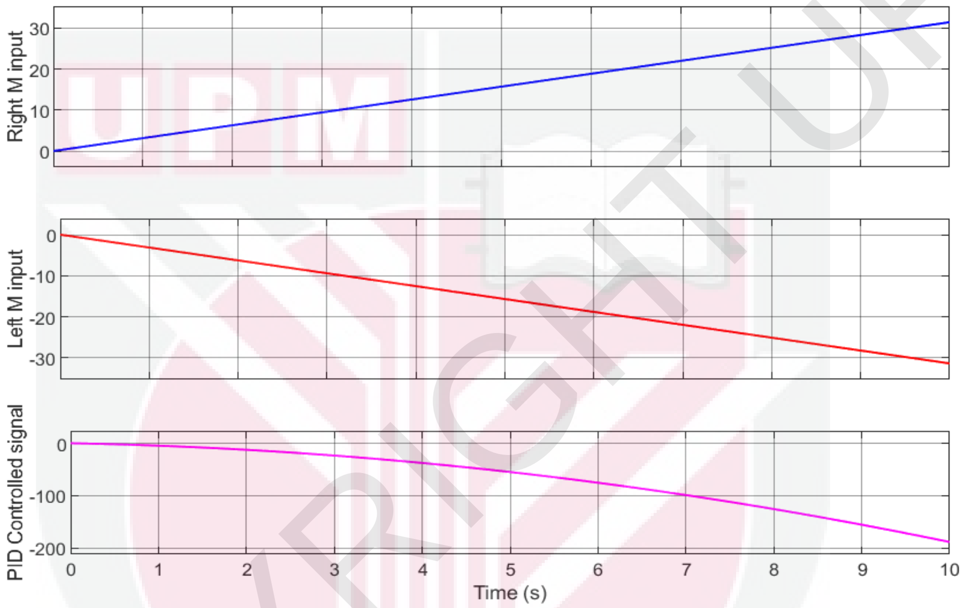

Figure 4.43 : Left and Right Motor Input Signals with PID Controlled Signal

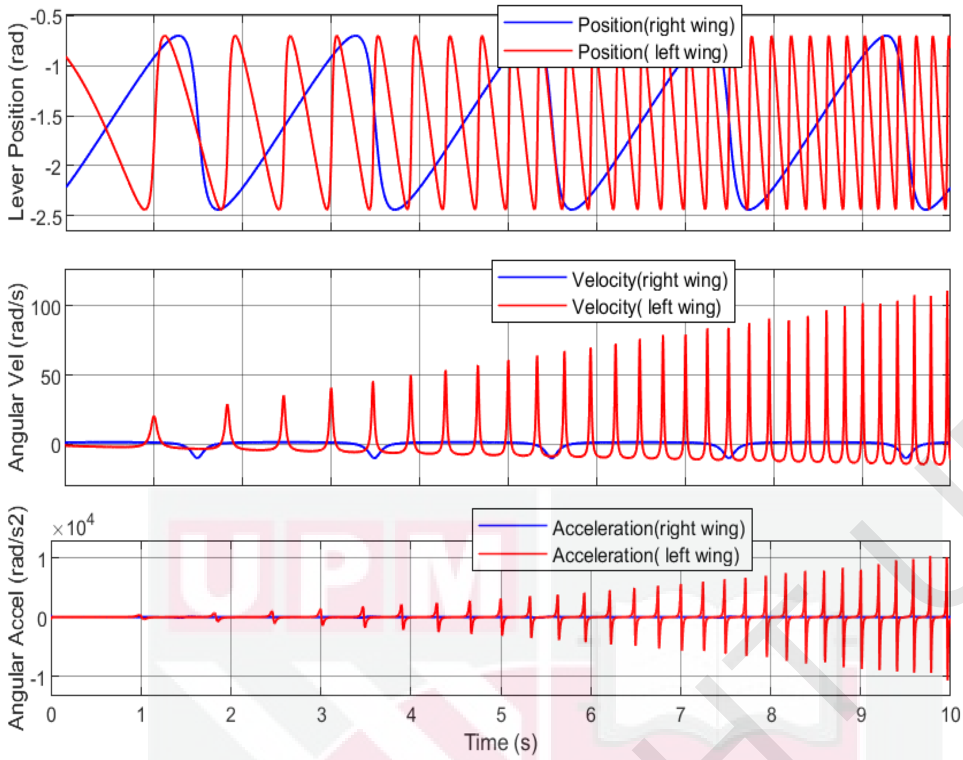

Figure 4.44 : PID Controlled Variations of Left Wing Lever Position, Velocity and Acceleration with Respect to Right Wing (without PID) of DC-SDL Mechanism

4.4.3 DC Motor with PID Controller Tuning

Simscape is a simulation tool within the MATLAB environment used for modelling and simulating physical systems, including electrical, mechanical, fluid, and thermal systems. To use Simscape for DC motor speed control in flapping wing design, following a series of process like the ones detailed here is very much important. By defining the DC motor parameters such as resistance, inductance, torque constant, and back EMF constant. Use Simscape components to build an electrical circuit that represents the DC motor. This will typically include a voltage source, electrical resistance, electrical inductance, and a rotational electromechanical converter. Model the flapping wing mechanism connected to the DC motor. This may involve rotational and translational spring-dampers, rigid bodies, and joints to represent the mechanical structure and motion of the wings. Implement a control strategy suitable for your flapping wing design and the desired motion. Typically, a PID controller is used for speed control of DC motors. In Simscape, the controllers are created within a Simulink block diagram using standard Simulink components and then interfacing it will be performed with the physical model by using Simulink-PS Converter and PS-Simulink Converter blocks. By referring Figure 3.44 in chapter 3, the Simscape modelled DC motor with PID controller, have been tuned for P as 0.026246 and the I value 52.4928, when D is zero. The obtained out put of dc motor after PID tuning can be seen at Figure 4.45 below.

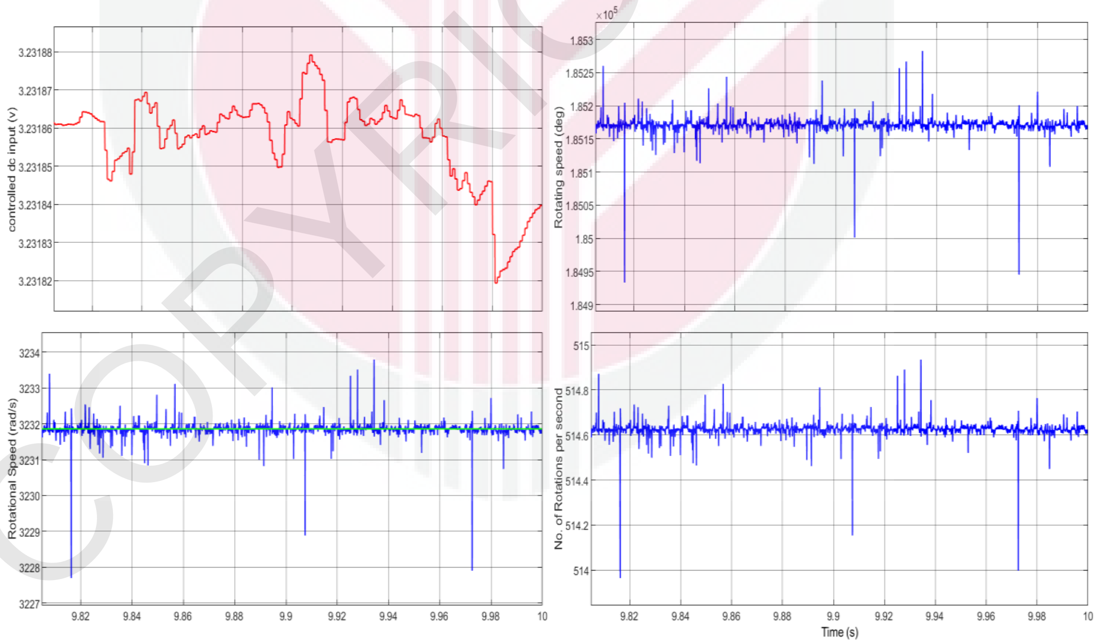

Figure 4.45 : DC Motor Output after PID Controller Tuning

4.4.4 PID Controlled DC Motor as Driving System at Right Lever of DC-SDL Model

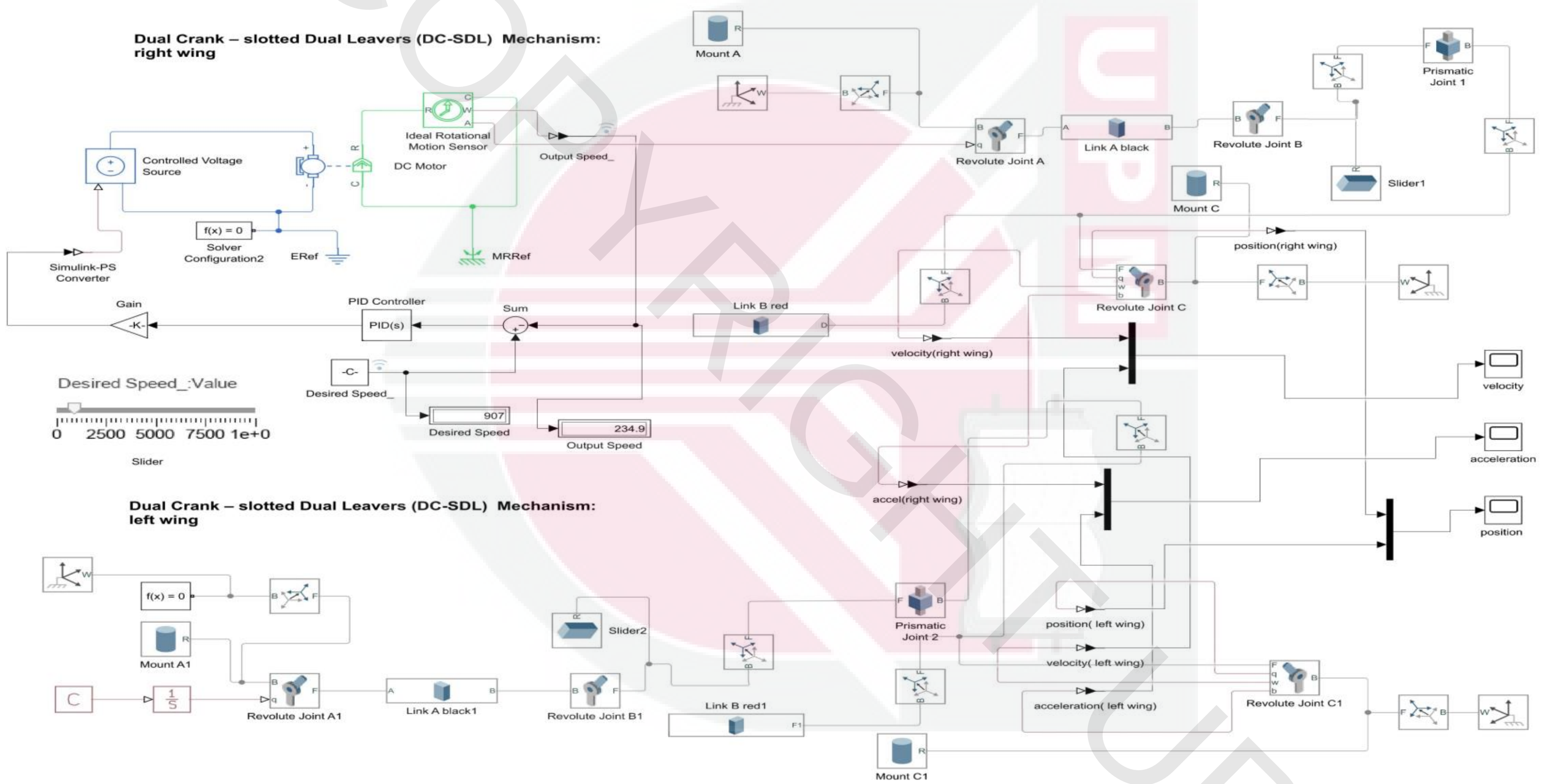

Figure 4.46 : PID Controlled DC Motor at Right Wing of Modelled Dual Crank – Slotted Dual Leavers (DC-SDL) Mechanism in Simscape

The above modeled DC motor has been added at right lever of modelled DC-SDL mechanism as in Figure 4.46 and Figure 4.47 with the desired speed as 907 rad/s. but the obtained results are with very less output speed i.e 234.9 rad per minute, which is greater than the simple PS-constant with PS-integrator block generated flapping as showed in Figure 4.48, Figure 4.49 and Figure 4.50.

The PID tuned DC motor model has offered greater speed at the right lever flapping when compared with the basic signal generated flapping at the left lever. As a result, the emulations are carried out by providing the PID tuned DC motor for both levers, as shown in Figure 4.51. This is because the model made it feasible to achieve a higher speed when fluttering the right lever. The results that were produced were outstanding; nevertheless, the speed matching between the left and right levers was not the same. They modeled a tiny new DC motor (as in Figure 4.52) with the parameters of the micro-DC motor and the factors that go into modeling micro-DC motors to eliminate the disparity between both levers.

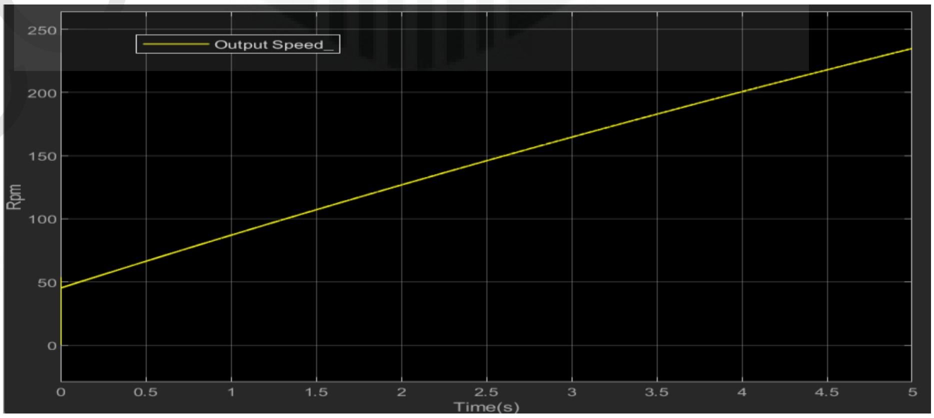

Figure 4.47 : PID Controlled Linearly Increasing DC Motor Speed

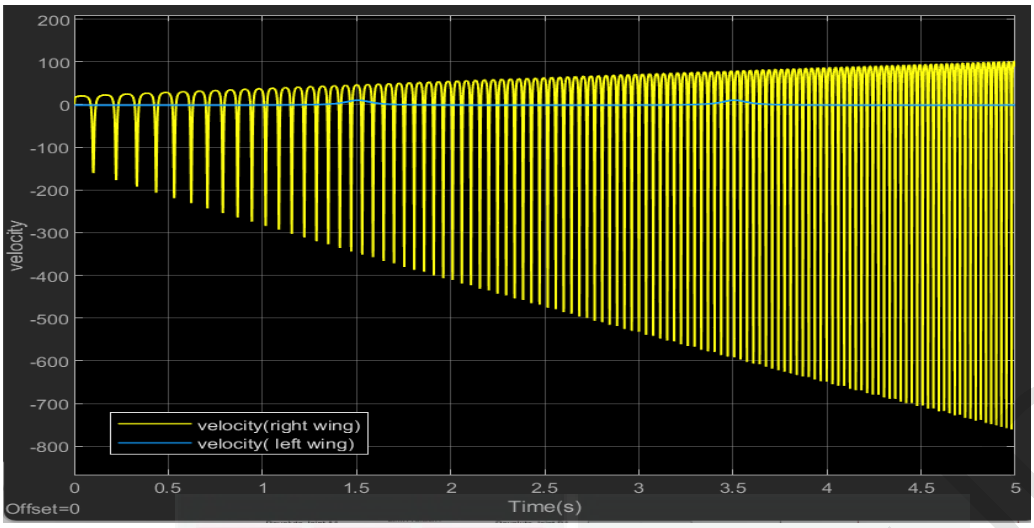

Figure 4.48 : Increased Right Wing Lever Flapping Velocity Compared to Left Wing

Hence, a PID (Proportional-Integral-Derivative) controlled micro-DC motor speed system provides an efficient method for sustaining accurate and stable motor speeds in a variety of applications. By adjusting the control input, the PID control algorithm incorporates proportional, integral, and derivative components to regulate the motor's speed. The PID controller can respond rapidly to deviations from the desired speed setpoint, ensuring accurate speed regulation even when disturbances or load changes occur. Combining proportional, integral, and derivative actions permits the controller to stabilize the system by addressing both steady-state errors and transient responses.

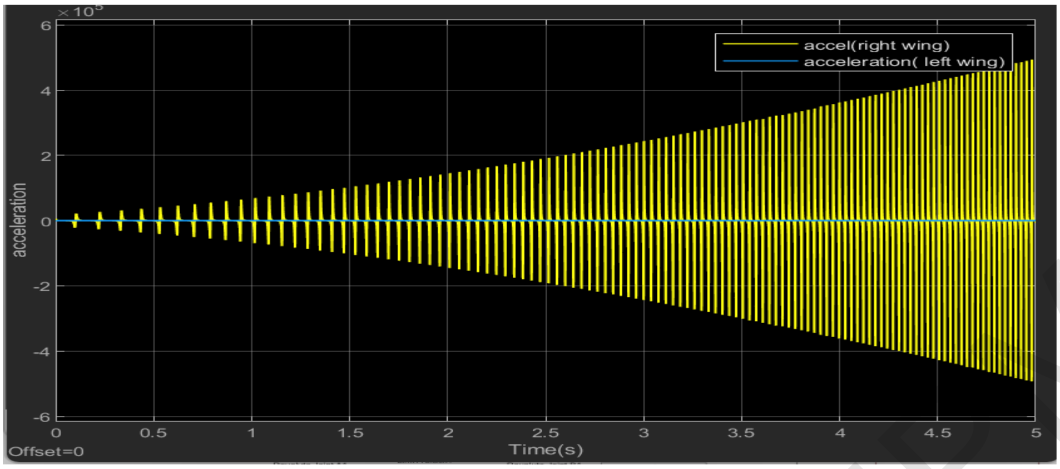

Figure 4.49 : Variation in Right Wing Lever Flapping Acceleration Compared to Left Wing

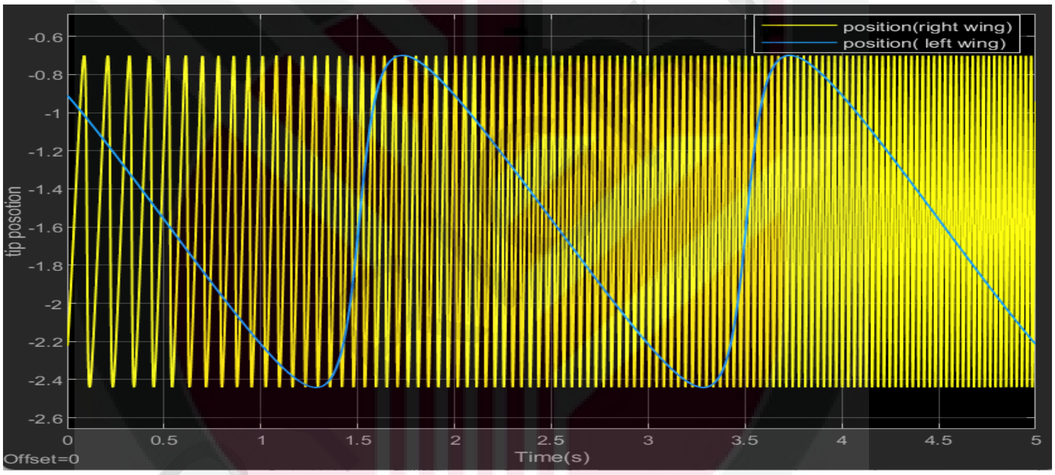

Figure 4.50 : Positional Tracking of Right-Wing Lever Tip

PID parameters can be modified to match the motor's and application's specific characteristics, making it adaptable to a wide range of operating conditions. A well-tuned PID controller can maintain stable performance despite external factors such as temperature variations, voltage fluctuations, and mechanical disturbances. Due to its simplicity and dependability, PID control is widely used in industrial and automation systems. It has a history of effective implementation in a variety of fields.

4.4.5 PID Controlled DC Motor as Driving System for Both the Levers of DC-SDL Model

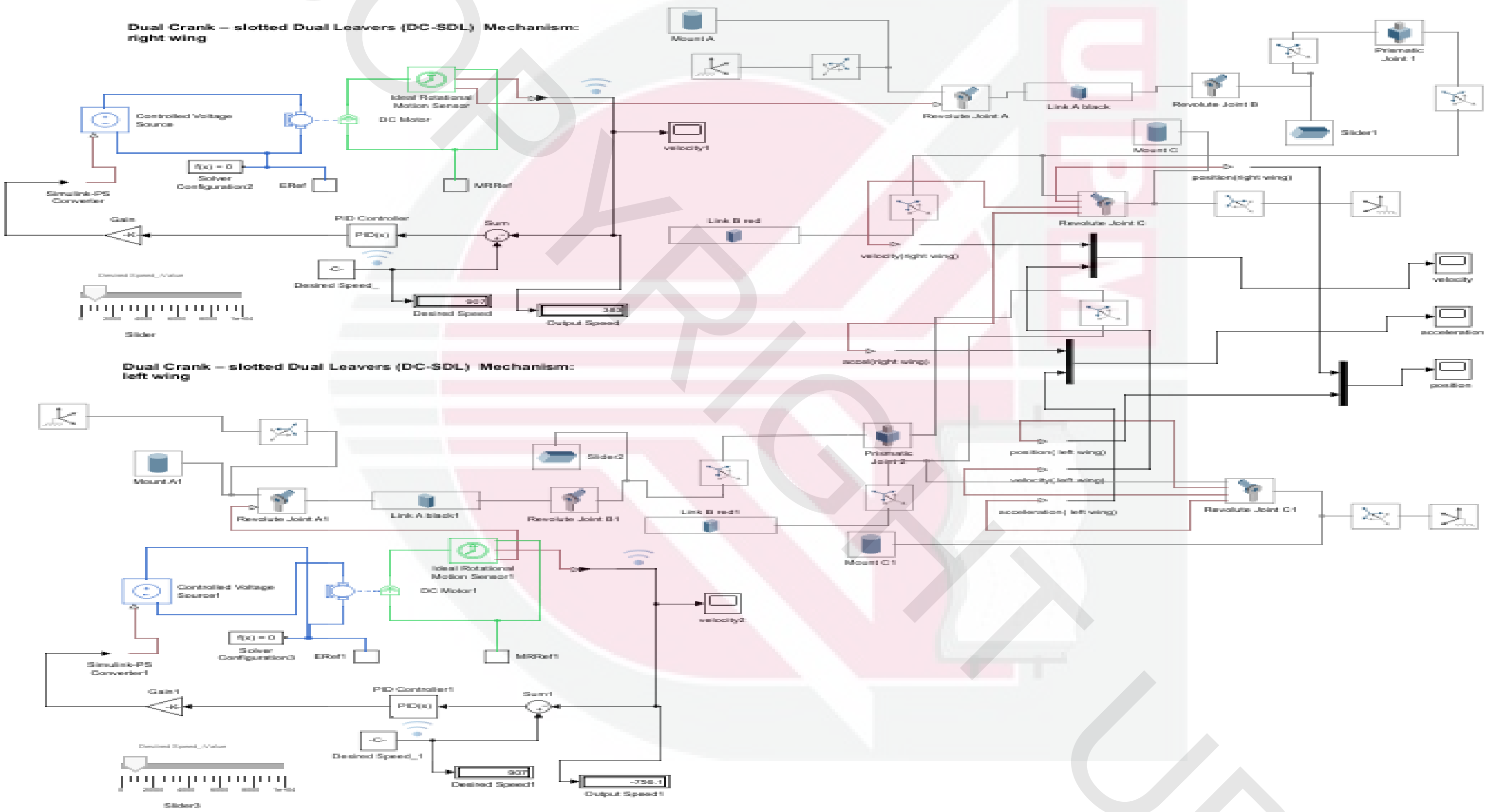

Figure 4.51 : PID Controlled DC Motor for Both the Levers of Modelled Dual Crank – Slotted Dual Leavers (DC-SDL) Mechanism in Simscape

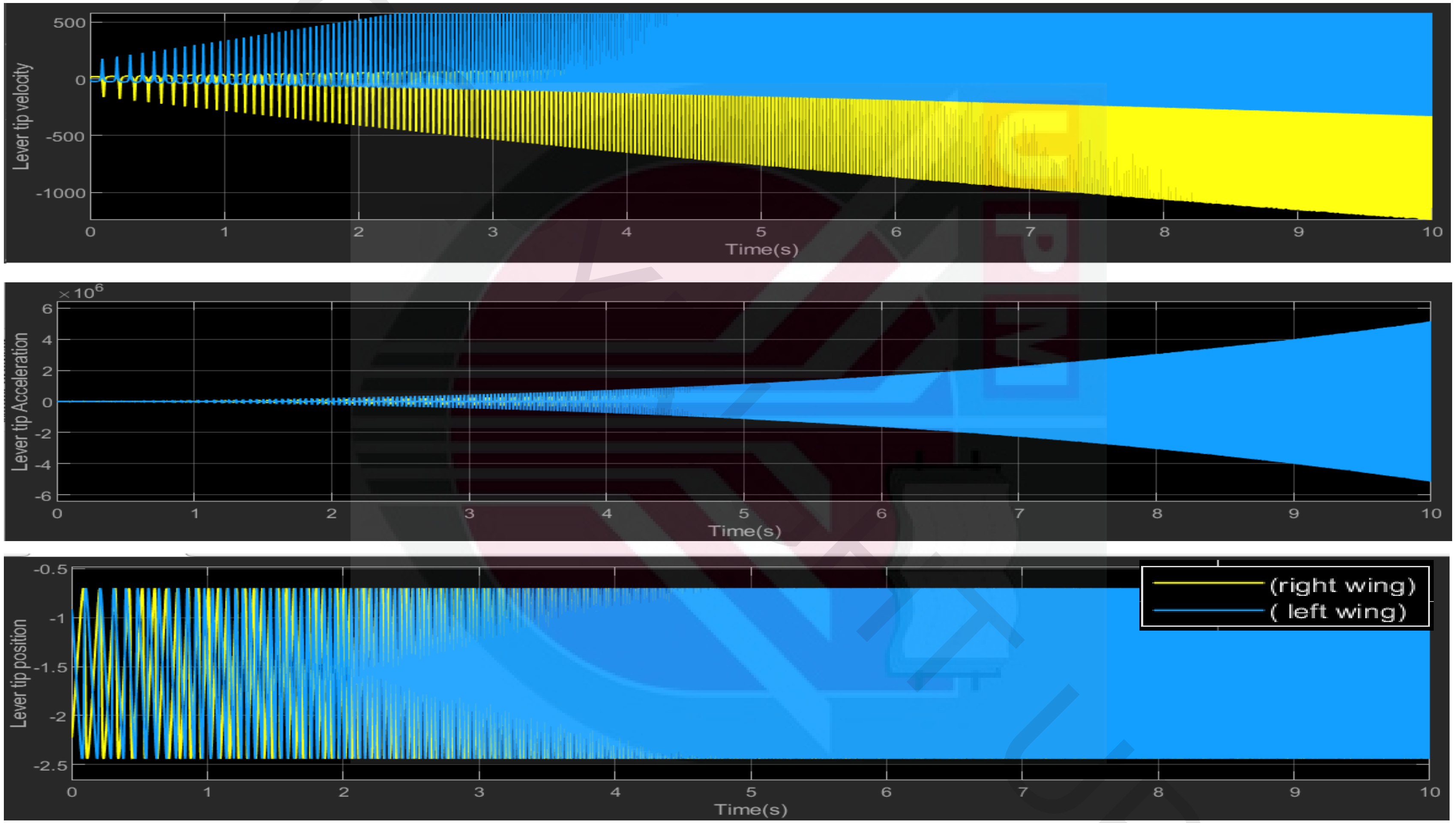

Figure 4.52 : Emulation Results of PID Controlled DC Motor for Both Levers of Modelled DC-SDL Mechanism

4.4.6 Implementation of Modelled New Micro DC Motor on DC-SDL Mechanism

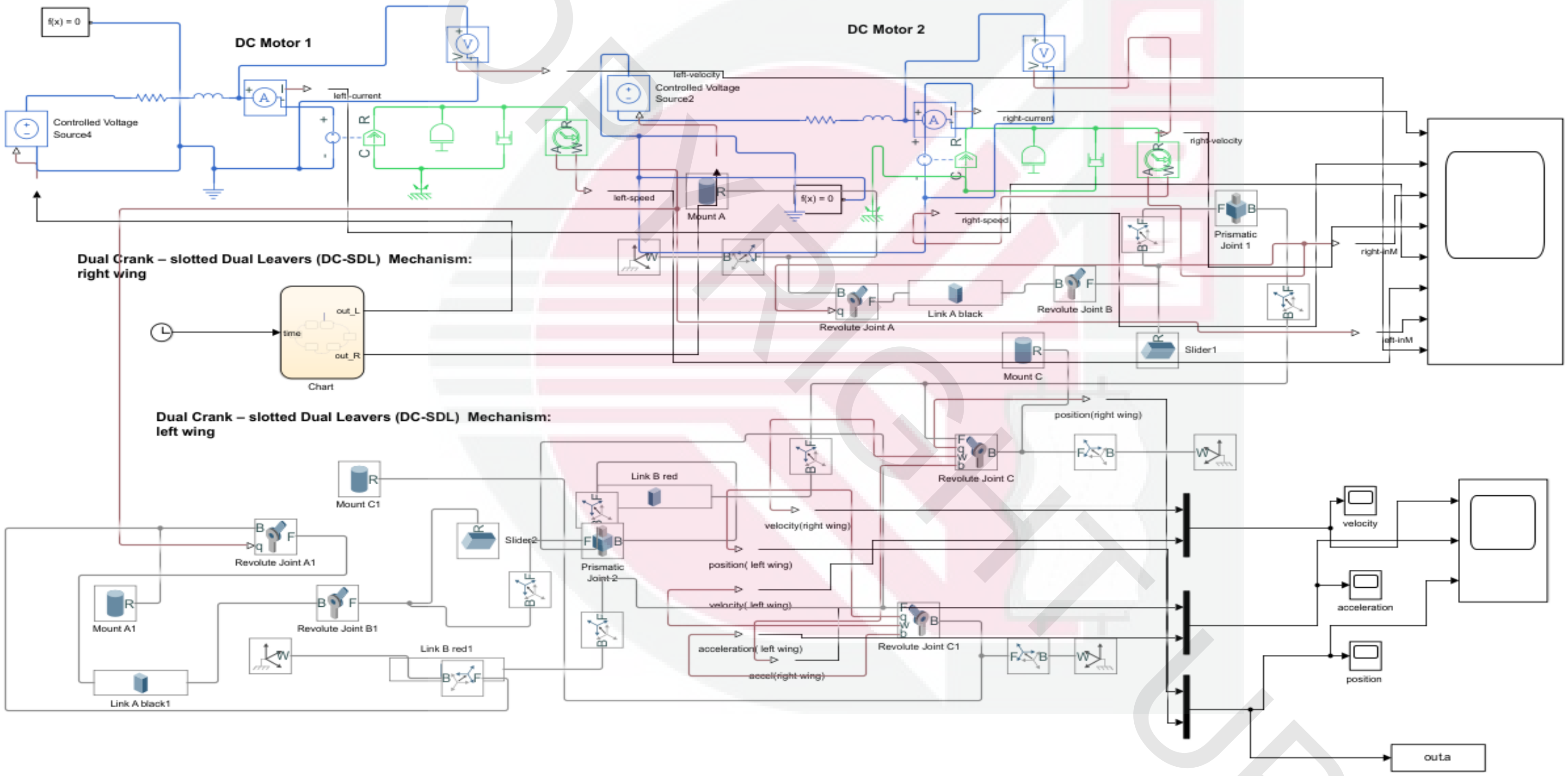

Figure 4.53 : Simscape Modelling of Micro-DC Motor-Controlled DC-SDL Mechanism with Chart Flow Process

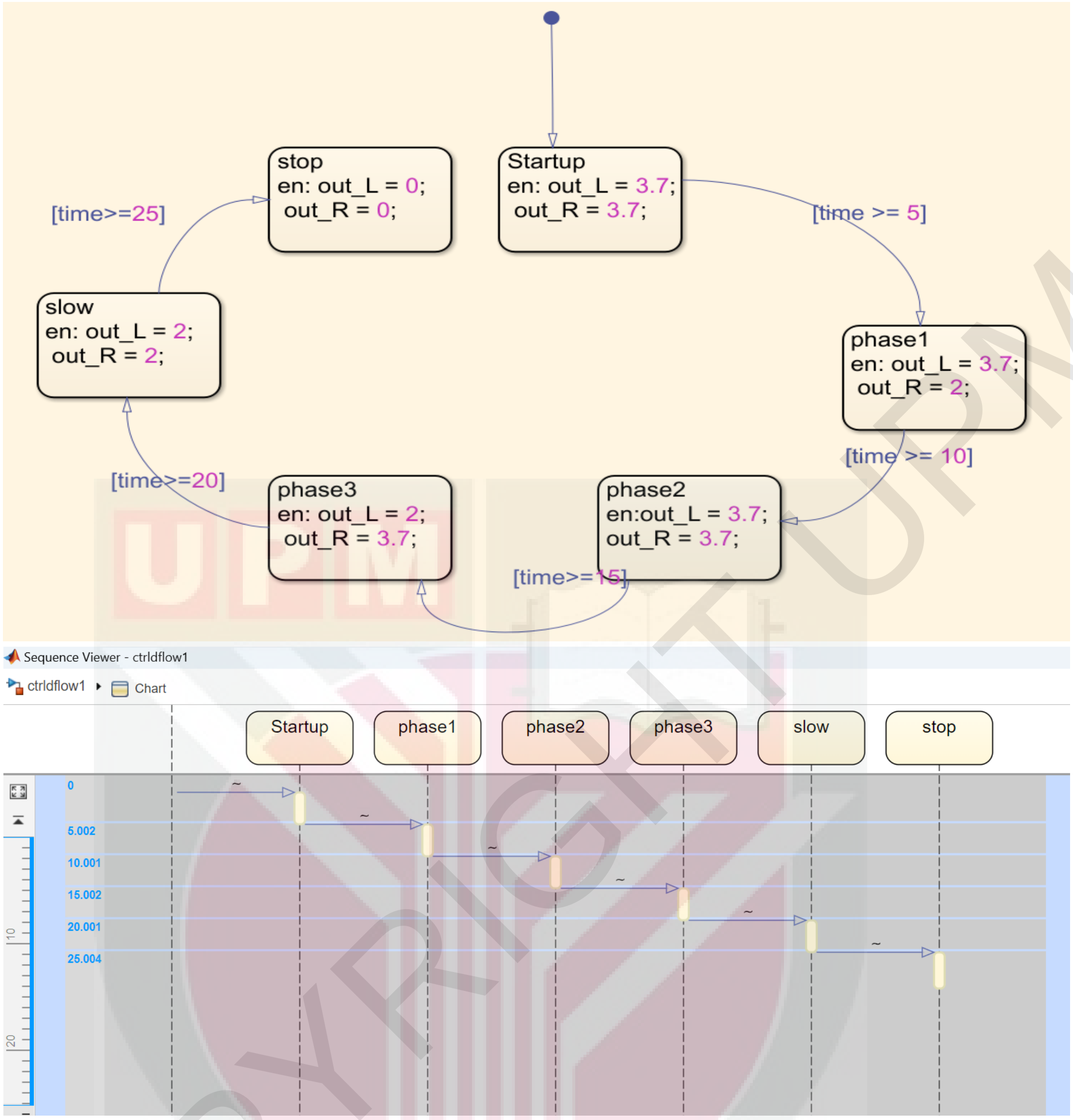

Figure 4.54 : Detailed Logic Chart for the Flapping Motion Control Process

For the simscape modelled Micro-DC motor-controlled DC-SDL design shown in Figure 4.53, altering the input voltage is necessary to adjust the speed of the flapping wings. The logic chart needed for this purpose has been constructed in simscape and is depicted in Figure 4.54. where out_L refers to the voltage control for the left lever and out_R refers to the voltage control for the right lever. The chart flow indicates that both wings will be beating at the same speed for the first five seconds. After that, the speed of the right wing will fluctuate for the following five seconds, and so on, in accordance with the flow given in Figure 4.54. In accordance with the chart's working flow, the variations that were provided at the motor's DC input voltage, as well as its related changes at the motor current, angular speed, and its accelerations, are depicted in Figure 4.55. These modifications transpired for both levers of the DC-SDL model emulations. Figure 4.56 depicts the output obtained as lever flapping variations every 5 seconds as per the chart.

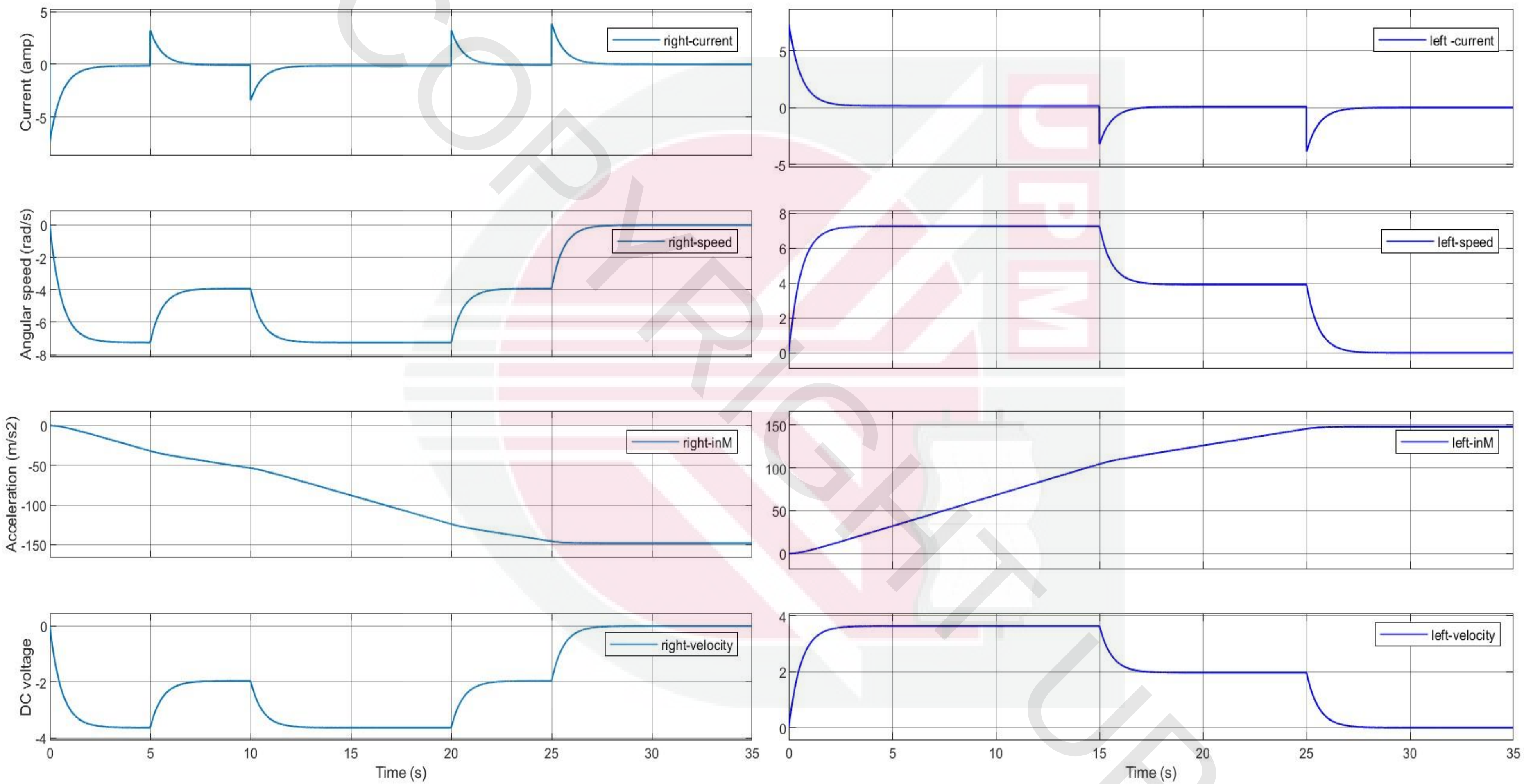

Figure 4.55 : Chart Controlled Inputs at Both Motors

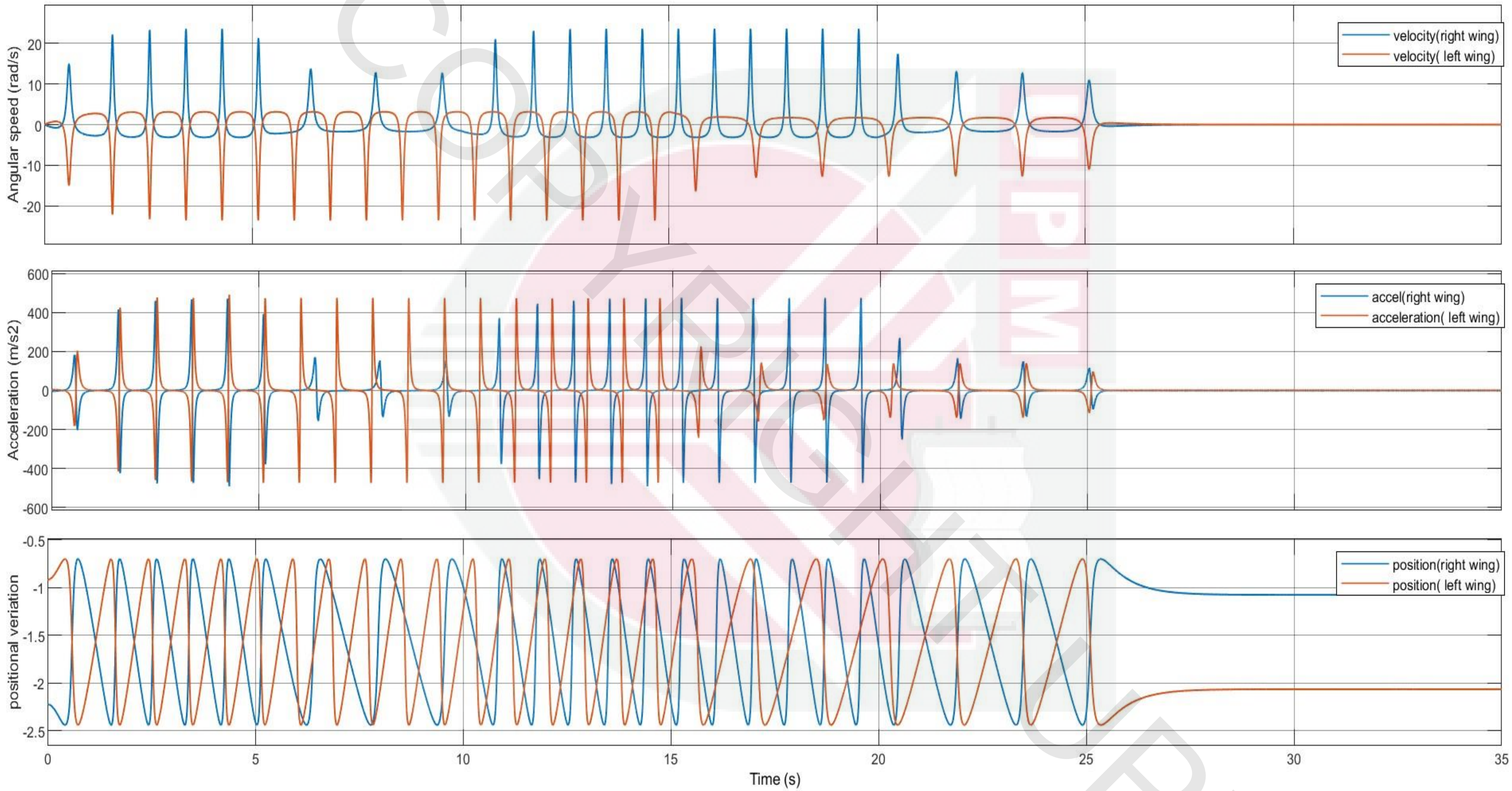

Figure 4.56 : Variations of the Flapping Lever Angular Speed, Acceleration and Position as Per the Chart Flow

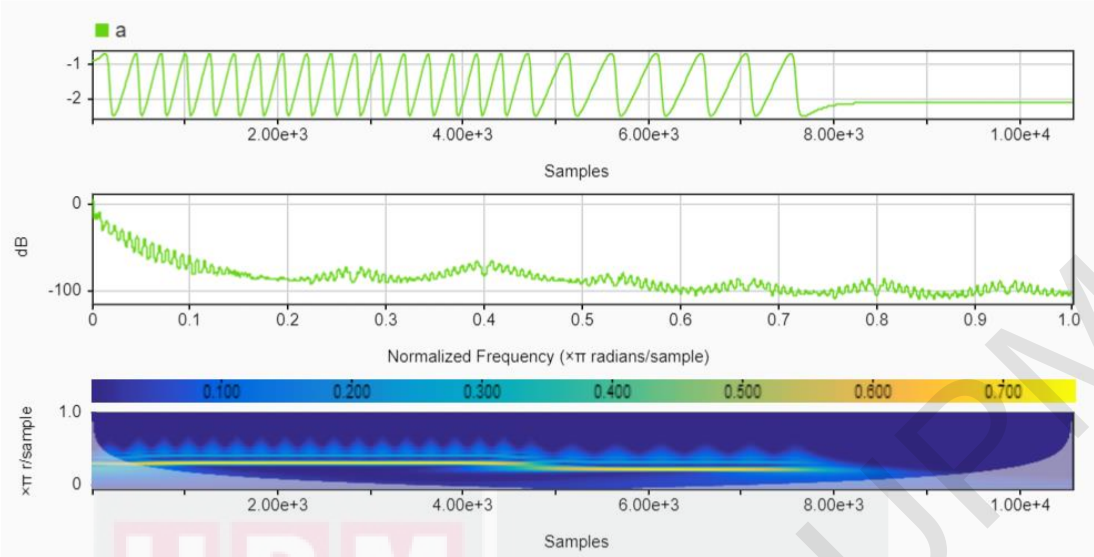

Figure 4.57 : Lever Position in to Normalized Frequency or Samples

Figure 4.56 is a representation of the variations that were obtained in terms of the angular speed, acceleration, and position of the flapping lever in accordance with the execution of the chart flow. Illustrating the lever position (Figure 4.56) in terms of the normalized frequency of samples is Figure 4.57. as per the figure 4.56, During the first five seconds, both wings progress forward at the same rate. It takes between 5 and 10 seconds to make a right turn by decelerating the right lever movement and maintaining optimum speed on the left wing. Within a 10- to 15-second interval, both wings resume forward motion with the same velocity. It takes between 15 and 20 seconds to make a left turn by decreasing the speed of the left wing's flapping and sustaining the speed of the right wing. Then, between 20 and 25 seconds, both wings will flutter at a reduced speed at 2 v input before stopping simultaneously. The insights of obtained results summarize the essence of the control innovations and their crucial role in achieving successful navigation in different directions via individual lever movement controllability.

4.5 Computational Fluid Dynamics

Computational Fluid Dynamics is a branch of fluid mechanics that uses numerical analysis and algorithms to solve and analyse problems involving fluid flows. Flapping wing aerodynamics is inherently complex due to unsteady, nonlinear, and three-dimensional flow fields. CFD provides detailed insights into these flows, which are challenging to capture through experimental methods alone. CFD allows for the calculation of aerodynamic forces and power requirements, which are crucial for determining the efficiency of a flapping wing system. By simulating different flapping motions, CFD helps to optimize wing kinematics for maximum lift, efficient thrust generation, and minimal energy consumption(Chimakurthi et al., 2009; Djojodihardjo & Rahim, 2015; Kudariyawar et al., 2016). As noted in studies such as the one by Hyunwoo Jung, Seung-Hoon Oh, and Haecheon Choi, CFD is instrumental in analysing the effects of the deviation motion (a figure-eight movement) on the aerodynamic performance of a mosquito wing. It shows how this motion can generate larger vertical forces more efficiently(H. Jung et al., 2024). For mosquitoes and other flapping wing insects, critical mechanisms such as leading-edge vortices and trailing-edge vortices significantly contribute to lift. CFD can visualize these vortices and quantify their impact. CFD allows the implementation of realistic and complex boundary conditions that mimic real-world scenarios, enhancing the reliability of analysis(L. G. Liu et al., 2020; Miller, 2017).

4.5.1 Analysis of the X-Pattern 4-bar FW through CFD

To computationally validate the kinematic results, 2D cross-sectional simplified geometry was used to determine the current suggested design. This simplification is appropriate since the extended arm starts a quick return "stiff body" motion that lacks pivots to consider the effects of flexibility on wing spar. A system to change the volume mesh at each interval must be created to represent the stream across the adjustable wing. The current work will confirm the MAV design without limiting the nuances and increased degree of freedom calculations by conducting a non-deforming, spatially dynamic, transient 2D evaluation of flapping wing cross section. The current design uses an articulated pitching mechanism to enable the pitching of rigid wings. The flappable movement is initiated via leading-edge-spars, having a 0.02094395 radians washout angle is considered for the root with tip chords. To reflect the Roget et al. more accurately, (Djojodihardjo, 2016; Roget et al., 2008, 2009) indicated effective thrust-propulsion distribution, 6.875-degree dihedral-angle is provided for the complete flapping-wing arrangement. In addition, a 2D geometry projection of the wing in the XY plane as a flat plate was considered with 3.7 cm in its height and width of 0.5 cm. Since this design concentrates on the wing-dynamics, the tail is not considered for CFD simulation (Muhammad Daffa Naufal, 2022) and just the wings are considered. To accurately represent the top and bottom models, which play a crucial part in the modelling of the computational domain, boundary conditions must be carefully considered. The top and bottom walls must be sufficiently modelled, for 12H–15H, to avoid the flow rebounding effects.

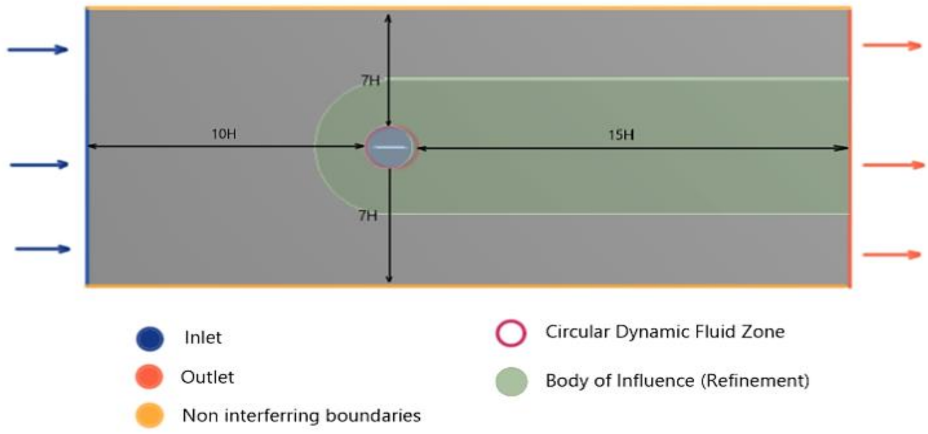

Figure 4.58 : Discretized Domain Dimensions

The top and bottom limits are simulated as symmetric zones with a 7H clearance from the flat plate zone, respectively, even though doing so significantly lengthens computation time. Finally, a circle with a diameter of 42 mm and C grid type bodies with arbitrary dimensions were made to use it as a body of influence to take into account the dynamical mobility of such plating inside the grids as well as the localized refinement of the trailing-edge region. A graphical illustration of the computational domain is in Figure 4.58. The domain was discretized using solver-specific grid generation techniques, and the incompressible Reynolds averaged Navier-Stokes equation was employed to solve the problem (RANS). RANS equations were essentially created by averaging the N.S. Equations across time. A 20-layer inflation layer with a growth rate of 1.247 was built over the surface of the flat plate in compliance with the mathematical requirement for the inflation reference length.

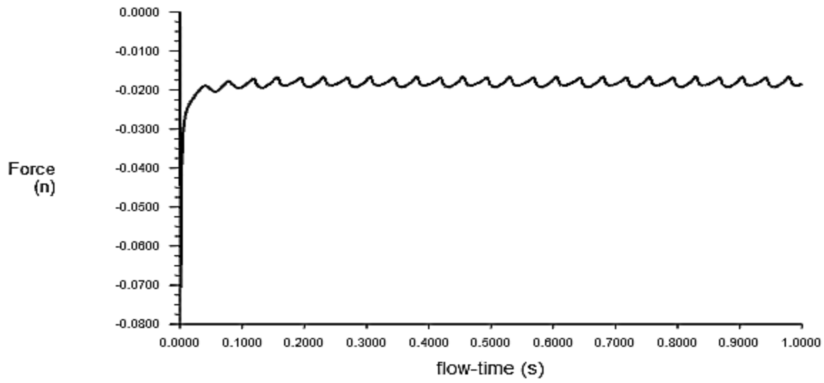

Figure 4.59 : Transient Thrust Force Plot

CFD solver methods can be implemented for the mathematical adjustment of nodes or grids. UDF scripting was used to simulate the circular area surrounding the planar plate of the flappable body. The script was compiled and run utilizing the CFD built-in with C++ codes interpreter to create flappable movements for the round regions. While high angles-of-attack (AOA) limitations for the flappable design, the dynamics of skewing's-nature of the mesh compromises the mesh orthogonal quality and overall mesh quality.

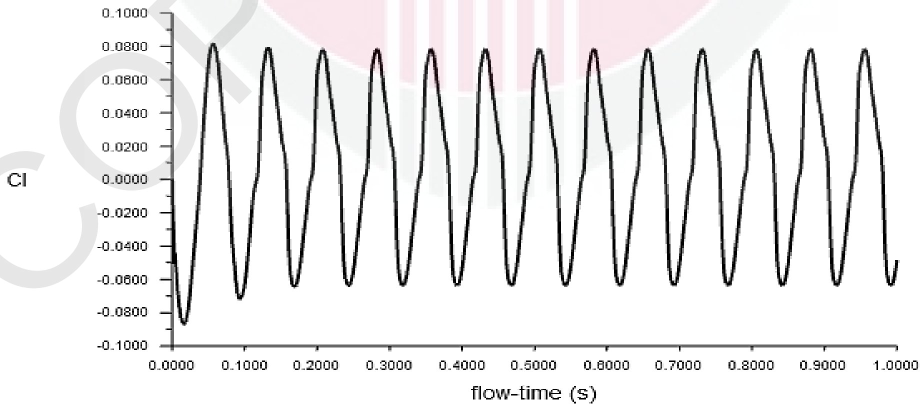

Figure 4.60 : Transient Coefficient of Lift Plot

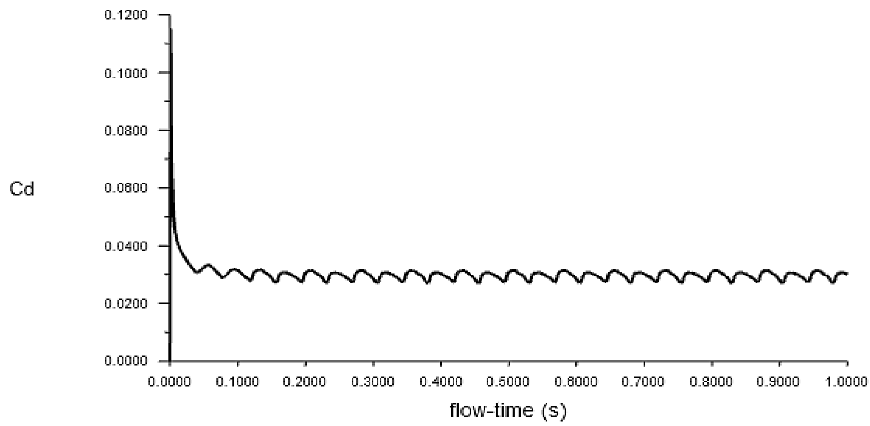

Figure 4.61 : Transient Coefficient of Drag Plot

The low speed of operation was considered to calculate the turbulences during the inviscid of flow-domain using a pressure-oriented solvers having iterative 2 equation k-omega SST RANS turbulence-computation and correction for low Reynolds number. The air had an incoming wind of 3.5 m/s operating in the +x direction under normal atmospheric circumstances. Dynamic frame and mesh motion, which were simulated with UDF for each of the exterior and interior interfaces, is essential to creating the flutter motion. To comprehend the transient effects and determine the net thrust generated along the axial direction, the simulation was run for 43,500 iterations, with time steps of 0.001 seconds to get the total simulation result for 1 second. The inviscid fluxes are assessed using a Roe upwind-biased flux-difference method. For time-accurate simulations, a 2nd order COUPLED-scheme is employed, and Newtons-type sub-iteration methods are used to resolve factorizing errors for restoring 2nd order accuracies. For spatial-discretization, a linear way-oriented path of Least Square Cell Based method was utilized, along with a third order MUSCL approach for additional flow and turbulent parameters and a second order iterative pressure calculation(Yusoff et al., 2022).

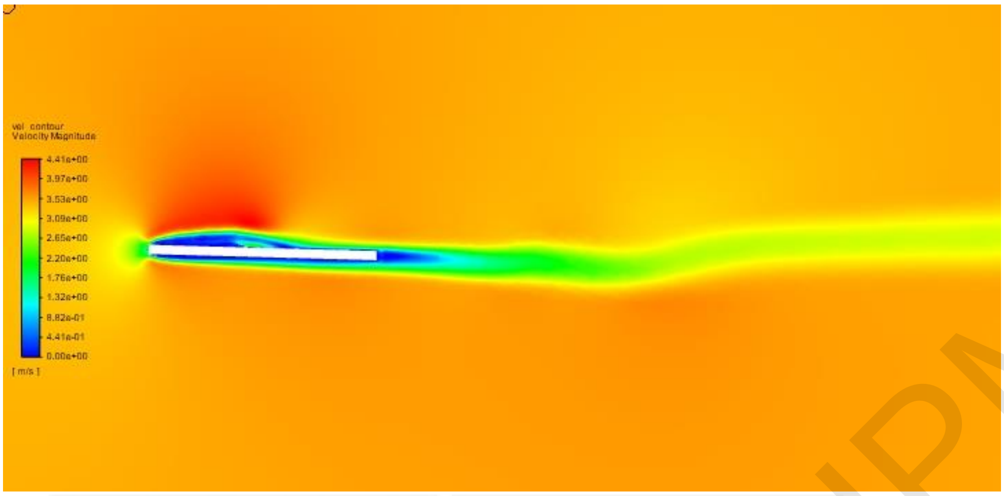

Figure 4.62 : Downstroke Flapping-Wing Plate with Velocity-Magnitude Contours at the 150 / 314-Time Frames

From the computational studies for the proposed design, it is noticed that with higher frequency of flap, there is a severe compromise in the resultant lift and drag coefficients. In previous study performed by S.Singh et.al., (S. Singh, Muralidharan, et al., 2022), for similar geometric modifications, it was inferred that an unsymmetric parabolic trend is noticed in the variation of the flapping frequency for a particular geometric configuration, where increasing the flapping frequency only increased the crucial fluid dynamic properties only to a certain extent. Any modifications further resulted in a gradual drop in the performance.

It was noticed that the peak coefficient of lift (attained at approximately 0.05 seconds – periodically) is just about 0.08, which is 72% - 84% lower than the peak lift coefficients obtained in previous explorations made by S.Singh et. al.(S. Singh, Muralidharan, et al., 2022) A similar trend is also noticed in the obtained force and coefficient of drag metric, as depicted in Figures 4.59, 4.60, 4.61 and 4.62.

4.5.2 Computational Fluid Dynamic Study and Results of Design Mechanism-III

A comprehensive investigation of the dynamics and critical aerodynamic flow parameters for design mechanism- III aids in juxtaposition of its aerial kinematics against other proposed research models of the MAV whilst ensuring its validation as a prospective novel build. Mathematical formulations in the early investigations of a flapping wing and propellers leveraged the capabilities of steady aerodynamic theory to flapping biomimetics. This study aimed to convey the influence of flapping frequencies, pitching angles and diverse combinations of wing designs over static thrust and generated power from the flapping motion. Utilization of time marching stroke averaged analytical schemes was done in this study to understand the important aspects of flapping aeromechanics in addition to lift and drag estimation such as dihedral offset, stiffness of wing material, constraint of wing edge motion, variation in wing size, alteration of stroke plane angle from horizontal to vertical, application of momentum-theory for oscillating wing, designing FWMAV. Liu et al. presented a fast and efficient method (X. Liu et al., 2006; Y. Wang et al., 2015) based on Delaunay graph mapping for computationally analyzing the flexible wing dynamics in a 3-Dimensional setup. In addition, a variety of computational schemes were put to test to evaluate the kinematics design process for controlling the insects/ birds motion based on the variations in proportion to the number of chosen wings, their layout, and wing design characteristics.

For the present proposed design, a geometrically simplified 2D cross sectional model was considered. Probing into the dynamics of the proposed design mechanism-III, this simulation simplification is well justified as the extended arm initiates a fast return “rigid body” motion without any pivots to account for the flexibility of the spar of the wing. To model the stream across the adaptable wing, a mechanism must be developed to modify the volume mesh at each interval. 3-Dimensional analysis with higher order solvers accounting for greater degrees of freedom has merits to capture the near tip wake, fluid-turbulence interactions and associated stagnation and transition effects. However, the flexible sheath over the rigid spar in the 3D study will be subjected to noticeable and computationally significant deformation, which poses immense challenges in domain discretization and hence makes the convergence of turbulent Kinetic energy (k) and Specific dissipation rate (omega) challenging. Presently two ways to solve the mesh deformation problem: the spring analogy method and the elastic body analogy method. Spring analogy model utilizes the method of connecting each node in the neighboring cells by springs, within which the governing equations for the fluid flow and the equations of motion for the mesh deformation is integrated in time to compute the reformed mesh cell position. This method works well for small motions but leads to high skewness and eventually grid invalidity for larger motions. Contrarily, in the elastic body analogy, the entire grid itself is considered as an elastic body where for the entire domain, the fundamental partial-differential-equations are resolved. While it does resolve the issues of its counterpart, it takes its toll in terms of computation and in a few cases in terms of accuracy (specifically for unsteady and highly turbulent flow problems) owing to the spatial discretization schemes employed. The scope of the current study, being to validate the MAV design while restricting the nuances and higher degree of freedom computation, a non-deforming, spatially dynamic, transient 2D study of a frequency controlled flapping wing cross section will solve the purpose. Kinematically analyzed heave and sink motion of the quick return flapping wing from the analysis data mentioned in section A could be imposed in the CFD methodology to assign necessary initial conditions for computing the aerodynamic loads. Acquired data post proper grid independence verification can be probed further to increase the study of the aerodynamic systems of flexible wing-flapping (Fairuz et al., 2016).

4.5.2.1 Geometry Simplification

In design mechanism-III, pitching of rigid wings is realized with the help of articulated pitching mechanism. The flapping motion is actuated by a leading-edge spar over which a flexible membrane with a 1.2-degree washout between the root and the tip is attached. 0.12 rad dihedral angle is given for the entire flapping wing setup to better account for effective thrust-propulsion distribution as suggested by Roget et.al (Djojodihardjo, 2016; Roget et al., 2008, 2009). A two-dimensional wing projection in the XY plane as flat plate having dimensions of 37 mm length with net assumed thickness of 5 mm was modelled within the Space claim CAD modelling tool. For CFD simulation, the tail is not modelled, and only the pair of wings is considered, as design mechanism-III focusses on the wing dynamics.

The dynamic action of the flapping wing, being subjected to varying angle of attack amplitudes, will obviously be the victim of turbulence induced flow separations and flow obstructing wake, dead zone formation. To better capture the effects of turbulence and to support steady flow development before interaction with the wing projection, a computational domain long enough, specifically after the trailing edge was modelled. Considering H as the reference length, which in most cases could be made synonymous to the chord length of the wing projection, the computational domain ahead of the leading edge was considered as 10H and the domain to the rear as 15H.

Boundary conditions playing a significant role in the modelling of computational domain, careful modelling of the top and the bottom models are to be considered. Specifically for flows with varying degrees of angle of attack, flow rebound effects will be more pronounced if the top and bottom bounding surfaces are modelled as walls. To evade from this flow rebounding effects, the top and bottom walls are to be modelled far enough, say 12H-15H. However, as it immensely increases the computational time, the top and bottom boundaries are modelled as symmetric zones with 7H clearance from the flat plate zone, each. Finally, to account for dynamic motion of the flat plate within the grid and to locally refine the trailing edge zone, a circle of 42 mm diameter and a C grid type bodies of arbitrary dimensions were created to utilize it as body of influence, respectively. A graphical depiction of the created computational domain is illustrated in Figure 4.58.

4.5.2.2 Domain Discretization

Scientific literature and various studies corroborate the information that the element size has a direct influence on the accuracy of the computational results. This greatly depends on the kind of algorithm adopted to decompose the domain. While a highly fine mesh yields reliable numerical predictions with minimal error in contrast to its coarser counterpart, a finer mesh takes its toll on the computational cost, time and effort.

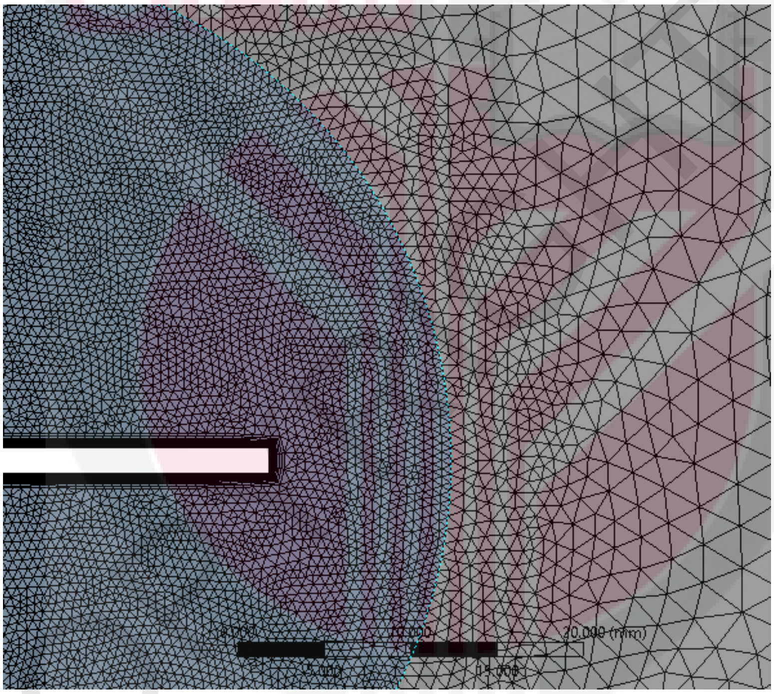

Figure 4.63 : Local Refinement within the Dynamic and Static Fluid Zones for Uniform Residual Convergence

Solver specific tried and tested grid generation methods were used to discretize the entire domain and solve using Incompressible Reynolds Averaged Navier-Stokes's equation (RANS). Basically, RANS equations were constructed by averaging over time, of the N.S. Equations. By simulating Reynolds stresses, the impact of disturbance can be approximated. Probing into the literature, conventionally three types of grids are commonly incorporated, namely, structured, block-structured and unstructured grids. Original mathematical formulations for Finite element, Finite difference and Finite volume are based on the consideration that the entire domain is divided uniformly into square grids. The underlying flux transfer and node parameters pre-conditioning is also based on this assumption. So, while using structured grids seems like an ideal choice, considering the merit of cell order and efficient flow field computation, it definitely is a challenging fit for complex geometries or dynamic meshes. A flat plate is not a complex geometry, but the dynamics of the flat plate for the parametric flapping frequency study is indeed the prime focus, for which unstructured grid offers better fit and mesh quality over its structured counterpart (Aaroh et al., 2018).

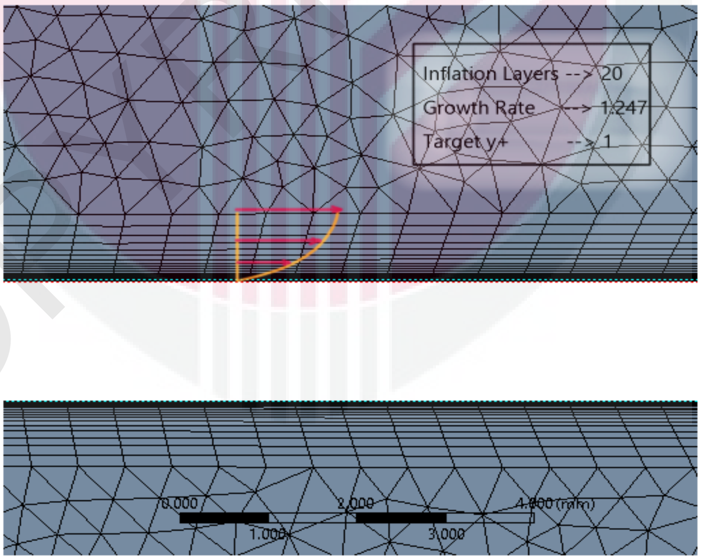

Figure 4.64 : Boundary Layer Inflation Zone in Close Proximity to the Flat Plate

The simulation is set up for a parametric study with 4 flapping frequencies from 20 Hz to 45 Hz. The entire computational domain was split into triangulated grids with a uniform grid element size of 10 mm. This grid size is gradually clustered towards the circular zone enclosing the flat plate, to account for better capture of the near wall effects as shown in Figure 4.63. The clustering towards the circular region was unbiased with a linear element order and a curvature capture minimum size of the order of 0.1 mm. Mesh defeaturing, although toggled on, was not of prime concern here, due to the fairly simplistic geometrical consideration devoid of higher order curvatures.

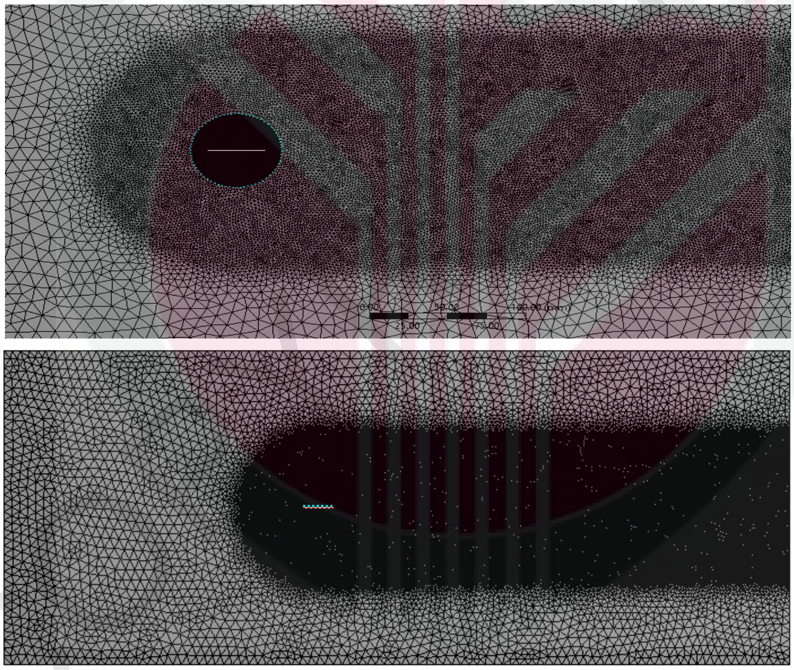

Figure 4.65 : Local Capsular Discretization to Capture the Wake Distribution of the Separated Flow

In accordance with the inflation layer mathematical requirement for the considered reference length, a 20-layer inflation layer over the surface of the flat plate with a growth rate of 1.247 was constructed (see Figure 4.64). This grid clustering near the surface is paramount to predict the aerodynamic forces and the varying static pressure over the geometry. Boundary layer is a very minute zone within which the viscous effects of the fluid become more pronounced. This tugging action of the fluid has its direct influence over the drag estimation. Hence, inflation layer control is required to create thin elements that can capture the normal gradient with minimal cell count.

$$y^+ = \frac{\rho y_p u_T}{\mu} \tag{4.41}$$

As specified earlier, wake capturing is key to understand the aggregate flow separation effect, which in turn also determines the thrust-lift distribution due to the flapping motion. Hence a body of influence meshing criteria was given for the C shaped body stretching till the end of the domain as shown in Figure 4.65. Each element within this body was sized at 2 mm.

Table 4.1 : Mesh Quality Metric Evaluation

Total number of elements in the domain			**90730**	
Mesh Quality Metric	Minimum value	Maximum value	Overall quality	Zone of concern
Aspect Ratio (AR)	6.34	133	99.12% < AR = 7	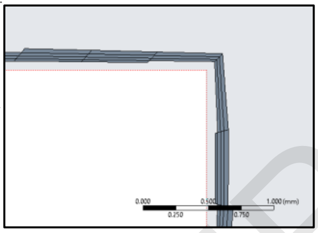
Orthogonal Quality (OQ)	0.171	0.956	98.76% > OQ = 0.85	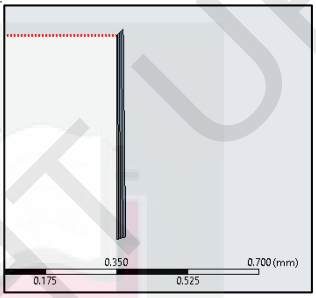
Skewness (SK)	0.0292	0.437	96.38% < 0.15 SK	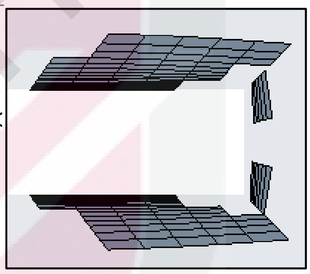

For such dynamic flapping motion, it is possible to implement CFD solver algorithms to mathematically morph the nodes and the grids to support the motion of the flat plate. ANSYS FLUENT supports a variety of mesh motion techniques to aid in transiently morphing the grids in accordance with the varying shape of the flat plate. In this regard, the circular region enclosing the flat plate was modelled as a flapping body with the aid of UDF scripting. Using the in-built CFD C++ code interpreter, the script was compiled and executed to induce flapping motion for the circular region. A prime focus was to attain the necessary motion ensuring quality, efficiency and robustness. With all these considerations, smoothing dynamic mesh motion was implemented and the entire domain was discretized (see Figure 4.65). Due to the dynamic skewing nature of the morphing mesh between the interacting interface of the circular zone (here, the internal region enclosing the flapping flat plate) and the outer zone, representing the fluid domain, the mesh orthogonal quality and the overall mesh quality gets compromised at higher angles of attack (AOA) limits for the flapping mechanism. In such cases, the readers are suggested to prefer geometry motion instead of dynamic mesh motion. Owing to the lower AOA limits of operation and to the ease of case setup with dynamic mesh motion, the authors here have preferred this setup. Owing to the lower AOA limits of operation and to the ease of case setup with dynamic mesh motion, the authors here have preferred this setup and obtained suitable mesh quality as summarized in Table 4.1.

4.5.2.3 Solver Setup

The flapping movements are constrained to the stroke planes, in which two separate phases of pitching are considered. i.e pronation (forward-backward) and supination (i.e vice -versa). For the computation of turbulence in the inviscid flow domain, attributed to the low speed of operation, pressure-based solver with iterative 2 equation k-omega SST RANS turbulence and low Reynolds number correction was used.

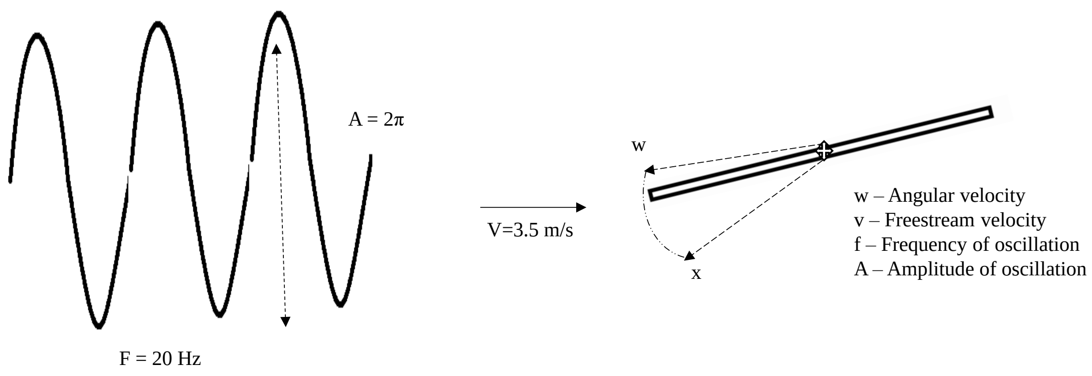

Figure 4.66 : Flapping Physics for the Computational Fluid Dynamic Ornithopter Analysis

The objective is to study the transient effects of the flow, due to which the entire simulation was carried out as a function of time. Incoming wind velocity was along the +x direction having a magnitude of 3.5 m/s operating at standard atmospheric condition. The key to setting up the flutter motion is to add dynamic frame and mesh motion, which, for each of the interior and exterior interface zones were modelled with UDF. Based on design mechanism-II experimentation results, the flapping frequency for the base design mechanism-III model was tested parametrically for 20 Hz, 30 Hz and 40 Hz with amplitude of 2*PI, fixed based on the degree of motion of the mechanical spar (see Figure 4.66). To better understand the transient effects and infer the net thrust force generated along the axial direction, the simulation was run for a total of 43,500 iterations, time stepping in every 0.001 seconds to obtain the total simulation result for 1 second. The evaluation of the inviscid fluxes is based on an upwind-biased flux-difference technique proposed by Roe (P. L. Roe, 1981; Roe, 1997) For time-accurate computations a second order COUPLED scheme in time is used, along with Newton-type sub-iterations to remove factorization errors and restore formal second order accuracy. For spatial discretization, a linearly governed Least Square Cell Based scheme was deployed with second order iterative computation for pressure and Third order MUSCL method for other flow and turbulent parameters.

4.5.2.4 Inferences

Based on the simulation data acquired from the aerodynamic analysis of the simplified ornithopter 2D geometry, it could be inferred that the design mechanism-III offers a feasible means of operation from aerodynamic standpoint. The flapping wing rendered a peak lift coefficient of 0.46 at its 0.2 second time of operation and a peak drag coefficient of 0.08. Transient Velocity contours were probed at 5 timestamps within its 1 second of operation to understand the dynamics of the flow upon its interaction with flapping flat plate geometry. During its initial state of operation, it was assumed that the flapping wing had no dihedral angle in relation to the body and hence an angle of attack of 0 degree was maintained. Incoming flow stagnates at the leading edge of the flapping wing's spar with a symmetric pressure distribution and a dead high-pressure zone at the rear as depicted in Figure 4.67.

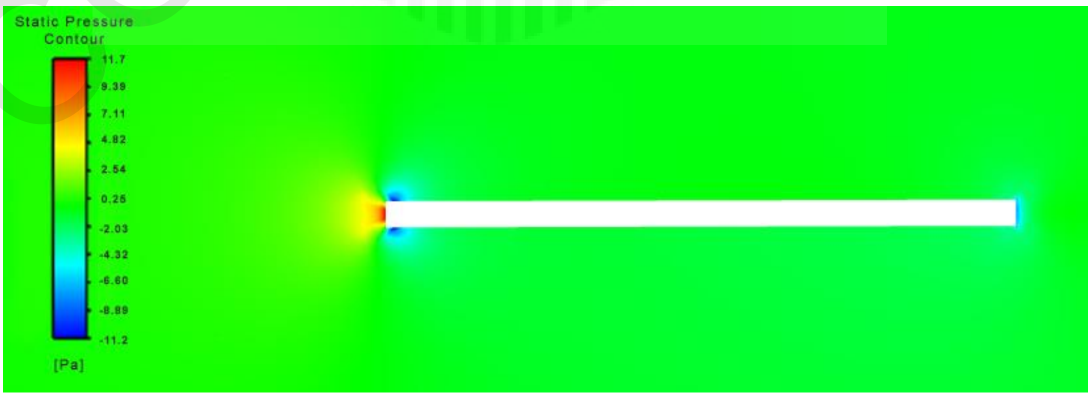

Figure 4.67 : Static Pressure Distribution over Flapping Flat Plate at t = 0.001

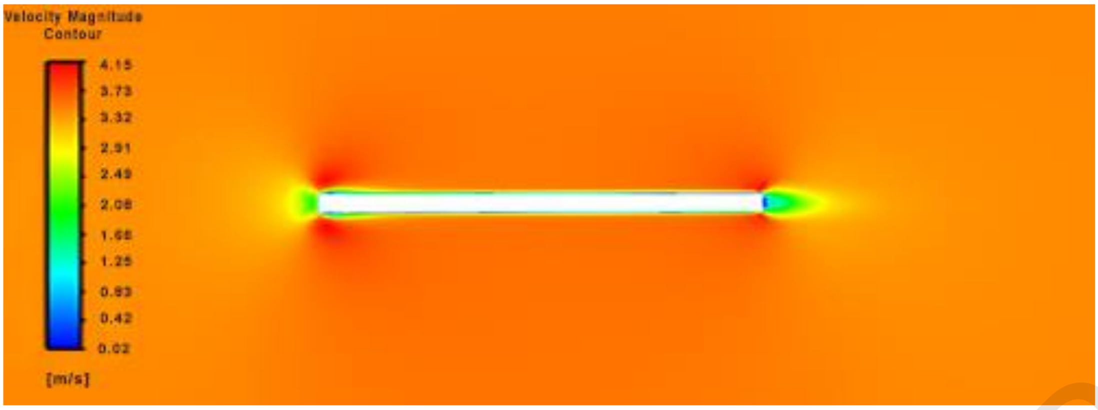

Figure 4.68 : Velocity Magnitude Contour over Flapping Flat Plate at t = 0.001

Owing to the tugging effect of the near wall shear, upon close encounter of the flow with the body and due to the gradual development plus external compression of the growth of the boundary layer by surrounding pressure, it can be noted that the incoming fluid takes a curvilinear trajectory (a characteristic of the subsonic fluid) and then tucks within a narrow layer near the body as shown in Figure 4.68.

Comparing its 150th and 314th flutter velocity contour (see Figure 4.69), separation produced on the upstroke and down-stroke is asymmetric, which in turn generates a larger flow separation on the lower side of the flapping body in contrast to its upper side. This could be attributed to the center of control where the flapping motion is initiated in our current design mechanism-III model and due to the adoption of bio-inspired quick return control mechanism. The resultant vortices created by the wing are pushed towards the rear, which creates a net horizontal momentum leading to thrust production.

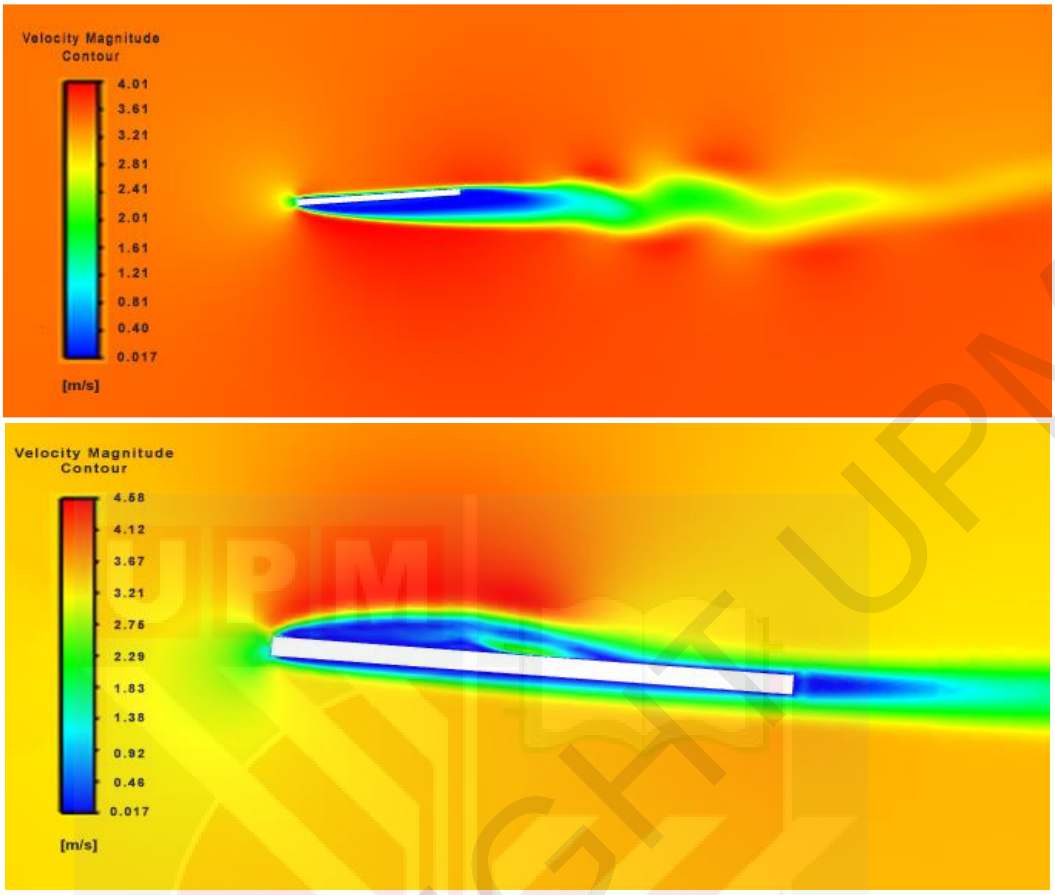

Figure 4.69 : Symmetrical (a) Downstroke and (b) Upstroke Velocity Magnitude Contours over Flapping Flat Plate at 150th and 314th Time Frame Respectively

As the flapping progressed, the wake disturbance from previous strokes had obvious and conspicuous impact over the flow adherence of upcoming strokes (see Figure 4.70), which resulted in larger wake formation and premature flow separation. These vortices were found to form along the leading edge with gradual motion towards 53% of the flat plate geometry, at which point the flow became highly unstable and detached from the plate's surface. This did take its toll over the net thrust produced, however the impact over the aggregate thrust drops due to the flow separation had little impact.

It appeared that the thrust force is higher for higher dihedral angle. One common observation was that a higher dihedral angle extended the zone of flapping rendering higher thrust force, but with an obvious bottleneck of limitation in the stall angle. However, the non-uniform pressure distribution with dynamic flapping had a great merit over its fixed wing counterpart as flapping wings do not exhibit a typical, abrupt stall seen with the fixed wings. This offers greater flexibility and window for control. Graphical interpretation of results from the transient Computational Fluid Dynamic parametric study rendered key insights about the performance of the figure of eight flapping wing mechanism. Based on the simulation results from 1 second of operation for frequencies ranging from 20Hz to 40hz, fluid dynamic characteristics namely, coefficient of lift, coefficient of drag and effective thrust for both individual flapping plate and combined flapping wing mechanism was analyzed. Critical analysis of the performance from Figure 4.71 indicates that there is a gradual hike from 20Hz to 24Hz and a drastic dip from 24Hz to 40Hz in the effective lift and drag characteristics of the flapping flat plate.

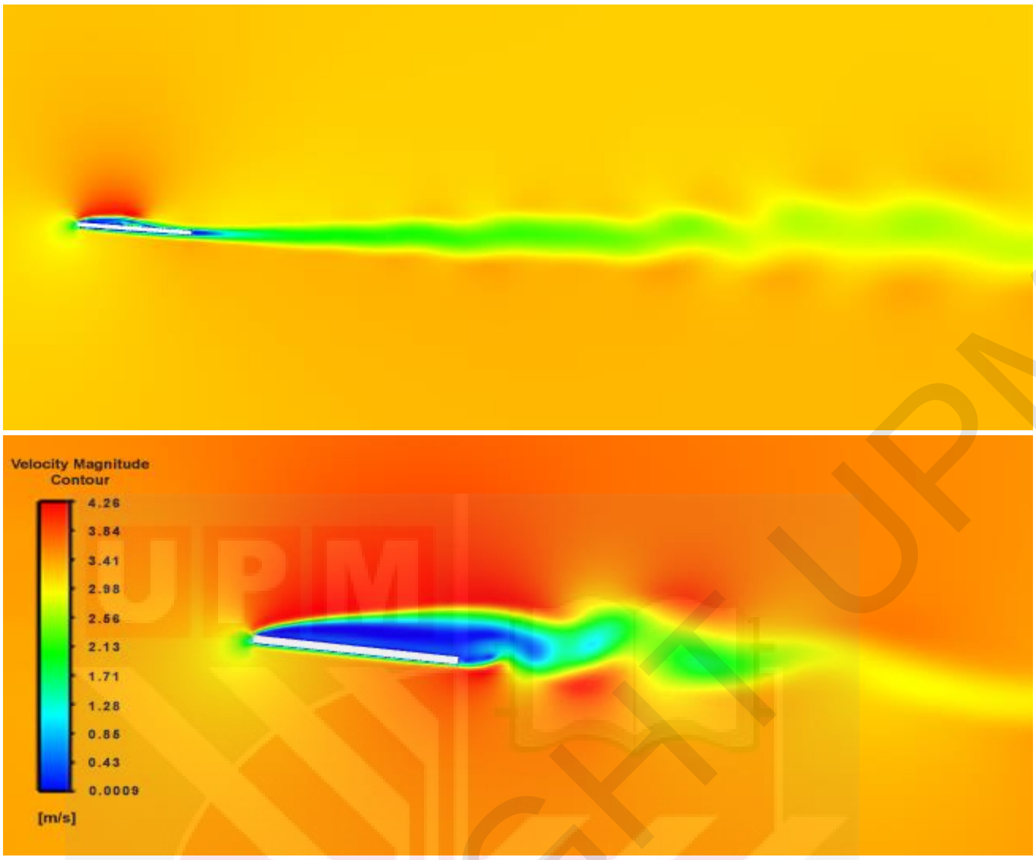

Figure 4.70 : Upheave Wake Induced Flow Separation over Flat Plate (a) Wake Distribution (b) Magnified View

While a higher flapping frequency guarantees effective improvement in the lift obtained due to the structure operating and turning larger mass flux of incoming air, the induced turbulence caused by the flat plate at higher frequency of operation outweighs the net benefit. In addition, as the wing at higher flapping frequencies are on the lower subsonic spectrum, the flow gets prewarned about the presence of the body upstream, which after certain flaps encounter an already disturbed flow leading to additional induced drag. Current test body with its flapping mechanism experiences a delay of 60 microseconds between the flaps of the right and left wing respectively. To simulate and interpret realistic flow conditions over the test body, the time delay between the flaps was accounted and by mathematically superimposing the phase difference, a weighted average was computed.

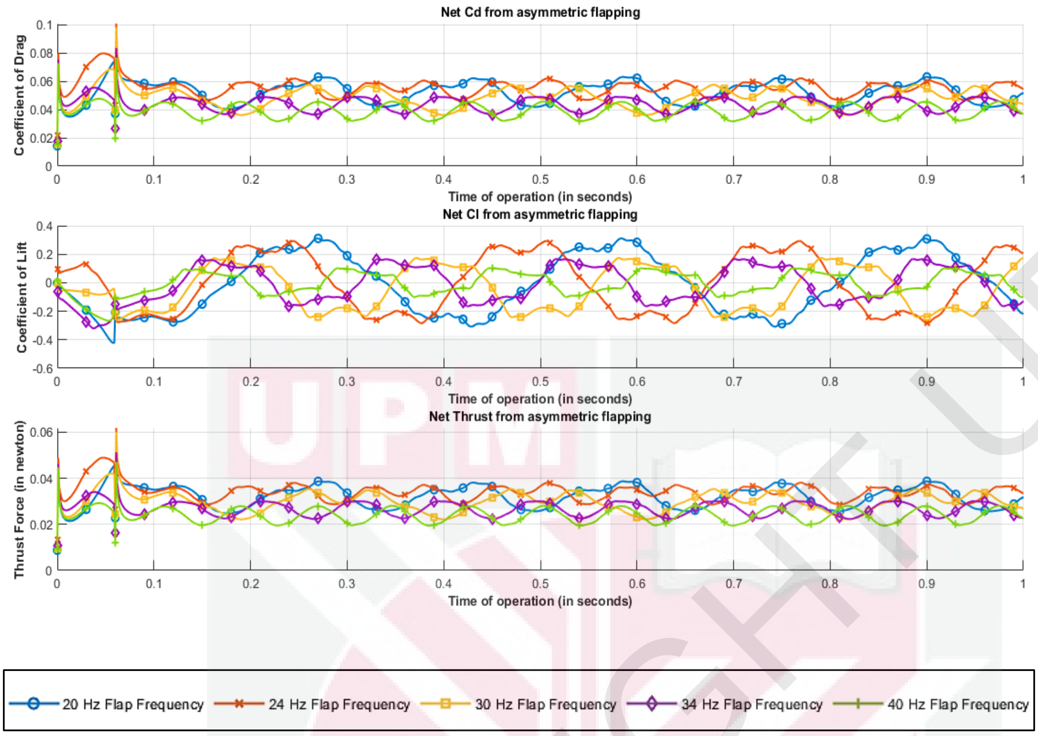

Figure 4.71 : Net Flow Field Metrics of Asymmetric Flapping Plate Configuration (a) Coefficient of Drag (b) Coefficient of Lift (c) Thrust Force along the Positive x Axis

Let ‘t’ be a column matrix of dimension mx1 denoting the simulation time of the ornithopter study from 0 to 1 second in steps of 0.001 seconds. At 60ms, the corresponding index of the 0.06s time stamp is calculated as

$$0.06 = 0 + (n-1)*0.001 \qquad (4.42)$$

$$n = \frac{0.06}{0.001} + 1 = 61 \qquad (4.43)$$

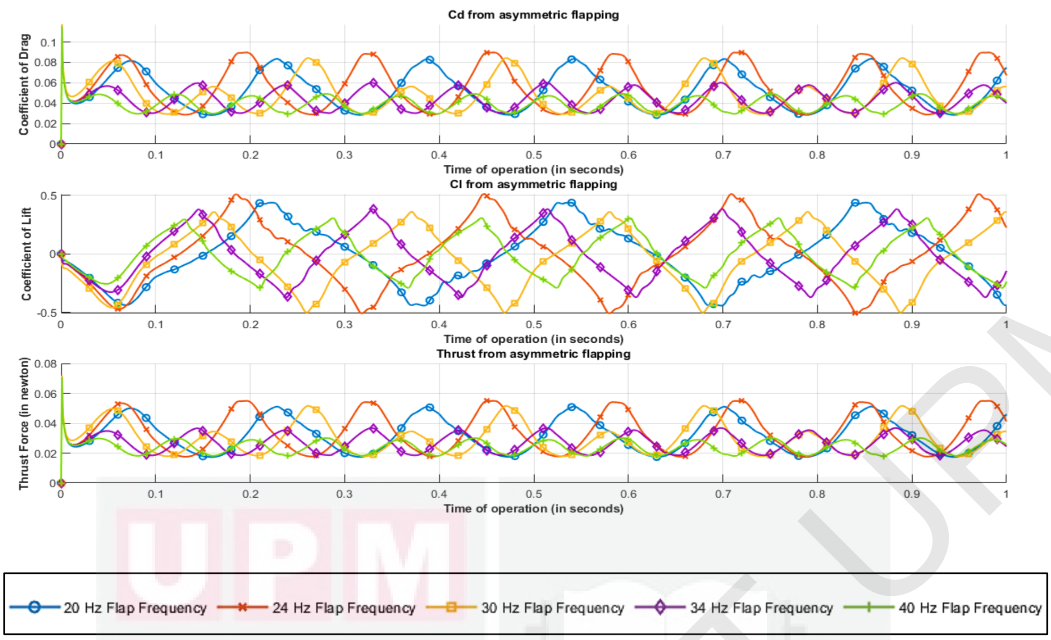

Figure 4.72 : Averaged Flow Field Metrics of Left and Right Asymmetric Flapping Plate Configuration (a) Coefficient of Drag (b) Coefficient of Lift (c) Thrust Force along the Positive x Axis

If $C_{L(R)}$ denotes the lift coefficient matrix of the right wing, which is having the same matrix dimension as that of 't' matrix (i.r mx1) than the $C_{L(L)}$ Matrix (i.e the lift coefficient matrix for the left wing is represented as,

$$C_{L(L)} = \left[\left[C_{L(R)}[m-61:m]_{61x1} \right]; \left[C_{L(R)}[61:m-61] \right]_{m-61x1} \right] \qquad (4.44)$$

i.e due to a shift by 60ms, the 1st $C_{L(L)}$ value will be equivalent to the 61st $C_{L(R)}$ value. The last 60 values of $C_{L(R)}$ will be the starting logged coefficient for the left wing. The resulting values for the left and the right wing are averaged to compute the net coefficient of lift, coefficient of drag and the resultant thrust as shown in Figure 4.72. The fluctuation in the simulated and computed parameters from 0 to 0.1 second is a relic of the emulation of gradual velocity ramping in the CFD simulation like that of a wind tunnel blower from 0 to 3.5

m/s. This gradual ramping tries to emulate the initial unstable inertial effects over the test body, synonymous to those induced over the body in actual experimental conditions till the flow gets stabilized in the test section. However, for any meaningful interpretation of inn obtained result, it is fair to neglect the logged results from 0 to 0.1 seconds.

Based on the results obtained from parametric study, a flapping frequency of 24hz seems ideal for the following reasons

→ The increase in the net coefficient of lift is more pronounced than the increase in drag by a factor of 22.7%

→ The power required to induce a flapping frequency of 24hz is relatively low compared to its higher frequency counterparts thus giving better output for 3 volts input.

→ From body's vibrational standpoint, although explicit study hasn't been performed to validate any claim, it is an engineering consideration that a high frequency requires faster mechanical motions, sometimes pushing the mechanical limit of micro-components resulting in vibrational and thermal management issues leading to reduced life span.

4.6 Experimental (Real-Time Results) of Fabricated FW-Prototypes

The importance of experimental (real-time) results of fabricated flapping wing (FW) prototypes is multifaceted, encompassing several critical aspects that contribute to the advancement, validation, and practical application of flapping wing technologies. Testing prototypes can reveal discrepancies between expected and actual performance, highlighting areas where models may need adjustment or refinement.

4.6.1 Experimental Setup and Results of 3C Model

By referring the circuit design of the setup, from Figure 3.20 and 3.21 of chapter 3, the flapping frequency have been obtained for different input voltage variations as shown in Figure 4.73 below**.**

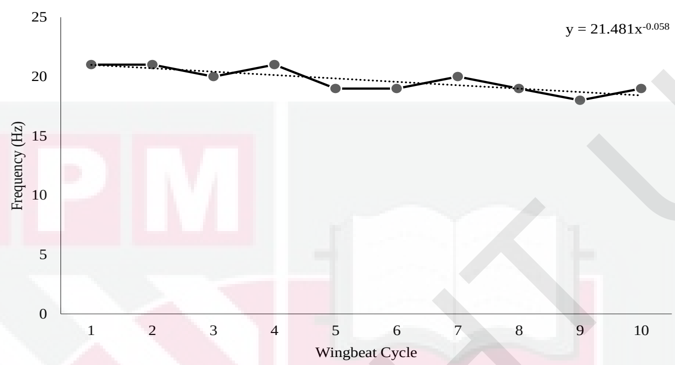

Figure 4.73 : Measured Flapping Frequency

According to Figure 4.73, they obtained a flapping frequency variation of between 18 and 21 hz for a 9v input voltage. The wing motion is clearly distinct relative to the stroke line, i.e. the wing beat frequency decreases concurrently (Figure 4.73). The frequency plot clearly shows a significant decrease / variation in frequency with respect to wing-beat cycles. This is strongly associated with the variation in flapping wing velocity as well. However, by varying the input voltage, the corresponding flapping frequency fluctuated. As illustrated in Figure 4.74a, as the input voltage is increased from 2.6v to 4v, the flapping frequency also increases and reaches 40hz. However, when the input voltage is 4.5 volts, the flapping frequency drops abruptly to 19 hz and then rises to 40hz as the input voltage is increased to 6v.

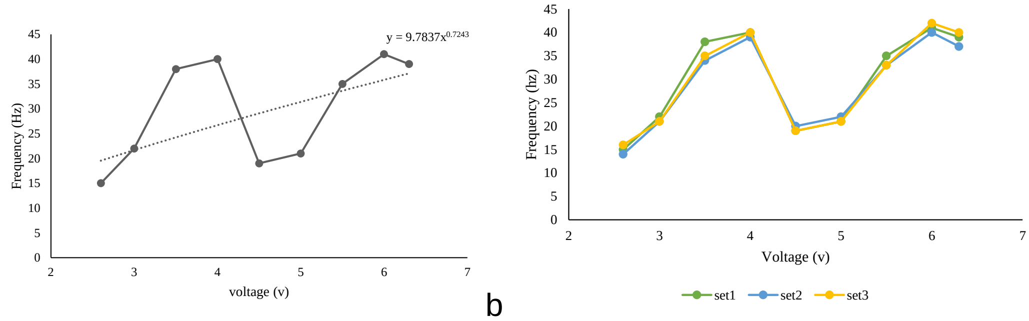

Figure 4.74 : a).Variation in Flapping Frequency as a Function of Increased Input Voltage. b). Multiple Set of Tests for Flapping Frequency Analysis

Since the obtained flapping frequency was not linear with increasing voltage, hence repeated the real-time experiments to obtain multiple sets of readings for the same. As shown in Figure 4.74b, it could obtain a similar wave graph of flapping frequency variation as a function of increasing voltage. As a result of Figure 4.73 and Figure 4.74, it can conclude that the design mechanism produces a higher flapping frequency by lowering the input voltage. However, the abrupt decrease in flapping frequency at 4.5v remains a puzzle, which were still attempting to solve. In general, however, the required battery voltage for MAVs is 3.5 volts when considering their mass limits. Accordingly, the obtained flapping frequency up to 3.5 volts is more than adequate. Hence the proposed mechanism is suitable for flapping wing drones' application.

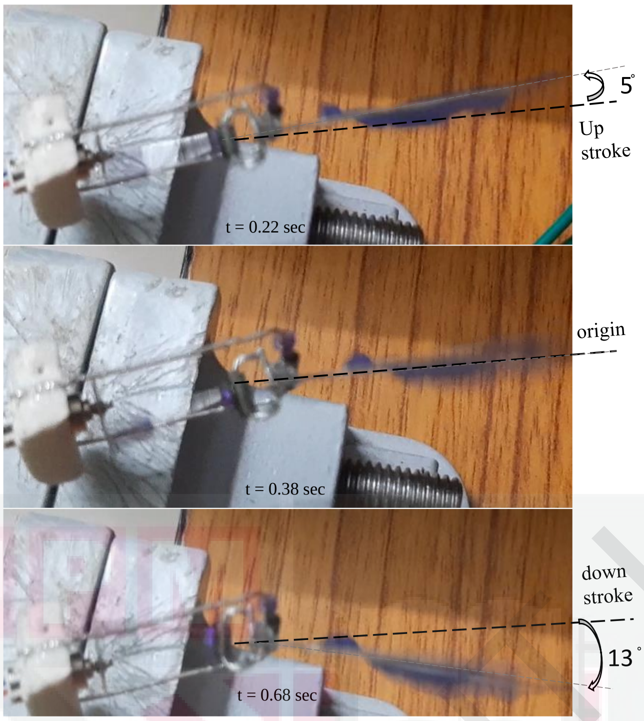

Figure 4.75 : Sequential Flapping Captured Frames of the Proposed Mechanism

The successive frames of the proposed mechanism for low flapping frequency are also depicted in Figure 4.75. When 3.5 volt is supplied to capture flapping action, frames are collected every 0.20 seconds. At separate times, they could observe the changing angular movements of both wings. During the up stroke and down stroke movement the obtained flapping angle with respect to the considered position as origin is depicted as in Figure 4.75. while the up-stroke movement, it could achieve 5 degree of angle and during down stroke, 13 degree of angle, hence over all its flapping angle is 18 degree. As an extension of this research work for the future, it is intended to publish an additional experimental analysis with parametric study for thrust and lift generation with variable set, size, and material of wings. This will be done as part of the parametric study.

Table 4.2 : Design Specifications of the Proposed 3C Design Test Bench Prototype

Overall mass	1.6 g (mechanism+wing+motor+supporting structure)
Motor weight	0.60 g
Wingspan	36mm
Wing area	3.6 x 2 (LxB)
Flapping frequency	38hz
Input voltage	3.5v DC
Angular velocity	ω1 = 0.401426/ 0.46 = 0.87 rad/sec)

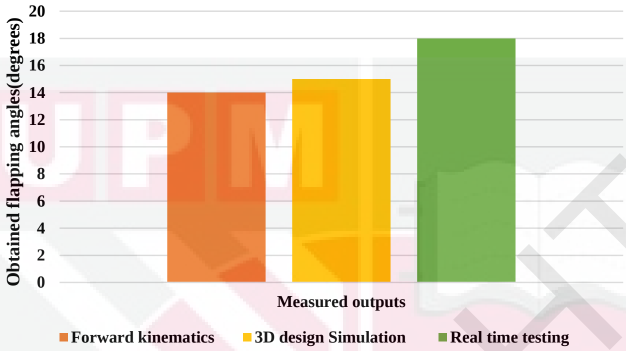

Figure 4.76 : Comparison of Obtained Flapping Angle from Forward Kinematics to Real Time Testing

The maximum displacement of the flapping wing is determined by using a distance measurement sensor, which is then transformed into an angle before being checked against the structural flappable workspace in both the vertical and horizontal directions. As can be seen in Figure 4.75, is achieved by flapping the wing at an angle ranging from 18 to 20 degrees. It is the angle of flapping that is obtained for each cycle of the wing beat. The proposed design mechanism's structural specifications are as outlined in Table 4.2, which may be seen here. Additionally, a comparison of the observed outputs of all the forward kinematics, 3D design simulation, and real time testing is carried out for the flapping angle as shown in Figure 4.76. There are not many variances in outputs, and there is similarity in all the angles obtained through flapping.

Because the overall prototype design is made with maximum possible reduction in its size, the obtained flapping angle is 18 degrees, if the connecting links sizes are varied the angle of flapping can be varied. This effort has produced a simple model that can aid in the design of FWMAVs inspired by insects. FWMAVs at centimeter or millimeter length scales are typically propelled by piezoelectric, dielectric/electrostatic elastomers, electromagnetic, or other reciprocating actuators. In any event, the rigidity of the actuator itself resembles that of the insect thorax most closely. Slight displacements of links in actuator can be converted into wing rotation by a mechanical transmission that acts in a manner like the insect wing hinge. Hence the proposed mechanism is resizable depending on the requirements.

4.6.2 Experimental Setup and Results: Design Mechanism-III

By considering SC-SDL design as in figure 3.27 of chapter 3, with circuit setup, the variations of frequencies obtained for varied voltage inputs can be seen in Figure 4.77 below. As shown in Figure 4.77, the frequency readings from an IR sensor vary based on the motor's input voltage. As the input voltage increases from 1.5 to 4.5 volts, the IR sensor's flapping measurement exhibits a modest linear variation. Figure 4.77 illustrates that our proposed prototype can achieve a maximum frequency of 35 Hz at a maximum voltage of 4.5v. Where F1 to F7 are the several sets of measurements conducted to observe the differences in flapping frequency measurements. It is seen that the greatest fluctuation in flaps per second occurs between the 2.5 to 4 volts range of input.

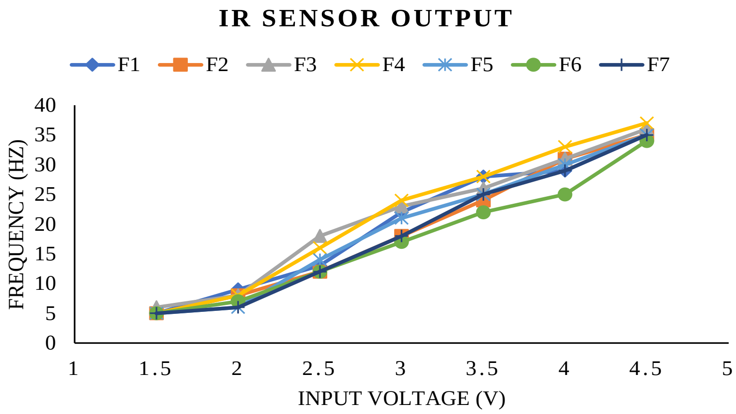

Figure 4.77 : Variation in Flapping Frequency Due to the Variable Input Voltage of the Motor

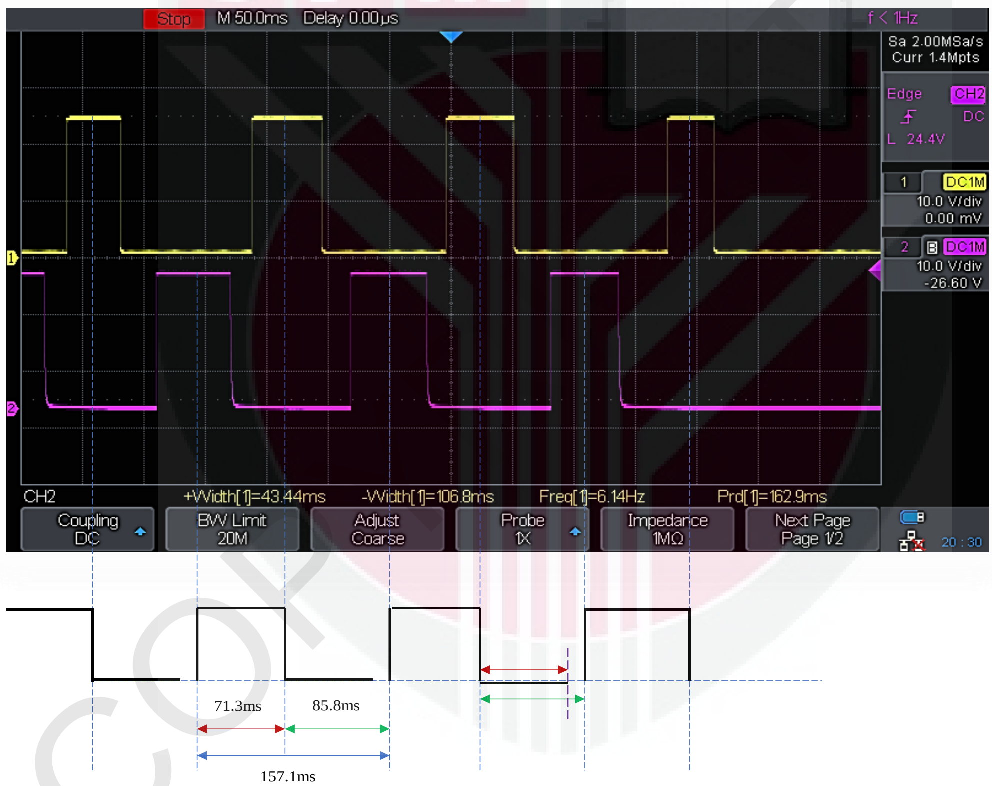

Figure 4.78 : Digital CRO Forward and Reverse Stroke Time Difference Measurement

Two IR sensors are positioned side-by-side, and the flapping wing is situated between both sensor wavelengths at 75mm such that the sensors can detect the forward stroke edge and return stroke edge. The time difference between forward and reverse strokes is determined using the CRO channels associated to each sensor. Figure 4.78 depicts the signals collected from the CRO, where the yellow signal shows the detection of the forward stroke edge, and the pink signal indicates the detection of the return stroke edge by the sensors. Figure 4.78 reveals that the forward stroke time space is 85.8 milliseconds, and the return stroke time space is 71.3 milliseconds based on the time space between the yellow and pink signals. As the forward stroke requires more time than the return stroke, this confirms that the quick return mechanism in this system is functional. The above obtained signals are for 6.14hz flapping frequency at an input voltage of 1.5v.

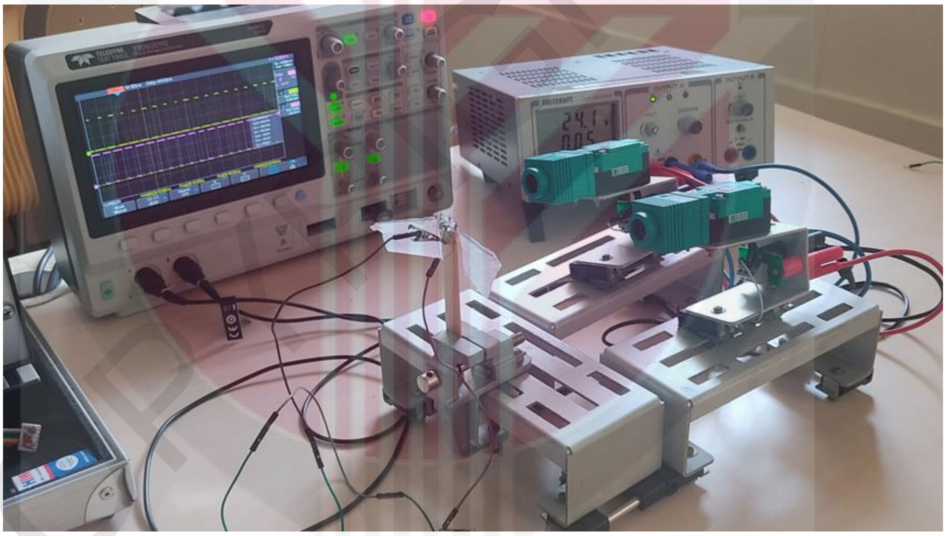

Figure 4.79 : Phase Lag between Left- and Right-Wing Measuring Setup

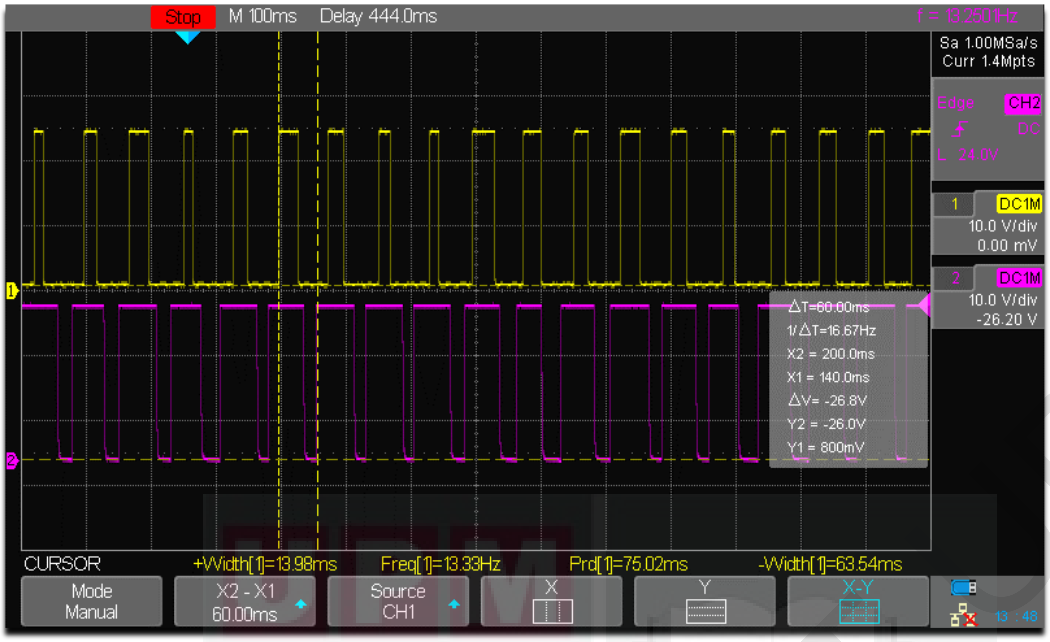

Figure 4.80 : Phase Lag between Left and Right Wing

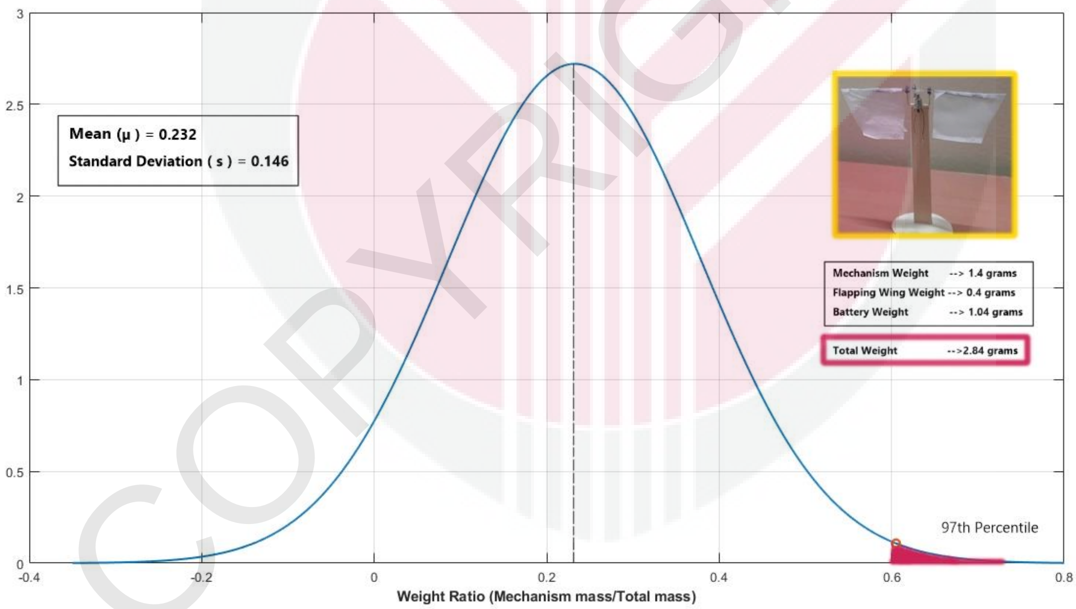

Figure 4.81 : Normal Distribution Comparison of Proposed Design Configuration's Metric against Existing Flapping Wing Design Weight Ratio Metric

As shown in simulations, structural design constraints caused a delay between the left- and right-wing positions during its flapping movements. i.e., approximately 2 degrees of angular position lag in one of its wings. In the proposed experimental setup using the prototype, it is attempted to evaluate the positional lag between the wing's movements by mounting two IR sensors side-by-side, focused on each wing tip, as depicted in Figure 4.79. CRO channels are connected to both the sensor and a 24v DC input source that activates the sensors. As illustrated in Figure 4.80, the prototype is accelerated by an input voltage of 2.5v, and able to acquire the flapping frequency of the wings measured at CRO as 13.33 Hz and 13.250 Hz. In the typical 'clicking mechanism prototype' of Y.W.Chin (Y.-W. Chin & Lau, 2013) , the click-happens when the stroke reaches a vital point. When a position lockout occurred in the crank slider mechanism, the study shows a fast, rapid flap stroke (click) could raise wing-joint strains and splinter the wing at its joint interconnection. It was projected that the click mechanism will yield more kinetic energy in flapping than a resonant system, assuming for the specific work. It is seen that our mechanism is superior than clicking mechanisms in terms of flapping frequency actuation (as individual wing is controllable), reduced weight, and low power consumption. The overall weight of the prototype is 2.84 gram (where weight of: motor = 0.54g, battery = 1.04g, two wings = 0.4g, mechanism with only supporting structure = 0.86g). For the proposed prototype Design III configuration, the weight ratio calculation obtained is around 0.634. which safely fall in the 97th percentile (as shown in Figure 4.81) of all the nine best available weight ratios for micro flapping wing designs of crank slider type mechanism from the previous literature (S. Singh, Zuber, et al., 2022a), such as SF-3 prototype (Zdunich et al., 2007) , Nguyen's Beetle (Q. V. Nguyen et al., 2009), Flapping robot (Lever crank mechanism)(Kudo et al., 2012), Lung-Jieh Yang's MAV (L. J. Yang et al., 2015) , untethered 3.2g FWMAV (Rosen et al., 2016) , Rotor-Bee (Yi et al., 2018), Evans Modified 3D printed Mechanism (Kompala et al., 2019), FWR MAV (DONG et al., 2020), and Hassanalian's FWMAV2 (Lane et al., 2020).

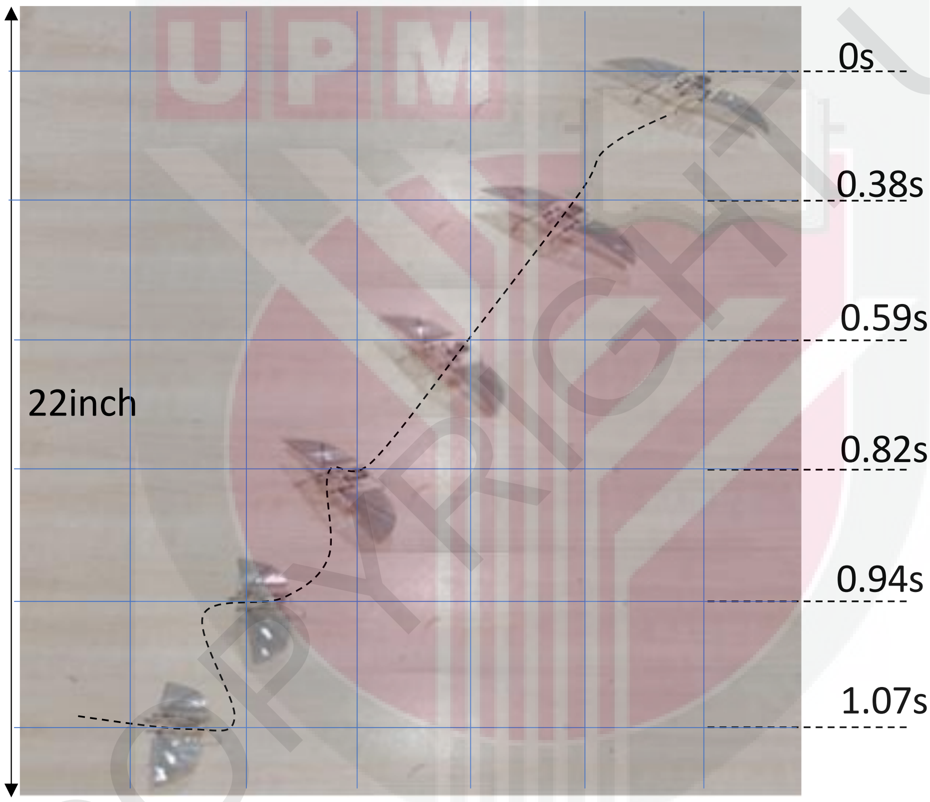

Figure 4.82 : The Captured Path of Movement by the Final Prototype

Also, attempted to substitute the tissue paper wing with a plastic wing in the shape of a mosquito wing. When the power supply is offered, however, it begins traveling in the reverse direction Figure 4.82. To make it move forward, once more attempted to alter the wing shape. As the supply was provided, the prototype began to move forward, indicating that it is generating thrust as in

Figure 4.82. However, it was not producing lift. The movement of the final prototype with respect to time is captured as depicted in Figure 4.82 clearly.

4.6.3 Experimental Setup and Results: Design Mechanism-IV

For the variation in flapping measurement and analysis, the authors have conducted the experimentation of distance detection through ultrasonic sensor in accordance with an Ultra 3000 software. With the ultrasonic sensor setup positioned at a maximum distance of 72mm from the prototype wing, they were able to test the distance measurement in relation to the flapping motion. The Ultra 3000 software is connected across it which shows us the sensor information and measured distance value at its port monitor with respect to time. Also, in Figure 4.83 the mili Amphere (mA) and Voltage (V) variation at its right top corner, as the variation in distance is measured by the ultrasonic sensor. Variation in wing position in terms of measured distance is plotted based on the dynamic data values acquired from the port monitor with respect to time as shown in Figure 4.84. But this distance measurement could give us the angle of motion covered through the lever length calculation, i.e 47degree. The design specifications of fabricated test bench DC-SDL design are listed in Table 4.3 below.

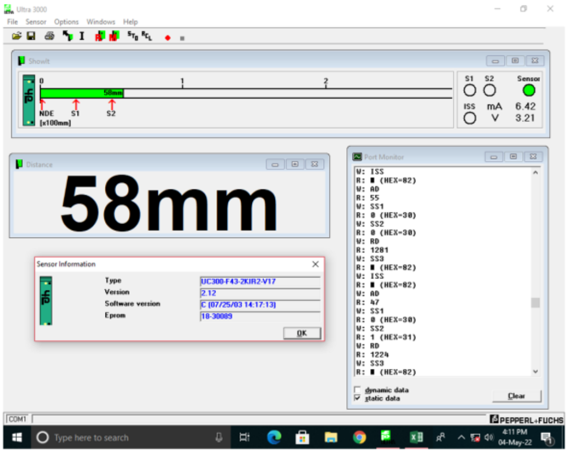

Figure 4.83 : Ultrasonic Sensor Measurement Interfaced with Ultra2000 Software

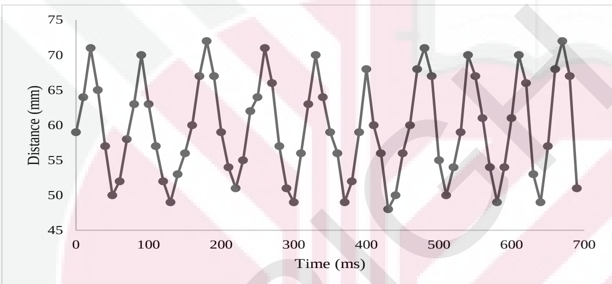

Figure 4.84 : Distance Variation Measured by an Ultrasonic Sensor throughout Wing Flapping

Table 4.3 : Design Specifications of the Test Bench DC-SDL Prototype

Over all weight	1.82g (without battery & with wings)
Each motor weight	0.60g
Wing span	78mm
Wing area	3.4 x 1.8 (LxB)
Flapping frequency	70hz
Input voltage	3.5v DC
Angular velocity	Forward stroke (ω1 = 0.925025/ 0.045 = 20.556 rad/sec) Return stroke (ω2 = 0.925025/ 0.027 = 34.2601 rad/sec)
Linkage length of test bench prototype	L1=6, L2=2.5, L3=11, all in mm (fig 1 labels)

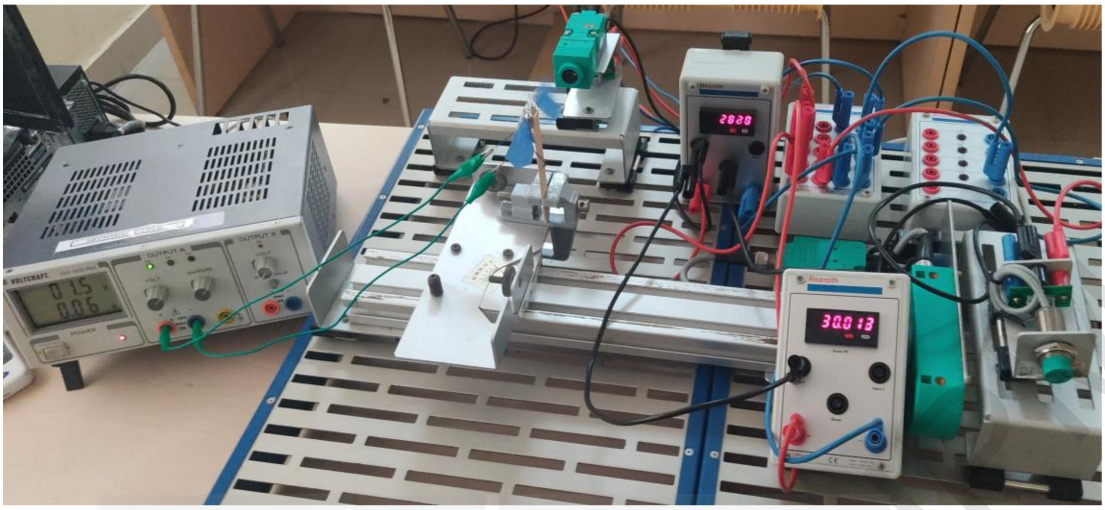

Figure 4.85 : IR Sensor Circuit Setup for Frequency Measurement

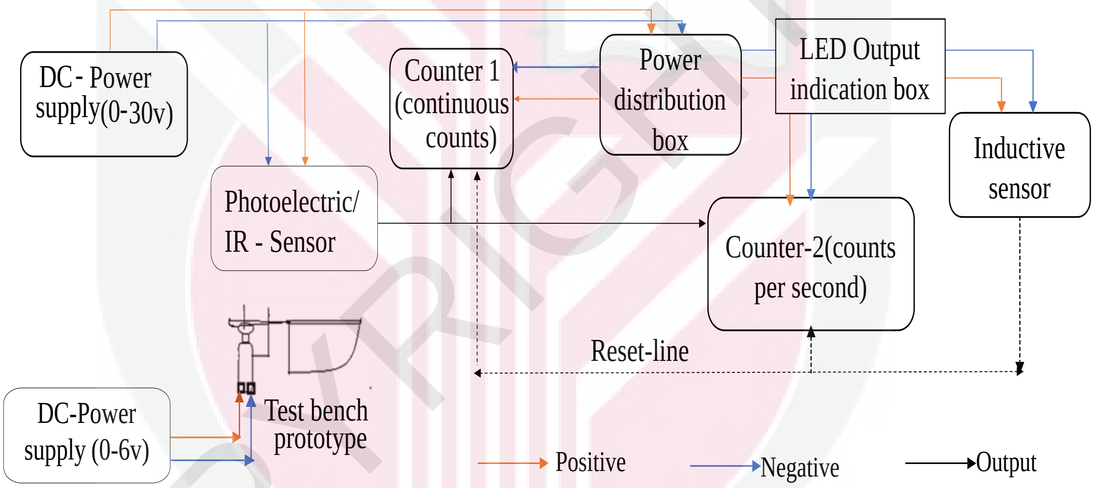

Figure 4.86 : Schematic Diagram of Flapping Frequency Measuring IR Sensor Circuit Setup

The consistency of the actuator's flapping is measured using an IR (infrared) sensor, and its flapping frequency is determined through a counter and tachometer, as seen in Figure 4.85. the Figure 4.86 depicts schematic Diagram of the Flapping Frequency Measuring Setup, which specifies the circuit connections in detail of Figure 4.85 As depicted in the Figure 4.85**,** an IR sensor is calibrated and set to a detection distance of 60mm using our prototype wing as a reference. As the IR sensor receives a DC input voltage of 24 volts and the motor connected to the prototype receives 1.5 volts, obtain the number of flaps continuously (i.e 2828) detected by the sensor at the counter-1. Also, counter-2 is programmed for tachometer readings to count the number of flaps per second (i.e 30.013), as shown in the 4.85**.** Also**,** an inductive sensor is connected to reset the counter value. Figure 4.86 clearly displays the positive, negative, and output wire connections of the circuit representing Figure 14's components. Authors have employed a non-contact but automatic laser sensor/tachometer to validate the IR sensor's measurements of the original prototype to compare their respective values.

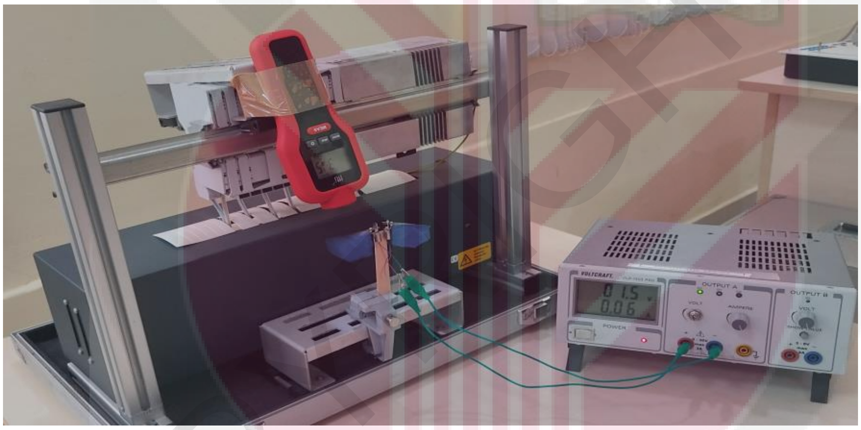

Figure 4.87 ***:*** **Flapping Frequency Measurement Setup with Laser Tachometer**

Figure 4.87 depicts the arrangement of the prototype across the laser tachometer with a vertical distance of 40mm from the top view with the input voltage of 1.5v across the motor. The frequency readings from two distinct sensors, an infrared (IR) sensor and a laser tachometer, are plotted separately for various input voltages at the motor, as shown in Figure 4.88. As the input voltage is increased from 1v to 3.5 v, the flapping measurement of both sensors demonstrated a linear change.

Figure 4.88 depicts a graph demonstrating that our proposed prototype can achieve a maximum frequency of 70 Hz at a maximum input voltage of 3.5v. In comparison to the clicking mechanism of yao wei (Y.-W. Chin & Lau, 2013)(i.e 15hz at 3.5v), our obtained flapping frequency is superior. Individual wing motion control is also possible in our proposed mechanism due to the independent motors dedicated to each wing, resulting in advantageous flight control overall.

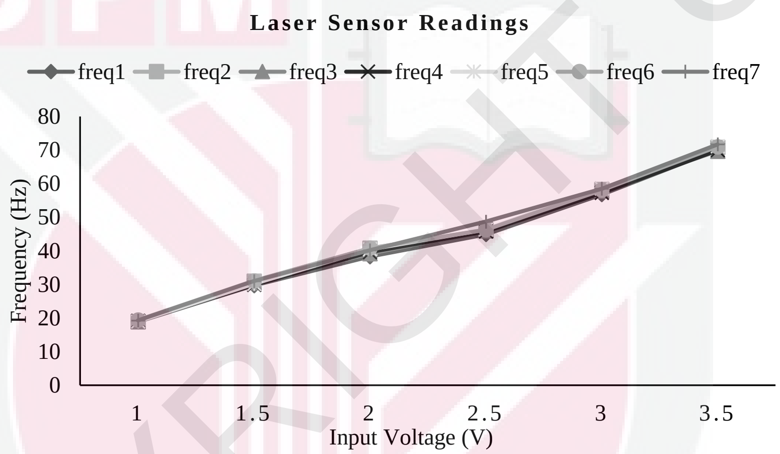

a).

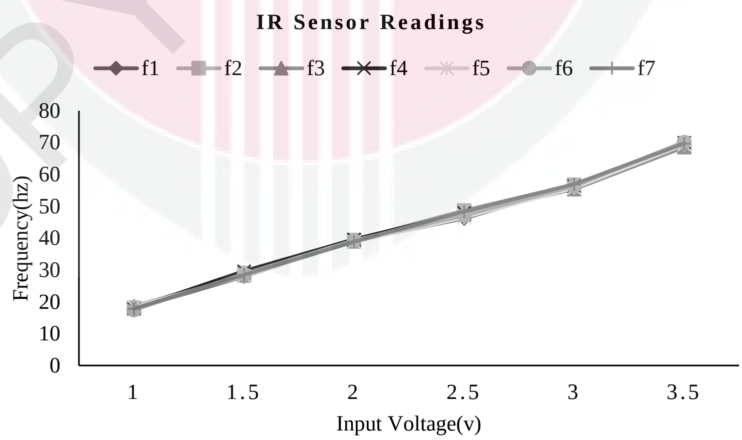

b).

Figure 4.88 : Variation in Flapping Frequency a) by Laser Sensor and b) IR Sensor Based on the Varied Input Voltage of the Motor

Whereas in the clicking mechanism flight control is not possible due to the single-motor dual-wing configuration. In clicking mechanism, the power required for flapping actuation is 3-9v which is very high. But it is advantageous in our proposed mechanism as they have tested for 1-3.5v maximum. Hence indirectly it will reduce the battery weight, by contributing to the overall weight reduction.

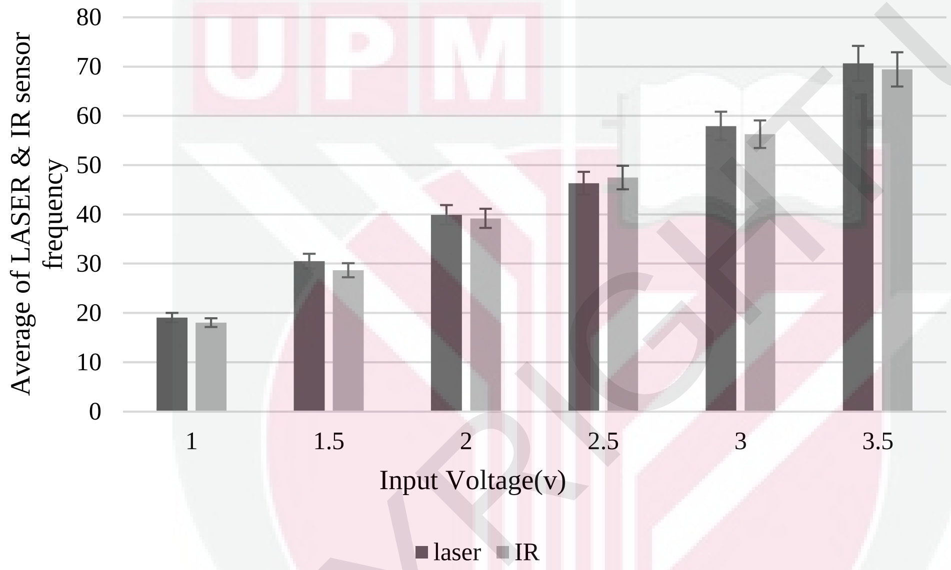

Figure 4.89 : Average of Laser Tachometer and IR Sensor Flapping Frequency Readings

Figure 4.89 depicts the difference between the average values obtained for IR Sensor and laser tachometer readings about the prototype flapping frequency. Figure 4.90 depicts the difference between the flapping frequency obtained for linear change in input voltage across the motor. i.e the 7 set of various readings that are performed is considered for the error range detection. The seven sets of readings are represented in different colors with labeling f1 to f7 for it. The error range obtained at Figure 4.89 and Figure 4.90 are between +

2.5HZ to -2.5HZ which is negligible. Consequently, the frequency measurement validation is performed and compared successfully.

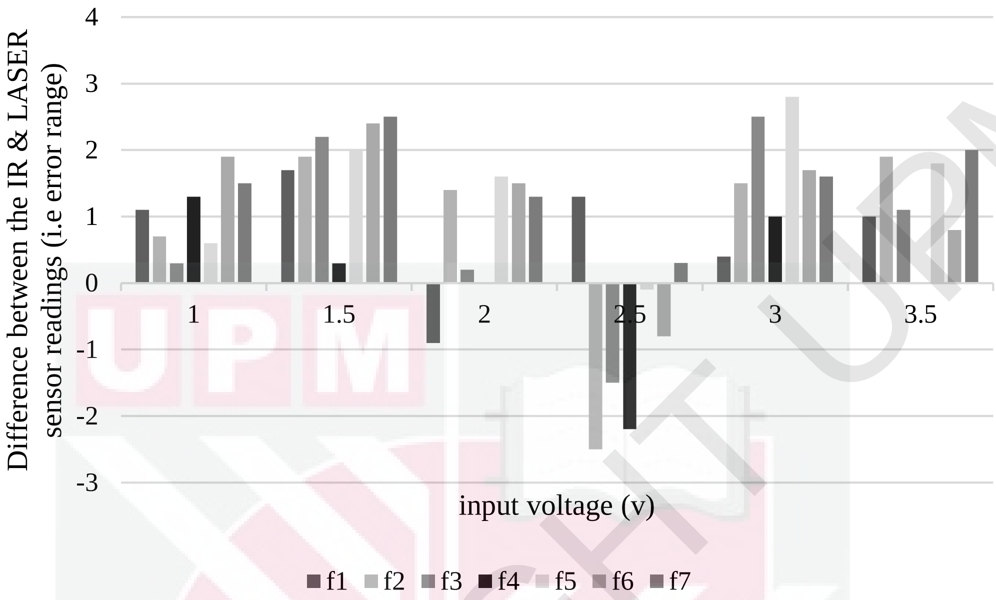

Figure 4.90 : Difference between the IR Sensor and Laser Tachometer Flapping Frequency Readings (i.e the Error Obtained) for 7set of Testing Performed

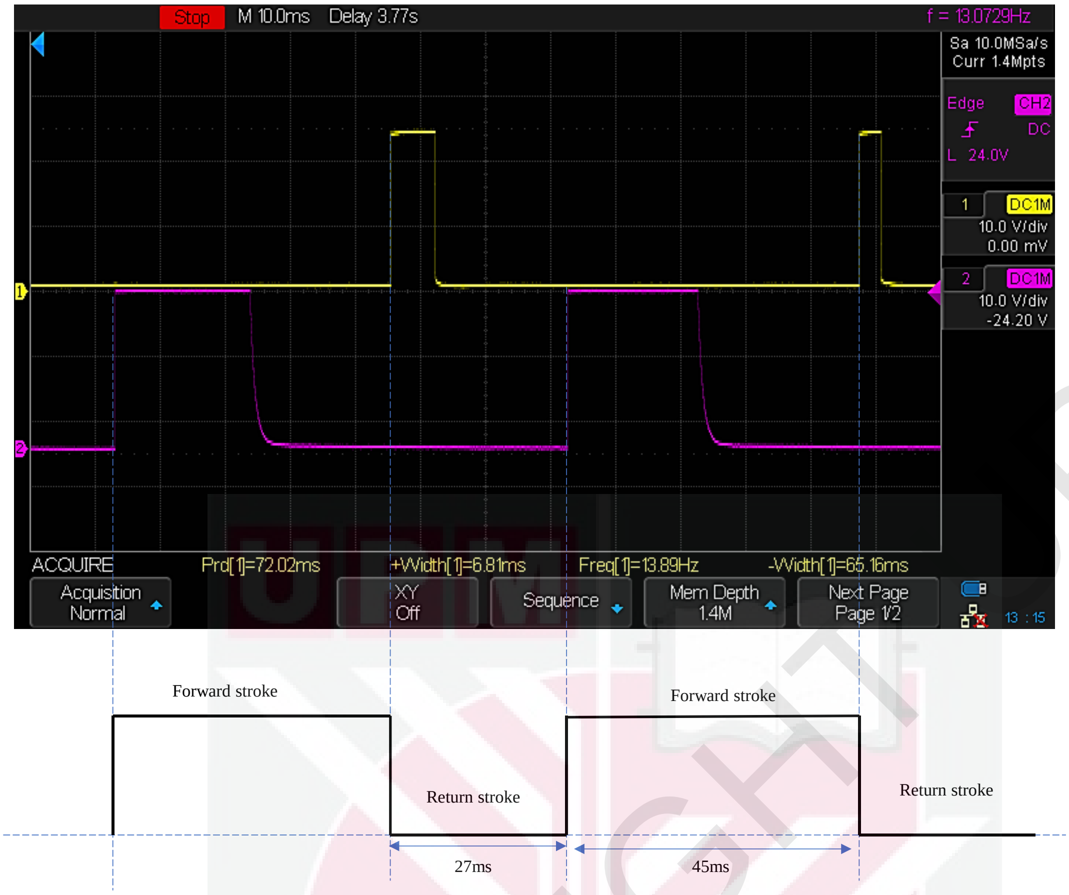

Figure 4.91 : Digital CRO Forward and Reverse Stroke Time lag Measurement

To measure the forward and return stroke time difference of the wing flapping, two distinct infrared sensors are mounted side by side at a certain distance facing the extreme ends of the wing tip. The IR sensor-1 output is connected to channel-1 of the Digital CRO, similarly IR sensor-2 output is connected to channel-2 of it. The forward and reverse stroke time lag measurement output obtained at CRO can be seen at Figure 4.91. The yellow signal represents the output obtained at channel-1, while the pink signal represents the output at channel- 2.the difference between both the signal gives us the period of forward stroke and the return stroke as in Figure 20. As the authors know that the angle of flapping performed by the prototype, calculating the velocity of both the strokes is easier. Flappable frequency is the number of flaps count per sec (i.e 1000ms). They got flapping frequency at channel-2 is 13.89 Hz and the cycle period between individual flap is 72.02ms as per the above obtained CRO plot. 72.02 x 13.89 = 1000.3578ms. The difference between the channel-1 and channel-2 raising edge of the signals are as shown in Figure 4.91, i.e 27ms is the obtained period for return stroke (Td) and 45ms for the forward stroke (Tu) period. Therefore, 37 percent of the period has been consumed by the return stroke, which is much faster than the forward stroke, which consumed 63 percent of the cycle period.Hence, it can be said that the obtained time ratio of forward and return stroke is 2:1, that generates a favorable lift force across flappable wing period. This validates us regarding the sliding lever concept of movement, also variation in time and speed of flapping for both strokes seen at analytical results, simulation results and real time testing as well. The frequency of flapping obtained by the 3d printed DC-SDL mechanism at an input of 3.5v is as shown in Figure 4.92. they can see that the obtained average flapping frequency from the IR sensor is 32.88hz. When compared to the prototype of the 3D printed DC-SDL model, the flapping frequency obtained by the handmade DC-SDL model is significantly greater. In fact, it is almost twice as high as the frequency acquired by the 3D printed model.

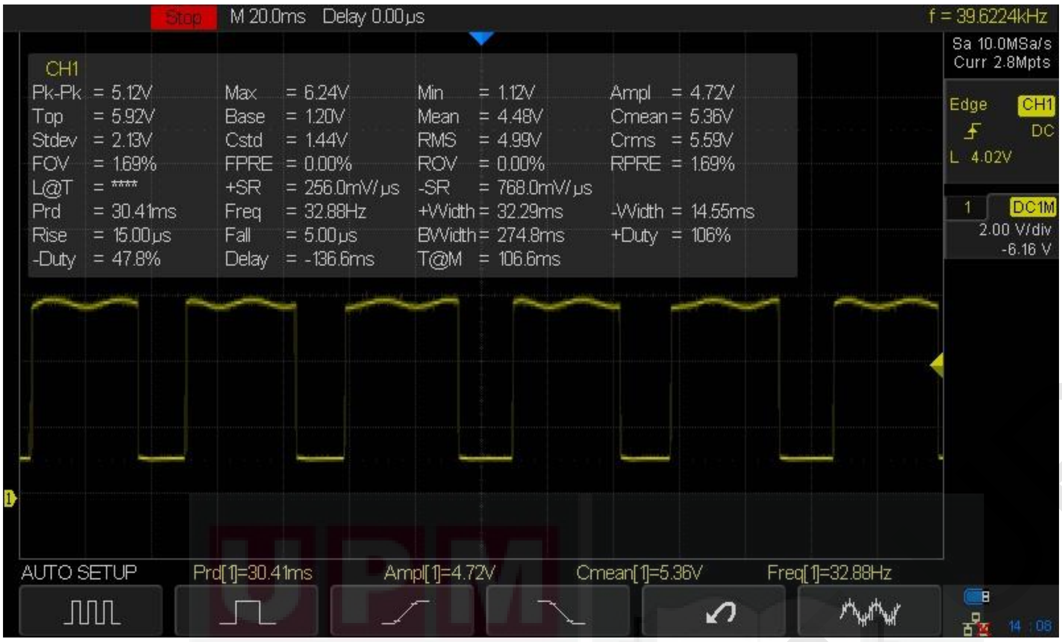

Figure 4.92 : Frequency Measurement of 3D Printed DC-SDL Mechanism with Micro DC Motor Design at an Input Voltage of 3.5v

4.6.4 Experimental Setup and Results: Button Motor Driven SC-SDL Design

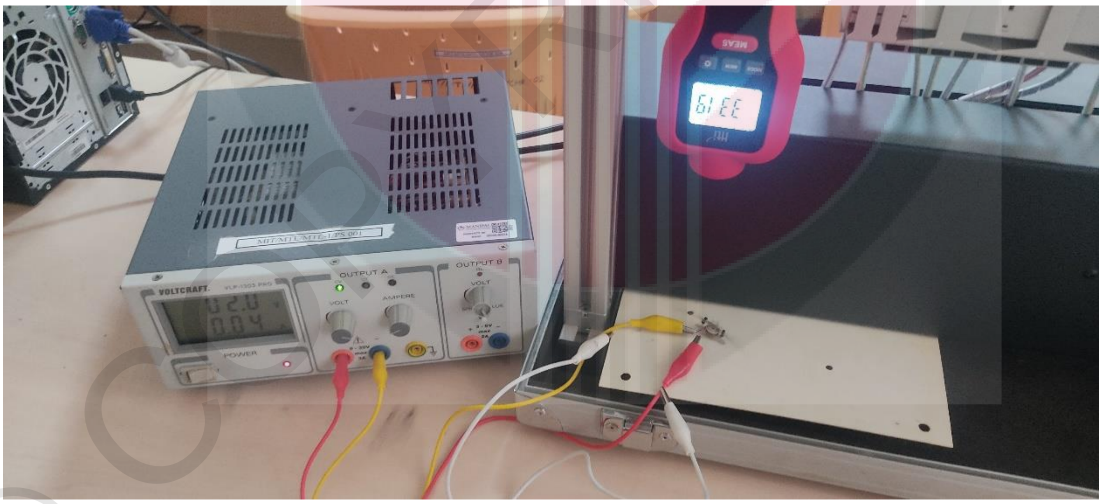

Figure 4.93 : Hand-Made SC-SDL Design with a Button Motor Frequency Testing Setup

Figure 3.39 in chapter 3, shows a hand-made SC-SDL design with a button motor. This design is connected to a variable dc power supply and a laser tachometer (as shown in Figure 4.93) so that the flapping frequency can been measured and recorded separately depending on the supply voltage. When the input voltage is changed from 1 volt to 5 volts, several sets of measurements are produced as shown in Figure 4.94; the highest flapping frequency obtained is 76.3 hertz when the voltage is 5 volts. The left- and right-wing flapping frequency are measured, and the difference obtained is projected in Figure 4.95 below. The obtained difference of flapping frequency is minor hence it can be negligible. The same flapping frequency verification validated for 1v by measuring it through IR sensor and it has produced 20hz as shown in Figure 4.96 below.

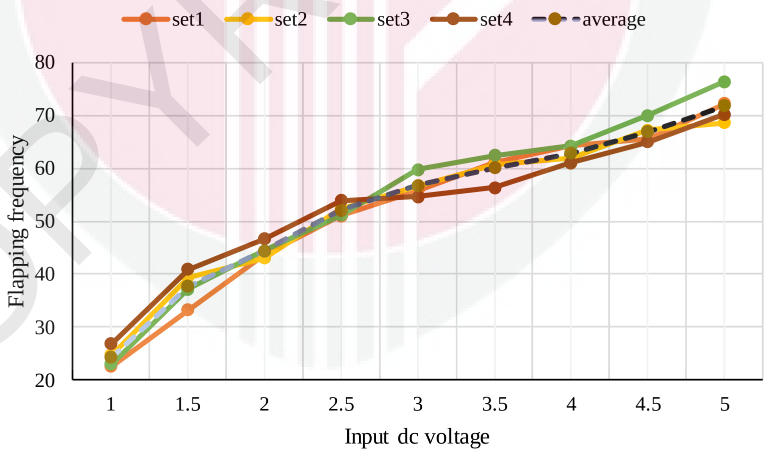

Figure 4.94 : Obtained Set of Flapping Frequencies from Button Motor Driven SC-SDL Model

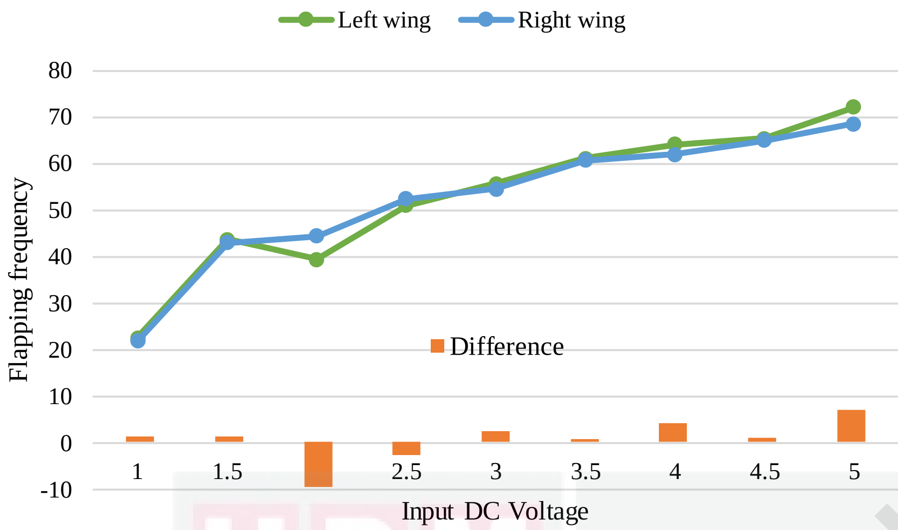

Figure 4.95 : Difference of Flapping Frequency Obtained between Left and Right Wing of Button Motor Driven SC-SDL Model

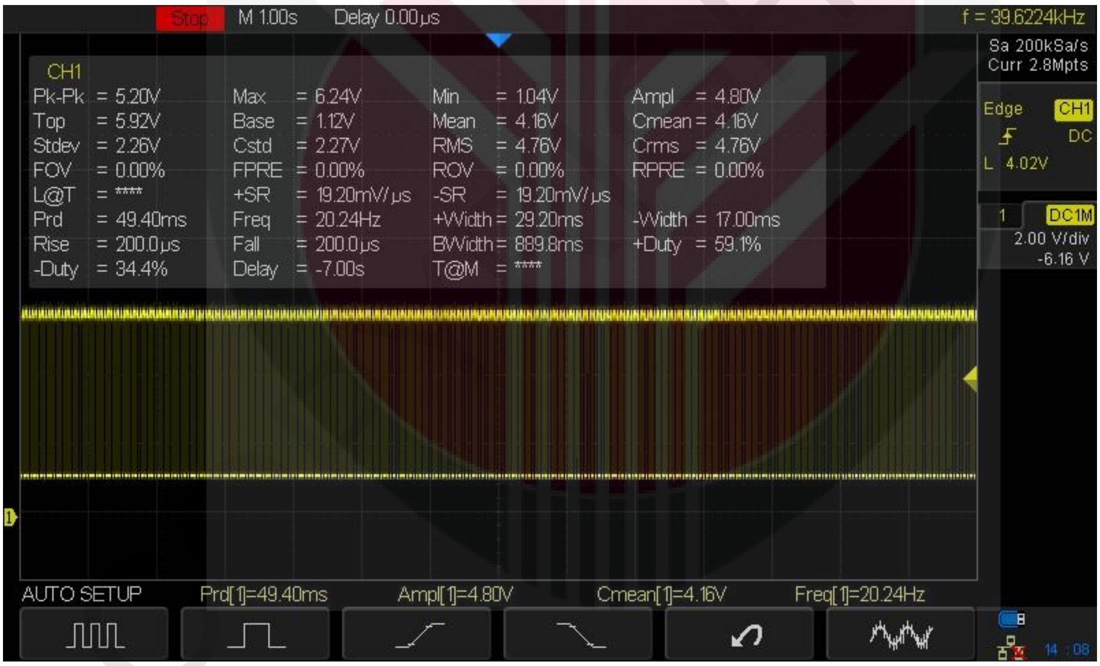

Figure 4.96 : IR Sensor Measured Frequency Measurement of Handmade SC-SDL Mechanism with Button Vibration Motor Design at 1v Input Dc Voltage

The detailed list of the overall flapping wing actuating mechanisms designed and fabricated are tabulated with its specifications for the ease of comparison are, as seen in Table 4.4 below. The details of simulations and real time experimental analysis done, has been tick marked in the list as shown in Table 4.5 below. Out of seven flapping wing designs (from design 3C to design VI), design IV **(**DC-SDL mechanism) has produced a high flapping frequency of 70 hz, with least prototype weight of 1.87g.

Table 4.4 : List of All Modelled Designs and its Specifications

Design	3C	I	II	III	IV	V	VI
CAD	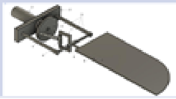	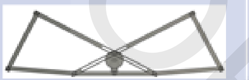	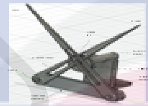				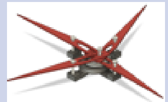
Design name	Motor Actuated 3C Joint Mechanism	X-pattern crank-slider Four-bar mechanism	X pattern SC-SDL mechanism	Modified Single Crank – Slotted Dual Leavers (SC-SDL) mechanism	Dual Crank – Slotted Dual Leavers (DC-SDL) mechanism	Button motor driven Slotted Dual Leavers mechanism	Button motor driven Slotted Quad Leavers mechanism
Input DC voltage	1.5 - 3.5v	1.5 - 4.5v	1.5 - 4.5v	1.5 - 4.5v	1.5 - 4.5v	1.5 - 3.5v	1.5 - 3.5v
Wingspan	36mm	120mm	105mm	66mm	80mm	48mm	48mm
Prototype weight	1.6g		3.14 g	1.18 g	1.87 g	0.88 g	1.07 g
Motor size weight & RPM	4mmx8mm, 0.60g & 25k rpm	6mmx10mm, 2.43g & 20k rpm	6mmx10mm, 2.43g & 20k rpm	4mmx8mm, 0.60g & 25k rpm	3mmx7mm, 0.54g & 70k rpm	10mmx3mm, 0.68g	10mmx3mm, 0.68g
Flapping angle	18 deg	38deg	31 deg	21 deg	43 to 51deg	23 deg	19deg
Flapping frequency	38hz	14hz	20hz	24hz	70hz	61hz	40hz
Design type	complex	simple	simple	simple	simple	simple	complex
Hand made designs					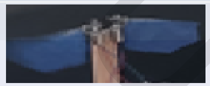	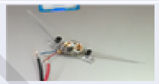	
3d printed designs							

Table 4.5 : List of Simulations and Experiments Performed for All Designs

Design types	Motor Actuated 3C-Joint Model	Crank-Slider Models					
Methodology steps		X-pattern crank-slider Four-bar mechanism Design -I	X-pattern Single Crank - Slotted Dual Lever (SC-SDL) mechanism Design -II	Modified Single Crank - Slotted Dual Lever (SC-SDL) mechanism Design -III	Dual Crank - Slotted Dual Lever (DC-SDL) mechanism Design -IV	Button Motor driven Slotted Dual Leavers mechanism Design - V	Button motor driven Slotted Quad Leavers mechanism Design - VI
Design concepts with kinematic modelling	✓	✓	✓				
CAD Design	✓	✓	✓	✓	✓	✓	✓
Actual Design Fabrication	✓	✓	✓	✓	✓	✓	✓
Controller implementation					✓		
Simulations							
2D /3D simulations using CompMech GIM	✓	✓	✓	✓	✓		✓
MATLAB Simscape	✓			✓	✓		

4.7 Summary of the Simulations and Results

This chapter examines the simulations and real-time testing of six novel test bench models for flapping wing actuation mechanisms. The purpose is to provide simulated findings for comparison and validation, with the goal of improving the mechanisms of bionic micro aerial vehicles (MAVs). The authors provide a detailed examination of the kinematics of two important mechanisms: the crank-driven 3C slidable and the crank slider mechanisms. The crank slider mechanism, within the 3C-joint mechanism, provides a lightweight and minimal-link design that is well-suited for Micro Aerial Vehicles (MAVs). The designs were subjected to 2D and 3D simulations to assess the performance of the flapping motion and trace the path of the flapping link tip. This was done using two distinct software tools. The simulation results were analysed and compared in terms of flapping frequency, angle, position, angular velocity, and angular accelerations. Using fabricated prototypes and motion analysis, it shows that the simulated findings aligned with the anticipated kinematics.

Developing a micro-DC motor system with PID control for flapping wing actuation provides accurate, steady, and quick control, taking inspiration from the flight patterns seen in nature. The impact of the controller on the flight control system is accurately replicated and observed in Simulink's Simscape environment, with manoeuvres executed in different directions every 5 seconds. The benefits of this technology encompass precise flapping, stable flight, effective energy utilization, and adjustable parameters. Nevertheless, it is important to tackle obstacles such as mechanical limitations, fluctuating conditions, incorporation with navigation systems, and susceptibility to temperature variations. Utilizing advanced modelling and adaptive control systems can significantly improve performance.

CHAPTER 5

CONCLUSION AND RECOMMENDATIONS FOR FUTURE RESEARCH

5.1 Concluding Remarks

Researchers have long been fascinated by the incredible flight capabilities of small insects like flies and mosquitoes. These natural creatures exhibit remarkable aerodynamic performance with their lightweight and compact flapping wing designs. While previous studies have extensively explored the wing aerodynamics of mosquitoes and developed various piezo or linear actuated nano-scale flapping wing prototypes, fewer attempts have been made to miniaturize motor-actuated flapping wing mechanisms for insect-scale applications. Mosquitoes exhibit highly efficient flight mechanics optimized through millions of years of evolution. Mimicking these mechanics allows for the development of MAVs that can achieve similar aerodynamic efficiency. Mosquito-like designs are well-suited for low Reynolds number flight conditions, which are typical at small scales, leading to improved flight stability and control. Mimicking the flapping patterns and wing kinematics of mosquitoes can result in MAVs with exceptional maneuverability, capable of performing agile and precise movements in cluttered environments. These designs can potentially enable stable hovering, an essential feature for various surveillance and inspection applications too.

These MAVs can be deployed for surveillance and reconnaissance in military operations, providing real-time data without being easily detected. Useful for monitoring borders and assisting law enforcement in covert operations. Their small size and quiet operation make them ideal for observing wildlife without disturbing the natural behavior of animals. Can be equipped with sensors to monitor air quality and detect pollutants in hard-to-reach areas. Can navigate through rubble and confined spaces to locate survivors in disaster-stricken areas. Useful for inspecting damaged infrastructure such as buildings, bridges, and tunnels post-disaster. Can be used to study the flight mechanics and behavior of real mosquitoes and other insects in their natural habitat. Potentially capable of delivering small medical payloads or sensors to specific locations within the human body or to remote areas. Useful for monitoring crop health, detecting pests, and assessing field conditions. Can assist in pollination, especially in environments where natural pollinators are declining. MAVs can inspect hard-to-reach urban infrastructure such as high-rise buildings, bridges, and utility lines. mosquito-mimicking flapping wing MAVs offer significant advantages in terms of efficiency, maneuverability, and stealth, with a wide range of applications spanning from military and surveillance to environmental monitoring and disaster response.

Literature study chapter 2 reviews various flapping-wing systems, focusing on actuation mechanisms, structure-based designs, and hybrid techniques for flapping enhancement. It categorizes flapping-wing drones by rotary/motor, hybrid, and linear-driven mechanisms and deconstructs basic actuation mechanisms into block diagrams. The authors propose alternative approaches and key parameters for micro to nano-size flapping-wing systems, emphasizing high flapping frequency and stroke angle controllability. The chapter highlights long-term stability from flapping patterns/flight modes and yearly progress in FWAV prototypes over two decades, ranking the best by flight modes and lift generation. Current motor-driven flapping mechanisms are deemed simplest, while piezo and electrostatic actuated models face issues like short flight times and variable flapping frequencies. The need for wireless electricity in bio-inspired drones is noted, with new molecular-level actuation systems under exploration. A demand for lightweight, simple FWMAV designs is identified, necessitating new mechanisms to transform rotary action into flapping movement. Future chapters will delve deeper into tested designs.

Through the literature survey - a lot of research gaps have been identified. Out of which few gaps have been considered for addressing it through this research. From the literature review data, of fully flyable FW-Models – under motor driven mechanisms the researchers have achieved max 45 hz flapping frequency, where in linear driven models (piezo, shape memory alloy, electro active polymer, electrostatic & electromagnetic. etc) researchers have achieved nearly 200hz. This research aims to address these gaps by proposing novel and improved designs for miniaturized motor-driven flapping wing actuation mechanisms. As highlighted in the literature, researchers such as Bomphrey, Wood, Lung, and Nguyen have made significant contributions to the field of flapping wing robotics. Through a comprehensive literature review, it is identified that the several research opportunities have guided the objectives and methodology of this research study.

In order to accomplish the above goals, a methodology has been developed consisting of four distinct steps, as illustrated here. Stage 1 involves the invention or selection of a design for the flapping actuation, together with the necessary drive source. Developing a mathematical model for it using kinematic measurements. The following stage, Stage 2, involves conducting design simulations of kinematic measurements using 2D/3D analysis in computational mechanics GIM software, as well as in MATLAB SimScape Multibody software. In Stage 3, it attempted to create several models using both manual fabrication and 3D printing methods. Additionally, they conducted experimental validation by monitoring several parameters such as the flapping frequency and angle. Finally, in stage 4, they executed the controller implementation for the moving of the system using MATLAB Simulink modelling.

The objectives addressed in each level are as indicated below. They have built 2 distinct systems here. The first mechanism is referred to as a 3C mechanism, which stands for a mechanism with three cylindrical joints that are coupled in a mutually perpendicular manner in series. The second mechanism is a crank slider design, which has been further changed into six distinct patterns. In the under crank slider design, the initial design, referred to as Design 1, involves connecting the sliding levers in an x pattern using a combination of a 4-bar mechanism. This mechanism is operated by a single motor, as depicted here. Design 1 was modified to design 2 by eliminating the side links in order to simplify the design and reduce its complexity. The single crank-slotted dual lever mechanism is being referred to. However, there was a lack of coordination between the left and right wing in this case, as evidenced by design 2, where the left wing is positioned 10 degrees behind the right wing. The lever tip position study was conducted using the Compmech GIM software to simulate and determine the angular velocity and accelerations for each design.

Therefore, they altered design 2 to design 3 by moving the crank slider position to a precise alignment between the left and right lever supporting hinges. In design 3, the difference in angle between the left and right wing was modest, specifically 2 degrees. The reason design 3 and 5 are written together is because the design of mechanism 5 is like that of mechanism 3, with the only difference being the replacement of the DC motor with a different button motor, as described in the fabrication section. However, with this design including a 3& 5 mechanism, the delay between the levers was a result of the construction design, namely the use of a single motor to drive both levers. Consequently, they made further modifications to the design by adding an additional motor to enable independent control of each lever's movement. That is, design number 4. In design 4, the flapping coordination of the left and right wings was adequate. Subsequently, they attempted to incorporate an additional pair of sliding levers into design 5, controlled by a button motor, resulting in a quadruple lever configuration referred to as design 6. The lever tip position analysis was conducted using Compmech gim software as simulations. The resulting angular velocity and accelerations for each design are displayed here. Now let's proceed to stage 3, which is the fabrication phase: The design of 3C, as depicted below, is a manually crafted design that achieves a maximum flapping frequency of 38 Hz. The obtained flapping angle is 18 degrees, as depicted in the illustration. Despite the novelty of this design, they opted for several variations of the crank slider design concept because to the complicated exploitation of 3 joints for rotational to flapping conversion. That is, design 1 - as seen in this image. The object was created using 3D printing technology. Subsequently, it was modified to create design 2, which features a handcrafted wooden aesthetic. They have the ability to observe its motions. Following When it comes to designs 3, 5, and 6, they will begin by examining design 3. The item is a manually crafted piece, with a significantly small size, as demonstrated by its comparison to a 10-cent coin. This device demonstrated superior flapping performance even when powered by a little 1-volt button battery, as depicted above. Subsequently, they attempted to validate the test bench model by employing several dummy wings, as depicted in the accompanying illustration. This pertains to the measuring of the flapping frequency of an IR sensor. The researchers conducted live testing to analyse the flapping behaviour of the object. The testing revealed that it could generate a force ranging from 1.6 to over 2g. That is why it can move randomly on the table. However, it has demonstrated a flapping frequency of 24 Hz with a flapping angle of 21 degrees when supplied with 3.4V DC. Next, it will proceed to design 5, which utilizes a button vibrator as a motor. Button vibrators are typically utilized in mobile devices or tablets for the purpose of generating vibrations. To change these vibrators, individuals have opened their outer casing and removed the additional weight. This alteration effectively eliminates the vibration function, allowing the device to be used as a motor. The crank revolves in the air due to the electromagnetic effect, even though it only has indirect contact with its bottom shaft. The design demonstrated a flapping frequency of 61 Hz and a flapping angle of 23 degrees. Subsequently, in the fifth iteration of the design, two additional levers were incorporated, resulting in the creation of the sixth design. Notably, in this design, there is a lack of coordination between the wings. Therefore, a separate motor is installed at each lever in design 3 in order to achieve design 4. As demonstrated in this example. Within This design has demonstrated the capacity to control the flapping of each wing independently, which is beneficial for moving in any direction. The specifications table displays that at a voltage of 3.5 V, it has achieved the maximum flapping frequency of 70 Hz, surpassing the previously stated designs. The oscilloscope displays the differences in both the forward and return strokes, as depicted above. The actuation mechanism of the design has been simulated using Matlab Simulink Multibody. The controller has been implemented to enable movement in both left and right directions over time. The CAD designs have been imported and implemented with a micro-DC motor configuration according to the specified specifications. The flow chart demonstrates its operational control every 5 seconds by adjusting the input velocity of each motor individually.

for the controller implemented model, the fluctuations in input voltage, velocity, current, and acceleration of the motors on the left and right sides are recorded every 5 seconds. In chapter 4, the obtained outputs of flapping wing design 4 for the given flow control configuration are shown in relation to changes in lever position, angular velocity, and acceleration for the purpose of comparison. Based on the acquired output, it can be inferred that during the first 5 minutes, when both levers flapped at the same speed, the FW design moved forward. Within the next 5 seconds, if the speed of the right-wing flapping is decreased in comparison to the left wing, the object will change its direction towards the right side. For the next 5 seconds, it continues to move ahead and to the right before coming to a stop. The authors have utilized CAD to create 7 distinct flapping actuating mechanism designs. These designs were then subjected to kinematic modelling and 2D/3D design analysis using Comp-mech GIM software. The parameters of each model are outlined in chapter 4. The simulations are conducted to acquire a positional analysis of the flapping lever and its angular velocity, as well as to compare the measured accelerations. Additionally, they have created several designs using a 3D printer and others using a manual, handmade method. Among the 7 concepts that were proposed, design IV, which utilizes a dual motor operated slotted twin levers mechanism, stands out as the most compact, least complicated, and lightest in terms of overall weight. In addition, the design IV demonstrated a flapping frequency of 70 Hz, which was the highest recorded, using a 3.5v DC input supply. This accomplishment is in line with our goal in motorized designs to achieve a flapping frequency above 45 Hz, a characteristic evocative to mosquitoes. The utilization of a button vibrator as a motor for a miniature FWD (flapping wing drone) system has been a unique contribution from this team, as this type of vibrator has not been before employed in any FW (flapping wing) applications. For future research on these proposed design models, it is recommended to develop a wing that considers aerodynamic considerations in order to create a fully functional flying model. Which will be the topic of another doctoral dissertation, as future work to make it fully flyable bio-mimicking models.

5.2 Overall Conclusion

Biomimetic flapping actuation models utilizing different mechanisms like 3C, SC-SDL, SC-SQL, and DC-SDL approximating a crank and sliding lever system is investigated. The model exhibited thrust by utilizing the disparity in momentum between the forward and return strokes. To determine wing angular velocity, acceleration, and flapping frequency, the structural kinematic analyses are performed by subjecting the mechanism to varying input voltage (i.e 1v-5v). CAD design modelling of the proposed designs are carried out and its structural movement analysis is performed in Compmech GIM software in 2d and 3d analysis for simulation validations. emulations of the mechanisms are performed by modelling the design with control inputs at MATLAV Simscape Multibody. Utilizing a PID-controlled micro-DC motor speed variation system in simulation with simscape multibody with simscape electrical proves to be a practical and efficient approach for managing flapping actuation systems in devices inspired by natural flight patterns. This method ensures precise and controlled wing movements, resulting in stable flight and maneuverability. PID-controlled micro-DC motor speed systems present a valuable solution for achieving accurate and steady wing motion in micro air vehicles, with potential for further improvement through advancements in control theory and technology. The 3D-printed prototype is contrasted with a handcrafted model. The validation of flapping frequency for the handmade design and 3d printed design fabrications are performed using measurements from both infrared sensors and a laser tachometer, paying close attention to variations in forward and reverse stroke velocity. Compared to all seven designs, the design IV (dc-sdl) mechanism has superior flapping frequency actuation, reduced weight, and least power consumption. Hence the slotted-sliding lever mechanism is optimal for micro air vehicles with oscillating wings due to its maneuverability, reduced complexity, lightweight structure, and individual motor control for flight direction changes. Also, the proposed all four objectives have been achieved.

5.3 Future Work /Suggestions

When comparing the performance of the actual bird to that of the bird-mimicking flapping-wing drones, the latter suffers, because it is impossible to perfectly imitate creatures like birds and insects. As a result, an effective combination of biomimetic and biomorphic designs may be the best solution for the development of future flapping-wing drones. Designing any lightweight flapping-wing systems with minimal size and structure development is a challenging aspect. It is better to opt for a directly driven mechanism with a minimal compliant structure in its components. Under rotary actuated systems flying machines with crank shaft design and novel flapping wing rotors with crank shaft design are the lightest fully flyable flapping-wing drone models. The design mechanism must be in such a way that the speed ratios at the two reversals are as high as possible in a single full cycle. Compliant conveyance mechanisms like hinges can be incorporated into forthcoming system designs. For reducing the influence of friction, with the elasticity stored in the hinge can aid in the initial acceleration of the wing throughout each cycle. In hybrid actuated systems, the smaller yoke within the scotch-yoke mechanism

(K. Moses et al., 2020) is the latest design with less mass system. The best option for producing a flapping mechanism in NAVs is by using an improved piezoelectric actuator of 5-millimeter size. As the amplification frame is in its construction, smooth and flexible displacement can be produced, that could maximize mechanical efficiency internally. Investigation of various types of elastomers to mitigate tangent loss may theoretically optimize the electrical requirements. Lift is normally proportional to the number of wings utilized and the amount of flapping created. Increased wing numbers enable slower stroke motion with less energy usage. However, four-winged mechanisms should be prioritized above two-winged systems due to the excessive oscillations and noise generated by the two-winged systems. Because the angular pitching performance of wings is very important, it is necessary to investigate novel mechanism designs that incorporate flexible material and multiple wing configurations with angular pitching techniques. Controlling the flapping or lagging motions of both the wings is accomplished by utilizing nonlinear equations with the implementation of control vectors to achieve model stabilization and tracking.

Hence, Future work should concentrate on increasing the integration of onboard systems to improve control capabilities and on improving coordination through the establishment of compliant, electrostatic, and electromagnetic actuated mechanisms. However, cost savings, optimal wing layout for better lift outputs, aerodynamic modifications, clap & fling impact, and the development of a downward flow must be prioritized. Rotary pico-motors may be the future option for generating flapping in PAVs at the molecular level, as they work by adjusting the magnetic interactions between the gathered nano-scale elements. It's indeed essential to investigate innovative mechanism designs that integrate pico-motors at the molecular level for flapping actuation in PAV designs. In future work, it may be necessary to design a MEMS transmission for rotational to linear conversion to use it for flapping-wing PAV. Surprisingly, only a small amount of progress has been made in improving endurance and increasing the number of fully flyable vehicles built since Microbat in 2003, particularly over the last two centuries, as elaborated in chapter 2. Consequently, there is a need for the development of new types of driving mechanisms capable of producing better lift and long-duration flight.

REFERENCES

Aaroh, Zuber, M., Khader, S. M. A., Kalburgi, S., Basri, E. I., & Ahmad, K. A. (2018). Performance of a monarch butterfly for various flapping angle. *International Journal of Engineering and Technology (UAE)*, *7*(4).

Aerodynamics of Flapping Flight. (n.d.).

Agrawal, A., & Agrawal, S. K. (2009). Design of bio-inspired flexible wings for flapping-wing micro-sized air vehicle applications. *Advanced Robotics*, *23*(7–8), 979–1002. https://doi.org/10.1163/156855309X443133

Ahmad, A., Rama Rao, V., & Radha Krishma, P. (2000). On speed and aerodynamic forces of mosquito. *Indian Journal of Experimental Biology*, *38*(8).

Ahmed, M., Tahir, N. M., Zimit, A. Y., Idi, M., Abubakar, K. A., & Jalo, S. A. (2021). Improved PID Controller for DC Motor Control. *IOP Conference Series: Materials Science and Engineering*, *1052*(1). https://doi.org/10.1088/ 1757-899x/1052/1/012058

Analooee, A., & Ghayour, M. (2020). Flowchart-aided design of a novel spatial flapping wing mechanism. *Proceedings of the Institution of Mechanical Engineers, Part C: Journal of Mechanical Engineering Science*, *234*(22), 4462–4477. https://doi.org/10.1177/0954406220924695

Anderson, M. L., Sladek, N. J., & Cobb, R. G. (2011). Design, fabrication, and testing of an insect-sized MAV wing flapping mechanism. *49th AIAA Aerospace Sciences Meeting Including the New Horizons Forum and Aerospace Exposition*. https://doi.org/10.2514/6.2011-549

Andrzej Harlecki, & Andrzej Urbaś. (2016). Dynamic Analysis of a Selected Spatial One-DOF Linkage Mechanism with Friction in Joints. *J. of Control Science and Engineering*, *4*(1). https://doi.org/10.17265/2328-2231/2016.01.002

Avadhanula, S., Wood, R. J., Campolo, D., & Fearing, R. S. (2002). Dynamically tuned design of the MFI thorax. *Proceedings - IEEE International Conference on Robotics and Automation*, *1*, 52–59. https://doi.org/10.1109/ROBOT.2002.1013338

Baek, S. S., Ma, K. Y., & Fearing, R. S. (2009). Efficient resonant drive of flapping-wing robots. *2009 IEEE/RSJ International Conference on Intelligent Robots and Systems, IROS 2009*, 2854–2860. https://doi.org/10.1109/IROS.2009.5354725

Ballas, R. G., Schlaak, H. F., & Schmid, A. J. (2006). The constituent equations of piezoelectric multilayer bending actuators in closed analytical form and experimental results. *Sensors and Actuators, A: Physical*, *130–131*(SPEC. ISS.), 91–98. https://doi.org/10.1016/j.sna.2005.11.034

Banala, S. K., & Agrawal, S. K. (2005). Design and optimization of a mechanism for out-of-plane insect winglike motion with twist. *Journal of Mechanical Design, Transactions of the ASME*, *127*(4), 841–844. https://doi.org/10.1115/1.1924474

Basaeri, H., Yousefi-Koma, A., Zakerzadeh, M. R., & Mohtasebi, S. S. (2014). Experimental study of a bio-inspired robotic morphing wing mechanism actuated by shape memory alloy wires. *Mechatronics*, *24*(8), 1231–1241. https://doi.org/10.1016/j.mechatronics.2014.10.010

Bashir, M., & Rajendran, P. (2018). A review on electroactive polymers development for aerospace applications. In *Journal of Intelligent Material Systems and Structures* (Vol. 29, Issue 19, pp. 3681–3695). https://doi.org/10.1177/1045389X18798951

Bejgerowski, W., Ananthanarayanan, A., Mueller, D., & Gupta, S. K. (2009). Integrated product and process design for a flapping wing drive mechanism. *Journal of Mechanical Design, Transactions of the ASME*, *131*(6), 0610061–0610069. https://doi.org/10.1115/1.3116258

Bejgerowski, W., Gerdes, J. W., Gupta, S. K., & Bruck, H. A. (2011). Design and fabrication of miniature compliant hinges for multi-material compliant mechanisms. *International Journal of Advanced Manufacturing Technology*, *57*(5–8), 437–452. https://doi.org/10.1007/s00170-011-3301-y

Bejgerowski, W., Gerdes, J. W., Gupta, S. K., Bruck, H. A., & Wilkerson, S. (2010). Design and fabrication of a multi-material compliant flapping wing drive mechanism for miniature air vehicles. *Proceedings of the ASME Design Engineering Technical Conference*, *2*(PARTS A AND B), 69–80. https://doi.org/10.1115/DETC2010-28519

bin Abas, M. F., bin Mohd Rafie, A. S., bin Yusoff, H., & bin Ahmad, K. A. (2016). Flapping wing micro-aerial-vehicle: Kinematics, membranes, and flapping mechanisms of ornithopter and insect flight. In *Chinese Journal of Aeronautics* (Vol. 29, Issue 5, pp. 1159–1177). https://doi.org/10.1016/j.cja.2016.08.003

Bluman, J. E., Sridhar, M. K., & Kang, C. K. (2018). Chordwise wing flexibility may passively stabilize hovering insects. *Journal of the Royal Society Interface*, *15*(147). https://doi.org/10.1098/rsif.2018.0409

Bolsman, C. T., Goosen, J. F. L., & van Keulen, F. (2008). Insect-inspired wing actuation structures based on ring-type resonators. *Active and Passive Smart Structures and Integrated Systems 2008*, *6928*, 69281I. https://doi.org/10.1117/12.776084

Bolsman, C. T., Goosen, J. F. L., & van Keulen, F. (2009a). Design and realization of resonant mechanisms for wing actuation in flapping wing micro air vehicles. *Integrity, Reliability and …*, *July*, 20–24. http://paginas.fe.up.pt/clme/IRF2009/PROCEEDINGS/PAPERS/P029

0.pdf

Bolsman, C. T., Goosen, J. F. L., & van Keulen, F. (2009b). Design Overview of a Resonant Wing Actuation Mechanism for Application in Flapping Wing MAVs. *International Journal of Micro Air Vehicles*, *1*(4), 263–272. https://doi.org/10.1260/175682909790291500

Bomphrey, R. J., Nakata, T., Phillips, N., & Walker, S. M. (2017). Smart wing rotation and trailing-edge vortices enable high frequency mosquito flight. *Nature*, *544*(7648). https://doi.org/10.1038/nature21727

Bontemps, A., Vanneste, T., Paquet, J. B., Dietsch, T., Grondel, S., & Cattan, E. (2013). Design and performance of an insect-inspired nano air vehicle. *Smart Materials and Structures*, *22*(1). https://doi.org/10.1088/0964-1726/22/1/014008

Breuer, K. (2019). Flight of the RoboBee. In *Nature* (Vol. 570, Issue 7762). https://doi.org/10.1038/d41586-019-01964-3

Burgess, S. C., Ling, C. S., Conn, A., Araromi, S., Wang, J., & Vaidyanathan, R. (2009). Development of a novel Electro Active Polymer (EAP) actuator for driving the wings of flapping micro air vehicle. *WIT Transactions on the Built Environment*, *106*, 207–217. https://doi.org/10.2495/OP090191

Cao, C., Burgess, S., & Conn, A. T. (2018). Flapping at resonance: Realization of an electroactive elastic thorax. *2018 IEEE International Conference on Soft Robotics, RoboSoft 2018*, 327–332. https://doi.org/10.1109/ROBOSOFT.2018.8404940

Cao, C., Burgess, S., & Conn, A. T. (2019). Toward a dielectric elastomer resonator driven flapping wing micro air vehicle. *Frontiers Robotics AI*, *6*(JAN). https://doi.org/10.3389/frobt.2018.00137

Chao, Z. (2016). Design and Control of Flapping Wing Micro Air Vehicles. *Department of Aeronautics and Astronautics*, *Doctor of*, 212.

Chattaraj, N., Ananthasuresh, G. K., & Ganguli, R. (2021). Design of a distributed compliant mechanism using spring-lever model and topology optimization for piezoelectrically actuated flapping wings. *Mechanics of Advanced Materials and Structures*, *28*(2), 118–126. https://doi.org/10.1080/15376494.2018.1549295

Chen, C., Tang, Y., Wang, H., & Wang, Y. (2013). A review of fabrication options and power electronics for flapping-wing robotic insects. *International Journal of Advanced Robotic Systems*, *10*, 779–786. https://doi.org/10.5772/51186

Chen, C., & Zhang, T. (2019). A review of design and fabrication of the bionic flapping wing micro air vehicles. In *Micromachines* (Vol. 10, Issue 2). https://doi.org/10.3390/mi10020144

CHEN, L., ZHANG, Y., CHEN, Z., XU, J., & Wu, J. (2020). Topology optimization in lightweight design of a 3D-printed flapping-wing micro aerial vehicle. *Chinese Journal of Aeronautics*. https://doi.org/10.1016/j.cja.2020.04.013

Chen, L., Zhang, Y., & Wu, J. (2018). Study on lift enhancement of a flapping rotary wing by a bore-hole design. *Proceedings of the Institution of Mechanical Engineers, Part G: Journal of Aerospace Engineering*, *232*(7), 1315–1333. https://doi.org/10.1177/0954410016688927

Chen, S., Wang, L., Guo, S., Zhao, C., & Tong, M. (2020). A bio-inspired flappingwing rotor of variant frequency driven by ultrasonic motor. *Applied Sciences (Switzerland)*, *10*(1). https://doi.org/10.3390/app10010412

Chen, Y., Helbling, E. F., Gravish, N., Ma, K., & Wood, R. J. (2015). Hybrid aerial and aquatic locomotion in an at-scale robotic insect. *IEEE International Conference on Intelligent Robots and Systems*, *2015-December*. https://doi.org/10.1109/IROS.2015.7353394

Chen, Y., Wang, H., Helbling, E. F., Jafferis, N. T., Zufferey, R., Ong, A., Ma, K., Gravish, N., Chirarattananon, P., Kovac, M., & Wood, R. J. (2017). A biologically inspired, flapping-wing, hybrid aerial-aquatic microrobot. *Science Robotics*, *2*(11). https://doi.org/10.1126/scirobotics.aao5619

Chen, Y., Zhao, H., Mao, J., Chirarattananon, P., Helbling, E. F., Hyun, N. seung P., Clarke, D. R., & Wood, R. J. (2019). Controlled flight of a microrobot powered by soft artificial muscles. *Nature*, *575*(7782), 324–329. https://doi.org/10.1038/s41586-019-1737-7

Chen, Z., Wu, J., & Zhang, Y. (2018). Topology optimization of transmission system of flapping-wing micro aerial vehicle via 3D printing. *IOP Conference Series: Materials Science and Engineering*, *397*(1). https://doi.org/10.1088/1757-899X/397/1/012121

Chen, Z., Xu, J., Liu, B., Zhang, Y. L., & Wu, J. (2019). Structural integrity analysis of transmission structure in flapping-wing micro aerial vehicle via 3D printing. *Engineering Failure Analysis*, *96*, 18–30. https://doi.org/10.1016/j.engfailanal.2018.09.017

Cheng, T. H., Xuan, D. J., Li, Z. Z., & Shen, Y. de. (2011). Development of IPMC actuator for flapping motion of dragonfly. *Advanced Materials Research*, *150–151*, 1301–1304. https://doi.org/10.4028/www.scientific.net/AMR.150-151.1301

Chimakurthi, S. K., Cesnik, C. E. S., & Stanford, B. K. (2011). Flapping-wing structural dynamics formulation based on a corotational shell finite element. *AIAA Journal*, *49*(1). https://doi.org/10.2514/1.J050494

Chimakurthi, S. K., Stanford, B. K., Cesnik, C. E. S., & Shyy, W. (2009). Flapping wing CFD/CSD aeroelastic formulation based on a corotational shell finite element. *Collection of Technical Papers - AIAA/ASME/ASCE/AHS/ASC Structures, Structural Dynamics and Materials Conference*. https://doi.org/10.2514/6.2009-2412

Chin, Y. W., Kok, J. M., Zhu, Y. Q., Chan, W. L., Chahl, J. S., Khoo, B. C., & Lau, G. K. (2020). Efficient flapping wing drone arrests high-speed flight using post-stall soaring. *Science Robotics*, *5*(44). https://doi.org/10.1126/scirobotics.aba2386

Chin, Y.-W., & Lau, G.-K. (2013). Is clicking mechanism good for flapping wing micro aerial vehicle? *Bioinspiration, Biomimetics, and Bioreplication 2013*, *8686*, 86860W. https://doi.org/10.1117/12.2009627

Chirarattananon, P., Ma, K. Y., Cheng, R., & Wood, R. J. (2015). Wind disturbance rejection for an insect-scale flapping-wing robot. *IEEE International Conference on Intelligent Robots and Systems*, *2015-Decem*, 60–67. https://doi.org/10.1109/IROS.2015.7353355

Chirarattananon, P., Ma, K. Y., & Wood, R. J. (2014). Adaptive control of a millimeter-scale flapping-wing robot. *Bioinspiration and Biomimetics*, *9*(2). https://doi.org/10.1088/1748-3182/9/2/025004

Chukewad, Y., & Fuller, S. (2021). Yaw Control of a Hovering Flapping-Wing Aerial Vehicle with a Passive Wing Hinge. *IEEE Robotics and Automation Letters*, *6*(2). https://doi.org/10.1109/LRA.2021.3060726

Chukewad, Y. M., Singh, A. T., James, J. M., & Fuller, S. B. (2018). A New Robot Fly Design That is Easier to Fabricate and Capable of Flight and Ground Locomotion. *IEEE International Conference on Intelligent Robots and Systems*, 4875–4882. https://doi.org/10.1109/IROS.2018.8593972

Chung, H. C., Kummari, K. L., Croucher, S. J., Lawson, N. J., Guo, S., & Huang, Z. (2008). Coupled piezoelectric fans with two degree of freedom motion for the application of flapping wing micro aerial vehicles. *Sensors and Actuators, A: Physical*, *147*(2), 607–612. https://doi.org/10.1016/j.sna.2008.06.017

Chung, H. C., Kummari, K. L., Croucher, S. J., Lawson, N. J., Guo, S., Whatmore, R. W., & Huang, Z. (2009). Development of piezoelectric fans for flapping wing application. *Sensors and Actuators, A: Physical*, *149*(1), 136–142. https://doi.org/10.1016/j.sna.2008.10.004

Chung, H.-C., Kummari, K. L., J.Croucher, S., J.Lawson, N., Guo, S., & Huang, Z. (2008). Sensors and Actuators A-Physical, 2008, Vol 147, Iss 2, pp607-612. *Sensors and Actuators A-Physical*.

Ciuti, G., Pateromichelakis, N., Sfakiotakis, M., Valdastri, P., Menciassi, A., Tsakiris, D. P., & Dario, P. (2012). A wireless module for vibratory motor control and inertial sensing in capsule endoscopy. *Sensors and Actuators, A: Physical*, *186*. https://doi.org/10.1016/j.sna.2011.12.024

Clawson, T. S., Ferrari, S., Helbling, E. F., Wood, R. J., Fu, B., Ruina, A., & Wang, Z. J. (2020). Full flight envelope and trim map of flapping-wing micro aerial vehicles. *Journal of Guidance, Control, and Dynamics*, *43*(12). https://doi.org/10.2514/1.G004754

Coleman, D. A., & Benedict, M. (2016). On the development of a robotic hummingbird. *54th AIAA Aerospace Sciences Meeting*, *0*. https://doi.org/10.2514/6.2016-0144

Coleman, D., Benedict, M., Hirishikeshaven, V., & Chopra, I. (2017). Development of a robotic hummingbird capable of controlled hover. *Journal of the American Helicopter Society*, *62*(3). https://doi.org/10.4050/JAHS.62.032003

Coleman, D., Benedict, M., Hrishikeshavan, V., & Chopra, I. (2015). Design, development and flight-testing of a robotic hummingbird. *Annual Forum Proceedings - AHS International*, *1*(January), 132–149.

Colmenares, D., Kania, R., Zhang, W., & Sitti, M. (2015). Compliant wing design for a flapping wing micro air vehicle. *IEEE International Conference on Intelligent Robots and Systems*, *2015-Decem*, 32–39. https://doi.org/10.1109/IROS.2015.7353111

Combes, S. A., & Daniel, T. L. (2003). Flexural stiffness in insect wings I. Scaling and the influence of wing venation. *Journal of Experimental Biology*, *206*(17), 2979–2987. https://doi.org/10.1242/jeb.00523

Conn, A., Burgess, S., Hyde, R., & Ling, C. S. (2006). From natural flyers to the mechanical realization of a flapping wing micro air vehicle. *2006 IEEE International Conference on Robotics and Biomimetics, ROBIO 2006*, 439–444. https://doi.org/10.1109/ROBIO.2006.340232

Conn, A. T., Burgess, S. C., & Ling, C. S. (2007). Design of a parallel crank-rocker flapping mechanism for insect-inspired micro air vehicles. *Proceedings of the Institution of Mechanical Engineers, Part C: Journal of Mechanical Engineering Science*, *221*(10), 1211–1222. https://doi.org/10.1243/09544062JMES517

Cox, A., Monopoli, D. J., Goldfarb, M., & Garcia, E. (1999). Development of piezoelectrically actuated elastodynamic flapping micro-aerial vehicles. *American Society of Mechanical Engineers, Aerospace Division (Publication) AD*, *59*, 257–262.

Dargent, T., Bao, X. Q., Grondel, S., Brun, G. le, Paquet, J. B., Soyer, C., & Cattan, E. (2009). Micromachining of an SU-8 flapping-wing flying micro-electro-mechanical system. *Journal of Micromechanics and Microengineering*, *19*(8). https://doi.org/10.1088/0960-1317/19/8/085028

de Croon, G. C. H. E., de Clercq, K. M. E., Ruijsink, R., Remes, B., & de Wagter, C. (2009). Design, Aerodynamics, and Vision-Based Control of the DelFly. *International Journal of Micro Air Vehicles*, *1*(2), 71–97. https://doi.org/10.1260/175682909789498288

De Croon, G. C. H. E., Groen, M. A., De Wagter, C., Remes, B., Ruijsink, R., & Van Oudheusden, B. W. (2012). Design, aerodynamics and autonomy of the DelFly. *Bioinspiration and Biomimetics*, *7*(2). https://doi.org/10.1088/1748-3182/7/2/025003

de Wagter, C., Karasek, M., & Croon, G. C. H. E. de. (2017). Quad-thopter: Tailless Flapping Wing Robot with 4 Pairs of Wings. *9th International Micro Air Vehicles Conference and Competition*.

de Wagter, C., Karásek, M., & de Croon, G. (2018). Quad-thopter: Tailless flapping wing robot with four pairs of wings. *International Journal of Micro Air Vehicles*, *10*(3), 244–253. https://doi.org/10.1177/1756829318794972

de Wagter, C., Tijmons, S., Remes, B. D. W., & de Croon, G. C. H. E. (2014a). Autonomous flight of a 20-gram Flapping Wing MAV with a 4-gram onboard stereo vision system. *Proceedings - IEEE International Conference on Robotics and Automation*. https://doi.org/10.1109/ICRA.2014.6907589

de Wagter, C., Tijmons, S., Remes, B. D. W., & de Croon, G. C. H. E. (2014b). Autonomous flight of a 20-gram Flapping Wing MAV with a 4-gram onboard stereo vision system. *Proceedings - IEEE International Conference on Robotics and Automation*, 4982–4987. https://doi.org/10.1109/ICRA.2014.6907589

Dementyev, A., Olwal, A., & Lyon, R. F. (2020). Haptics with input: Back-EMF in linear resonant actuators to enable touch, pressure and environmental awareness. *UIST 2020 - Proceedings of the 33rd Annual ACM Symposium on User Interface Software and Technology*. https://doi.org/10.1145/3379337.3415823

Deora, T., Singh, A. K., & Sane, S. P. (2015). Biomechanical basis of wing and haltere coordination in flies. *Proceedings of the National Academy of Sciences of the United States of America*, *112*(5), 1481–1486. https://doi.org/10.1073/pnas.1412279112

Dhingra, D., Chukewad, Y. M., & Fuller, S. B. (2020). A Device for Rapid, Automated Trimming of Insect-Sized Flying Robots. *IEEE Robotics and Automation Letters*, *5*(2), 1373–1380. https://doi.org/10.1109/LRA.2020.2967318

Dickinson, M. H., & Tu, M. S. (1997). The function of dipteran flight muscle. In *Comparative Biochemistry and Physiology - A Physiology* (Vol. 116, Issue 3, pp. 223–238). https://doi.org/10.1016/S0300-9629(96)00162-4

Djojodihardjo, H. (2016). Analysis and computational study of the aerodynamics, aeroelasticity and flight dynamics of flapping wing ornithopter using linear approximation. *54th AIAA Aerospace Sciences Meeting*, *0*. https://doi.org/10.2514/6.2016-2027

Djojodihardjo, H., & Rahim, K. A. A. (2015). Two-dimensional CFD simulation for visualization of flapping wing ornithopter studies. *ARPN Journal of Engineering and Applied Sciences*, *10*(21).

DONG, X., LI, D., XIANG, J., & WANG, Z. (2020). Design and experimental study of a new flapping wing rotor micro aerial vehicle. *Chinese Journal of Aeronautics*. https://doi.org/10.1016/j.cja.2020.04.024

Dragonfly, I. (2013). BionicOpter. *FESTO_Projects*.

Du, L., & Sun, X. (2015). Effect of flapping frequency on aerodynamics of wing in freely hovering flight. *Computers and Fluids*, *117*, 79–87. https://doi.org/10.1016/j.compfluid.2015.05.004

E.El-Telbany, M. (2013). Tuning PID Controller for DC Motor: An Artificial Bees Optimization Approach. *International Journal of Computer Applications*, *77*(15). https://doi.org/10.5120/13559-1341

F. Sukarman, M. G . M. H. M . M. M. A.. M. S. and A. F.. K. (2017). Parallelogram Linkage Leg Structure for Stabilized Walking Gaits in Humanoid Robot. *Journal of Advanced Research in Applied Sciences and Engineering Technology*, *9*(1), 22–31.

Fairuz, Z. M., Abdullah, M. Z., Zubair, M., Abdul Mujeebu, M., Abdullah, M. K., Yusoff, H., & Abdul Aziz, M. S. (2016). Effect of Wing Deformation on the Aerodynamic Performance of Flapping Wings: Fluid-Structure Interaction Approach. *Journal of Aerospace Engineering*, *29*(4). https://doi.org/10.1061/(asce)as.1943-5525.0000548

Fearday, C., Ward, T. A., Soin, N., Hashim, U., & Karim, N. M. (2017). Development of an inductor incorporated onto a carbon fiber MAV structural component. *Microsystem Technologies*, *23*(5), 1433–1442. https://doi.org/10.1007/s00542-016-2958-4

Fearing, R. S., Chiang, K. H., Dickinson, M. H., Pick, D. L., Sitti, M., & Yan, J. (2000). Wing transmission for a micromechanical flying insect. *Proceedings - IEEE International Conference on Robotics and Automation*, *2*, 1509–1516. https://doi.org/10.1163/1568563017 60132123

Fearing, R. S., & Wood, R. J. (2010). Challenges for 100 milligram flapping flight. In *Flying Insects and Robots* (pp. 219–229). https://doi.org/10.1007/978-3-540-89393-6_16

Fenelon, M. A. A., & Furukawa, T. (2010). Design of an active flapping wing mechanism and a micro aerial vehicle using a rotary actuator.

Mechanism and Machine Theory, *45*(2), 137–146. https://doi.org/10.1016/j.mechmachtheory.2009.01.007

FESTO. (2013). *BionicOpter: Inspiration, Dragonfly Flight*. Festo AG & Co. .

Fixed and Flapping Wing Aerodynamics for Micro Air Vehicle Applications. (2001). In *Fixed and Flapping Wing Aerodynamics for Micro Air Vehicle Applications*. https://doi.org/10.2514/4.866654

Four-bar linkage - Wikipedia. (n.d.). Retrieved December 4, 2021, from https://en.wikipedia.org/wiki/Four-bar_linkage

Fuller, S. B. (2019). Four Wings: An Insect-Sized Aerial Robot with Steering Ability and Payload Capacity for Autonomy. *IEEE Robotics and Automation Letters*, *4*(2). https://doi.org/10.1109/LRA.2019.2891086

Furst, S. J., Bunget, G., & Seelecke, S. (2013). Design and fabrication of a bat-inspired flapping-flight platform using shape memory alloy muscles and joints. *Smart Materials and Structures*, *22*(1). https://doi.org/10.1088/0964-1726/22/1/014011

Furst, S. J., Peele, B., & Seelecke, S. (2012). Design and fabrication of an SMA actuated bat. *ASME 2012 Conference on Smart Materials, Adaptive Structures and Intelligent Systems, SMASIS 2012*, *2*, 697–706. https://doi.org/10.1115/SMASIS2012-8198

Gaissert, N., Mugrauer, R., Mugrauer, G., Jebens, A., Jebens, K., & Knubben, E. M. (2014). Inventing a micro aerial vehicle inspired by the mechanics of dragonfly flight. *Lecture Notes in Computer Science (Including Subseries Lecture Notes in Artificial Intelligence and Lecture Notes in Bioinformatics)*, *8069 LNAI*, 90–100. https://doi.org/10.1007/978-3-662-43645-5_11

Galiński, C., & Zbikowski, R. (2005). Insect-like flapping wing mechanism based on a double spherical Scotch yoke. *Journal of the Royal Society Interface*, *2*(3), 223–235. https://doi.org/10.1098/rsif.2005.0031

Gan, Y., & Xu, C. (2020). Research on Single-Input Multiple-Output Converter for Rotorcraft Unmanned Aerial Vehicle. *IOP Conference Series: Materials Science and Engineering*, *719*(1). https://doi.org/10.1088/1757-899X/719/1/012025

Ganor, Y., Shilo, D., Zarrouati, N., & James, R. D. (2009). Ferromagnetic shape memory flapper. In *Sensors and Actuators, A: Physical* (Vol. 150, Issue 2, pp. 277–279). https://doi.org/10.1016/j.sna.2009.01.001

Garcia-Valle, G., Arranz-Paraiso, S., Serrano-Pedraza, I., & Ferre, M. (2021). Estimation of Torso Vibrotactile Thresholds Using Eccentric Rotating Mass Motors. *IEEE Transactions on Haptics*, *14*(3). https://doi.org/10.1109/TOH.2020.3048290

Gong, D. H., Lee, D. W., Shin, S. J., & Kim, S. Y. (2018). Design and experiment of string-based flapping mechanism and modulized trailing edge control system for insect-like FWMAV. *AIAA Information Systems-AIAA Infotech at Aerospace, 2018*, *209989*. https://doi.org/10.2514/6.2018-0987

Gong, D. H., Lee, D. W., Shin, S. J., & Kim, S. Y. (2019). String-based flapping mechanism and modularized trailing edge control system for insect-type FWMAV. *International Journal of Micro Air Vehicles*, *11*. https://doi.org/10.1177/1756829319842547

Graule, M. A., Chirarattananon, P., Fuller, S. B., Jafferis, N. T., Ma, K. Y., Spenko, M., Kornbluh, R., & Wood, R. J. (2016). Perching and takeoff of a robotic insect on overhangs using switchable electrostatic adhesion. *Science*, *352*(6288), 978–982. https://doi.org/10.1126/science.aaf1092

Guo, S., Li, D., & Wu, J. (2012). Theoretical and experimental study of a piezoelectric flapping wing rotor for micro aerial vehicle. *Aerospace Science and Technology*, *23*(1), 429–438. https://doi.org/10.1016/j.ast.2011.10.002

Guo, S., Li, H., Zhou, C., Zhang, Y. L., He, Y., & Wu, J. H. (2018). Analysis and experiment of a bio-inspired flyable micro flapping wing rotor. *Aerospace Science and Technology*, *79*, 506–517. https://doi.org/10.1016/j.ast.2018.06.009

Gursul, I. (2007). Introduction to the Design of Fixed-Wing Micro Air Vehicles: including Three Case Studies T.J. Muelleret al. American Institute of Aeronautics and Astronautics, 1801 Alexander Bell Drive, Suite 500, Reston, VA 20191-4344, USA. 2007. 287pp. Illustrated. $6. *The Aeronautical Journal*, *111*(1120), 405. https://doi.org/10.1017/s0001924000086954

Ha, N. S., Truong, Q. T., Goo, N. S., & Park, H. C. (2013). Relationship between wingbeat frequency and resonant frequency of the wing in insects. *Bioinspiration and Biomimetics*, *8*(4). https://doi.org/10.1088/1748-3182/8/4/046008

Han, J.-H., Lee, J.-S., & Kim, D.-K. (2009). Bio-inspired flapping UAV design: a university perspective. *Health Monitoring of Structural and Biological Systems 2009*, *7295*, 72951I. https://doi.org/10.1117/12.815337

Hao, Z. Y., Wang, T., Cao, X., Gan, Y., & Yu, Q. (2022). Modeling and control of rotating eccentric mass block vibration damping electric actuator. *Zhendong Gongcheng Xuebao/Journal of Vibration Engineering*, *35*(1). https://doi.org/10.16385/j.cnki.issn.1004-4523.2022.01.023

Harlecki, A., & Urbaś, A. (2015). Forward dynamics of selected spatial one-dof linkage mechanisms with the Dahl friction model in revolute joints. *Proceedings of the ECCOMAS Thematic Conference on Multibody*

Dynamics 2015, Multibody Dynamics 2015.

Hartenburg, R. S., Denavit, J., & Freudenstein, F. (1965). Kinematic Synthesis of Linkages. *Journal of Applied Mechanics*, *32*(2), 477–477. https://doi.org/10.1115/1.3625860

Hassanalian, M., & Abdelkefi, A. (2016). Effective design of flapping wing actuation mechanisms: Theory and experiments. *54th AIAA Aerospace Sciences Meeting*, *0*. https://doi.org/10.2514/6.2016-1745

Hassanalian, M., & Abdelkefi, A. (2017). Classifications, applications, and design challenges of drones: A review. In *Progress in Aerospace Sciences* (Vol. 91, pp. 99–131). https://doi.org/10.1016/j.paerosci.2017.04.003

Hassanalian, M., & Abdelkefi, A. (2019a). Towards improved hybrid actuation mechanisms for flapping wing micro air vehicles: Analytical and experimental investigations. *Drones*, *3*(3), 1–21. https://doi.org/10.3390/drones3030073

Hassanalian, M., & Abdelkefi, A. (2019b). Towards improved hybrid actuation mechanisms for flapping wing micro air vehicles: Analytical and experimental investigations. *Drones*, *3*(3), 1–21. https://doi.org/10.3390/drones3030073

Hassanalian, M. M. A. (2014). Increasing Flight Endurance of MAVs using Multiple Quantum Well Solar Cells. *International Journal of Aeronautical and Space Sciences*, *15*(2), 212–217. https://doi.org/10.5139/IJASS.2014.15.2.212

Hassanalian, M., Throneberry, G., & Abdelkefi, A. (2017). Wing shape and dynamic twist design of bio-inspired nano air vehicles for forward flight purposes. *Aerospace Science and Technology*, *68*, 518–529. https://doi.org/10.1016/J.AST.2017.06.010

Hawkes, E. W., & Lentink, D. (2016). Fruit fly scale robots can hover longer with flapping wings than with spinning wings. *Journal of the Royal Society Interface*, *13*(123). https://doi.org/10.1098/rsif.2016.0730

Higuchi, T., Yamagata, Y., Furutani, K., & Kudoh, K. (1990). Precise positioning mechanism utilizing rapid deformations of piezoelectric elements. *Proceedings. IEEE Micro Electro Mechanical Systems-An Investigation of Micro Structures, Sensors, Actuators, Machines*, 222–226. https://doi.org/10.1109/memsys.1990.110280

Hines, L., Arabagi, V., & Sitti, M. (2012). Shape memory polymer-based flexure stiffness control in a miniature flapping-wing robot. *IEEE Transactions on Robotics*, *28*(4), 987–990. https://doi.org/10.1109/TRO.2012.2197313

Hines, L., Campolo, D., & Sitti, M. (2014). Liftoff of a motor-driven, flapping-wing microaerial vehicle capable of resonance. *IEEE Transactions on Robotics*, *30*(1), 220–232. https://doi.org/10.1109/TRO.2013.2280057

Hines, L., Colmenares, D., & Sitti, M. (2015). Platform design and tethered flight of a motor-driven flapping-wing system. *Proceedings - IEEE International Conference on Robotics and Automation*, *2015-June*(June), 5838–5845. https://doi.org/10.1109/ICRA.2015.7140016

Ho, S., Nassef, H., Pornsinsirirak, N., Tai, Y. C., & Ho, C. M. (2003). Unsteady aerodynamics and flow control for flapping wing flyers. In *Progress in Aerospace Sciences* (Vol. 39, Issue 8, pp. 635–681). https://doi.org/10.1016/j.paerosci.2003.04.001

Hollar, S., Flynn, A., Bellew, C., & Pister, K. S. J. (2003). Solar powered 10 mg silicon robot. *Proceedings of the IEEE Micro Electro Mechanical Systems (MEMS)*, 706–711. https://doi.org/10.1109/memsys.2003.1189847

Hong, Y., & Altman, A. (2008). Lift from spanwise flow in simple flapping wings. *Journal of Aircraft*, *45*(4), 1206–1216. https://doi.org/10.2514/1.34100

Hsiao, F. Y., Yang, L. J., Lin, S. H., Chen, C. L., & Shen, J. F. (2012). Autopilots for ultra lightweight robotic birds: Automatic altitude control and system integration of a sub-10 g weight flapping-wing micro air vehicle. *IEEE Control Systems*, *32*(5), 35–48. https://doi.org/10.1109/MCS.2012.2205475

Hu, H., Kumar, A. G., Abate, G., & Albertani, R. (2010). An experimental investigation on the aerodynamic performances of flexible membrane wings in flapping flight. *Aerospace Science and Technology*, *14*(8), 575–586. https://doi.org/10.1016/j.ast.2010.05.003

Hussain, H. A. (2019). A novel contactless rotary-to-linear magnetic actuator. *2019 IEEE International Electric Machines and Drives Conference, IEMDC 2019*, 1081–1086. https://doi.org/10.1109/IEMDC.2019.8785222

Introduction (Chapter 1) - An Introduction to Flapping Wing Aerodynamics. (n.d.). Retrieved July 24, 2021, from https://www.cambridge.org/core/books/an-introduction-to-flapping-wing-aerodynamics/introduction/2B8A40CE9F9D3D0C81AE8A02B60109F9

Jafferis, N. T., Helbling, E. F., Karpelson, M., & Wood, R. J. (2019). Untethered flight of an insect-sized flapping-wing microscale aerial vehicle. *Nature*, *570*(7762), 491–495. https://doi.org/10.1038/s41586-019-1322-0

Jang, J. H., & Yang, G. H. (2018). Design of wing root rotation mechanism for dragonfly-inspired micro air vehicle. *Applied Sciences (Switzerland)*, *8*(10). https://doi.org/10.3390/app8101868

Jayender, J., Patel, R. v., Nikumb, S., & Ostojic, M. (2008). Modeling and control of shape memory alloy actuators. *IEEE Transactions on Control Systems Technology*, *16*(2), 279–287. https://doi.org/10.1109/TCST.2007.903391

Jeon, J. H., Cho, H., Kim, Y., Lee, J. H., Gong, D. H., Shin, S. J., & Kim, C. (2017). Design and analysis of the link mechanism for the flapping wing MAV using flexible multi-body dynamic analysis. *International Journal of Micro Air Vehicles*, *9*(4), 253–269. https://doi.org/10.1177/1756829316682148

Jiang, H., Zhou, C., & Xie, P. (2017). Design and kinematic analysis of seagull inspired flapping wing robot. *2016 IEEE International Conference on Information and Automation, IEEE ICIA 2016*. https://doi.org/10.1109/ICInfA.2016.7832035

Jiang, T., Yang, X., Wang, H., Gai, W., & Cui, L. (2019). Longitudinal Modeling and Control of Tailed Flapping-Wings Micro Air Vehicles near Hovering. *Journal of Robotics*, *2019*. https://doi.org/10.1155/2019/9341012

Jiaxin, Z., Weiping, Z., Chenyang, W., Yang, Z., & Jiahao, W. (2019). Current Status of insect-inspired Flapping Wing Micro Air Vehicles. *Proceedings of the 2019 IEEE International Conference on Unmanned Systems, ICUS 2019*, 894–898. https://doi.org/10.1109/ICUS48101.2019.8996060

Jimbo, T., Ozaki, T., Amano, Y., & Fujimoto, K. (2020). Flight control of flapping-wing robot with three paired direct-driven piezoelectric actuators. *IFAC-PapersOnLine*, *53*(2). https://doi.org/10.1016/j.ifacol.2020.12.2408

Jones, K. D., Bradshaw, C. J., Papadopoulos, J., & Platzer, M. F. (2004). Improved performance and control of flapping-wing propelled micro air vehicles. *AIAA Paper*. https://doi.org/10.2514/6.2004-399

Jones, K. D., Bradshaw, C. J., Papadopoulos, J., & Platzer, M. F. (2005). Bio-inspired design of flapping-wing micro air vehicles. *Aeronautical Journal*, *109*(1098), 385–393. https://doi.org/10.1017/S0001924000000804

Jones, K. D., Bradsliaw, C. J., Papadopoulos, J., & Platzer, M. F. (2003). Development and flight testing of flapping-wing propelled micro air vehicles. *2nd AIAA "Unmanned Unlimited" Conference and Workshop and Exhibit*. https://doi.org/10.2514/6.2003-6549

Jones, K. D., & Platzer, M. F. (2003). Experimental investigation of the aerodynamic characteristics of flapping-wing micro air vehicles. *41st Aerospace Sciences Meeting and Exhibit*. https://doi.org/10.2514/6.2003-418

Jones, K. D., & Platzer, M. F. (2006a). Bio-inspired design of flapping wing micro air vehicles - An engineer’s perspective. *Collection of Technical Papers - 44th AIAA Aerospace Sciences Meeting*, *1*, 463–476. https://doi.org/10.2514/6.2006-37

Jones, K. D., & Platzer, M. F. (2006b). Flapping-wing aerohydromechanics in nature and engineering. *WIT Transactions on Ecology and the Environment*, *87*, 3–11. https://doi.org/10.2495/DN060011

Jones, K. D., & Platzer, M. F. (2010). Flow control using flapping wings for an efficient low-speed micro-air vehicle. In *Flying Insects and Robots* (pp. 159–169). https://doi.org/10.1007/978-3-540-89393-6_12

Jumat, N. A., Abdullah, E. J., & Mazlan, N. (2019). Effect of polydimethylsiloxane (PDMS) coating on the behavior of Shape Memory Alloy (SMA) actuator. *International Journal of Recent Technology and Engineering*, *8*(1), 275–280.

Jung, H. K., Choi, J. S., Wang, C., & Park, G. J. (2015). Analysis and fabrication of unconventional flapping wing air vehicles. *International Journal of Micro Air Vehicles*, *7*(1). https://doi.org/10.1260/1756-8293.7.1.71

Jung, H., Oh, S., & Choi, H. (2024). Role of the deviation motion on the aerodynamic performance of a mosquito wing in hover. *Computers and Fluids*, *270*. https://doi.org/10.1016/j.compfluid.2023.106146

Kamaruzaman, N. F., & Abdullah, E. J. (2017). Design and testing of shape memory alloy actuation mechanism for flapping wing micro unmanned aerial vehicles. *IOP Conference Series: Materials Science and Engineering*, *270*(1). https://doi.org/10.1088/1757-899X/270/1/012017

Karásek, M., Hua, A., Nan, Y., Lalami, M., & Preumont, A. (2014). Pitch and roll control mechanism for a hovering flapping wing MAV. *International Journal of Micro Air Vehicles*, *6*(4), 253–264. https://doi.org/10.1260/1756-8293.6.4.253

Karasek, M., Muijres, F. T., Wagter, C. de, Remes, B. D. W., & de Croon, G. C. H. E. (2018). A tailless aerial robotic flapper reveals that flies use torque coupling in rapid banked turns. *Science*, *361*(6407), 1089–1094. https://doi.org/10.1126/science.aat0350

Karnavas, Y. L., & Chasiotis, I. D. (2016). PMDC coreless micro-motor parameters estimation through Grey Wolf Optimizer. *Proceedings - 2016 22nd International Conference on Electrical Machines, ICEM 2016*. https://doi.org/10.1109/ICELMACH.2016.7732627

Karpelson, M., Whitney, J. P., Wei, G. Y., & Wood, R. J. (2011). Design and fabrication of ultralight high-voltage power circuits for flapping-wing robotic insects. *Conference Proceedings - IEEE Applied Power Electronics Conference and Exposition - APEC*, 2070–2077.

https://doi.org/10.1109/APEC.2011.5744882

Kawamura, Y., Souda, S., Nishimoto, S., & Ellington, C. P. (2008). Clapping-wing micro air vehicle of insect size. *Bio-Mechanisms of Swimming and Flying: Fluid Dynamics, Biomimetic Robots, and Sports Science*. https://doi.org/10.1007/978-4-431-73380-5_26

Keennon, M., Klingebiel, K., Won, H., & Andriukov, A. (2012a). Development of the nano hummingbird: A tailless flapping Wing Micro Air Vehicle. *50th AIAA Aerospace Sciences Meeting Including the New Horizons Forum and Aerospace Exposition*. https://doi.org/10.2514/6.2012-588

Keennon, M., Klingebiel, K., Won, H., & Andriukov, A. (2012b). Tailless flapping wing propulsion and control development for the nano hummingbird micro air vehicle. *American Helicopter Society International - Future Vertical Lift Aircraft Design Conference 2012*, 15–51.

Keennon, M., Klingebiel, K., Won, H., & Andriukov, A. (2012c). Tailless flapping wing propulsion and control development for the nano hummingbird micro air vehicle. *American Helicopter Society International - Future Vertical Lift Aircraft Design Conference 2012*, 15–51.

Keennon, M. T., & Grasmeyer, J. M. (2003a). Development of the Black Widow and Microbat MAVs and a vision of the future of MAV design. *AIAA\ICAS International Air and Space Symposium and Exposition: The Next 100 Years*.

Keennon, M. T., & Grasmeyer, J. M. (2003b). Development of the Black Widow and Microbat MAVs and a vision of the future of MAV design. *AIAA\ICAS International Air and Space Symposium and Exposition: The Next 100 Years*.

Khan, Z. A., & Agrawal, S. K. (2007). Design and optimization of a biologically inspired flapping mechanism for flapping wing micro air vehicles. *Proceedings - IEEE International Conference on Robotics and Automation*, 373–378. https://doi.org/10.1109/ROBOT.2007.363815

Khan, Z. A., & Agrawal, S. K. (2011). Study of biologically inspired flapping mechanism for micro air vehicles. *AIAA Journal*, *49*(7), 1354–1365. https://doi.org/10.2514/1.J050447

Khan, Z., Steelman, K., & Agrawal, S. (2009). Development of insect thorax based flapping mechanism. *Proceedings - IEEE International Conference on Robotics and Automation*, 3651–3656. https://doi.org/10.1109/ROBOT.2009.5152822

Kim, C. J., Pisano, A. P., Muller, R. S., & Lim, M. G. (1997). POlysilicon microgripper. In *Micromechanics and MEMS: Classic and Seminal Papers to 1990* (pp. 203–206). https://doi.org/10.1109/

9780470545263.sect3

Kimber, M., Suzuki, K., Kitsunai, N., Seki, K., & Garimella, S. v. (2009). Pressure and flow rate performance of piezoelectric fans. *IEEE Transactions on Components and Packaging Technologies*, *32*(4), 766–775. https://doi.org/10.1109/TCAPT.2008.2012169

Kommepalli, H. K. R., Yu, H. G., Muhlstein, C. L., Trolier-McKinstry, S., Rahn, C. D., & Tadigadapa, S. A. (2009). Design, fabrication, and performance of a piezoelectric uniflex microactuator. *Journal of Microelectromechanical Systems*, *18*(3), 616–625. https://doi.org/10.1109/JMEMS.2009.2015480

Kompala, S., Esakki, B., Yang, L. J., Wang, W. C., Reshmi, W., & Chin, Y. J. (2019). Fabrication of Flapping Wing Mechanism Using Fused Deposition Modeling and Measurement of Aerodynamic Forces. *Journal of Aeronautics, Astronautics and Aviation* , *51*(1), 131–140. https://doi.org/10.6125/JoAAA.201903_51(1).09

Kong, G., & Su, Y. (2019). A dual-stage low-power converter driving for piezoelectric actuator applied in flapping-wing micro aerial vehicles. *International Journal of Advanced Robotic Systems*, *16*(3). https://doi.org/10.1177/1729881419851710

Krulevitch, P., Lee, A. P., Ramsey, P. B., Trevino, J. C., Hamilton, J., & Northrup, M. A. (1996). Thin film shape memory alloy microactuators. *Journal of Microelectromechanical Systems*, *5*(4), 270–282. https://doi.org/10.1109/84.546407

Kudariyawar, J. Y., Vaidya, A. M., Maheshwari, N. K., & Satyamurthy, P. (2016). Computational study of instabilities in a rectangular natural circulation loop using 3D CFD simulation. *International Journal of Thermal Sciences*, *101*. https://doi.org/10.1016/j.ijthermalsci.2015.11.003

Kudo, K., Suzuki, K., Takanobu, H., & Miura, H. (2012). Study on flapping-wing robot utilizing resonant drive. *Nihon Kikai Gakkai Ronbunshu, C Hen/Transactions of the Japan Society of Mechanical Engineers, Part C*, *78*(792), 2914–2923. https://doi.org/10.1299/kikaic.78.2914

Lai, J. C. S., & Platzer, M. F. (2001). Characteristics of a plunging airfoil at zero freestream velocity. *AIAA Journal*, *39*(3). https://doi.org/10.2514/2.1340

Lane, P., Throneberry, G., Fernandez, I., Hassanalian, M., Vasconcellos, R., & Abdelkefi, A. (2020). Towards bio-inspiration, development, and manufacturing of a flapping-wing micro air vehicle. *Drones*, *4*(3). https://doi.org/10.3390/drones4030039

Lau, G. K., Chin, Y. W., Goh, J. T. W., & Wood, R. J. (2014). Dipteran-insect-inspired thoracic mechanism with nonlinear stiffness to save inertial power of flapping-wing flight. *IEEE Transactions on Robotics*, *30*(5), 1187–1197. https://doi.org/10.1109/TRO.2014.2333112

Lau, G. K., Lim, H. T., Teo, J. Y., & Chin, Y. W. (2014). Lightweight mechanical amplifiers for rolled dielectric elastomer actuators and their integration with bio-inspired wing flappers. *Smart Materials and Structures*, *23*(2). https://doi.org/10.1088/0964-1726/23/2/025021

Lau, G.-K., Chin, Y.-W., & La, T.-G. (2017). Development of elastomeric flight muscles for flapping wing micro air vehicles. *Electroactive Polymer Actuators and Devices (EAPAD) 2017*, *10163*, 1016320. https://doi.org/10.1117/12.2260422

Lee, S. G., Park, H. C., Pandita, S. D., & Yoo, Y. (2006). Performance improvement of IPMC (Ionic Polymer Metal Composites) for a flapping actuator. *International Journal of Control, Automation and Systems*, *4*(6), 748–755.

Lentink, D., Jongerius, S. R., & Bradshaw, N. L. (2010). The scalable design of flapping micro-air vehicles inspired by insect flight. In *Flying Insects and Robots*. https://doi.org/10.1007/978-3-540-89393-6_14

Lindholm, G. J., & Cobb, R. G. (2014). Passive rotation joint design considerations for lift and thrust generation for a biomimetic flapping wing. *International Journal of Micro Air Vehicles*, *6*(3), 141–154. https://doi.org/10.1260/1756-8293.6.3.141

Liu, L. G., Du, G., & Sun, M. (2020). Aerodynamic-force production mechanisms in hovering mosquitoes. *Journal of Fluid Mechanics*, *898*. https://doi.org/10.1017/jfm.2020.386

Liu, Q., Li, Q., Zhou, X., Xu, P., Ren, L., & Pan, S. (2019). Development of a novel flapping wing micro aerial vehicle with elliptical wingtip trajectory. *Mechanical Sciences*, *10*(2), 355–362. https://doi.org/10.5194/ms-10-355-2019

Liu, X., Qin, N., & Xia, H. (2006). Fast dynamic grid deformation based on Delaunay graph mapping. *Journal of Computational Physics*, *211*(2). https://doi.org/10.1016/j.jcp.2005.05.025

Liu, Z., & Moschetta, J.-M. (2009). Rotary vs. Flapping-Wing Nano Air Vehicles: Comparing Hovering Power. *European Micro Air Vehicle Conference and Flight Competition 2009 (EMAV2009)*, 21–27.

Liu, Z., Yan, X., Qi, M., Huang, D., Zhang, X., & Lin, L. (2018). Electrostatic flapping-wing actuator with improved lift force by the pivot-spar bracket design. *Sensors and Actuators, A: Physical*, *280*, 295–302. https://doi.org/10.1016/j.sna.2018.07.054

Liu, Z., Yan, X., Qi, M., & Lin, L. (2016). Electrostatic flapping wings with pivot-spar brackets for high lift force. *Proceedings of the IEEE International*

Conference on Micro Electro Mechanical Systems (MEMS), *2016-Febru*, 1133–1136. https://doi.org/10.1109/MEMSYS.2016.7421835

Liu, Z., Yan, X., Qi, M., Zhang, X., & Lin, L. (2017). Low-voltage electromagnetic actuators for flapping-wing micro aerial vehicles. *Sensors and Actuators, A: Physical*, *265*, 1–9. https://doi.org/10.1016/j.sna.2017.08.027

Liu, Z., Yan, X., Qi, M., Zhu, Y., Huang, D., Zhang, X., & Lin, L. (2019). Design of flexible hinges in electromagnetically driven artificial flapping-wing insects for improved lift force. *Journal of Micromechanics and Microengineering*, *29*(1). https://doi.org/10.1088/1361-6439/aaf02d

Long, C., Wanfang, Y., & Jianghao, W. (2015). Experimental Validation on Lift Increment of a Flapping Rotary Wing with Boring-hole Design. *Procedia Engineering*, *99*, 1543–1547. https://doi.org/10.1016/j.proeng.2014.12.706

Lv, X., Wei, W., Mao, X., Chen, Y., Yang, J., & Yang, F. (2015). A novel MEMS electromagnetic actuator with large displacement. *Sensors and Actuators, A: Physical*, *221*, 22–28. https://doi.org/10.1016/j.sna.2014.10.028

Ma, C. C., Wang, R., Sun, Q. P., Zohar, Y., & Wong, M. (2000). Frequency response of TiNi shape memory alloy thin film micro-actuators. *Proceedings of the IEEE Micro Electro Mechanical Systems (MEMS)*, 370–374. https://doi.org/10.1109/memsys.2000.838545

Ma, K. Y., Chirarattananon, P., Fuller, S. B., & Wood, R. J. (2013). Controlled flight of a biologically inspired, insect-scale robot. *Science*, *340*(6132), 603–607. https://doi.org/10.1126/science.1231806

Ma, K. Y., Chirarattananon, P., & Wood, R. J. (2015). Design and fabrication of an insect-scale flying robot for control autonomy. *IEEE International Conference on Intelligent Robots and Systems*, *2015-Decem*, 1558–1564. https://doi.org/10.1109/IROS.2015.7353575

Ma, K. Y., Felton, S. M., & Wood, R. J. (2012). Design, fabrication, and modeling of the split actuator microrobotic bee. *IEEE International Conference on Intelligent Robots and Systems*. https://doi.org/10.1109/IROS.2012.6386192

Macho, E., Urízar, M., Petuya, V., & Hernández, A. (2021). Improving skills in mechanism and machine science using gim software. *Applied Sciences (Switzerland)*, *11*(17). https://doi.org/10.3390/app11177850

Madangopal, R., Khan, Z. A., & Agrawal, S. K. (2006). Energetics-based design of small flapping-wing micro air vehicles. *IEEE/ASME Transactions on Mechatronics*, *11*(4), 433–438. https://doi.org/10.1109/TMECH.2006.878525

Madill, D. R., & Wang, D. (1998). Modeling and L2-stability of a shape memory alloy position control system. *IEEE Transactions on Control Systems Technology*, *6*(4), 473–481. https://doi.org/10.1109/87.701339

Mahendra, A., Setiawan, I., & Denis, D. (2021). IMPLEMENTASI SENSOR INFRARED DAN PENGEREMAN DYNAMIC DENGAN INJECT DC PADA MOTOR INDUKSI 3 FASA BERBASIS ESP32 UNTUK APLIKASI SISTEM KONVEYOR TERKENDALI. *Transient: Jurnal Ilmiah Teknik Elektro*, *10*(1). https://doi.org/10.14710/transient.v10i1.176-183

Marimuthu, N., Abdullah, E. J., Majid, D. L. A., & Romli, F. I. (2014). Conceptual design of flapping wing using shape memory alloy actuator for micro unmanned aerial vehicle. *Applied Mechanics and Materials*, *629*, 152–157. https://doi.org/10.4028/www.scientific.net/AMM.629.152

Markose, S., Raja, S., & Peter, S. (2014). *Radio Control Based DC-DC Converter for Micro Air Vehicle Applications*. 444–451.

McCarthy, J. M., & Soh, G. S. (2011). Geometric Design of Linkages. *Interdisciplinary Applied Mathematics*, *11*, 1–448. https://doi.org/10.1115/ 1.1334345

McIvor, B., & Chahl, J. (2020). Energy efficiency of linear electromagnetic actuators for flapping wing micro aerial vehicles. *Energies*, *13*(5). https://doi.org/10.3390/en13051075

Michelson, R. C. (2010). Overview of Micro Air Vehicle System Design and Integration Issues. In *Encyclopedia of Aerospace Engineering*. https://doi.org/10.1002/9780470686652.eae401

Miller, L. A. (2017). Biomechanics: The aerodynamics buzz from mosquitoes. In *Nature* (Vol. 544, Issue 7648). https://doi.org/10.1038/nature21904

Moses, K. C., Michaels, S. C., Willis, M., & Quinn, R. D. (2017). Artificial Manduca sexta forewings for flapping-wing micro aerial vehicles: How wing structure affects performance. *Bioinspiration and Biomimetics*, *12*(5). https://doi.org/10.1088/1748-3190/aa7ea3

Moses, K. C., Prigg, D., Weisfeld, M., Bachmann, R. J., Willis, M., & Quinn, R. D. (2018). Simulating flapping wing mechanisms inspired by the Manduca sexta hawkmoth. *Lecture Notes in Computer Science (Including Subseries Lecture Notes in Artificial Intelligence and Lecture Notes in Bioinformatics)*, *10928 LNAI*, 326–337. https://doi.org/10.1007/978-3-319-95972-6_35

Moses, K., Willis, M., & Quinn, R. (2020). Biomimicry of the hawk moth, Manduca sexta (L.), produces an improved flapping-wing mechanism. *Biomimetics*, *5*(2). https://doi.org/10.3390/BIOMIMETICS5020025

Moubarak, P. M., & Ben-Tzvi, P. (2013). On the Dual-Rod Slider Rocker Mechanism and Its Applications to Tristate Rigid Active Docking. *Journal of Mechanisms and Robotics*, *5*(1). https://doi.org/10.1115/1.4023178

Mueller, D., Bruck, H. A., & Gupta, S. K. (2010). Measurement of thrust and lift forces associated with drag of compliant flapping wing for micro air vehicles using a new test stand design. *Experimental Mechanics*, *50*(6). https://doi.org/10.1007/s11340-009-9270-5

Muhammad Daffa Naufal, M. F. M. Y. and N. A. C. S. (2022). Modelling of Nanomaterial Growth with Flame Enhancement. *J. Adv. Res. Appl. Mech.*, *90*(1), 1–6.

Mukherjee, S., & Ganguli, R. (2010). A dragonfly inspired flapping wing actuated by electro active polymers. *Smart Structures and Systems*, *6*(7), 867–887. https://doi.org/10.12989/sss.2010.6.7.867

Muthuselvi, M., Bharathi, R., Gladina Sherby, M., Jeya Monica, J., & Reshma, S. (2022). Vibrating Motor based Wearable Vibrating Analog Alarm. *Proceedings - International Conference on Augmented Intelligence and Sustainable Systems, ICAISS 2022*. https://doi.org/10.1109/ICAISS55157.2022.10010851

Nagai, H., & Isogai, K. (2011). Effects of flapping wing kinematics on hovering and forward flight aerodynamics. *AIAA Journal*, *49*(8), 1750–1762. https://doi.org/10.2514/1.J050968

Natesan, A. K. (n.d.). *Kinematic analysis and synthesis of four-bar mechanisms for Kinematic analysis and synthesis of four-bar mechanisms for straight line coupler curves straight line coupler curves*. Retrieved December 4, 2021, from https://scholarworks.rit.edu/theses

Nguyen, C. T., & Choi, H. R. (2015). Properties and applications of dielectric elastomer actuator. In *Smart Materials Actuators: Recent Advances in Characterization and Applications* (pp. 235–248).

Nguyen, Q., Chan, W. L., & Debiasi, M. (2014). Design, Fabrication, and Performance Test of a Hovering-Based Flapping-Wing Micro Air Vehicle Capable of Sustained and Controlled Flight. *International Micro Air Vehicle Conference and Flight Competition*, *August*, 18–25.

Nguyen, Q. V., & Chan, W. L. (2019). Development and flight performance of a biologically-inspired tailless flapping-wing micro air vehicle with wing stroke plane modulation. *Bioinspiration and Biomimetics*, *14*(1). https://doi.org/10.1088/1748-3190/aaefa0

Nguyen, Q. V., Chan, W. L., & Debiasi, M. (2016). Hybrid Design and Performance Tests of a Hovering Insect-inspired Flapping-wing Micro Aerial Vehicle. *Journal of Bionic Engineering*, *13*(2), 235–248. https://doi.org/10.1016/S1672-6529(16)60297-4

Nguyen, Q. V., Park, H. C., Goo, N. S., & Byun, D. (2010). Characteristics of a Beetle's Free Flight and a Flapping-Wing System that Mimics Beetle Flight. *Journal of Bionic Engineering*, *7*(1), 77–86. https://doi.org/10.1016/S1672-6529(09)60195-5

Nguyen, Q. V., Truong, Q. T., Park, H. C., Goo, N. S., & Byun, D. (2009). A motor-driven flapping-wing system mimicking beetle flight. *2009 IEEE International Conference on Robotics and Biomimetics, ROBIO 2009*, 1087–1092. https://doi.org/10.1109/ROBIO.2009.5420860

Nguyen, Q. V., Truong, Q. T., Park, H. C., Goo, N. S., & Byun, D. (2010). Measurement of force produced by an insect-mimicking flapping-wing system. *Journal of Bionic Engineering*. https://doi.org/10.1016/S1672-6529(09)60222-5

Nguyen, Q.-V., Chan, W. L., & Debiasi, M. (2015). An insect-inspired flapping wing micro air vehicle with double wing clap-fling effects and capability of sustained hovering. *Bioinspiration, Biomimetics, and Bioreplication 2015*, *9429*, 94290U. https://doi.org/10.1117/12.2085714

Oldiges, A., & Bajaj, N. (2022). Control, Sensor Calibration, and Parasitic Torque Cancellation of a Dual-Rotor Haptic Actuator. *IEEE/ASME International Conference on Advanced Intelligent Mechatronics, AIM*, *2022-July*. https://doi.org/10.1109/AIM52237.2022.9863281

Onal, C. D., Wood, R. J., & Rus, D. (2013). An origami-inspired approach to worm robots. *IEEE/ASME Transactions on Mechatronics*, *18*(2). https://doi.org/10.1109/TMECH.2012.2210239

Oppenheimer, M. W., Sigthorsson, D. O., Weintraub, I. E., & Doman, D. B. (2017). Wing design and testing for a tailless flapping wing micro air vehicle. *AIAA Guidance, Navigation, and Control Conference, 2017*. https://doi.org/10.2514/6.2017-1271

Ozaki, T., & Hamaguchi, K. (2018a). Bioinspired Flapping-Wing Robot with Direct-Driven Piezoelectric Actuation and Its Takeoff Demonstration. *IEEE Robotics and Automation Letters*, *3*(4), 4217–4224. https://doi.org/10.1109/LRA.2018.2863104

Ozaki, T., & Hamaguchi, K. (2018b). Performance of direct-driven flapping-wing actuator with piezoelectric single-crystal PIN-PMN-PT. *Journal of Micromechanics and Microengineering*, *28*(2). https://doi.org/10.1088/1361-6439/aaa2c8

Ozaki, T., & Hamaguchi, K. (2020). Improved lift force of a resonant-driven flapping-wing micro aerial vehicle by suppressing wing–body and wing–wing vibration coupling. *Extreme Mechanics Letters*, *40*. https://doi.org/10.1016/j.eml.2020.100867

P. L. Roe. (1981). Approximate Riemann Solvers, Parameter Vectors, and Difference Schemes. *Journal of Computational Physics*, *43*.

Park, J. H., Yang, E. P., Zhang, C., & Agrawal, S. K. (2012). Kinematic design of an asymmetric in-phase flapping mechanism for MAVs. *Proceedings - IEEE International Conference on Robotics and Automation*. https://doi.org/10.1109/ICRA.2012.6225028

Pei, Q., Pelrine, R., Rosenthal, M. A., Stanford, S., Prahlad, H., & Kornbluh, R. D. (2004). Recent progress on electroelastomer artificial muscles and their application for biomimetic robots. *Smart Structures and Materials 2004: Electroactive Polymer Actuators and Devices (EAPAD)*, *5385*, 41. https://doi.org/10.1117/12.540462

Pelrine, R., & Kornbluh, R. (2016). Dielectric Elastomers as Electroactive Polymers (EAPs): Fundamentals. In *Electromechanically Active Polymers* (pp. 1–17). https://doi.org/10.1007/978-3-319-31767-0_30-1

Pelrine, R., Kornbluh, R., Qibing, P., Stanford, S., Seajin, O., Eckerle, J., Full, R. J., Rosenthal, M., & Meijer, K. (2017). Dielectric Elastomer Artificial Muscle Actuators: Toward Biomimetic Motion. *Smart Structures and Materials*, *4695*, 126–137.

Peng, K., Lin, F., & Chen, B. M. (2017). Modeling and control analysis of a flapping-wing micro aerial vehicle. *IEEE International Conference on Control and Automation, ICCA*. https://doi.org/10.1109/ICCA.2017.8003076

Peng, Y., Cao, J., Liu, L., & Yu, H. (2017). A piezo-driven flapping wing mechanism for micro air vehicles. *Microsystem Technologies*, *23*(4), 967–973. https://doi.org/10.1007/s00542-015-2762-6

Peng, Y. X., Gao, W., Kaneko, J., Arai, Y., Shimizu, Y., Okamoto, K., Chiba, M., & Aisawa, S. (2011). A linear micro-stage with a long stroke for precision positioning of micro-objects. *Nami Jishu Yu Jingmi Gongcheng/Nanotechnology and Precision Engineering*, *9*(3), 221–227.

Pérez-Arancibia, N. O., Ma, K. Y., Galloway, K. C., Greenberg, J. D., & Wood, R. J. (2011). First controlled vertical flight of a biologically inspired microrobot. *Bioinspiration and Biomimetics*, *6*(3). https://doi.org/10.1088/1748-3182/6/3/036009

Perseghetti, B. M., Roll, J. A., & Gallagher, J. C. (2014). Design constraints of a minimally actuated four bar linkage flapping-wing micro air vehicle. *Advances in Intelligent Systems and Computing*, *274*, 545–555. https://doi.org/10.1007/978-3-319-05582-4_47

Peters, H. J., Goosen, J. F. L., & Keulen, F. van. (2016). Methods to actively modify the dynamic response of cm-scale FWMAV designs. *Smart Materials and Structures*, *25*(5). https://doi.org/10.1088/0964-1726/25/5/055027

Petricca, L., Ohlckers, P., & Grinde, C. (2011). Micro- and nano-air vehicles: State of the art. *International Journal of Aerospace Engineering*, *2011*. https://doi.org/10.1155/2011/214549

Phan, H. V., Au, T. K. L., & Park, H. C. (2016). Clap-and-fling mechanism in a hovering insect-like two-winged flapping-wing micro air vehicle. *Royal Society Open Science*, *3*(12). https://doi.org/10.1098/rsos.160746

Phan, H. V., Aurecianus, S., Au, T. K. L., Kang, T., & Park, H. C. (2020). Towards the Long-Endurance Flight of an Insect-Inspired, Tailless, Two-Winged, Flapping-Wing Flying Robot. *IEEE Robotics and Automation Letters*, *5*(4), 5059–5066. https://doi.org/10.1109/LRA.2020.3005127

Phan, H. V., Aurecianus, S., Kang, T., & Park, H. C. (2019a). KUBeetle-S: An insect-like, tailless, hover-capable robot that can fly with a low-torque control mechanism. *International Journal of Micro Air Vehicles*, *11*. https://doi.org/10.1177/1756829319861371

Phan, H. V., Aurecianus, S., Kang, T., & Park, H. C. (2019b). KUBeetle-S: An insect-like, tailless, hover-capable robot that can fly with a low-torque control mechanism. *International Journal of Micro Air Vehicles*, *11*. https://doi.org/10.1177/1756829319861371

Phan, H. V., Kang, T., & Park, H. C. (2017). Design and stable flight of a 21 g insect-like tailless flapping wing micro air vehicle with angular rates feedback control. *Bioinspiration and Biomimetics*, *12*(3). https://doi.org/10.1088/1748-3190/aa65db

Phan, H. V., & Park, H. C. (2016). Pitch, roll, and yaw moment generator for insect-like tailless flapping-wing MAV. *Bioinspiration, Biomimetics, and Bioreplication 2016*, *9797*, 97970H. https://doi.org/10.1117/12.2219190

Phan, H. V., & Park, H. C. (2019). Insect-inspired, tailless, hover-capable flapping-wing robots: Recent progress, challenges, and future directions. In *Progress in Aerospace Sciences* (Vol. 111). https://doi.org/10.1016/j.paerosci.2019.100573

Phan, H. V., Truong, Q. T., Au, T. K. L., & Park, H. C. (2015). Effect of Wing Kinematics Modulation on Aerodynamic Force Generation in Hovering Insect-mimicking Flapping-wing Micro Air Vehicle. *Journal of Bionic Engineering*, *12*(4), 539–554. https://doi.org/10.1016/S1672-6529(14)60144-X

Phan, H. V., Truong, Q. T., Au, T. K. L., & Park, H. C. (2016). Optimal flapping wing for maximum vertical aerodynamic force in hover: Twisted or flat? *Bioinspiration and Biomimetics*, *11*(4). https://doi.org/10.1088/1748-3190/11/4/046007

Phan, H. V., Truong, Q. T., & Park, H. C. (2017). An experimental comparative study of the efficiency of twisted and flat flapping wings during hovering flight. *Bioinspiration and Biomimetics*, *12*(3). https://doi.org/10.1088/1748-3190/aa65e6

Pomplun, E., Thomas, A., Corrigan, E., Shah, V. A., Mrotek, L. A., & Scheidt, R. A. (2022). Vibrotactile Perception for Sensorimotor Augmentation: Perceptual Discrimination of Vibrotactile Stimuli Induced by Low-Cost Eccentric Rotating Mass Motors at Different Body Locations in Young, Middle-Aged, and Older Adults. *Frontiers in Rehabilitation Sciences*, *3*. https://doi.org/10.3389/fresc.2022.895036

Pornsin-Sirirak, T. N., Tai, Y. C., Nassef, H., & Ho, C. M. (2001). Titanium-alloy MEMS wing technology for a micro aerial vehicle application. *Sensors and Actuators, A: Physical*, *89*(1–2), 95–103. https://doi.org/10.1016/S0924-4247(00)00527-6

Pornsin-Sirirak, T. N., Tai, Y.-C., Ho, C.-M., & Keennon, M. (2001). Microbat: A palm-sized electrically powered ornithopter. *Proceedings of NASA/JPL Workshop on Biomorphic Robotics*, 14–17. http://ho.seas.ucla.edu/wp-content/uploads/2011/04/jpl10_2001.pdf

Pourtakdoust, S. H., & Aliabadi, S. K. (2012). Evaluation of flapping wing propulsion based on a new experimentally validated aeroelastic model. *Scientia Iranica*, *19*(3), 472–482. https://doi.org/10.1016/j.scient.2012.03.004

Prasanna, S., & Spearing, S. M. (2007). Materials selection and design of microelectrothermal bimaterial actuators. *Journal of Microelectromechanical Systems*, *16*(2), 248–259. https://doi.org/10.1109/JMEMS.2006.889528

Rashid, Y. G., & Hussain, A. M. A. (2021). Implementing optimization of PID controller for DC motor speed control. *Indonesian Journal of Electrical Engineering and Computer Science*, *23*(2). https://doi.org/10.11591/ijeecs.v23.i2.pp657-664

Ristroph, L., & Childress, S. (2014). Stable hovering of a jellyfish-like flying machine. *Journal of the Royal Society Interface*, *11*(92). https://doi.org/10.1098/rsif.2013.0992

Robbins, W. P., Polla, D. L., Tamagawa, T., Glumac, D. E., & Tjhen, W. (1991). Design of linear-motion microactuators using piezoelectric thin films. *Journal of Micromechanics and Microengineering*, *1*(4), 247–252. https://doi.org/10.1088/0960-1317/1/4/006

Roe, P. L. (1997). Approximate Riemann solvers, parameter vectors, and difference schemes. *Journal of Computational Physics*, *135*(2). https://doi.org/10.1006/jcph.1997.5705

Roget, B., Sitaraman, J., Harmon, R., Grauer, J., Conroy, J., Hubbard, J., & Humbert, S. (2008). A computational study of flexible wing ornithopter flight. *Collection of Technical Papers - AIAA Applied Aerodynamics Conference*. https://doi.org/10.2514/6.2008-6397

Roget, B., Sitaraman, J., Harmon, R., Grauer, J., Hubbard, J., & Humbert, S. (2009). Computational study of flexible wing ornithopter flight. *Journal of Aircraft*, *46*(6). https://doi.org/10.2514/1.43187

Roll, J. A., Cheng, B., & Deng, X. (2013). Design, fabrication, and experiments of an electromagnetic actuator for flapping wing micro air vehicles. *Proceedings - IEEE International Conference on Robotics and Automation*, 809–815. https://doi.org/10.1109/ICRA.2013.6630666

Rosen, M. H., le Pivain, G., Sahai, R., Jafferis, N. T., & Wood, R. J. (2016). Development of a 3.2g untethered flapping-wing platform for flight energetics and control experiments. *Proceedings - IEEE International Conference on Robotics and Automation*, *2016-June*, 3227–3233. https://doi.org/10.1109/ICRA.2016.7487492

Roshanbin, A., Altartouri, H., Karásek, M., & Preumont, A. (2017). COLIBRI: A hovering flapping twin-wing robot. *International Journal of Micro Air Vehicles*, *9*(4), 270–282. https://doi.org/10.1177/1756829317695563

Rosly, M. A., Yussof, H., Shaari, M. F., Samad, Z., Kamaruzaman, D., & Omar, A. R. (2018). Speed control mechanism for IPMC based biomimetic flapping thruster. *Proceedings - 2017 IEEE 5th International Symposium on Robotics and Intelligent Sensors, IRIS 2017*, *2018-Janua*, 218–223. https://doi.org/10.1109/IRIS.2017.8250125

Ryan, M., & Su, H. J. (2012). Classification of flapping wing mechanisms for micro air vehicles. *Proceedings of the ASME Design Engineering Technical Conference*, *4*(PARTS A AND B), 105–115. https://doi.org/10.1115/DETC2012-70953

Ryan, M., Venkiteswaran, V. K., & Su, H. J. (2013). Peak input torque minimization of a flapping wing mechanism for MAVs. *Collection of Technical Papers - AIAA/ASME/ASCE/AHS/ASC Structures, Structural Dynamics and Materials Conference*.

Sachs, G. (2016). Comparison of power requirements: Flapping vs. fixed wing vehicles. *Aerospace*, *3*(4). https://doi.org/10.3390/aerospace3040031

Sadia, B., Emgin, S. E., Sezgin, T. M., & Basdogan, C. (2020). Data-driven vibrotactile rendering of digital buttons on touchscreens. *International Journal of Human Computer Studies*, *135*. https://doi.org/10.1016/j.ijhcs.2019.09.005

Sahai, R., Avadhanula, S., Groff, R., Steltz, E., Wood, R., & Fearing, R. S. (2006). Towards a 3g crawling robot through the integration of microrobot technologies. *Proceedings - IEEE International Conference* *on Robotics and Automation*, *2006*, 296–302. https://doi.org/10.1109/ROBOT.2006.1641727

Sahai, R., Galloway, K. C., Karpelson, M., & Wood, R. J. (2012). A flapping-wing micro air vehicle with interchangeable parts for system integration studies. *IEEE International Conference on Intelligent Robots and Systems*, 501–506. https://doi.org/10.1109/IROS.2012.6386058

Sahai, R., Galloway, K. C., & Wood, R. J. (2013). Elastic element integration for improved flapping-wing micro air vehicle performance. *IEEE Transactions on Robotics*, *29*(1), 32–41. https://doi.org/10.1109/TRO.2012.2218936

Shen, Y., Lin, F., Wang, C., Liu, T., Ba, Z., Lu, L., Xu, W., & Ren, K. (2023). MotoPrint: Reconfigurable Vibration Motor Fingerprint Via Homologous Signals Learning. *IEEE Transactions on Dependable and Secure Computing*. https://doi.org/10.1109/TDSC.2023.3253507

Shreyas, J. v., Devranjan, S., & Sreenivas, K. R. (2011). Aerodynamics of bird and insect flight. In *Journal of the Indian Institute of Science* (Vol. 91, Issue 3).

Shyy, W., Aono, H., Kang, C., & Liu, H. (2013). Introduction. *An Introduction to Flapping Wing Aerodynamics*, 1–41. https://doi.org/10.1017/CBO9781139583916.004

Shyy, W., Kang, C. K., Chirarattananon, P., Ravi, S., & Liu, H. (2016). Aerodynamics, sensing and control of insect-scale flapping-wing flight. In *Proceedings of the Royal Society A: Mathematical, Physical and Engineering Sciences* (Vol. 472, Issue 2186). https://doi.org/10.1098/rspa.2015.0712

Singh, B., Yidris, N., Basri, A. A., Pai, R., & Ahmad, K. A. (2021). Study of mosquito aerodynamics for imitation as a small robot and flight in a low-density environment. *Micromachines*, *12*(5). https://doi.org/10.3390/mi12050511

Singh, S., Muralidharan, A. K., Radhakrishnan, J., Zuber, M., Basri, A. A., Mazlan, N., Hamidon, M. N., & Ahmad, K. A. (2022). Parametric Study and Experimental Investigations of a Single Crank–Slotted Dual Lever Mechanism for MAV Flapping Actuation. *Biomimetics*, *7*(4), 208. https://doi.org/10.3390/biomimetics7040208

Singh, S., Zuber, M., Hamidon, M. N., Mazlan, N., Basri, A. A., & Ahmad, K. A. (2022a). Classification of actuation mechanism designs with structural block diagrams for flapping-wing drones: A comprehensive review. *Progress in Aerospace Sciences*, *132*, 100833. https://doi.org/10.1016/J.PAEROSCI.2022.100833

Singh, S., Zuber, M., Hamidon, M. N., Mazlan, N., Basri, A. A., & Ahmad, K. A. (2022b). Classification of actuation mechanism designs with structural block diagrams for flapping-wing drones: A comprehensive review. *Progress in Aerospace Sciences*, *132*, 100833. https://doi.org/10.1016/J.PAEROSCI.2022.100833

Sitti, M. (2003). Piezoelectrically actuated four-bar mechanism with two flexible links for micromechanical flying insect thorax. *IEEE/ASME Transactions on Mechatronics*, *8*(1), 26–36. https://doi.org/10.1109/TMECH.2003.809126

Sitti, M., Campolo, D., Yan, J., Fearing, R. S., Su, T., Taylor, D., & Sands, T. D. (2001). Development of PZT and PZN-PT based unimorph actuators for micromechanical flapping mechanisms. *Proceedings - IEEE International Conference on Robotics and Automation*, *4*, 3839–3846. https://doi.org/10.1109/ROBOT.2001.933216

Sochacki, W., & Cekus, D. (2020). The new concept of power transmission to the entomopter wings. *Journal of Micro-Bio Robotics*, *16*(2), 225–235. https://doi.org/10.1007/s12213-020-00135-2

Sreetharan, P. S., Whitney, J. P., Strauss, M. D., & Wood, R. J. (2012). Monolithic fabrication of millimeter-scale machines. *Journal of Micromechanics and Microengineering*, *22*(5). https://doi.org/10.1088/0960-1317/22/5/055027

Stanford, B., & Beran, P. (2012). Optimal compliant flapping mechanism topologies with multiple load cases. *Journal of Mechanical Design, Transactions of the ASME*, *134*(5). https://doi.org/10.1115/1.4006438

Steltz, E., Avadhanula, S., & Fearing, R. S. (2007). High lift force with 275 Hz wing beat in MFI. *IEEE International Conference on Intelligent Robots and Systems*, 3987–3992. https://doi.org/10.1109/IROS.2007.4399068

Syaifuddin, M., Park, H. C., & Goo, N. S. (2006). Design and evaluation of a LIPCA-actuated flapping device. *Smart Materials and Structures*, *15*(5), 1225–1230. https://doi.org/10.1088/0964-1726/15/5/009

Takahashi, H., Abe, K., Takahata, T., & Shimoyama, I. (2018). Experimental study of the aerodynamic interaction between the forewing and hindwing of a beetle-type ornithopter. *Aerospace*, *5*(3). https://doi.org/10.3390/aerospace5030083

Tay, W. B., van Oudheusden, B. W., & Bijl, H. (2015). Numerical simulation of a flapping four-wing micro-aerial vehicle. *Journal of Fluids and Structures*, *55*, 237–261. https://doi.org/10.1016/j.jfluidstructs.2015.03.003

Teoh, Z. E., Fuller, S. B., Chirarattananon, P., Prez-Arancibia, N. O., Greenberg, J. D., & Wood, R. J. (2012). A hovering flapping-wing microrobot with altitude control and passive upright stability. *IEEE International Conference on Intelligent Robots and Systems*, 3209–3216. https://doi.org/10.1109/IROS.2012.6386151

The aerodynamics of hovering insect flight. VI. Lift and power requirements. (1984). *Philosophical Transactions of the Royal Society of London. B, Biological Sciences*, *305*(1122), 145–181. https://doi.org/10.1098/rstb.1984.0054

Thierry, J., Alain, F., & Laurent, D. (2009). Asymmetric Hovering Flapping Flight: a Computational Study. In *Aerial Vehicles*. https://doi.org/10.5772/6478

Toda, M. (1981). Voltage-induced large amplitude bending device-pvf2 bimorph-its properties and applications. *Ferroelectrics*, *32*(1), 127–133. https://doi.org/10.1080/00150198108238683

Toda, M., & Osaka, S. (1979). Vibrational Fan Using the Piezoelectric Polymer Pvf2. In *Proceedings of the IEEE* (Vol. 67, Issue 8, pp. 1171–1173). https://doi.org/10.1109/PROC.1979.11419

Tomozawa, M., Kim, H. Y., & Miyazaki, S. (2009). Shape memory behavior and internal structure of Ti-Ni-Cu shape memory alloy thin films and their application for microactuators. *Acta Materialia*, *57*(2), 441–452. https://doi.org/10.1016/j.actamat.2008.09.026

Truong, Q. T., Nguyen, Q. v., Park, H. C., Byun, D. Y., & Goo, N. S. (2011). Modification of a four-bar linkage system for a higher optimal flapping frequency. *Journal of Intelligent Material Systems and Structures*, *22*(1), 59–66. https://doi.org/10.1177/1045389X10392611

Truong, Q.-T., Nguyen, Q.-V., Park, H. C., Byun, D., & Goo, N. S. (2009). Dynamic behavior of LIPCA and modification of a four-bar linkage for mimicking insect flapping frequency. *Active and Passive Smart Structures and Integrated Systems 2009*, *7288*, 72880K. https://doi.org/10.1117/12.815904

Tyson, R. K., & Frazier, B. W. (2012). Electrostatic Actuators. In *Field Guide to Adaptive Optics, Second Edition* (pp. 52–52). https://doi.org/10.1117/3.923078.ch46

Uh, K., Yoon, B., Lee, C. W., & Kim, J. M. (2016). An Electrolyte-Free Conducting Polymer Actuator that Displays Electrothermal Bending and Flapping Wing Motions under a Magnetic Field. *ACS Applied Materials and Interfaces*, *8*(2), 1289–1296. https://doi.org/10.1021/acsami.5b09981

van Veen, W. G., van Leeuwen, J. L., & Muijres, F. T. (2020). Malaria mosquitoes use leg push-off forces to control body pitch during take-off. *Journal of Experimental Zoology Part A: Ecological and Integrative Physiology*, *333*(1). https://doi.org/10.1002/jez.2308

Viaña, J., Petuya, V., & Viaña, J. (2017). *A proposal for a formula of absolute pole velocities between relative poles A proposal for a formula of absolute pole velocities be-tween relative poles. Mechanism and*

Machine Theory A Proposal for a Formula of Absolute Pole velocities between Relative Poles. *114*, 74–84. https://doi.org/10.1016/j.mechmachtheory.2017.03.016ï

Vu Phan, H., Vu Phan, H., Vu Phan, H., Truong, Q. T., Park, H. C., Park, H. C., & Park, H. C. (2015). Implementation of initial passive stability in insect-mimicking flapping-wing micro air vehicle. *International Journal of Intelligent Unmanned Systems*, *3*(1), 18–38. https://doi.org/10.1108/IJIUS-12-2014-0010

Wait, S. M., Basak, S., Garimella, S. v., & Raman, A. (2007). Piezoelectric fans using higher flexural modes for electronics cooling applications. *IEEE Transactions on Components and Packaging Technologies*, *30*(1), 119–128. https://doi.org/10.1109/TCAPT.2007.892084

Wang, C., Zhang, W., Zou, Y., Meng, R., Zhao, J., & Wei, M. (2020). A Sub-100 mg Electromagnetically Driven Insect-inspired Flapping-wing Micro Robot Capable of Liftoff and Control Torques Modulation. *Journal of Bionic Engineering*, *17*(6), 1085–1095. https://doi.org/10.1007/s42235-020-0103-7

Wang, C., Zhou, C., Zhang, X., & Liu, C. (2010). An optimization on single-crank-double-rocker flapping wing mechanism. *Proceedings - 4th International Conference on Genetic and Evolutionary Computing, ICGEC 2010*, 337–340. https://doi.org/10.1109/ICGEC.2010.90

Wang, P. L., & McCarthy, J. M. (2018). Design of a flapping wing mechanism to coordinate both wing swing and wing pitch. *Journal of Mechanisms and Robotics*, *10*(2). https://doi.org/10.1115/1.4038979

Wang, P. L., Taha, H. E., & McCarthy, J. M. (2018). Synthesis of a flapping wing mechanism using a constrained spatial RRR serial chain. *Journal of Mechanisms and Robotics*, *10*(1). https://doi.org/10.1115/1.4038529

Wang, Q.-M., & Cross, L. E. (1998). Performance analysis of piezoelectric cantilever bending actuators. *Ferroelectrics*, *215*(1), 187–213. https://doi.org/10.1080/00150199808229562

Wang, Y., Qin, N., & Zhao, N. (2015). Delaunay graph and radial basis function for fast quality mesh deformation. *Journal of Computational Physics*, *294*. https://doi.org/10.1016/j.jcp.2015.03.046

WEIS-FOGH, T. (1973). Quick Estimates of Flight Fitness in Hovering Animals, Including Novel Mechanisms for Lift Production. *Journal of Experimental Biology*, *59*(1), 169–230. https://doi.org/10.1242/JEB.59.1.169

Wood, R. J. (2007). Liftoff of a 60mg flapping-wing MAV. *IEEE International Conference on Intelligent Robots and Systems*, 1889–1894. https://doi.org/10.1109/IROS.2007.4399502

Wood, R. J. (2008). The first takeoff of a biologically inspired at-scale robotic insect. *IEEE Transactions on Robotics*, *24*(2), 341–347. https://doi.org/10.1109/TRO.2008.916997

Wood, R. J., Avadhanula, S., Sahai, R., Steltz, E., & Fearing, R. S. (2008). Microrobot design using fiber reinforced composites. *Journal of Mechanical Design, Transactions of the ASME*, *130*(5). https://doi.org/10.1115/1.2885509

Wood, R. J., Finio, B., Karpelson, M., Ma, K., Pérez-Arancibia, N. O., Sreetharan, P. S., Tanaka, H., & Whitney, J. P. (2017). Progress on "pico" air vehicles. *Springer Tracts in Advanced Robotics*, *100*, 3–19. https://doi.org/10.1007/978-3-319-29363-9_1

Wood, R. J., Steltz, E., & Fearing, R. S. (2005). Optimal energy density piezoelectric bending actuators. *Sensors and Actuators, A: Physical*, *119*(2), 476–488. https://doi.org/10.1016/j.sna.2004.10.024

Wood, R., Nagpal, R., & Wei, G. Y. (2013). Flight of the robobees. *Scientific American*, *308*(3). https://doi.org/10.1038/scientificamerican0313-60

Yan, X., Qi, M., & Lin, L. (2015). Self-lifting artificial insect wings via electrostatic flapping actuators. *Proceedings of the IEEE International Conference on Micro Electro Mechanical Systems (MEMS)*, *2015-Febru*(February), 22–25. https://doi.org/10.1109/MEMSYS.2015.7050876

Yang, L. J. (2012). The Micro-air-vehicle golden snitch and its figure-of-8 flapping. *Journal of Applied Science and Engineering*, *15*(3), 197–212. https://doi.org/10.6180/jase.2012.15.3.01

Yang, L. J., Esakki, B., Chandrasekhar, U., Hung, K. C., & Cheng, C. M. (2015). Practical flapping mechanisms for 20 cm-span micro air vehicles. *International Journal of Micro Air Vehicles*, *7*(2), 181–202. https://doi.org/10.1260/1756-8293.7.2.181

Yang, L. J., Hsu, C. K., Han, H. C., & Miao, J. M. (2009). Light flapping micro aerial vehicle using electrical-discharge wire-cutting technique. *Journal of Aircraft*, *46*(6), 1866–1874. https://doi.org/10.2514/1.38862

Yang, L. J., Hsu, C. K., Ho, J. Y., & Feng, C. K. (2007). Flapping wings with PVDF sensors to modify the aerodynamic forces of a micro aerial vehicle. *Sensors and Actuators, A: Physical*, *139*(1-2 SPEC. ISS.), 95–103. https://doi.org/10.1016/j.sna.2007.03.026

Yang, L. J., Hsu, C. K., Hsiao, F. Y., Feng, C. K., & Shen, Y. K. (2009). A Micro-Aerial-Vehicle (MAV) with figure-of-eight flapping induced by flexible wing frames. *47th AIAA Aerospace Sciences Meeting Including the New Horizons Forum and Aerospace Exposition*. https://doi.org/10.2514/6.2009-875

Yang, L. J., Kao, C. Y., & Huang, C. K. (2012). Development of flapping ornithopters by precision injection molding. *Applied Mechanics and Materials*, *163*, 125–132. https://doi.org/10.4028/www.scientific.net/AMM.163.125

Yang, Y. (2016). *A Millimeter-Scale Electrostatic Flapping-wing Actuator with High Lift-to-Weight Ratio*. https://doi.org/10.2991/ismems-16.2016.67

Yi, S., Li, D., Jiaqi, J., Jinwu, X., & Wei, X. (2018). Design and experimental study of a new flapping wing rotor micro aerial vehicle. *Proceedings of 2017 IEEE International Conference on Unmanned Systems, ICUS 2017*, *2018-Janua*, 29–33. https://doi.org/10.1109/ICUS.2017.8278312

Yokoyama, T., Tanaka, K., & Ohtake, H. (2008). Development of a variable-wing mechanism based on flapping motion of birds. *Proceedings of the SICE Annual Conference*, 168–173. https://doi.org/10.1109/SICE.2008.4654643

Yousaf, R., Shahzad, A., Qadri, M. M., & Javed, A. (2020). Recent advancements in flapping mechanism and wing design of micro aerial vehicles. In *Proceedings of the Institution of Mechanical Engineers, Part C: Journal of Mechanical Engineering Science*. https://doi.org/10.1177/0954406220960783

Yu, Y., & Tong, B. (2005). Flow control mechanism in wing flapping with stroke asymmetry during insect forward flight. *Acta Mechanica Sinica/Lixue Xuebao*, *21*(3). https://doi.org/10.1007/s10409-005-0032-z

Yusoff, H., Abdullah, M. Z., Mujeebu, M. A., & Ahmad, K. A. (2013). Development of flexible wings and flapping mechanism with integrated electronic control system, for micro air vehicle research. *Experimental Techniques*, *37*(4), 25–37. https://doi.org/10.1111/j.1747-1567.2011.00729.x

Yusoff, H., Yamin, A. F. M., Halidi, S. N. A. M., Abdullah, N. S., Ghafar, H., Suhaimi, S., Hyie, K. M., & Mohamed, W. M. W. (2022). The Optimisation of Aerodynamic Performance Enhancement of a Flapping Wing using Response Surface Methodology. *Journal of Advanced Research in Fluid Mechanics and Thermal Sciences*, *91*(1). https://doi.org/10.37934/arfmts.91.1.6982

Zbikowski, R., Galiński, C., & Pedersen, C. B. (2005). Four-bar linkage mechanism for insectlike flapping wings in hover: Concept and an outline of its realization. *Journal of Mechanical Design, Transactions of the ASME*, *127*(4), 817–824. https://doi.org/10.1115/1.1829091

Zdunich, P., Bilyk, D., MacMaster, M., Loewen, D., DeLaurier, J., Kornbluh, R., Low, T., Stanford, S., & Holeman, D. (2007). Development and testing of the mentor flapping-wing micro air vehicle. *Journal of Aircraft*, *44*(5), 1701–1711. https://doi.org/10.2514/1.28463

Zhang, J. D., & Huang, W. X. (2019). On the role of vortical structures in aerodynamic performance of a hovering mosquito. *Physics of Fluids*, *31*(5). https://doi.org/10.1063/1.5090878

Zhang, T., Zhou, C., Wang, C., & Zhang, X. (2011). Flapping wing mechanism design based on mechanical creative design theory. *Proceedings 2011 International Conference on Mechatronic Science, Electric Engineering and Computer, MEC 2011*, 2237–2240. https://doi.org/10.1109/MEC.2011.6025937

Zhang, T., Zhou, C., Zhang, X., & Wang, C. (2011). Design, analysis, optimization and fabrication of a flapping wing MAV. *Proceedings 2011 International Conference on Mechatronic Science, Electric Engineering and Computer, MEC 2011*, 2241–2244. https://doi.org/10.1109/MEC.2011.6025938

Zhang, X., Deng, H., Xiao, S., Yang, L., & Ding, X. (2019). Bionic design and attitude control measurement in a double flapping-wing micro air vehicle. *Lecture Notes in Computer Science (Including Subseries Lecture Notes in Artificial Intelligence and Lecture Notes in Bioinformatics)*, *11745 LNAI*, 240–254. https://doi.org/10.1007/978-3-030-27529-7_22

Zhang, Y., Peng, Y., Cheng, Y., & Yu, H. (2020). A novel piezo-actuated flapping mechanism based on inertia drive. *Journal of Intelligent Material Systems and Structures*, *31*(15), 1782–1792. https://doi.org/10.1177/1045389X20935624

Zhang, Y., Wang, X., Zhang, G., & Yang, J. (2020). Design and analysis of single-degree-of-freedom flapping wing mechanism based on UG. *Journal of Physics: Conference Series*, *1629*(1). https://doi.org/10.1088/1742-6596/1629/1/012060

Zhang, Y., Zhu, R., Wu, J., & Wang, H. (2022). SimoBot: An Underactuated Miniature Robot Driven by a Single Motor. *IEEE/ASME Transactions on Mechatronics*, *27*(6). https://doi.org/10.1109/TMECH.2022.3189218

Zhao, J., Niu, J., McCoul, D., Leng, J., & Pei, Q. (2015). A rotary joint for a flapping wing actuated by dielectric elastomers: design and experiment. *Meccanica*, *50*(11), 2815–2824. https://doi.org/10.1007/s11012-015-0241-x

Zhao, J. S., Yan, Z. F., & Ye, L. (2014). Design of planar four-bar linkage with n specified positions for a flapping wing robot. *Mechanism and Machine Theory*, *82*, 33–55. https://doi.org/10.1016/j.mechmachtheory.2014.07.006

Zhao, Y., Xu, D., Sheng, J., Meng, Q., Wu, D., Wang, L., Xiao, J., Lv, W., Chen, Q., & Sun, D. (2018). Biomimetic beetle-inspired flapping air vehicle actuated by ionic polymer-metal composite actuator. *Applied Bionics and Biomechanics*, *2018*. https://doi.org/10.1155/2018/

3091579

Zhou, C., Zhang, R., & Wang, C. (2019). Flap–control mechanism for flapping-wing micro air vehicles. *Proceedings of the Institution of Mechanical Engineers, Part G: Journal of Aerospace Engineering*, *233*(4), 1537–1545. https://doi.org/10.1177/0954410017752708

Zou, Y., Zhang, W., & Zhang, Z. (2016). Liftoff of an Electromagnetically Driven Insect-Inspired Flapping-Wing Robot. *IEEE Transactions on Robotics*, *32*(5), 1285–1289. https://doi.org/10.1109/TRO.2016.2593449

APPENDICES

Appendix 1

(Note 1: Weight Ratio = Driving mechanism weight / Total Weight)
(Note 2: Lift to Weight Ratio = Lift Force / Total Weight)

Table A1 : Flapping-Wing System Characteristics of Varieties of Rotary Driven 4–Bar Linkage Mechanism

Flapping-wing system **prototypes with its Mechanism & References**	No. of wings & Tail	Motor Used	Flapping frequency	Figure of merit			Wing span	Flapping angle	Range & Endurance	Flight modes			Prototype		Hand /Auto launch	Flapping type	Mimic Type	Power supply used	Year
				Driving mechanism weight	Total weight	Weight ratio				Maneuverability	Hover ability	Forward flight	Test bench model	Fully flyable model					
Microbat (1st prototype) (T.Nick Pornsin-Sirirak et al. 2001)	2 & with tail	electric motor	-	2.8g	7.5g	0.373	15cm	10-45°	9sec	-	-	yes	-	yes	Hand	Pitching up & down	Bat	1-farad super capacitors	1998
Ornithopter MAV 4-bar mechanism (T. Nick Pornsin-Sirirak et al. 2001)	2 & with tail	DC motor	30hz	3.1g	10.5g	0.2953	15cm	45°	5-18sec	High lift free flight	-	yes	-	yes	Hand	Pitching up & down	Bat & cicada wings	rechargeable NiCd battery	2001
Microbat (4-bar common crank mechanism) by Caltech and Aerovironment (T.Nick Pornsin-Sirirak et al. 2001)	2 & with tail	Electrical Motor	-	2.8g	12.5g	0.224	25cm	-	42sec	turning left or right	-	yes	-	yes	Auto	Pitching up & down	Bat	rechargeable Ni-Cad battery	2002
SF-2.5 (IC powered Mentor) 4- bar linkage crank rocker mechanism (Zdunich et al. 2007)	4 & with tail	glow engine	30hz	108g	580g	0.1863	0.36 m	76°	1min	Vertical take-off	yes	yes	-	yes	Auto	Clap-fling	Hummingbird flight	8 _ 600 mAh NiCd cells	2002
AeroVironment Microbat MAV (4-bar single crank mechanism) (Keennon and Grasmeyer 2003a) (Keennon and Grasmeyer 2003b)	2 & with tail	DC	-	-	14g	-	23cm	-	22-25minute	turning left or right	No	yes	-	yes	Auto	Pitching up & down	Bat	two-cell Lithium-polymer battery	2003
Delfly [DFM] crank mechanism (de Croon et al. 2009)	4 & with tail	coreless pager	-	-	22g	-	35cm	-	15minute	forward flight	No	yes	-	yes	Auto	Clap & peel	biomorphic	rechargeable Lithium Polymer batteries	2005
Bristol's novel PCR mechanism (Parallel crank rocker mechanism) (A. T. Conn, Burgess, and Hyde 2006)	2	Brushed dc motor	31.7hz	-	62.6g	-	75mmeach	102°	-	-	-	yes	yes	No	-	-	Hawkmoth	-	2006
Lung-Jieh Yang's MAV , 4-bar linkage with pvdf wing B (Yang et al. 2007)	2 & with tail	DC	16hz	2g	10.67g	0.1875	28cm	39-61°	40meter & 10s	lift off and free flight	-	yes	-	yes	-	-	Nature bird	poly-lithium batteries	2007
Bristol's PCR prototype(parallel crank-rocker mechanism) (Conn et al. 2007)	2	DC micromotor	7.15hz	-	46g	-	75mm each	102°	-	Flat turn & banked turn	-	yes	yes	No	-	Pitch	Insect flight	-	2007
Delfly II [DF2] crank mechanism (Tay et al. 2015)	4 & with tail	brushless motor	13hz	-	16.07g	-	28cm	30-36°	15minutes	Turning and backward flight	yes	yes	No	yes	Auto	Clap & fling	biomorphic	-	2006-2007
SF-3 (electric-powered Mentor) 4- bar linkage T- flex mechanism (Zdunich et al. 2007)	4& with tail	Brush less DC motor	30hz	44g	440g	0.1	0.36 m	40°	1min	slow translational flight with Vertical take-off	yes	yes	-	yes	Auto	Clap-fling	Hummingbird flight	NiCd battery pack (8 cells,600 mAh each)	2007
Delfly micro [DFM] crank mechanism (de Croon et al. 2009)	4 & with tail	electric motor	37.5hz	0.5g	3.07g	0.162	10cm	25.5°	50meter & 3 minutes	forward flight	yes	yes	No	Yes	Auto	-	biomorphic	rechargeable Lithium Polymer batteries	2008
Lung-Jieh Yang's Golden Snitch,4-bar single crank linkage, 3 gear transmission (Yang et al. 2012) (Hsiao et al. 2012)(Yang, Hsu, Han, et al. 2009)	2& with tail	Dc motor	20 Hz	-	5.9 g	--	21.6cm	52.8-89°	107sec	Free stream	-	yes	No	Yes	-	-	Bird	poly-Lithium battery	2008
Figure 8 shape (spherical 4 bar mechanism) (Rehmat et al. 2010)	1 & tailless	Brushless DC servo gear motor	12.25hz	-	-	-	138mm	-	-	Flapping Test bench model	yes	-	yes	no	-	-	Humming bird	-	2009
Delfly II [DF2] crank mechanism (Lentink et al. 2010)	4 & with tail	Brushless electric motor	14-20hz	4.5g	14g	0.3214	28cm	30°	15minutes	Vertical takeoff & vertical landing	yes	yes	No	yes	Auto	Clap & fling	biomorphic	140 mA h lithium-polymer battery	2009

Fenelon's modified slider-crank (MSC) mechanism (Fenelon and Furukawa 2010)	2& tailless	Pager motor	11.5hz	-	6.55 g	-	9 cm	90°	-	constrained hover and forward flight	yes	yes	No	yes	Auto	-	dragonflies	External power of 4.4v at 220mA	2009
Fenelon's biomimetic FWAV(spatial mechanism) (Fenelon 2009)	2 & tailless	Dc brushless	15hz	-	98g	-	380mm	45°	3 sec	Vertical take off & landing	yes	yes	No	yes	Auto	Clap & fling	Dragon flies & humming bird	Lithium Polymer, 7.4V, 480mA	2009
Nguyen's Beetle (Scotch yoke with linkage) (Nguyen et al. 2009)	2 & tailless	DC pager	17 Hz	2.76g	10.26g	0.269	125mm	148°	3 sec	wired flight test	-	yes	No	yes	Guiding rail	Clap & fling	Insect beetle *Allomyrina dichotoma*) .	Lithium battery (3.7 V, 180 mAh)	2009
VAMP RC ornithopter(rigid-body mechanism) (Baek et al. 2009)	2	DC motor	16hz	-	5.8g	-	304mm	45°	-	Flapping test	-	-	yes	No	-	-	Bird	0.48w	2009
ultra-light, small size FWMAV(single crank mechanism) (Tsai and Fu 2009)	2 & horizontal tail	Dc motor	25.58hz	-	8g	-	15cm	73°	8 meter	Flutter & forward flight pattern	-	yes	no	yes	Hand	pitch	Insect	Li–H battery 3.7v	2009
Lung-Jieh Yang's Eagle-II 4-bar mechanism (Yang, Hsu, Hsiao, et al. 2009)(Yang, Hsu, Han, et al. 2009)	2& with tail	-	16hz	-	11g	-	30cm	56.3°	11sec	Free stream	-	Yes	No	Yes	-	-	Bird	-	2009
TADBIR Ornithopter 4-bar mechanism (Mazaheri and Ebrahimi 2010)	2 & with tail	Dc motor	0-10hz	-	230g	-	80cm	+30°,- 19°	5sec	Hovering flight	yes	-	yes	No	-	-	Bird	battery	2010
Nguyen's Beetle Coupler and crank mechanism (Nguyen, Truong, et al. 2010)	2& tailless	motor	25hz	1.57g	10.37g	0.1513	125mm	145°	2sec	wired flight test	-	yes	No	yes	Guiding rail	Clap & fling	Insect beetle	(lithium, 3.7 V, 180 mAh	2010
Lung-Jieh Yang's Golden Snitch MAV (Yang 2012)	2& with tail	Electrical	21.7hz	-	5.9g	-	20cm	38.9°	480 sec	Vertical take off	Yes	Yes	No	Yes	Auto	-	natural flyers/small bird	poly-lithium battery 30-50 mAh	2010
4-bar crank-rocker mechanism (Sahai et al. 2012)	2 & with tailed	Planetary Gear Pager	-	-	15g	-	36cm	90°	10sec	Flapping test bench model	-	-	Yes	No	-	-	Small Bird	0.4A , 6.5v	2012
Flapping robot (Lever crank mechanism) (Kudo et al. 2012)	4 & with tail	DC motor	11 Hz	3.8g	14.5g	0.262	330mm	50°	1.5sec	Free flight	-	yes	No	Yes	Hand	-	Bird	lithium polymer battery	2012
Crank-slider with guiding slots, rigid body mechanism (Chin and Lau 2013)	2 & tailless	DC motor	19hz	-	3.26g	-	6cm	100°	-	Flapping test bench model	-	-	yes	No	-	-	Insect Inspired	Battery 3-10v	2013
4-bar crank slider rigid-body mechanism (Lau, Chin, et al. 2014)	2 & tailless	dc motor	25hz	-	3.34g	-	100mm	79-85°	-	Flapping test bench model	-	-	yes	No	-	-	Insect Dipteran	0.927w	2014
Delfly Explorer (de Wagter et al. 2014a)	4	Brushless motor	-	-	20g	-	28cm	-	9 -10 minutes	-	yes	yes	No	yes	Auto	-	Bird Delfly	-	2014
Nguyen's FWMAV (crank-slider mechanisms and linkages) (Nguyen et al. 2015)	4 & with tail	Dc brushless, & 3 servos	13.7 Hz	-	16.6g	-	22cm	90°	2minutes	take-off and back forth , up down & turns & landing	yes	yes	No	yes	auto	Clap & fling	Insect inspired	single cell lithium-polymer (LiPo) 70mah (3.7 V)	2015
Lung-Jieh Yang's MAV, 4-bar linkage with Evans Mechanism EDWC (Yang et al. 2015)	2& with tail	motor	18.9hz	2.44g	9.62 g	0.253	20cm	100°	120 sec	Forward flight, Vertical take-off and landing	Yes	Yes	No	Yes	Auto	-	Bird	Battery 60mAH, 3.7 V	2015
slider crank mechanism (Long et al. 2015)	2 & tailless	electric micro	30hz	-	-	-	83mm	25°	-	Lift off & Flapping test bench model	-	-	yes	No	-	-	Biomorphic	-	2015
4-bar mechanism crank rocker (İşbitirici and Altuğ 2017) (Isbitirici and Altug 2016)	4 & tailless	DC servomotor	10hz	-	280.1g	-	-	90°	-	Flapping test bench model	-	-	yes	No	-	-	Biomorphic dragonfly	lithium-polymer battery	2016
Modified TADBIR crank-rod/shaft mechanism (Jahanbin et al. 2016)	2 & tailless	Dc motor	10hz	90g	230g	0.391	50cm	+30°, - 22°	-	Flapping test bench model & simulations	-	-	yes	No	-	-	Bird	lithium-polymer battery	2016
untethered 3.2g FWMAV (crank slider mechanism) (Rosen et al. 2016)	2 & horizontal tail	DC motor,	25hz	140mg	3.22g	0.043	16cm	-	1.4sec	-	No	Yes	No	yes	Hand	Flap - glide	Small Bird	LiPo Powerstream 8mAh battery	2016
Jumping and flapping-wing robot With Spatial 4-bar mechanism (Zhang, Dong, and Song 2018)	2 & 2 horizontal tail	Dc & 2- servo motors	-	-	500g	-	-	-	-	Jump & Take off	-	-	-	yes	Auto	-	Biomorphic	-	2017
RotorBee (4-bar slider rail mechanism) (Wei et al. 2018)	2 & tailless	coreless	8-18hz	-	15.9g		30cm	-	2m & 5sec	untethered vertical take-off and landing	-	-	No	yes	Auto	Pitch	Insect Bee	Battery 50mAh	2017
RotorBee (4-bar slider rail mechanism) (Yi et al. 2018)	2 & tailless	Motor	19hz	2.46g	12.51g	0.196	28cm	20°	2minutes	untethered vertical take-off and landing	-	-	No	yes	Hand	pitch	Insect Bee	Battery 50mAh	2018
spatial 4-bar (slide crank)ball screw mechanism (J. H. Jang and Yang 2018)	2 & tailless	Motor	15hz	-	-	-	180mm	90°	-	flapping test bench model	-	-	yes	No	-	-	Dragonfly	-	2018
4 bar linkage mechanism with camber-flat wing (J. Jang and Yang 2018)	2 & tailless	Dc motor	20hz	-	-	-	10cm	60°	-	Flapping test bench model	yes	yes	yes	No	-	-	Insect Dragonfly	0.011N lift	2018
4-bar linkage mechanism (Z. Chen et al. 2019)	2 & tailless	coreless DC motor	30hz	-	-	-	90mm	120°	-	Flapping test bench model	-	-	yes	No	-	-	Small bird /insect	-	2018
Delfly Nimble (a 4-bar mechanism) (Karasek et al. 2018)	4 & with tail	Mini brushless dc motor	17hz	-	29g	-	33cm	-	1km & 5minutes	Side ways flight	yes	yes	No	yes	Auto	Clap & fling	biomorphic	Battery	2018
MechFLY (crank-rocker mechanism) system (Chan and Nguyen 2019)	Tailless	Brushless motor	26-39hz	-	30g	-	-	28°	-	Flapping test bench model	Yes	-	yes	No	-	Clap & fling	Small bird	-	2019

Lung-Jieh Yang's MAV, 4-bar linkage with Evans Modified 3D printed Mechanism (Kompala et al. 2019b)	2 & with tail	motor	23hz	1.82g	5g	0.365	21.5cm	82.6°	-	-	-	Yes	No	Yes	-	-	Bird	poly-Lithium battery	2019
FlowerFly Crank slider (Jadhav, Lua, and Tay 2019)	4 & tailless	brushless motor	12.4 hz	-	16g	-	Length 11cm	90°	-	Flapping test bench model	-	-	yes	no	-	Clap & fling	Small bird/insect	DC power supply	2019
Flapping Wing Rotor Model Slider crank mechanism (Chen et al. 2020)	2 & tailless	DC& servo motor	3hz	-	50g	-	205mm	30°	-	vertical take-off and landing, flapping test bench model	-	-	yes	no	-	-	Biomorphic type	-	2020
FWR MAV 4-bar crank mechanism (DONG et al. 2020)	3 & with tail	Brushless motor	20hz	3g	32g	0.093	14cm length	20°	4 sec	Take off Indoor flight test	yes	yes	No	yes	Auto	Pitch	Biomorphic type	45mAh lithium micro battery	2020
Entomopter (slider rail type mechanism) (Sochacki and Cekus 2020)	2 & tailless	stepper motor	-	-	-	-	-	77°	-	Flapping test bench model	-	-	yes	no	-	-	Insect Beetle	battery	2020
Hassanalian's FWMAV2 (slider crank mechanism with alternating crank mechanism)	4 & with horizontal tail	Motor	20hz	69.5g	135.9g	0.511	-	-	-	Flapping test bench model	-	-	yes	-	-	-	Bird	Battery	2020

Table A2 : Flapping-Wing System Characteristics of Varieties of Rotary Driven 5-Bar Linkage Mechanism

Small Bird Planar 5-bar linkage (crank rocker mechanism) (Bejgerowski et al. 2010)	2 & with tail	Brushless motor	6.1hz	8g	71g	0.1126	63.5 cm	65°	15minute	sustained indoor & outdoor flight ascent, descent, steering and landing	-	-	-	Yes	Auto	-	Small bird	21.1g 3x250mAh-cell li-po battery	2010
David Coleman's Hummingbird modified 5-bar (crank-rocker) mechanism (Coleman et al. 2015)	2 & tailless	brushless out runner motor	22hz	16.8g	62g	0.27	12-inch	±60° to ±75°	1meter & 5sec	stable hovering flight , left & right with backward movements	yes	yes	no	yes	Auto	Pitch, roll , yaw	Hummingbird	3-cell LiPo battery	2015
David Coleman's Robotic humming bird (5-bar linkage mechanism) (Coleman et al. 2017)	2 & tailless	Servo motor	20hz	16.8 g	62.1g	0.27	14cm	20°	50-60sec	Hovering flight	yes	yes	no	yes	Auto	Pitch, roll, yaw	Hummingbird	one-cell 3.7 V 30 mAh Li–Po battery	2017

Table A3 : Flapping-Wing System Characteristics of Varieties of Rotary Driven 6-Bar Linkage Mechanism

FMAV (Planar Single-Crank Double-Rocker mechanism) (Zhang, Zhou, Zhang, et al. 2011)	2 & with horizontal tail	Mini motor	17hz	-	14.88g	-	22cm	70°	10minutes	Free flight	-	yes	no	yes	auto	-	Small bird	70 mA battery	2011
Lung-Jieh Yang's MAV Stephenson 6-bar linkage mechanism (Yang et al. 2015)	2 & with tail	Motor	14.3hz	-	10.46 g	-	20 cm	84°	57sec	forward flight, vertical take-off and landing	-	Yes	No	yes	Auto	-	Bird	Battery 60mAH, 3.7 V 14.02 W	2015
Hassanalian's Thunder I (slider-crank mechanism) (Mostafa Hassanalian et al. 2017) (Hassanalian and Abdelkefi 2016)(Hassanalian and Abdelkefi 2019b)	2 & with horizontal tail	Motor & servo motor	5.88- 9hz	-	350g	-	700mm	30°	13minutes	vertical take-off, flapping, gliding, bounding, and soaring	yes	Yes	No	yes	Hand	-	Bird	Lipo-3 Cell-800mAh	2016
6-bar linkage (quick return, crank slider mechanism) (Jeon et al. 2017)	2 & tailless	Dc & servo motor	37Hz	8.3g	20g	0.415	150mm	160°	-	vertical take-off, flapping, & gliding,	yes	-	no	yes	Auto	Pitch	Insect	Battery	2017
SDU-1 (Spatial RRSS-SSR mechanism) (Ji et al. 2020)	2 & tailless	(dc) brushless motor	2.1hz	-	74g	-	0.9m	54°	-	Flapping test bench model	-	-	yes	No	-	-	Bird-pigeon	-	2020

Table A4 : Flapping-Wing System Characteristics of Varieties of String-Based Rotary Driven Mechanism

Saturn Prototype (string-based dual lever flapping mechanism) (Keennon et al. 2012a)	2 & tailless	-	27.5hz	-	17.5g	-	15.8 cm	180°	11 minutes	hover and fly forward	yes	yes	No	Yes	Auto	-	Nano Hummingbird	Battery	2010
Ball-joint mechanism is adopted to twist wings flapping (Yoon, Kang, and Jo 2011)	2 & tailless	Voice Coil Motors (VCM)	68 Hz	1.09g	2.86 g	0.381	75mm	60°	-	Flapping test bench model also hover in midair	yes	-	yes	No	-	-	Bird	1.5 V/15 mAh mercury battery	2011
Nano Hummingbird with string-based mechanism (Keennon et al. 2012a)	2 & tailless	-	30Hz	-	19g	-	16.5cm	200°	4 minutes	hover and fly forward	yes	yes	No	yes	Auto	-	Nano Hummingbird	-	2012
FW Robot (TEC Mechanism) Pully string mechanism (Phan, Kang, and Park 2016)	2 & tailless	Dc motor	20hz	-	20g	-	156mm	180°	40 sec	Vertical flight	yes	yes	no	yes	Auto	Clap & fling	Insect beetle	-	2016
KUBeetle Pully string mechanism (Phan, Kang, et al. 2017)	2 & tailless	Dc motor	33hz	2.8g	21.4g	0.130	140mm	190°	14sec	Vertical flight	yes	yes	no	yes	Auto	Clap & fling	Insect beetle	7.4v li-poly	2017
String based FWMAV (Gong et al. 2019)	2 & tailless	DC motor	24 Hz	-	10.8 g	-	150mm	132.7°	--	Flapping & trailing edge test bench model	-	-	yes	no	-	-	Insect	Battery 4v	2019
KUBeetle-S Pully string mechanism (Phan et al. 2019b)	2 & tailless	Dc motor	23hz	2.6g	16.4g	0.158	170mm		3minutes	takeoff, forward/backward	yes	yes	no	yes	Auto	Clap & fling	Insect beetle	two-cell lithium-polymer 7.4 V, 70 mAh	2019
KUBeetle-S Pully string mechanism (Phan et al. 2020)	2 & tailless	Dc motor	17.3hz (10-30 hz)	2.6g	15.8g	0.164	20cm	90°	8.8 minutes	takeoff, forward/backward, and sideways flights	yes	yes	no	yes	Auto	Clap & fling	Insect Beetle	3.7v lithium polymer battery	2020

Table A5 : Flapping-Wing System Characteristics of Varieties of the Shaft–Based Rotary Driven Mechanism

MAV-sized biplane propulsion test model (crankshaft mechanism) (Jones, Duggan, and Platzer 2001) (Jones and Platzer 2009)(Kevin D. Jones and Platzer 2006)	2 oscillating airfoils	Small geared stepping motor	18hz	-	9g	-	15cm	-	-	Flapping test bench model	-	-	yes	no	-	-	Biomorphic	rechargeable lithium-polymer battery	2001
FWMAV first flew. (crank shaft mechanism) (Jones and Platzer 2003) (Jones et al. 2005)	2 fixed wing & 2 oscillating airfoils	Motor	30hz	1.10g	14.4g	0.076	30 & 25cm	-	2-3minutes	take-off and land vertically, hover, maneuver and fly forward	yes	yes	no	yes	Auto	pitch/plunge	Biomorphic	-	2002
Vertical takeoff MAV with cambering wings (Jones and Platzer 2003)	2 fixed-wing & 2 oscillating airfoils	motor	40hz	2.7g	9.5g	0.284	-	-	-	take-off and land vertically, hover, maneuver and fly forward	yes	yes	no	yes	Auto	pitch/plunge	Biomorphic	-	2003
Model 2 (crank shaft mechanism) (Jones et al. 2005)	2 fixed-wing & 2 oscillating airfoils	Motor	-	2.5g	13.4g	0.186	27cm	-	-	take-off and land vertically, hover, maneuver and fly forward	yes	yes	no	yes	Auto	pitch/plunge	Biomorphic	Battery 1.5W	2003
Improved NPS FWmodel (smallest version) (Jones and Platzer 2015)	2 fixed-wing & 2 oscillating airfoils		30hz	2.3g	11g	0.209	23cm		12 minute	take-off and land vertically, hover, maneuver and fly forward	yes	yes	no	yes	Auto	pitch/plunge	Biomorphic	Single chargeable lithium-polymer battery	2005
Radio controlled flapping-wing MAV (Model 3) (crankshaft mechanism) (Kevin D. Jones and Platzer 2006)(Jones et al. 2005)	2 fixed wing & 2 oscillating airfoils	Mini motor	32hz	2.3g	12.4-14g	0.164	25cm	-	15-20 minutes	Free stream flight	yes	yes	no	yes	Auto	pitch/plunge	Biomorphic	Lithium-polymer cell.	2005
Clapping wing MAV (common crank shaft mechanism) (Kawamura et al. 2008b)	2 & with tail	-	35hz	-	2.3g	-	10cm	100°	8 minutes	-	-	yes	no	yes	hand	clap	Hawkmoth	-	2008
Crank shaft mechanism with quad-rotor-like structure (van Breugel, Ern Teoh, and Lipson 2010)	8 wings & with tail	DC Motor	20hz	0.8g	24.22g	0.033	222.89 mm each	10°	33sec	passively stable hovering flapping flight	yes	-	no	yes	Auto	pitch/plunge	Biomorphic	3.7v, 90mAh Lipoly battery	2010
Flapping wing rotor MAV(U-shape lever mechanism) (Li et al. 2011)	2 & tailless	Mini Electric	25.10 Hz	-	9.1g	-	8cm length	35°	-	Flapping Test bench model	-	-	yes	No	-	-	insect	Lithium battery	2011
flying machine (crank shaft mechanism) (Ristroph and Childress 2014)	4 & tailless	Motor (Solarbotics, GM15)	5-19hz	1.1g	2.1g	0.523	10cm	-	1sec	Stable ascent, forward & hovering flight	yes	yes	no	yes	Auto	-	Jelly fish like flying machines, Bio morphic type	5.5v	2013

Hummingbird robot (direct drive with spring shaft connected mechanism) (Zhang et al. 2013)	1 wing-flapping test	Brushless DC motor	24hz	-	-	-	62.5mm	150v	-	Flapping Test bench model	-	-	yes	No	-	-	Humming bird	-	2013
BionicOpter by festo(crank shaft mechanism) (Gaissert et al. 2014)	4 & tailless	Brushless motor & servo motor	15-20hz	-	175g	-	63cm	80-130°	Several minutes (average 10 minutes)	Stabled forward flight	yes	yes	no	yes	Auto	-	Dragonfly	2 LiPo cells with 7.4 V	2014
Hummingbird robot prototype 1 (direct driven with spring shaft connected mechanism) (Fei et al. 2019; Zhang et al. 2015, 2017)	2 & tailless	Brushless DC-Servomotors	30hz	1g	7.5g	0.133	160mm	170°	1.5sec	Lift off from guide wires	-	-	no	yes	-	-	Humming bird	-	2015
Hummingbird robot prototype 2 (direct driven with spring shaft connected mechanism) (Zhang et al. 2017)	2 & tailless	Brushless DC-Servomotors	30hz	2.1g	12g	0.175	170mm	150°	2.7sec	Vertical Take off	yes	-	no	yes	Auto	-	Humming bird	battery	2017
Quad thopter (crank shaft mechanism) (de Wagter et al. 2017)	8 & tailless	Servo(small brushed motor)	15hz	-	33g	-	28cm	40°	9 minutes	Semi-transitioned & fast forward flight	yes	yes	no	yes	Auto	-	Bio-morphic	-	2017
Hummingbird robot FWMAV(direct driven with spring shaft connected mechanism) (Fei et al. 2019; Zhang et al. 2017)	2 & tailless	Brushless DC-Servomotors	40hz	1g	12.1g	0.082	167.9mm		40cm height in 11sec	vertical take-off and short hovering flight	yes	yes	no	yes	Auto	-	Humming bird		2019
bore-hole of a Flapping Rotary Wing (L. Chen et al. 2018)	2 & tailless	electric micro& coreless DC	28hz	2.98g	5.64g	0.528	-	10°-30°	-	Flapping Test bench model	-	-	yes	no	-	-	Bird	-	2017
novel flapping wing rotor with crank shaft mechanism (Guo et al. 2018)	2 & tailless	micro electric DC motor	11-24hz	1.45g	2.6g	0.557	20cm	35°-41°	4 sec	vertical take-off and short hovering fligh	yes	-	no	yes	Hand	Pitch	Insect	2.5-4.5v	2018
at-scale Hummingbird robot (shaft spring mechanism) Prototype 3 (Tu, Fei, Zhang, et al. 2020)	2 & tailless	Dual Dcmotor	34hz	2.1g	19.35g	0.108	170mm	150°	10 sec	sustained stable free flight & stable hovering	yes	-	no	yes	Auto	-	Hummingbird	Li–Po battery 7.4v	2020
at-scale Hummingbird robot (shaft spring mechanism) Prototype 3 (Tu, Fei, and Deng 2020)	2 & tailless	Dual brushless Dc motor	34hz	2.1g	20.4g	0.102	170mm	±78°	15meter in 20 sec	sustained stable free flight & stable hovering	yes	yes	no	yes	Auto	-	Hummingbird	Li–Po battery 7.4v	2020
at-scale Hummingbird robot (shaft spring mechanism) (Tu et al. 2021)	2 & tailless	Dual brushless Dc motor	-	-	12.5g	-	170mm	135-153°	350mm in 7sec	Vertical takeoff	Yes	-	no	yes	auto	-	Hawkmoth	-	2021

Table A6 : Flapping-Wing System Characteristics of Varieties of Compliant Structure Mechanisms for Flapping

4-bar with spring mechanism (Madangopal, Khan, and Agrawal 2005)	2 & with tail	DC motor	-	-	15g	-	36cm	-	-	Forward flight	-	yes	no	yes	Auto	-	Bird	-	2005
Bejgerowski's (Crank rocker mechanism) (Bejgerowski et al. 2009)	2 & with tail	DC pager motor	7-12.1hz	1.5g	12.76g	0.117	152mm	65°	5 minutes	sustained flight with ascent & descent 0.15 N lift	-	yes	no	yes	Hand	-	Bird	Battery	2009
4-bar Baek's compliant mechanism(crank-arm mechanism coupled to a mass-spring system) (Baek et al. 2009)	2 & tailless	DC motor, & Linear spring	10-30hz	-	5.8g	-	80mm	55°	-	Flapping test bench model	-	-	yes	No	-	-	Bird	2.65V	2009
Bejgerowski's Small Bird (Crank rocker mechanism with short compliant segments) (Bejgerowski et al. 2011)	2 & with tail	Servo motor	5.2hz	-	72.5g	-	63.5cm	65°	15 minutes	Sustained indoor & outdoor flight	-	yes	no	yes	Auto	-	Bird	21.1g 3x250mAh-cell li-po battery	2011
Sahai's 4-bar compliant mechanism (Sahai et al. 2013)	2 & tailless	Planetary Gear Pager	16-18hz	-	3g	-	124mm	100°	-	Flapping bench model	-	-	yes	No	-	-	Insect	Battery	2013
Clicking mechanism with Crank-slider-driven compliant structure (Chin and Lau 2013)	2 & tailless	dc motor	19hz	-	3.78g	-	6cm	115°	8 ms	Flapping test bench model	-	-	yes	No	-	-	Insect Inspired	Battery 3-10v	2013
Hines novel minimalist FWMAV (motor spring mechanism) (Hines et al. 2014a)	2 & tailless	Solarbotics GM15 motor	10hz	1.21g	2.7g	0.448	7cm each	180°	0.616 sec	Lift off and hovering flight	yes	-	no	yes	Auto	-	Nano Hummingbird	Battery power	2013
4-bar (crank slider) Shell Structure Compliant thoracic mechanism (Lau, Chin, et al. 2014)	2 & tailless	Dc motor	25hz	-	3.51g	-	10cm	56-80°	-	Flapping test bench model	-	-	yes	No	-	-	Insect Dipteran	0.681w electrical power	2014
Hines two wing FWMAV (motor spring mechanism) (Hines et al. 2015)	2 & tailless	Solarbotics GM15 motor	10hz	2g	3.1g	0.645	210mm	180°	1.25sec	Lift off and hovering flight	yes	-	no	yes	Auto	-	Nano Hummingbird	Battery power	2015
Hines four wing prototype (motor spring mechanism) (Hines et al. 2015)	4 & tailless	Solarbotics GM15 motor	10hz	5g	6.9g	0.7 24	210mm	180°	1.2sec	Lift off and hovering flight	yes	-	no	yes	Auto	-	Nano Hummingbird	Battery power	2015

Table A7 : Flapping-Wing System Characteristics of Varieties of Hybrid Driven Mechanism

FWMAV prototypes with its Mechanism & References	No. of wings & Tail	Motor Used	Flapping frequency	Driving mechanism weight	Total weight	Weight ratio	Wing span	Flapping angle	Range & Endurance	Flight modes	Hover ability	Forward flight	Test bench model	Fully flyable model	Hand /Auto launch	Flapping type	Mimic Type	Power supply used	Year
Dual spherical scotch yoke mechanism (Galiński and Zbikowski 2005)	2 & tailless	DC motor	20hz	-	50-100g	-	150mm	±90°	-	Flapping test bench model	-	-	yes	no	-	-	Insect Diptera	-	2005
Scotch-yoke mechanism and linkage system (Nguyen, Park, et al. 2010)	2 & tailless	DC pager motor	45hz		10.26g		125mm	140°	-	Flapping test bench model	-	-	yes	no	-	-	Insect Beetle	lithium battery (3.7 V, 180 mAh),	2010
four-bar with single-crank slider mechanism (Yusoff et al. 2013)	2 & tailless	DC mini motor	6-9hz	-	-	-	270mm	40-60°	-	Flapping test bench model	-	yes	yes	No	-	-	Bat Mormopterus Planiceps	DC power supply	2011
Matěj Karásek FWMAV (Crank Slider with rocker and 4-bar linkage mechanism) (Karásek et al. 2014)	2 & tailless	brush-less DC motor	18 hz	-	21.4g	-	15cm	±40°	-	Flapping test bench model	Yes	-	yes	no	-	-	Nano hummingbird	4Wsupply , lift force 90 mN	2014
Scotch-yoke and slider crank (rack rocker)mechanism (Truong et al. 2014)	2 & tailless	motor	40hz	-	-	-	110mm	100 °	3sec	Vertical flight	-	-	no	yes	Auto	pitch	Insect beetle	-	2014
Tailless FWMAV (Scotch-yoke and crank slider mechanism) (Vu Phan et al. 2015)	2 & tailless	DC motor	39-43hz	2.4g	7.36g	0.326	12.5cm	150°	1sec	Free vertical take-off	-	-	no	yes	Auto	pitch	Insect Beetle Allomyrina dichotoma	lithium polymer battery 3.7 V, 20 mAh,	2015
Tailless FWMAV (slider-crank and pulley-string mechanisms) (Phan et al. 2015)	2 & tailless	motor	40hz	-	10g	-	10mm each	140 °	-	Flapping Test bench model	yes	-	yes	no	-	-	Insect beetle	External power supply	2015
Tailless FWMAV (4-bar linkage and a pulley-string mechanism) (Phan and Park 2016)	2 & tailless	motor	25 ± 0.2 Hz.	-	-	-	156mm	180 °	-	Flapping Test bench model	yes	-	yes	no	-	-	Insect Allomyrina Dichotoma	external power supply	2016
Tailless FWMAV (4-bar link and a pulley-string mechanism) (Phan, Au, et al. 2016)	2 & tailless	Carbon/epoxy panels	20hz	-	-	-	70mm	192°	-	Flapping test bench model	yes	-	yes	no	-	Clap & fling	Insect rhinoceros beetle	external power supply -	2016
Two planar 4-bar linkages mimicking insect's thorax(crank -coupler rocker-mechanism) (Nguyen et al. 2016)	4 & with tail	3.1 g brushless motor, servos	12.4hz	3.3g	14.6g	0.226	22cm	126.66°	3 minute	Vertical takeoff & turning flight	yes	yes	no	yes	auto	Clap & fling	Insect	3.7 V-70mAh single cell lithium polymer	2016
Colibri (slider crank with 4-bar mechanism) (Roshanbin et al. 2017)	2 & tailless	(EPS8-Brushed DC)	22hz	5.98g	22.02g	0.271	21cm	±60° to ±70°	15-20sec	Hovering flight	Yes	-	no	yes	Auto	Pitch & roll	Hummingbird	(Nanotech Lipoly 160 mah 25 C	2016
Kubeetle (4-bar linkage and pully string mechanism) (Phan, Kang, et al. 2017)	2 & tailless	3.5g coreless DC motor	29-35hz	2.8g	21g	0.133	-	190°	14 sec	Hovering & straight vertical takeoff flight	yes	yes	no	yes	auto	Clap & fling	Insect Beetle	2-cell 7.4 V lithium polymer battery	2017
Flower fly (Two crank slider mechanism with two linkages) (Nguyen, Chan, and Debiasi 2017)	4 & Tail less	Brushless motor	9-14hz	2.5g	14.5g	0.172	110mm	90°	-	Hovering & vertical take off flight	Yes	-	yes	No	-	Clap & fling	Insect Flower fly	3.7v single cell LiPo battery	2017
Delfly II FWMAV (two symmetric 4-bar mechanisms coupled) (Tijmons, Karásek, and de Croon 2018)	4 & With Tail	DC &Double Linear Servo	12-15hz	2.7g	21.1g	0.127	28cm	83°	1 minute	Hovering, Forward flight, take off & land vertically	yes	yes	no	yes	auto	Clap & fling	Biomorphic	180 mAh LiPo battery	2018
FWMAV (crank-slider and double-pendulum mechanism) (Zhou et al. 2019)	2 & with tail	-	-	-	78g	-	40cm	45°	-	fast turning & stable straight flight	-	yes	no	yes	hand	-	Insect bilateral wing approach	-	2018
Nguyen's NUS robotic bird crank-slider-rocker mechanism (Nguyen and Chan 2019)	4 & Tail less	Brushless motor & linear servo	12-14hz	-	27g	-	22cm	90°	4 minute	Left & right turns, hovering, forward & backward flight, Vertical takeoff & landing	Yes	Yes	No	yes	Auto	Clap & fling	Nano hummingbird	220 mAh LiPo battery	2019
Crank rocker and double rocker mechanism (Zhang et al. 2019)	4 & tailless	Brush & linear servo motor	23hz	-	32.8g		-	-	-	Flapping test bench model	-	--	yes	no	-	-	Insect Rhinoceros beetle	battery	2019
Crank and coupler sliding with rocker (Q. Liu et al. 2019)	2 & with tail	brushless motor	11-12hz	-	23g		29cm	140°	-	Flapping test bench model	-	-	yes	no	-	-	Insect cicadas	DC voltage stabilizer	2019
FW assisted jumping robot (slider-crank and rack-pinion mechanism) (Truong, Phan, and Park 2019)	2 & tailless	DC motor	19hz	-	23.5g	-	-	140°	0.56 sec	Jump and lift off Lift force 2.78 N	-	yes	no	yes	auto	-	Insect Schistocerca gregaria	External power supply	2019
double-cracker-rocker (Chin et al. 2020)	4 & with tail	Servo and small motor	15hz	-	26g	-	280mm	50°	8.43sec	Vertical Lift off, flight and dart	yes	yes	no	yes	auto	Clap & fling	Bird	7.36mNm torque at 4.2V	2020
smaller yoke within the scotch-yoke mechanism (Moses et al. 2020)	2 & tailless	DC motor	21.6hz	-	1.2g	-	24mm	-	-	Flapping test bench model	-	-	yes	no	-	-	Insect Hawkmoth Manduca sexta	3-10v DC	2020
Hassanalian's FWMAV1 (slider-crank mechanism with alternating crank mechanism)	4 & with horizontal tail	Motor	20hz	152.1g	218.5g	0.696	-	-	-	Flapping test bench model	-	-	yes	no	-	-	Bird	Battery	2020
Single crank -double rocker mechanism (Deng et al. 2021)	2 & tailless	Micro motor	30hz	-	23.1g	-	19cm	160°	-	Flapping test bench model	-	-	yes	no	-	-	Insect dichotoma	7.4v	2021

Table A8 : Flapping-Wing System Characteristics of Varieties of Piezo Driven Mechanisms

FW Aerial Vehicle & references	No. of wings & Tail	Actuation Mechanism /Materials used	Flapping frequency	Driving mechanism weight	Total weight	Weight ratio	Wing span	Flapping angle	Endurance	Model Type & flight mode	Hovering ability	Forward flight	Test bench model	Fully flyable model	Launch type	Flapping type	Power used	Lift force	Lift to wing span ratio (N/m)	year
UC Berkeley Micro mechanical flying insect [MFI]model (Deng, Schenato, and Sastry 2001) (Deng et al. 2006)	2	Piezoelectric actuators(piezo PZN-PT unimorph) 4 bar mechanism	150hz	40mg	43-100mg	0.4	25mm	45°	600miliseconds	Insect blow fly Calliphora	yes	-	no	yes	Auto	pitch	Battery 20mW	-	-	2001-2006
Micro mechanical flying insect (Sitti 2003)	2 & tailless	PZT 5H actuator (4 bar mechanism)	29hz	-	-	-	-	90°	-	Insect Test bench model	-	-	yes	no	-	-	-	-	-	2003
LIPCA(4 bar linkae system) (Syaifuddin et al. 2006)	2 & tailless	Unimorp piezo ceramic actuator	9hz	-	20g	-	12cm	80°	-	Insect,	-	-	yes	no	-	-	$300V_{p-p}$	-	-	2006
Nguyen's LIPCA(Lightweight Piezo Composite Actuator) (Nguyen et al. 2007)	2	piezo actuated 4 bar mechanism	9hz	6.10g	10.38g	0.587	12cm	110°	-	Insect, Wired flight	No	No	yes	No	Auto wired flight	Clap & fling	Interface power supply 300Vpp	0.022N	0.183	2007
Lightweight Piezocomposite actuator (LIPCA) (Nguyen et al. 2008)	2	Unimorph Piezoceramic,	17 Hz	-	3.6g	-	Wing size 27.5 cm2	92°	-	Insect	No	No	yes	No	-	Clap & fling	150V	Average vertical force 3.6 (gf)	-	2008
1st take-off at scale robotic insect (Wood 2008) (Wood 2007)	2 & tail less	single-drive piezo actuated (PZT biomorph) mechanism	110hz	44mg	60mg	0.733	3cm	±50°	400 mili ssec	Insect Vertical take off	yes	-	no	Yes	Auto Guide rail	-	100Wkg−1	-	-	2007 2008
Nguyen's LIPCA (modif4 bar) (Nguyen et al. 2007; Truong et al. 2009)	2	piezo actuated 4 bar mechanism	15hz	-	-	-	14cm	97°	-	Insect,	No	No	yes	No	-	Clap & fling	Interface power supply 300Vpp	0.022N	0.157	2009
UC Berkeley MFI (4 bar slider-crank mechanism with piezo actuation) (Fearing and Wood 2010)(Steltz et al. 2007)	2 & tailless	PZT bimorph actuator	275hz	-	130mg	-	25mm	±35°	-	Insect honeybee Flapping test bench model	-	-	yes	no	-	-	LiPoly battery 27 mW, 600Wkg−1	1400 μN	0.056	2007 2010
THUNDER TH-8R (Guo et al. 2012)	2 & tailless	piezoelectric thunder 8r actuator	77-125hz	-	0.15-0.27g	-	90mm each	-	-	Insect Flapping test bench model	No	No	yes	No	-	-	65v	2.20 mN	0.012	2011
Micro robotic fly (Pérez-Arancibia et al. 2011)	2 & tailless	piezoelectric bimorph actuator	90-110 hz	-	56mg	-	3cm		10sec	Insect diptera vertical take-off	yes	-	no	yes	Auto Guide rail	pitch	300v	-	-	2011
Mocro robotic bee (Ma et al. 2012)	2 & tailless	PZT-5H	95-105hz	25mg	70mg	0.357	3cm	90°	23ms	Insect diptera vertical take off	-	-	no	yes	Auto	pitch	105v	1.3mN	0.043	2012
FW Microrobot	2 & tailless	piezoelectric bending bimorph cantilever actuator	110hz	-	101mg	-	30mm	-	9cm in 33sec	Insect diptera vertical take-off	yes	-	no	yes	Auto Guide rail	pitch	-	-	-	2012

Lionfly (Mateti, Byrne-Dugan, Tadigadapa, et al. 2013)	2 & tailless	SUEX dry film and powered by piezoelectric bimorph actuator	37 Hz	-	112mg	-	19.89mm	46°	-	Insect Flapping test bench model	-	-	yes	no	-	-	75 V DC	71 μN	0.0035	2012
Harvard Robobee (Teoh et al. 2012)	2 & tailless	(piezoelectric actuator)-	105-120Hz	-	61mg+45mg =106mg	-	30mm	45°	1.2 sec	Insect stable vertical take-off	yes	-	no	yes	Auto	pitch	200-256V external supply	-	-	2012
Mobee (Sreetharan et al. 2012)	2 & tailless	bimorph piezo actuator	-	-	90mg	-	39mm	90°	-	Insect Bee Test bench model	-	-	yes	no	-	-	-	-	-	2012
Half-scale prototype (spherical 4-bar mechanism) (Arabagi et al. 2012)	2 & tailless	spherical 4-bar (PZT-5H)	37 Hz	-	160 mg	-	37 mm	20-40°	-	Insect Test bench model	yes	-	yes	no	-	-	340v	0.58 mN	0.0156	2012
full-scale prototype (spherical 4-bar mechanism) (Arabagi et al. 2012)	2 & tailless	spherical 4-bar (PZT-5H)	26 Hz	-	650mg	-	70 mm	90°	-	Insect Test bench model	yes	-	yes	no	-	-	180v	1.05 mN	0.015	2012
LionFly prototype LF07 (Mateti, Byrne-Dugan, Rahn, et al. 2013)	1 & tailless	PZT-5H bimorph actuator	49.13 ± 1.43 Hz	-	54mg+18.70mg =72.7mg	-	5mm each	75°	-	Insect Flapping test bench model	-	-	yes	no	-	-	150 VDC	-	-	2013
Robotic fly (Ma et al. 2013)	2 & tailless	Voltage driven piezoelectric bimorph actuator	120hz	-	80mg	-	3cm	110°	9 -20 sec	Insect diptera vertical take-off	yes	-	no	yes	auto	pitch	External supply	1.3mN	0.0433	2013
FW microrobot (Chirarattananon et al. 2014)	2 & tailless	Tw piezoelectric bimorph actuator	120hz	-	80g	-	35mm	110°	7sec	Insect vertical take off	yes	-	no	yes	auto	pitch	19mw	-	-	2014
Robo Bee (aerial & aquatic) (Chen et al. 2015)	2 & tailless	Bimorph piezoelectric actuaor	120-140hz in air, 4.1-5hz in water	-	80mg	-	3cm	70°	8.8 sec	Insect vertical take off	yes	-	no	yes	auto	pitch	200V	1.1mN	0.0366	2015
MicroRobotic insect with adhesion (Graule et al. 2016)	2 & tailless	piezoelectric actuator with electrostatic adhesion	-	-	100mg	-	3cm	-	12.28 sec	Insect diptera take off	yes	-	no	yes	auto	pitch	External supply	-	-	2016
Hybrid Aerial aquatic microbot (Chen et al. 2017)	2 & tailless	Pair of piezoelectric actuators	5-15hz	-	175mg	-	-	14.80°	60ms	Insect take off & landing	yes	-	no	yes	auto	pitch	<300V	11mN	-	2017
Aerial aquatic microbot (Chen et al. 2017)	2 & tailless	Pair of piezoelectric actuators	9-11hz	-	85mg	-	3cm	-	2.4 sec	Insect Take off	-	-	no	yes	auto	pitch	-	1.8mN	0.06	2017
self-lifting sub 100 mg FW Robot (Zou et al. 2017)	2 & tailless	Piezo actuator PZT-5H	100hz	55mg	84mg	0.654	35mm	± 60°	7 sec	Take off along guide rail	-	-	no	yes	Guide rail	-	V_{pp} 250v	-	-	2017
Robofly Flapping wing NAV (James et al. 2018)	2 & tailless	two piezo-electric actuators driven by a 976 nm laser source and a photovoltaic (PV) cell.	170 Hz	73.7mg	190mg	0.387	20mm	90°	250ms	Insect honeybee Lift off	yes	-	no	yes	auto	pitch	a 976 nm laser – Powered, 200-300 mW,25 mA.	-	-	2018
FW ROBOT Direct driven piezo (Ozaki and Hamaguchi 2018a)	2 & tailless	Piezo electric unimorph actuator	110hz	368mg	598mg	0.615	114mm	66.2°	1 sec	Insect Vertical Take-off flight	-	-	no	yes	auto	clap	100v voltage	6.52 mN (665 mgf)	0.0571	2018
Robofly (Chukewad et al. 2018)	2 & tailless	Piezoelectric two cantilever actuator	70-140hz	-	74mg	-	13mm each	90°	200 ms	Insect Lift off Bio-morphic type	-	-	no	yes	auto	-	250v	-	-	2018
Robobee X wing Untethered flight (Jafferis et al. 2019)	4 & tailless	alumina-reinforced piezoelectric actuators with 4 wings	165-173hz	-	91mg-259m	-	3.5cm	88°	0.3 sec	Insect Lift off Bio-morphic type	-	-	no	yes	auto	-	190-210v	-	-	2019
SDAB1 fly with four wing (Jafferis et al. 2019)	4 & tailless	for 4 wings alumina-reinforced piezoelectric actuators	165-172hz	-	270-372 mg	-	3.5cm	95.5°-98°	0.7 sec	Insect Lift off Bio-morphic type	-	-	no	yes	auto	-	185-210v	-	-	2019

Bee+ (Yang et al. 2019)	4 & tailless	Twin piezoelectric unimorph actuator	100hz	56mg	95mg	0.589	33mm	65°	2 sec	Insect Vertical Take-off flight	yes	yes	no	yes	auto	Clap & fling	260v	1.4mN	0.0424	2019
Aerial robot with 4 wings (Fuller 2019)	4 & tailless	twin piezoelectric unimorph actuator	160h	10mg	143mg	0.0699	56mm	90°	5 sec	Insect Lift off Bio-morphic type	yes	yes	no	yes	auto	Clap & fling	190v	4mN	0.0714	2019
Novel Piezo actuation based on inertia drive (Yangkun Zhang et al. 2020)	1 & tailless	multilayer piezoelectric actuator (AL1.65 3 1.65 3 5D-4F from NEC TOKIN)	20hz-30hz	-	-	-	8 x 3 x1 mm^3 each flapper size	-25° to 25°	-	Insect Flapping test bench model	-	-	yes	no	-	-	60v	-	-	2020
3 paired wing resonant drive robot (Ozaki and Hamaguchi 2020)	6 & tailless	piezoelectric unimorph actuator	120-124hz	696mg	1.12g	0.621	114mm	-	0.4 sec	Vertical Lift off Bio-morphic type	-	-	no	yes	auto	clap	150 V external power supply	-	1.49	2020
3 paired wing direct driven piezo (Jimbo et al. 2020)	6 & tailless	piezoelectric unimorph actuator PIN–PMN–PT	115hz	-	1.15g	-	115mm	-	1.3sec	Vertical Lift off Bio-morphic type	-	-	no	yes	auto	clap	150 V external power supply	-	-	2020
two-winged MAV model (Kumar et al. 2020)	2 & tailless	piezoelectric bending actuator	20hz	-	0.61g	-	90.14mm	-	-	Insect Dragonfly Flapping test bench model	-	-	yes	no	-	-	-	-	-	2020
four-winged MAV model (Kumar et al. 2020)	4 & tailless	Cantilever type piezoelectric actuator	17.25-20hz	-	1.14g	-	Front 100mm & back80mm	-	-	Insect Dragonfly Flapping test Bio-morphic type	-	-	yes	no	-	-	-	-	-	2020
Dragonfly Micro Flapping Wing model (Regulski and Leang 2020)	4 & tailless	Dual piezo bimorph actuator	10-250hz	-	-	-	each wing length 10mm	30°	-	Insect Dragonfly Flapping test bench model	-	-	yes	no	-	-	$200V_{p\text{-}p}$	-	-	2020
Hovering robofly (Dhingra et al. 2020)	2 & tailless	piezoelectric actuator	150hz	-	-	-	-	-	12cm, in 5sec	Insect	yes	-	no	yes	auto	pitch	180v			2020
UW Robofly-expanded (Chukewad and Fuller 2021)	2 & tailless	piezoelectric actuator	170-190hz	-	160mg	-	-	54°	0.2meter in 2sec	Insect Biomorphic type Vertical take-off & landing	yes	-	no	yes	auto	pitch	250V	-	-	2021

Table A9 : Flapping-Wing System Characteristics of Varieties of SMA Driven Mechanisms

Bat with shoulder SMA muscles (Furst et al. 2013)	2 & tailless	SMA actuator wires	10hz	-	-	-	15cm	75°	-	Bat Flapping test bench model	-	-	yes	no	-	-	-	-	-	2013
Batbot with SMA-muscles (Colorado et al. 2013)	2 & tailless	SMA NiTi metal strips & wire	2.5-8hz	-	79g	-	53cm	120°	-	Bat Flapping test bench model	-	-	yes	no	-	-	Lipo battery	-	-	2013
SMA actuated Mechanism (Marimuthu et al. 2014)	2 & with tail	Ti-Ni, SMA wire actuators	-	-	30g	-	10cm	-	-	Bird-Lift with forward velocity	-	yes	no	yes	-	Clap & fling	0.62V, 1.5A	-	-	2014

Batbot with SMA-muscles (Colorado et al. 2015)	2 & tailless	SMA NiTi metal strips & wire	2.5-6.6hz	78.85g	125g	0.630	53cm	50°	0.4sec	Bat forward & turning flight	-	yes	no	yes	-	-	Lipo battery 800mAh	0.97N	1.83	2015
SMA actuated FWMUAV (Kamaruzaman and Abdullah 2017)	2 & with tail	SMA Nickel Titanium spring & wire	-	-	-	-	195mm	26.45°	-	Flapping test bench model	-	-	yes	no	-	-	3.5v , 0.51A& 7v, 2.23A	-	-	2017

Table A10 : Flapping-Wing System Characteristics of Varieties of Electro Active Polymer (EAP) Driven Mechanisms

IPMC Flapping wing actuator with pinion rack arrangement (Lee et al. 2006)	1 & tailless	gold-coated thick IPMC (Nafion)	0.5-15hz	-	-	-	-	15°-85°	-	Insect Flapping test bench model	-	-	yes	no	-	-	3-4v	-	-	2006
IPMC actuated dragonfly (Mukherjee and Ganguli 2010)	4 & tailless	IPMC	21hz	-	1.87g	-	5cm each	12°	-	Insect dragonfly Flapping test bench model	-	-	yes	no	-	-	7v	0.0115N Lift force	-	2010
Pre-strain Rolled DEA FWMAV (Lau, Lim, et al. 2014)	2 & tailless	Silicone BJB TC-5005 ,CFRP shell amplifier	1hz	5.3g	7- 10.47g	0.506	-	5-10°	-	Insect Flapping test bench model	-	-	yes	no	-	-	power supply 3kv	-	-	2014
DEMES FWMAV (Zhao et al. 2015)	2 & tailless	VHBTM 4910 & Graphite electrode	3-5hz	-	1.2g	-	100mm	60°	-	Small bird Flapping test bench model	-	-	yes	no	-	-	5kv	-	-	2015
IPMC actuated FWMAV (Zhao et al. 2018)	2 & tailless	casted Nafion, PET film	7-8hz	-	-	-	42mm each	12.5°	-	Insect Beetle Flapping test bench model	-	-	yes	no	-	-	4.5v DC	-	-	2018
Double cone DEA actuated model (Cao et al. 2019)	2 & tailless	Polyacrylate tape VHB ,silicone elastomers	18hz	0.12g	1.26g	0.095	80 mm each	63°	-	Insect, Lift off flapping test bench model	-	-	yes	no	-	-	-	-	-	2019
Flapping micro robot model 1 (Y. Chen et al. 2019)	2 & tailless	Driven by one DEA actuator (1 set of wings)	100-280hz	100mg	155mg	0.645	9.9mm	36-42°	1200ms	Insect, Vertical take-off	yes	yes	no	yes	auto	pitch	-	1.8mN	0.181	2019
Flapping micro robot model 2 (Y. Chen et al. 2019)	4 & tailless	Driven by two DEA actuators (2 set of wings)	100-280hz	200mg	320mg	0.625	9.9mm	36-42°	900ms	Insect, Lift off Bio morphic type	yes	-	no	yes	Auto	pitch	600v	1.8mN	0.181	2019
Flapping micro robot model 3 (Y. Chen et al. 2019)	8 & tailless	Driven by four DEA actuators (4 set of wings)	100-280hz	400mg	660mg	0.666	9.9mm	36-42°	10-16 sec	Insect, Lift off & hovering Bio morphic type	yes	-	no	yes	auto	pitch	-	1.8mN	0.181	2019

Dielectric elastomers for resonant FW model (Cao et al. 2020)	2 & tailless	Double cone DEA, electrodes, rack &pinion arrangement	30.2hz	-	1.6g	-	165mm	31°	-	Insect Flapping test bench model	-	-	yes	no	-	-	-	-	-	2019

Table A11 : Flapping-Wing System Characteristics of Varieties of Electrostatic (ES) Driven Mechanism

self-lifting artificial insect (Yan et al. 2015)	2 & tailless	fulcrum bars, metal beams, electrodes	50-70Hz	-	3.1mg	-	12mm each	50°	10 sec	Insect Vertical take-off	-	-	no	yes	U shape rail	-	DC power source 5kv	-		2015
Electrostatic flapping actuator (Liu et al. 2016)	2 & tailless	PVC Sheet, PET membrane, aluminum foil, electrode, ni-ti alloy	-	-	330mg	-	56mm	30-50°	-	Insect Flapping test bench model	-	-	yes	no	-	-	DC power source 3.25KV	82.4 µN	0.00147	2016
mm-scale electrostatic FW actuator (Yang 2016)	2 & tailless	carbon-fiber-reinforced polymer (CFRP)	80hz	3mg	7mg	0.428	10mm each	80°	-	Insect Flapping test bench model	-	-	yes	no	-	-	DC power source	15 µN	-	2016
Electrostatic FW actuator (Liu et al. 2018)	2 & tailless	PET Plate, electrodes, pivot spar brackets, carbon fiber sheets	35hz	-	50mg	-	56mm	40-60°	-	Insect honey bee Flapping test bench model	-	-	yes	no	-	-	DC voltage, pre charged capacitors	79.2 µN	0.00141	2018

Table A12 : Flapping-Wing System Characteristics of Varieties of Electromagnetic (EM) Driven Mechanisms

Ring type - Solenoid Actuated mechanism (Bolsman, J. F. L. Goosen, et al. 2009)(Bolsman et al. 2008)	2 & 4 winged models(tailless)	Voice coil actuator	28hz	-	4g	-	10cm	67.5°	0.1-0.5sec	Insect inspired, Hovering & horizontal flight	yes	yes	no	yes	-	-	-	-	-	2008 2009
Su-8 Electromagnetic Actuator (Dargent et al. 2009)	2 & tailless	SU-8 2035 film coated with aluminum	110hz	-	37mg	-	10-30mm	40°	-	Insect Calliphora species. Flapping test	-	-	yes	no	-	-	power of 7 mW	-	-	2009
Electromagnetic MEMS (Meng et al. 2012)	2 & tailless	New LIGA like process with SU-8 photoresist technology	130hz	107mg	143 mg	0.748	3.5 cm	27°	-	Insect Syrphid hoverflies Flapping test bench model	-	-	yes	no	-	-	Low driving voltage	-	-	2011
Electromagnetic Actuated FW NAV mechanism (Bontemps et al. 2013)	2 & tailless	SU-8 EPOXY(photoresist resin) with coil & magnet	100hz	11.3mg	22 mg	0.513	3.5 cm	51°-60°	-	Insect Flapping test bench model	-	-	yes	no	-	-	7 to 75 mW& 300 mA to 1 A	4 µN	0.0001212	2012

Electromagnetic actuated High Frequency FWMAV (Roll, Bardroff, and Deng 2016; Roll et al. 2013) (Roll, Cheng, and Deng 2015)	2 & tailless	N52 NdFeB disc magnets	33-70hz	-	2.61g	-	-	±70°	-	Insect Flapping test bench model	-	-	yes	no	-	-	24 V	-	-	2013 -2015
Electromagnetic actuated High Frequency FWMAV (Roll et al. 2016)	2 & tailless	Neodymium magnet (NdFeB N5) with coil	90hz	1.5g	4g	0.375	8.6cm	±60°	0.38sec	Insect Lift-off vertical guid rail	-	-	no	yes	Guide wire	-	24v	-	-	2016
SJFLY I (EM Actuated With Two 4-Bar Combination) (Zou et al. 2016)	2 & tailless	neodymium iron boron magnet Ni-N52	80hz	65mg	80mg	0.8125	3.5cm	±70°	7 min	Insect Lift-off vertical guide rail	-	-	no	yes	Guide rail	-	1.2 W	50mN	1.51	2016
Artificial flapping wing (Yan et al. 2016)	2 & tailless	Electromagnetically driven	80hz	-	3764mg	-	12mm each	60°	-	Insect Flapping test bench model	-	-	yes	no	-	-	5.5v	-	-	2016
Artificial flapping wing(Yan et al. 2016)	2 & tailless	Electromagnetically driven	60hz	-	197.2mg	-	12mm each	18°	-	Insect Flapping test bench model	-	-	yes	no	-	-	5v	-	-	2016
Em-Actuated FWMAV (Liu, Yan, Qi, Zhang, et al. 2017)	2 & tailless	Ni-Ti , Si-Al bonding wire	75 Hz	-	51.2 mg	-	10mm	30°-46°	-	Insect Flapping test bench model	-	-	yes	no	-	-	5.5v and 400mA	-	-	2017
Low voltage electromagnetic driven FW insect (Liu, Yan, Qi, Yang, et al. 2017)	2 & tailless	permanent magnet, Cantilever, electromagnet	51.3hz	65.8mg	90mg	0.7311	3cm	100.4°	12sec	Insect Horizontal guide rail	-	-	no	yes	Guide rail	-	5v	116.5 µN	0.0038	2017
Electromagnetic Actuated FW NAV mechanism SU-8 skeleton(Faux et al. 2018) (Bontemps et al. 2013)	2 & tailless	SU-8 EPOXY(photoresist resin) with coil & magnet	133.5hz	-	22mg	-	22mm	20°	-	Insect	-	-	no	yes	-	-	-	240 µN	0.0109	2018
Electromagnetically Driven (Z. Liu et al. 2019)	2 & tailless	Mylar as permanent magnet, cantilever-plate, and an EM- iron core.	65hz	-	84 mg	-	3.6 cm	101.2°	4sec	Insect Horizontal guide rail	-	-	no	yes	Guide rail	-	AC current 420 mA (AC voltage 0.5 V),	384.5 µN	0.01068	2019
Sub-miligram FWAV (Bhushan and Tomlin 2019)	1 & tailless	Magnet coil system	132hz	0.71mg	0.73mg	0.927	3.5cm	90`	-	Insect Flapping test bench model	-	-	yes	no	-	-	±70mV applied square wave voltage	0.01mN	0.00028	2019
SJFLY II EM driven FW micro robot (Wang et al. 2020)	2 & tailless	Ni-N52 magnet, spherical 4-bar transmission	80-90hz	-	96mg	-	35mm	130`	1200ms	Insect Vertical guide rail & Lift off	-	-	no	yes	Guide rail	-	AC supply (0.5-1.5 V)	0.457 µN	0.0000130	2020

LIST OF PUBLICATIONS

Spoorthi Singh, Mohammad Zuber, Mohd Nizar Hamidon, Norkhairunnisa Mazlan, Adi Azriff Basri, Kamarul Arifin Ahmad, " Classification of actuation mechanism designs with structural block diagrams for flapping-wing drones: A comprehensive review", Progress in Aerospace Sciences, Volume 132, 1 July, 2022, 100833, https://doi.org/10.1016/j.paerosci.2022.100833, Impact factor: 8.934 Q1.

Spoorthi Singh, Aravind K M, Jayakrishnan R, Mohammad Zuber, Adi Azriff Basri, Norkhairunnisa Mazlan, Mohd Nizar Hamidon, Kamarul Arifin Ahmad," Parametric Study and Experimental Investigations of a Single Crank–Slotted Dual Lever Mechanism for MAV Flapping Actuation", Biomimetics MDPI, Volume 7(4), 21, Nov 2022, 208, Impact factor: 4.5 Q2.

Spoorthi Singh, Mohammad Zuber, Mohd Nizar Hamidon, Adi Azriff Basri, Norkhairunnisa Mazlan, Kamarul Arifin Ahmad, "Kinematic Investigations of a Novel Flapping Actuation Design with Mutually Perpendicular 3 Cylindrical Joint Approach for FW-Drones", Biomimetics MDPI, Volume 8 , issue 2, 17th April 2023, https://doi.org/10.3390/biomimetics8020160, Impact factor: 4.5, Q2.

Spoorthi Singh, Aravind K M, Jayakrishnan R, Mohammad Zuber, Adi Azriff Basri, Norkhairunnisa Mazlan, Mohd Nizar Hamidon, Kamarul Arifin Ahmad, "Study of X-Pattern Crank-Activated 4-Bar Fast Return Mechanism for Flapping Actuation in Robo Drones", Journal of Advanced Research in Fluid Mechanics and Thermal Sciences, Volume 105 (2), May 2023 https://doi.org/10.37934/arfmts.105.2.115128,

Conference publication:

"Study of X-Pattern Crank-Activated 4-Bar Fast Return Mechanism for Flapping Actuation in Robo Drones", published in proceedings of International Conference on Recent Advances in Fluid Mechanics (ICRAFM)(4-6 Oct 2022).